VOLTAGE AND CURRENT PROFILES

AND

LOW-ORDER APPROXIMATION

OF FREQUENCY-DEPENDENT TRANSMISSION LINE PARAMETERS

by

LUIS MARTI

Elec. Engr., Central University of Venezuela, 1979

A THESIS SUBMITTED IN PARTIAL FULFILLMENT OF
THE REQUIREMENTS FOR THE DEGREE OF

MASTER OF APPLIED SCIENCE

in

THE FACULTY OF GRADUATE STUDIES
Department of Electrical Engineering

We accept this thesis as conforming
to the required standard

THE UNIVERSITY OF BRITISH COLUMBIA
April 1982

© Luis Marti, 1982

In presenting this thesis in partial fulfilment of the requirements for an advanced degree at the University of British Columbia, I agree that the Library shall make it freely available for reference and study. I further agree that permission for extensive copying of this thesis for scholarly purposes may be granted by the head of my department or by his or her representatives. It is understood that copying or publication of this thesis for financial gain shall not be allowed without my written permission.

Department of Electrical Engineering

The University of British Columbia
1956 Main Mall
Vancouver, Canada
V6T 1Y3

Date April 27th 1982

DE-6 (3/81)

ABSTRACT

In this thesis project, two models related to the simulation of electromagnetic transients in power systems, have been developed.

The first model has been designed to find voltages and currents at a number of intermediate, equally spaced points along the line ("profile"), from the solution at the end points (taking into account the frequency dependence of the line parameters). This "profile model" is derived from the cascade connection of n equivalent circuits, each one representing a segment of the line. The solution is carried out with an internal time step which is an exact submultiple of the travel time of the propagation mode in consideration.

A series of tests shows that the results obtained with this model are more accurate than those obtained if the standard practice of segmenting the line is followed.

With the aid of the profile routines, a movie which illustrates the propagation of transients along a line, has been produced as well.

The second part of this thesis describes the development of a low-order approximation of the frequency-dependence of line parameters, from a reduced amount of information. Using the electrical parameters at power frequency and dc conductor resistances, the tower configuration of the line is reconstructed. This equivalent line configuration permits the evaluation of the line parameters over a wide frequency range. Rational functions are then used to approximate the frequency-dependence of these parameters over a limited frequency range with a reduced order model.

Analytical tests and transient simulations, indicate that the model is reasonably accurate over the frequency range of interest in most practical applications.

Both models have been incorporated into the UBC version of the Electromagnetic Transients Program (EMTP).

TABLE OF CONTENTS

ACKNOWLEDGEMENT

It is impossible to thank all the individuals and institutions that directly or indirectly collaborated in the completion of this thesis project. However, risking ingratitude towards those not mentioned below, I must give special thanks,

To the "girls", in the main office of the Department of Electrical Engineering, for often going out of their way to give me a hand.

To Dr. Dommel, for his insight, help and unshakeable patience.

To my brother, Jose, whose genius lit the way of our shared dream.

To Debby, for her love.

To my parents.

PART I

VOLTAGE AND CURRENT PROFILES

ALONG A TRANSMISSION LINE

INTRODUCTION

When a power system is disturbed from its normal steady-state operation, a transition between the original state and the new steady-state conditions (with possible changes in the network) must occur. This transition period begins with very fast electromagnetic transients (in the order of milliseconds), which usually involve transient overvoltages or high transient currents. This is followed by slower electromechanical transients (in the order of seconds), which are not discussed in this thesis.

Protection devices are used to limit the magnitude of transient overvoltages across expensive equipment in order to prevent damage in this equipment and subsequent substation failures.

The selection and the co-ordination of these devices require detailed system studies. The efficiency and accuracy of computer programs used for such studies, become more important as systems grow in size and complexity.

Programs such as the Electromagnetic Transients Program (EMTP) are capable of simulating a large variety of transient conditions, for systems of varying size and complexity. This program, originally developed by Dommel [1], [2], has evolved and grown as simulation models have been improved by other researchers.

In the last decade or so, much effort has been devoted to the accurate modelling of transmission lines, taking into account the frequency dependence of their parameters. One such model has recently been developed and implemented by J.R. Marti [3]. The simplicity and computational flexibility of this model have provided the basic tools for the development of other related models (in particular, those discussed in

this thesis).

Most line models, either with frequency-dependent or constant parameters, give voltage and current information only at the end points of the line. This information usually satisfies the needs for most simulations. There are situations, however, when the information at the end points of the line may not be enough to give a clear picture of the overall behaviour of the line (e.g., when lightning arresters are considered).

The usual practice, when voltages and currents at intermediate places are needed, is to segment the line into shorter sections, and to examine the response at the end points of each segment. This procedure, however, can be inaccurate and is certainly time consuming.

Very few attempts to determine the voltage and current profile (without explicitly segmenting the line) can be found in the literature. The only model found [4], which takes frequency-dependence into account, is based on Semlyen's approach to the frequency-dependence problem [5]. In this model, the voltages and currents are found at only one intermediate point along the line. A profile can thus be obtained by repeated calculations with different segmentation ratios.

It is the purpose of the first part of this project, to develop a profile model for any number of equally spaced points along the line.

Such a model should meet the following requirements:

1. It should be more accurate than the conventional "external" segmentation of the line.
2. The computer routines must be designed to permit a simple and efficient interconnection with the frequency-dependence version of the EMTP.
3. The routines should be easy to use, and should require a minimum amount of effort on the part of the user.

CHAPTER 1

THEORETICAL CONSIDERATIONS

1.1 Description of the Profile Model in the Frequency Domain

Consider an m-phase transmission line with ground return, as represented in Figure 1.1

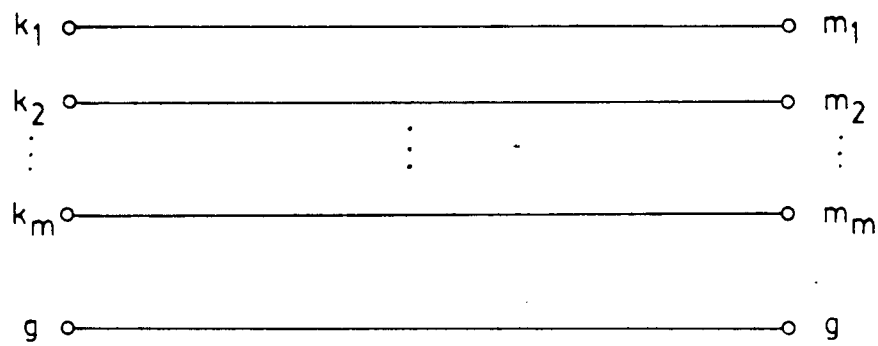

Fig. 1.1: Representation of an m-phase transmission line with ground return

After the appropriate modal transformations have been made, as described in appendix I-A, the behaviour of the line can be analyzed in the modal domain, where it can be studied as a set of m, single-phase lines. Each of these single-phase lines can then be described in terms of its modal surge impedance $Z_c(\omega)$ and propagation function $A_1(\omega)$. The equations obtained from this single-phase model, are applicable to any line mode, and therefore sufficient to describe the line in the phase domain.

Consider then, the representation of one of the line's propagation modes, shown in Figure 1.2

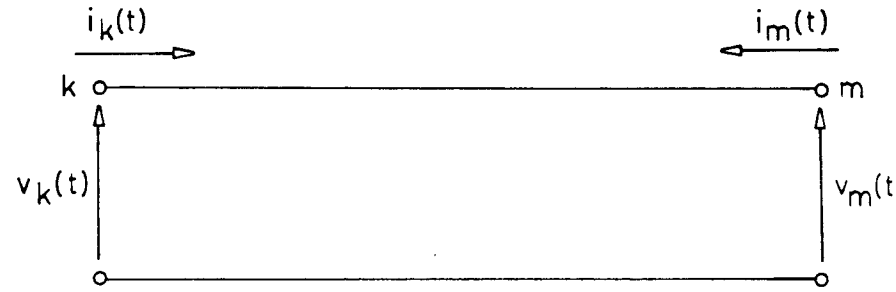

Fig. 1.2: Modal representation.

In the frequency domain, this line can be described by the (frequency-dependent) model of Figure 1.3, as described in appendix I-B.

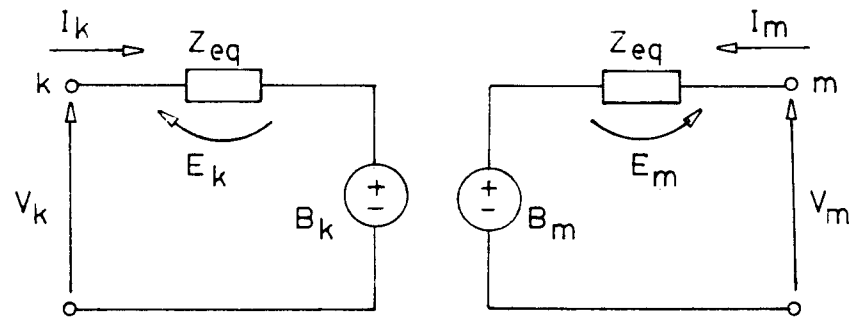

Fig. 1.3: Line model in the frequency domain.

where,

$$\left.\begin{aligned} B_k &= V_k - I_k Z_{eq} \\ B_m &= V_m - I_m Z_{eq} \end{aligned}\right| \quad \text{(backward travelling functions)} \qquad (1.1)$$

$$\left.\begin{aligned} F_k &= V_k + I_k Z_{eq} \\ F_m &= V_m + I_m Z_{eq} \end{aligned}\right| \quad \text{(forward travelling functions)} \qquad (1.2)$$

The relationship between forward and backward travelling functions is given by

$$B_k = A_{1,c}\, F_m \qquad (1.3)$$

where,

$$A_{1,c} = e^{-\gamma(\omega)\,\ell_c} \qquad (1.4)$$

$\gamma(\omega) = \sqrt{Z'Y'}$

Z' is the modal series impedance $(R'(\omega) + j\omega L'(\omega))$ per unit length (Ω/km)

Y' is the modal shunt admittance $(G' + j\omega C')$ per unit length (mhos/km)

ℓ_c is the line length in km

If we connect in cascade (n + 1) of the circuits in Figure 1.3, each representing a line segment of length ℓ, we obtain the equivalent circuit of Figure 1.4

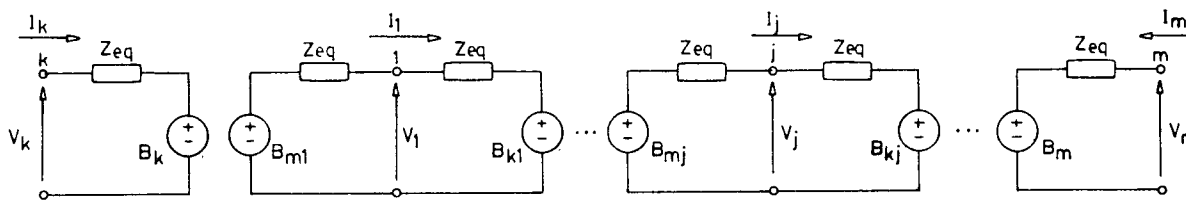

Fig. 1.4: Cascade connection of (n + 1) equivalent line circuits.

Note that to connect (n + 1) segments of length ℓ is equivalent to divide a line of length $\ell_c = \ell(n + 1)$ into (n + 1) segments of length

ℓ. This results in n nodes with n intermediate voltages and currents.

The following definitions can easily be extended from equations (1.1) to (1.4) for the forward and backward travelling functions of each segment j.

$$\left.\begin{aligned} B_k &= V_k - I_k Z_{eq} \\ B_m &= V_m - I_m Z_{eq} \end{aligned}\right| \qquad (1.5)$$

$$\left.\begin{aligned} B_{k,j} &= V_j - I_j Z_{eq} \\ B_{m,j} &= V_j + I_j Z_{eq} \end{aligned}\right| \qquad (1.6)$$

$$\left.\begin{aligned} F_k &= V_k + I_k Z_{eq} \\ F_m &= V_m + I_m Z_{eq} \end{aligned}\right| \qquad (1.7)$$

$$\left.\begin{aligned} F_{k,j} &= V_j + I_j Z_{eq} \\ F_{m,j} &= V_j - I_j Z_{eq}, \end{aligned}\right| \qquad (1.8)$$

where V_j and I_j (j = 1,2,..., n) are the voltages and currents at each of the n intermediate nodes.

The relationships between forward and backward travelling functions can be summarized as follows,

$$B_{m,1} = A_1 F_k \qquad (1.9)$$

$$B_{k,n} = A_1 F_m \qquad (1.10)$$

$$B_{m,j} = A_1 F_{k,j-1} \quad (j = 2, \ldots, n) \qquad (1.11)$$

$$B_{k,j} = A_1 F_{m,j+1} \quad (j = 1, \ldots, n-1), \qquad (1.12)$$

where,

$$A_1 = e^{-\gamma(\omega)\ell} \qquad (1.13)$$

and,

$$\ell = \ell_c/(n + 1)$$

Note that ℓ is the length of a segment, and ℓ_c is the length of the complete line. Also note that the relationships between the end

points of the line (equations (1.1) through (1.4)) still hold true, regardless of the number of segments connected.

From the equivalent circuit of Figure 1.4,

$$V_j = I_j Z_{eq} + B_{k,j}$$

$$V_j = -I_j Z_{eq} + B_{m,j}.$$

Adding up these two equations,

$$2 V_j = B_{k,j} + B_{m,j}. \tag{1.14}$$

Also, from the equivalent circuit,

$$2 I_j Z_{eq} = B_{m,j} - B_{k,j}. \tag{1.15}$$

Addition of (1.14) and (1.15) gives,

$$V_j + I_j Z_{eq} = B_{m,j}.$$

Subtraction of (1.14) from (1.15) gives,

$$V_j - I_j Z_{eq} = B_{k,j}.$$

Comparing the last two equations with (1.8) we finally obtain,

$$F_{k,j} = B_{m,j} \tag{1.16}$$

$$F_{m,j} = B_{k,j}. \tag{1.17}$$

Equations (1.11) and (1.12) can now be expressed in terms of backward travelling functions alone,

$$B_{m,j} = A_1 B_{m,j-1} \quad (j = 2, \ldots, n) \tag{1.18}$$

$$B_{k,j} = A_1 B_{k,j+1} \quad (j = 1, \ldots, n+1). \tag{1.19}$$

If the intermediate backward travelling functions $B_{k,j}$ and $B_{m,j}$ are known, the intermediate voltages and currents V_j and I_j are uniquely determined by equations (1.14) and (1.15). Also, $B_{k,j}$ and $B_{m,j}$ can be determined if the forward travelling functions F_k and F_m (end points) are known. For example, with F_k known from equation (1.9), $B_{m,1}$ can be obtained; with $B_{m,1}$ known, $B_{m,j}$ (j=2,...,n) is determined by equation (1.18). An analogous procedure can be followed for $B_{k,j}$, starting from F_m.

At this point it can be seen that the only information needed to evaluate the internal voltages and currents is given by F_k and F_m. This permits the evaluation of the intermediate voltages and currents in a way which is independent of the solution method being used for the complete line. This presents certain advantages that will be discussed later.

The propagation function $A_1(\omega)$ is identical for each segment, and it is approximated by rational functions in the same way as for the propagation function $A_{1,c}(\omega)$ of the complete line (see appendix II-B).

The partial fractions expansion of the rational functions yields,

$$A_1(\omega) = \frac{k_1}{s + \beta_1} + \frac{k_2}{s + \beta_1} + \ldots + \frac{k_m}{s + \beta_m} e^{-j\omega\tau} \qquad (1.20)$$

Since the surge impedance is independent of the length of the line, the same approximation used for the solution of the complete line is used for the evaluation of the profile, that is,

$$Z_c(\omega) = k_o + \frac{k_1}{s + \alpha_1} + \frac{k_2}{s + \alpha_2} + \ldots + \frac{k_m'}{s + \alpha_m'} \qquad (1.21)$$

1.2 Solution in the Time Domain

The intermediate voltages and currents are determined by the backward travelling functions, and these can be sequentially determined from the forward travelling functions at the end points of the line.

Consider equation (1.9)

$$B_{m,1} = A_1 F_k.$$

The time domain counterpart is obtained using the Inverse Fourier Transform,

$$b_{m,1}(t) = a_1 * f_k(t). \tag{1.23}$$

The convolution (indicated by "*") can be solved by recursive methods, as explained in appendix II-B, giving,

$$b_{m,1}(t) = \sum_{i=1}^{m} b_{m,1,i}(t) \tag{1.24}$$

with,

$$b_{m,1,i}(t) = g_i\, b_{m,1,i}(t-\Delta t) + c_i f_k(t-\tau) + d_i\, f_k(t-\tau-\Delta t) \tag{1.25}$$

where, g_i, c_i and d_i are the integration constants from the convolution integral (1.23), and are given by,

$$g_i = e^{-\beta_i \Delta t}$$

$$h_i = \frac{1 - g_i}{\beta_i \Delta t}$$

$$c_i = \frac{k_i\,(1 - h_i)}{\beta_i}$$

$$d_i = -\frac{k_i\,(g_i - h_i)}{\beta_i},$$

k_i and β_i are obtained from the rational-functions approximation of $A_1(\omega)$ for the length of one segment (see equation (1.20)).

Similarly, $b_{k,n}(t)$ is obtained from equation (1.10),

$$b_{k,n}(t) = a_1(t) * f_m(t) \tag{1.26}$$

$$b_{k,n}(t) = \sum_{i=1}^{m} b_{k,n,i}(t) \tag{1.27}$$

with,

$$b_{k,n,i}(t) = g_i\, b_{k,n,i}(t-\Delta t) + c_i\, f_m(t-\tau) + d_i\, f_m(t-\tau-\Delta t). \tag{1.28}$$

The intermediate functions $b_{k,j}(t)$ and $b_{m,j}(t)$ are obtained in a similar fashion from equations (1.18) and (1.19).

$$b_{m,j}(t) = a_1(t) * b_{m,j-1}(t) \tag{1.29}$$

$$b_{m,j}(t) = \sum_{i-1}^{m} b_{m,j,i}(t) \tag{1.30}$$

$$b_{m,j,i}(t) = g_i\, b_{m,j,i}(t-\Delta t) + c_i\, b_{m,j-1}(t-\tau) + d_i\, b_{m,j-1}(t-\tau-\Delta t), \tag{1.31}$$

and,

$$b_{k,j}(t) = a_1(t) * b_{k,j+1}(t) \tag{1.32}$$

$$b_{k,j}(t) = \sum_{i=1}^{m} b_{k,j,i}(t) \tag{1.33}$$

$$b_{k,j,i}(t) = g_i\, b_{k,j,i}(t-\Delta t) + c_i\, b_{k,j+1}(t-\tau) + d_i\, b_{k,j+1}(t-\tau-\Delta t) \tag{1.34}$$

As mentioned in the previous section, with $b_{k,j}$ and $b_{m,j}$ known, the intermediate voltages are obtained using equation (1.14) in the time domain,

$$v_j(t) = \frac{1}{2}(b_{k,j}(t) + b_{m,j}(t)). \tag{1.35}$$

The intermediate currents can be obtained from equation (1.15) in the time domain

$$2e_j(t) = b_{m,j}(t) - b_{k,j}(t), \tag{1.36}$$

where,

$$e_j(t) = i_j(t) * z_{eq}(t). \tag{1.37}$$

From equation (1.21),

$$z_{eq}(t) = [k_o\,\delta(t) + k_1\,e^{-\alpha_1 t} + \ldots + k_m\,e^{-\alpha_{m'} t}]\,u(t). \tag{1.38}$$

Introducing (1.38) into (1.37)

$$e_j(t) = e_{j,o}(t) + \sum_{i=1}^{m'} e_{j,i}(t), \tag{1.39}$$

where,

$$e_{j,o}(t) = k_o\,i_j(t) \tag{1.40}$$

$$e_{j,i}(t) = m_i\,e_{j,i}(t-\Delta t) + p_i\,i_j(t) + g_i\,i_j(t-\Delta t). \tag{1.41}$$

The coefficients for the recursive convolution of equation (1.37) (see appendix I-B) m_i, p_i and g_i are given by,

$$m_i = e^{-\alpha_i \Delta t}$$

$$h_i = \frac{1 - m_i}{\alpha_i \Delta t}$$

$$p_i = \frac{k_i\,(1 - h_i)}{\alpha_i}$$

$$g_i = -\frac{k_i\,(m_i - h_i)}{\alpha_i}\,.$$

Introducing equations (1.40) and (1.41) into (1.36) we obtain, after some algebraic manipulations,

$$i_j(t) = \frac{1}{p}\left[\frac{1}{2}(b_{m,j}(t) - b_{k,j}(t)) - q\,i_j(t-\Delta t) - \sum_{i=1}^{m'} m_i\,e_{j,i}(t-\Delta t)\right], \tag{1.42}$$

where,

$$p = k_o + \sum_{i=1}^{m'} p_i$$

$$q = \sum_{i=1}^{m'} q_i$$

1.3 Initial Conditions

With equations (1.36) and (1.42), the current and voltage profiles on a given line can be obtained when the past history terms of the forward travelling functions for the end points (f_j and f_m) are known.

Note that a record of past history terms for the intermediate parameters must be kept for the solution. When $t = 0$, these history vectors must be evaluated from the initial conditions of the simulation. If the currents and voltages at the ends of the line are zero, all the history terms are set initially to zero. If linear, ac steady-state conditions exist prior to $t = 0$, the past history terms can be evaluated from the phasor quantities associated with e_j, $b_{m,j}$, $b_{k,j}$ and i_k,

$$e_j(t) \longleftrightarrow \bar{E}_j(\omega)$$

$$b_{m,j}(t) \longleftrightarrow \bar{B}_{m,j}(\omega)$$

$$b_{k,j}(t) \longleftrightarrow \bar{B}_{k,j}(\omega)$$

$$i_j(t) \longleftrightarrow \bar{I}_j(\omega)$$

From equation (1.20)

$$A_1(\omega) = \sum_{i=1}^{m} A_{1,i}(\omega),$$

where,

$$A_{1,i}(\omega) = \frac{k_i}{j\omega + \beta_i} e^{-j\omega\tau}$$

Since $\bar{F}_k$ and $\bar{F}_m$ are known from the steady-state solution of the system, $\bar{B}_{k,j,i}(\omega)$ and $\bar{B}_{m,j,i}(\omega)$ can be obtained from equations (1.9), (1.10), (1.18), and (1.19),

$$\bar{B}_{m,1,i}(\omega) = A_{1,i}(\omega)\ \bar{F}_k(\omega) \qquad (1.43)$$

$$\bar{B}_{m,j,i}(\omega) = A_{1,i}(\omega)\ \bar{B}_{m,j-1,i}(\omega) \quad (j=2,\ldots,n) \qquad (1.44)$$

$$\bar{B}_{k,n,i}(\omega) = A_{1,i}(\omega)\ \bar{F}_m(\omega) \tag{1.45}$$

$$\bar{B}_{k,j,i}(\omega) = A_{1,i}(\omega)\ \bar{B}_{k,j+1,i}(\omega) \quad (j=1,\ldots,n-1) \tag{1.46}$$

The intermediate steady-state currents can be found using equation (1.15)

$$\bar{I}_j(\omega) = \frac{\bar{B}_{m,i}(\omega) - \bar{B}_{k,j}(\omega)}{2\ Z_{eq}(\omega)}\ , \tag{1.47}$$

with $Z_{eq}(\omega)$ given by equation (1.21).

Also, from equation (1.21)

$$Z_{eq}(\omega) = k_o + \frac{k_1}{j\omega+\alpha_1} + \ldots + \frac{k_{m'}}{j\omega+\alpha_{m'}}$$

$$Z_{eq,i}(\omega) = \frac{k_i}{j\omega + \alpha_i}$$

Introducing $Z_{eq}(\omega)$ into equation (1.37) in the frequency domain

$$\bar{E}_j(\omega) = Z_{eq}(\omega)\ \bar{I}_j(\omega) \tag{1.48}$$

results in,

$$\bar{E}_{j,i}(\omega) = Z_{eq,i}(\omega)\ \bar{I}_j(\omega). \tag{1.49}$$

The time domain equivalents of these phasor quantities are then given by,

$$b_{b,j}(t) = |\bar{B}_{m,j}(\omega)| \cos(\omega t + \arg(\bar{B}_{m,j}(\omega)))$$

$$b_{k,j}(t) = |\bar{B}_{k,j}(\omega)| \cos(\omega t + \arg(\bar{B}_{k,j}(\omega)))$$

$$i_j(t) = |\bar{I}_j(\omega)| \cos(\omega t + \arg(\bar{I}_j(\omega)))$$

$$e_{j,i}(t) = |\bar{E}_{j,i}(\omega)| \cos(\omega t + \arg(E_{j,i}(\omega))).$$

Note that in the case of dc initial conditions (i.e., trapped charge), ω is simply set to zero in the equations above.

CHAPTER 2

IMPLEMENTATION OF THE SOLUTION METHOD

2.1 General Considerations

The model and equations described in Chapter 1 have been implemented into UBC's frequency-dependence version of the EMTP. Since the profile model requires a relatively small amount of information from the solution of the line at the end points, the interconnection with the EMTP is very simple and straightforward. Less than 90 FORTRAN statements had to be added to the main program, and all profile calculations are made in subroutines.

The profile calculations proceed simultaneously with the solution for the end points (actually, there is a delay of one time step in order to avoid numerical instability when the time step is very close to the travel time of the complete line). This method was preferred over the alternative of post-processing, in order to decrease memory requirements and to increase computational efficiency.

The profile model presents some important advantages over the external segmentation of the line. The most obvious one is that, from the user's point of view, it is easier and faster to request profile calculations with only one command, (see appendix I-C) than it is to set up several line segments.

The number of numerical convolutions (one of the most time consuming operations in the frequency-dependent solution of a line) is reduced by a factor of $(3n + 4)/(4n + 4)$, where n is the number of intermediate nodes.

The difference, although not spectacular for a small number of intermediate points, can be considerable for relatively large values of n. These savings range from 12.5% for 1 intermediate node, to 24.75% for 100 intermediate modes.

The most important advantage, however, is the increase in accuracy. Some of the computational aspects leading to this improved accuracy are discussed next.

2.2 Internal Time Step $\Delta t'$

In the solution of transmission lines at discrete time intervals, the main source of error is the fact that the time step Δt is not an exact fraction of the travel time τ of the line [6]. This error, in the case of frequency-dependent solutions, occurs when the past history terms $f(t-\tau)$ and $f(t-\Delta t-\tau)$ are evaluated. If $\tau/\Delta t$ is not an integer number, linear or higher-order interpolation is needed. For example, $f(t-\tau)$ must be interpolated between $f(t-\tau-\Delta t)$ and $f(t-\tau+\Delta t)$. The interpolation error can be reduced by using a small Δt, or it can be eliminated by choosing Δt to be an exact submultiple of τ.

The profile routines select an internal time step $\Delta t'$ that is the closest (and largest) submultiple of τ for the line mode considered. Although there is still a certain amount of interpolation involved when $f(t-\Delta t'-\tau)$ and $f(t-\tau)$ are evaluated at the end points, no additional interpolation is needed for the intermediate segments.

The accuracy gained, in comparison with the external segmentation method, increases with the number of sections considered. The improvement becomes more evident when the line has more than one phase, and it is no longer possible to choose an external Δt which is a submultiple of τ for all propagation modes.

The use of an internal time step slows down the profile calculations because the number of time steps needed is greater than, or equal to the number of time steps necessary to solve the line at the end points. Note that the intermediate currents and voltages for each mode will be evaluated at slightly different points in time, therefore, an additional interpolation is needed to obtain the phase domain quantities.

The interpolation for phase voltages and currents introduces a minimal amount of error because it is not a cumulative process: the phase

voltages for one section are not needed to evaluate the phase voltages of the next section; and once all the voltages are obtained for one time step, they are no longer needed for any future calculations.

When the line is segmented externally, care must be taken to choose a time step that is smaller than the travel time of the fastest propagation mode of the shortest section.

Therefore, as the number of intermediate sections increases, Δt must be decreased accordingly. When the segmented line is part of a larger system, this reduction is usually not justifiable for the rest of the components of the network. This results in an unnecessary (and often prohibitive) increase in computing costs.

This problem is alleviated with the profile routines, because the decrease in Δt is confined to the profile solution only, while the rest of the network can be solved with a larger Δt. When (for a given mode) Δt is larger than the travel time of the smallest section, the internal time step $\Delta t'$ is automatically set equal to τ. If larger accuracy is desired, the profile routines provide the option to decrease $\Delta t'$ to $\Delta t'/m$, where m is an integer number supplied by the user (see appendix I-C).

2.3 Approximation of $A_1(\omega)$

The rational-functions approximation of $A_1(\omega)$ can be obtained with very high accuracy over the frequency range of interest in transient studies. However, with the best approximations attainable with the approximating routines presently available at UBC(*), peak errors of 0.5% are not uncommon for values of $|A_1(\omega)|$ between 1.0 and 0.1 (higher errors in the region where $|A_1(\omega)| < 0.1$ are not significant in most applications).

These errors tend to accumulate when the line is segmented. Suppose, for example, that a 500 km line is segmented into 10 sections. Let $|A_1(\omega_o)|_{50}$ and $|A_1(\omega_o)|_{500}$ be the actual magnitudes of $A_1(\omega)$ at $\omega = \omega_o$ for a 50 km and 500 km line, respectively.

$$|A_1(\omega_o)|_{50} = 0.980$$

$$|A_1(\omega_o)|_{500} = 0.81707$$

Let us now suppose that the approximation of $|A_1(\omega_o)|_{50}$ is off by 0.51% at $\omega = \omega_o$;

$$|A_1'(\omega_o)|_{50} = 0.985$$

If we calculate $|A_1'(\omega_o)|_{500}$ from $|A_1'(\omega_o)|_{50}$ we obtain,

$$|A_1'(\omega_o)|_{500} = [|A_1(\omega_o)|_{50}]^{10} = 0.85973$$

Comparing $|A_1'(\omega_o)|_{500}$ with $|A_1(\omega_o)|_{500}$ we can see that an error of 0.51% in the approximation of the 50 km segment, yields an error of 5.22% in the estimated value of $|A_1(\omega_o)|_{500}$.

(*) Jose R. Marti has been working (at the time this thesis is being written) on more refined versions of the approximating routines available at UBC. Preliminary results have been encouraging, and the new routines can be expected to yield even more accurate approximations in the near future.

The preceding example illustrates how the errors in the approximation of $A_1(\omega)$ accumulate when several lines are connected in cascade. Note that the error increases with the number of sections, as the error of one section is transmitted to the next.

This is an unavoidable source of error in any calculation involving line sectioning. The model developed in Chapter 1 is also affected by the quality of the approximation of $A_1(\omega)$, but to a lesser extent than the external segmentation procedure. Since the evaluation of the convolutions $a_1(t)*b_{k,j}(t)$ and $a_1(t)*b_{m,j}(t)$ start at opposite ends of the line, (see section 1.2) the error does not accumulate at one end only, but it is averaged along the line. This can be more easily visualized in the frequency domain from equations (1.18) and (1.19)

$$B_{m,j} = A_1 B_{m,j-1} \qquad (j=2,\ldots,n)$$

$$B_{k,j} = A_1 B_{k,j+1} \qquad (j=1,\ldots,n-1)$$

Suppose that the line has 10 intermediate nodes. Starting from node k,

$$B_{m,1} = A_1 F_k$$

$$B_{m,2} = A_1 B_{m,1} = A_1^2 F_k$$

$$B_{m,3} = A_1 B_{m,2} = A_1^3 F_k$$

$$\vdots$$

$$B_{m,10} = A_1 B_{m,9} = A_1^{10} F_k$$

Starting from node m,

$$B_{k,10} = A_1 F_m$$

$$B_{k,9} = A_1 B_{k,10} = A_1^2 F_m$$

$$B_{k,8} = A_1 B_{k,9} = A_1^3 F_m$$

$$\vdots$$

$$B_{k,1} = A_1 B_{k,2} = A_1^{10} F_m$$

It can then be seen that, when the error is maximum in $B_{k,j}$, it is minimum in $B_{m,j}$ and viceversa. The result is an approximately constant error level for all sections.

2.4 Animated Motion Picture of Travelling Waves Along the Line

Suppose that the intermediate voltages (or currents) at a given time t are known. If the number of intermediate points is large enough, it is possible to plot these voltages against the length of the line, and obtain a smooth curve, as shown in Figure 2.1

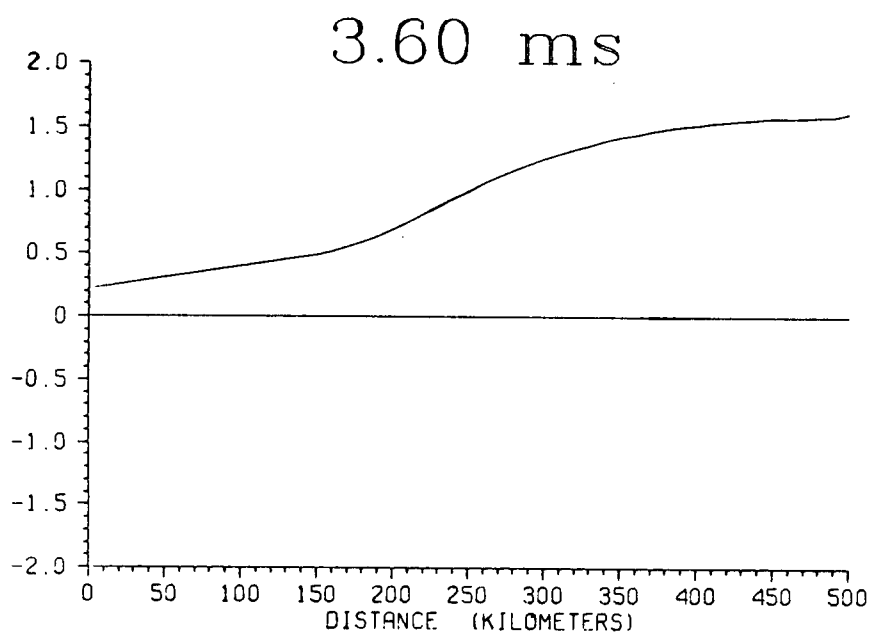

Fig. 2.1: Voltage profile 3.6 ms after the energization of an open ended, single-phase line.

This plot of v(t) vs ℓ can be visualized as a still picture of a voltage wave at time t. If several of these still frames were displayed sequentially, for increasing values of t, the effect of "a moving wave" could then be created.

To demonstrate the possibilities of this procedure as a teaching tool, an animated movie of travelling waves along a transmission line was produced as part of this project.

For the generation of this movie, the line from John Day to Lower Monumental of the Bonneville Power Administration (BPA) was used as an example. To demonstrate the behaviour of the different propagation modes, the line was assumed to be single-phase, either with zero or positive sequence parameters. Several transient situations were simulated on the line, and voltages and currents were obtained at 49 intermediate points (51 points per time step after including the end points).

These voltages and currents were plotted against the line length (as shown in Figure 2.1) at every time step on the IBM 3279 colour terminal, and photographed with a 16 mm movie camera. The number of exposures per plot was co-ordinated with the time step of the transient simulation to create a relatively smooth motion at a projection speed of 18 frames per second.

The result is a movie (13 min. long), in which transient phenomena are seen as waves propagating on a line (*).

Figure 2.2 shows a few selected frames extracted from the movie. The situation simulated in this case was the injection of a unit voltage pulse of 0.5 ms duration into the 500 km line, with the receiving end open. Positive sequence parameters were used in this particular case.

This movie permits a visualization of the transient phenomena in a way which is very difficult to obtain from the usual plots (voltage or current vs time at any fixed point on the line). The possibilities as a teaching aid are considerable, and the benefits as an analysis tool cannot be lightly disregarded.

(*) Copies of this movie can be borrowed by contacting Dr. H.W. Dommel in the Department of Electrical Engineering at UBC.

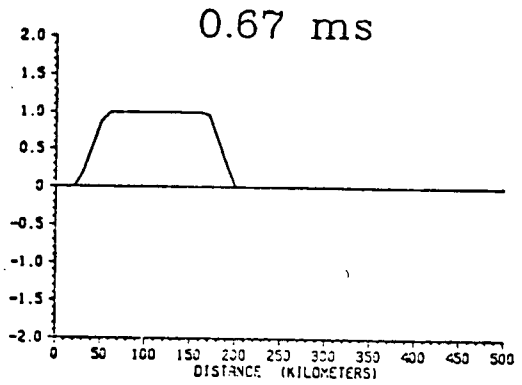

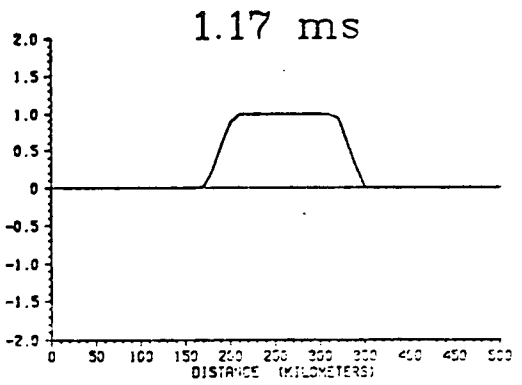

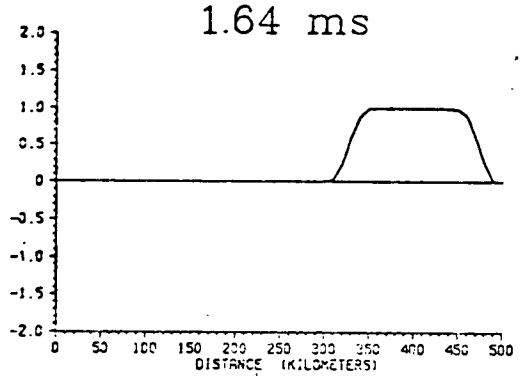

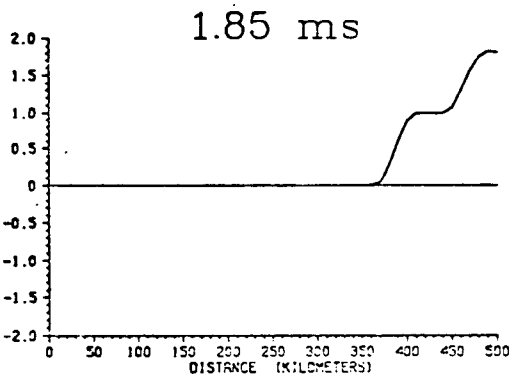

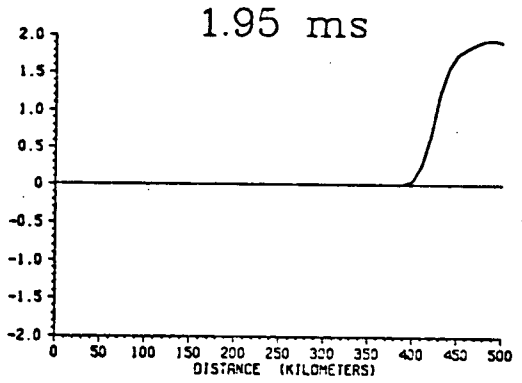

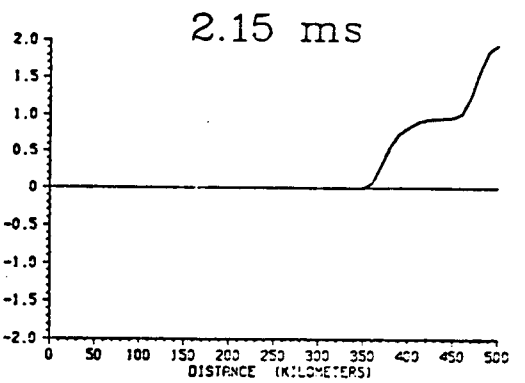

Fig. 2.2: Selected frames from the Travelling Waves Movie.

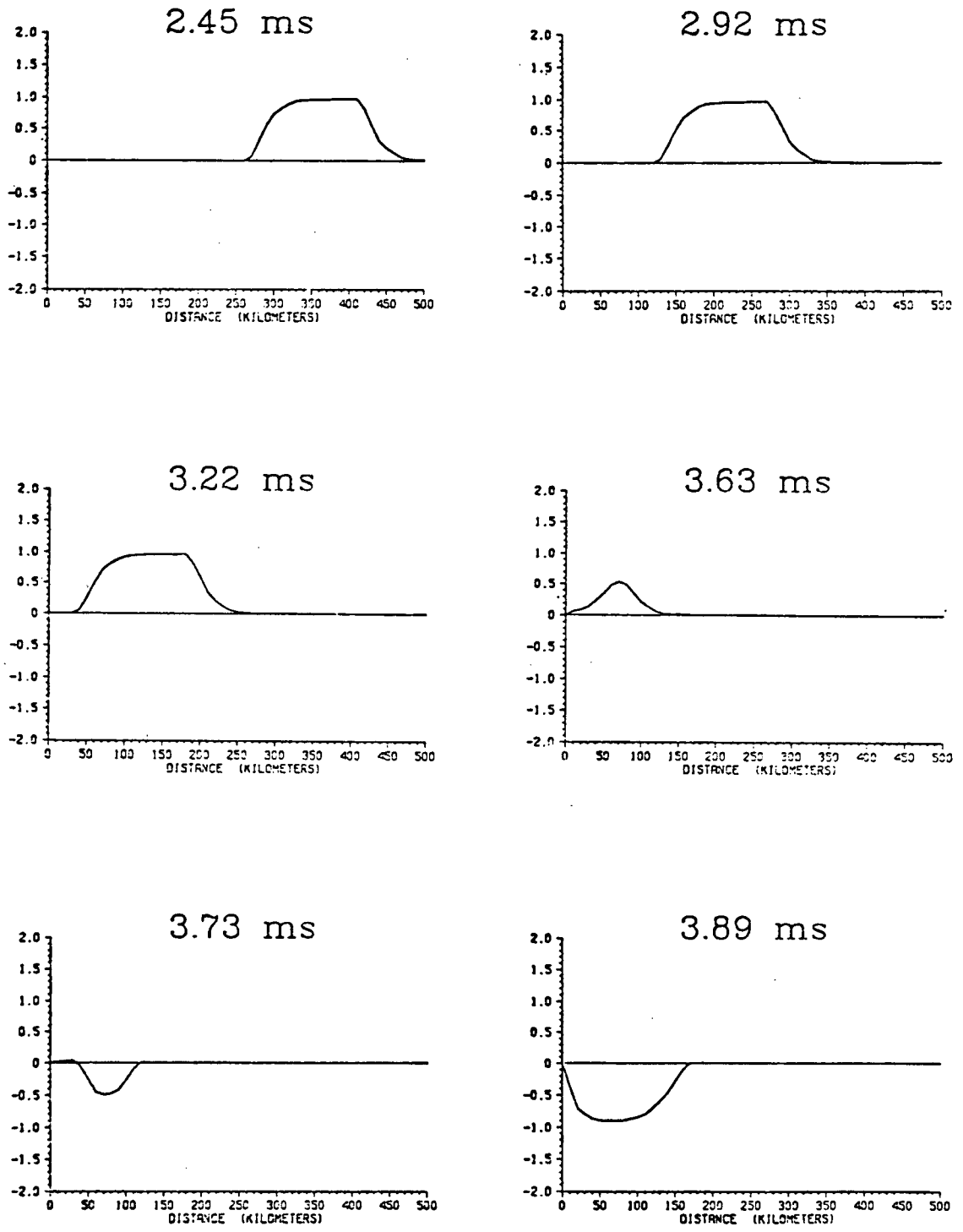

Fig. 2.2: (continuation)

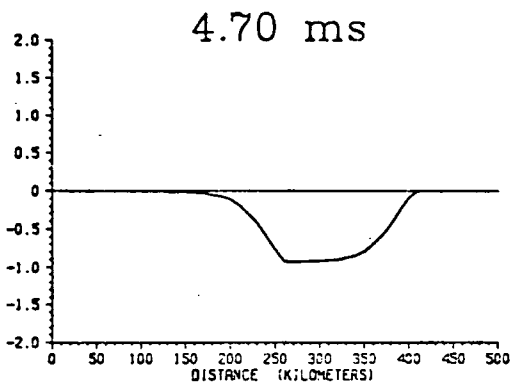

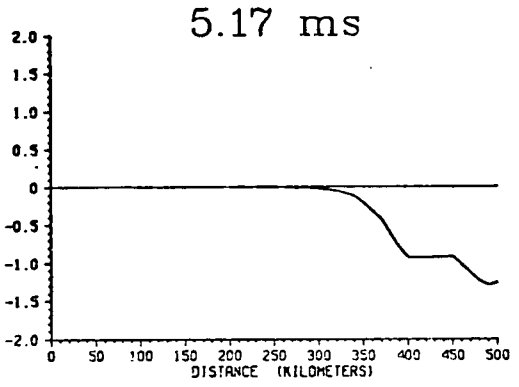

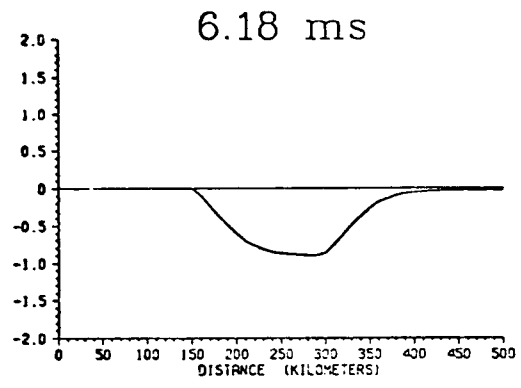

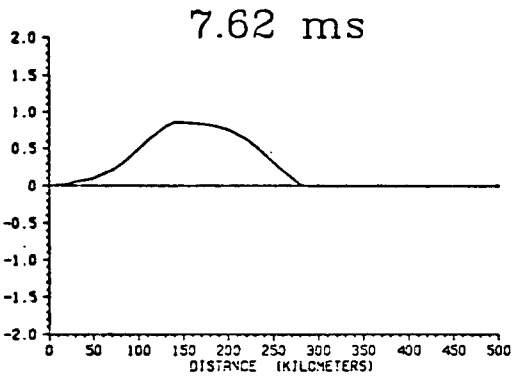

Fig. 2.2: (continuation)

For example, when a voltage limiting device such as a lightning arrester is connected to the end of the line, it is sometimes erroneously assumed that the voltages along the line will not exceed the voltage determined by the characteristic of the lightning arrester. To prove this assumption wrong, it is sufficient to segment the line and to observe some of the intermediate overvoltages. However, when the voltage wave is seen reflecting back and forth along the line, the interpretation of the phenomena becomes much simpler.

An animated movie can obviously not be produced every time a transient simulation is performed, but such movies can be made for selected cases for teaching purposes. The best solution for routine visualization of power transients would be to display the wave motion on a suitable graphics terminal.

At the time this thesis is being written, some work is being done in this direction in the Department of Electrical Engineering at UBC, using the Megatek 4000, fast-refresh, graphic station. It can therefore be expected that in the near future, routine examination of wave motion will become possible after the execution of a transient simulation.

CHAPTER 3

NUMERICAL RESULTS

3.1 Introduction

The results from a series of tests and comparisons will be shown in this chapter in order to assess the performance of the profile model. In these tests the parameters of a typical 500 KV line will be used (i.e., BPA's John Day to Lower Monumental transmission line). The length of the line is assumed to be 500 km. The tower configuration is shown in Figure 3.1, and the physical characteristics of the conductors are listed below:

a) Phase conductors

dc resistance = 0.032405 Ω/km

tube thickness/outside diameter = 0.3636

(stranded conductor is approximated as a tube, with the effects of the steel core ignored)

diameter = 4.0691 cm

b) Ground wires (assumed to be semented or "T-connected" (*))

dc resistance = 1.6218 Ω/km

tube thickness/outside diameter = 0.5

diameter = 0.98044 cm

(*) Grounded at one tower, and insulated, as well as series interrupted at the adjacent towers. This arrangement provides electrostatic shielding (ground wires considered in capacitance calculations), but eliminates circulating currents (ground wires ignored in impedance calculations).

c) Ground resistivity = 100 Ω-m

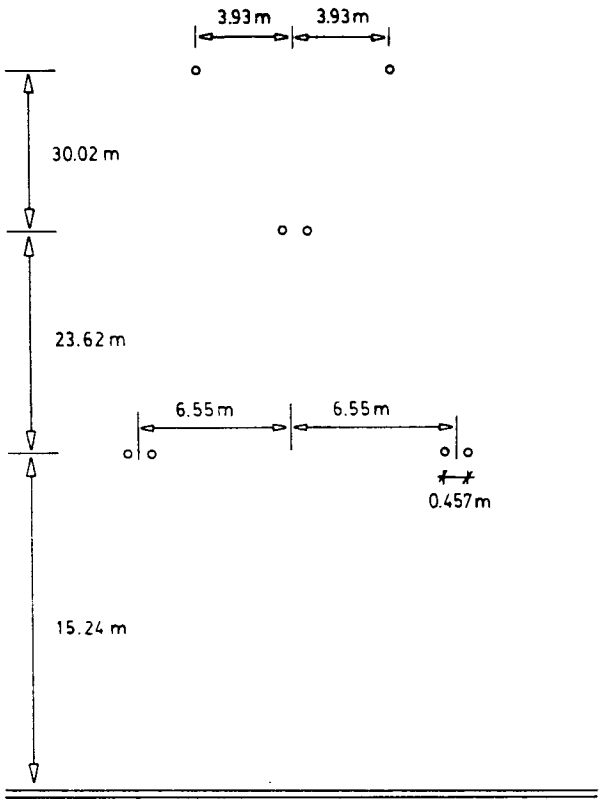

Fig. 3.1: Tower configuration of BPA's John Day to Lower Monumental 500 KV transmission line. Height shown is average height above ground.

3.2 Truncation and Segmentation Effects

The two major sources of error in the calculation of intermediate voltages and currents are the truncation errors due to linear interpolation in the forward travelling functions (caused when $\tau/\Delta t$ is not an integer number), and the segmentation errors caused by the accumulation of errors from the solution of one section to the next.

These two effects will be illustrated in this section. For this purpose, a simple energization test will be performed, with the receiving end being open (see Figure 3.2)

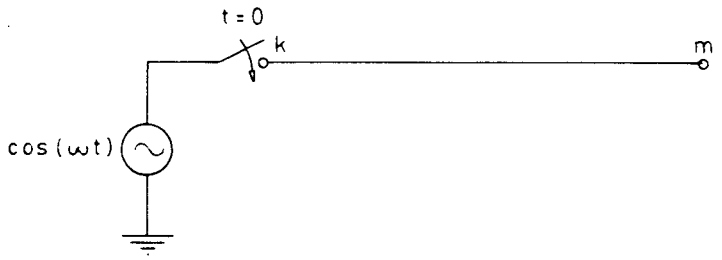

Fig. 3.2: Energization test.

The line will be assumed to be single-phase with positive sequence parameters. The length of the line is 500 km, and 10 sections or 9 intermediate nodes will be considered.

In order to isolate truncation from segmentation effects, for the first set of tests the time step Δt has been chosen to be exactly 1/20th of the travel time; this implies that $\Delta t = \tau_{50}/2$ (where τ_{50} is the travel time for a 50 km section), and that no truncation errors will be present in the results.

It was mentioned in Chapter 2 that the main source of segmentation errors is the approximation of the propagation function for each line segment (50 km in this case). Graph 1.1 shows the error function of the rational-functions approximation of $|A_1(\omega)|_{50}$ and $|A_1(\omega)|_{500}$ (with the output from the line constants program being used as the reference), for values of $|A_1(\omega)|$ between 1.0 and 0.1. Lower values of $|A_1(\omega)|$ are not significant for the purposes of this project.

Graph 1.2 shows the error function for $[|A_1(\omega)|_{50}]^{10}$ compared to the rational-functions approximation of $|A_1(\omega)|_{500}$). The travel time for the 500 km line is 1.6798 ms, while τ_{50} is 1.679 ms. The difference between $10.\tau_{50}$ and τ_{500} is very small in this case (approximately -0.074%).

Graph 1.3 shows the receiving end voltage when the line is externally segmented (compared to the unsegmented line).

The assessment of the accuracy of the profile model presents a practical difficulty because it is not clear what reference or accurate results should be used for comparison purposes. If only single-frequency signals were injected into the line, an exact theoretical response could be obtained using the solution of the line equations in the frequency domain (see appendix I-A). However, this would be a rather impractical and time consuming process. A simpler alternative (although not as accurate) would be to use only two line segments and adjust the respective lengths to the intermediate point of interest. This should give a reasonably accurate reference model, assuming that the partitioning of the line into two segments does not introduce significant errors. In the following simulations such two-segment models will be used as a reference for comparison purposes.

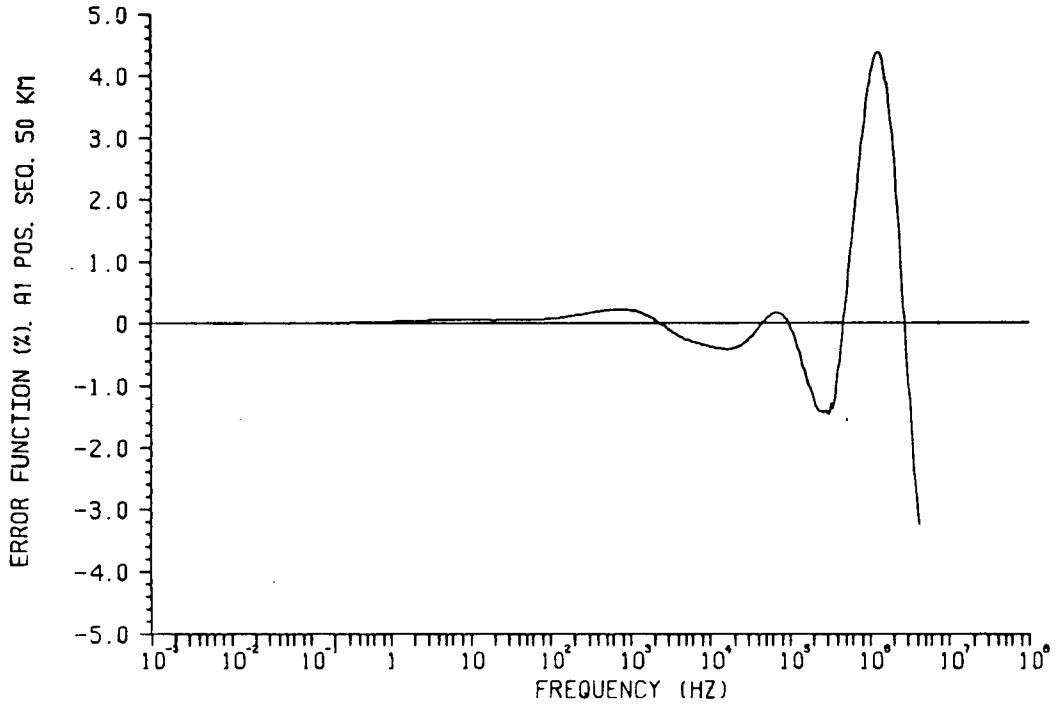

(a)

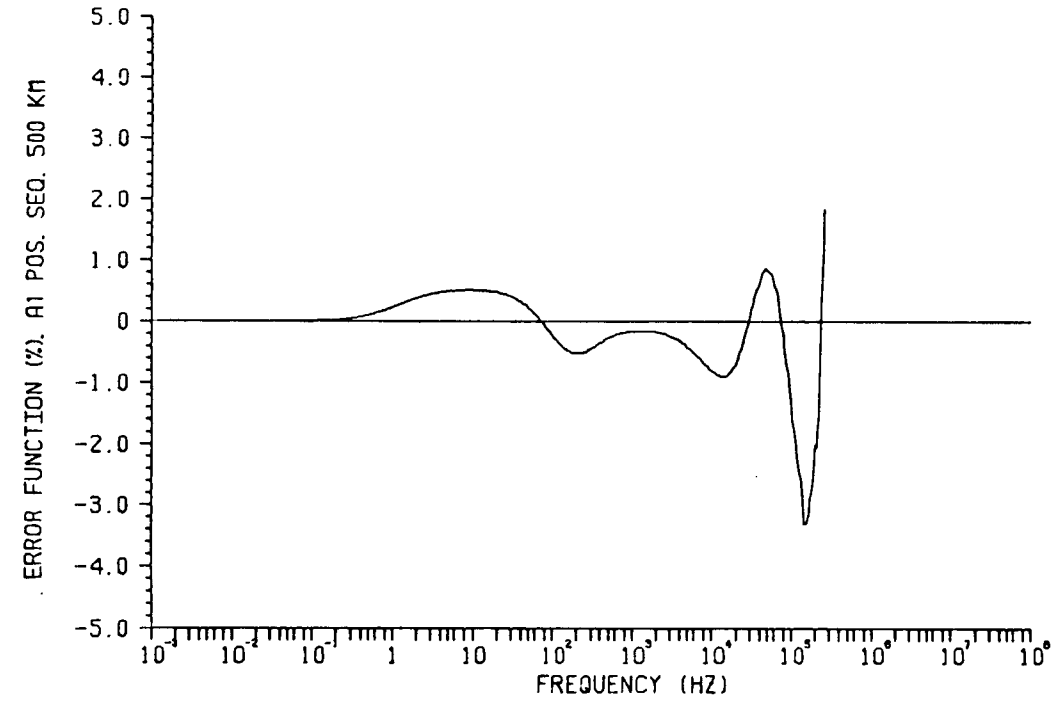

(b)

Graph 1.1: Error functions for the magnitudes of $|A_1(\omega)|$.
(a) 50 km. (b) 500 km.

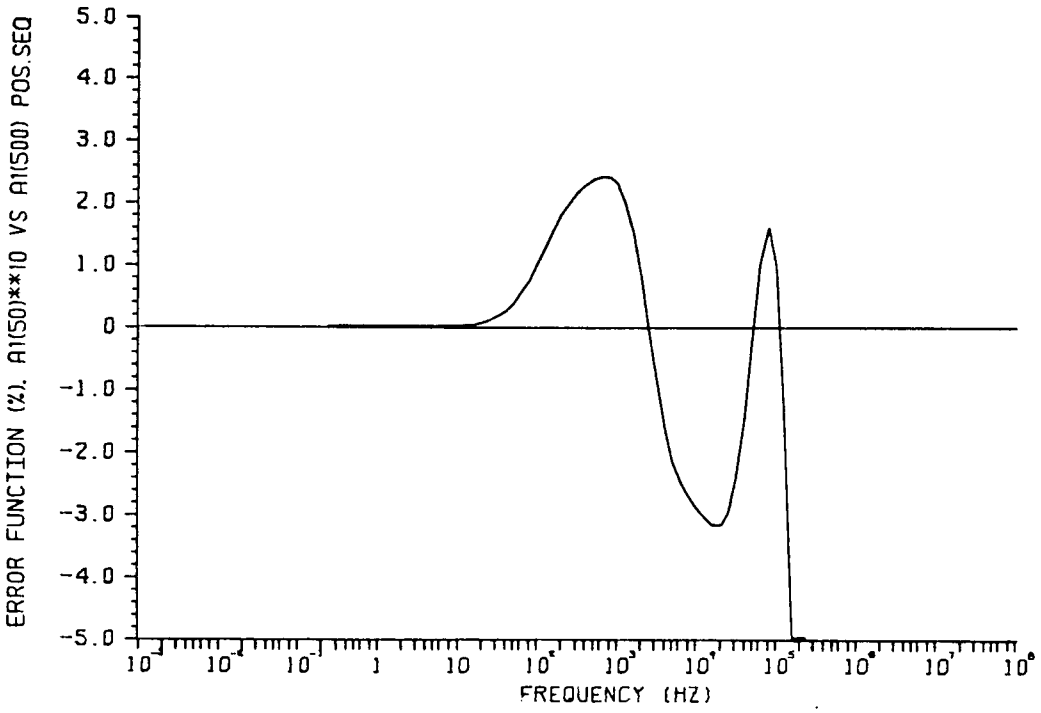

Graph 1.2: Error function of $|A_1(\omega)|_{500}$ estimated from $|A_1(\omega)|_{50}$.

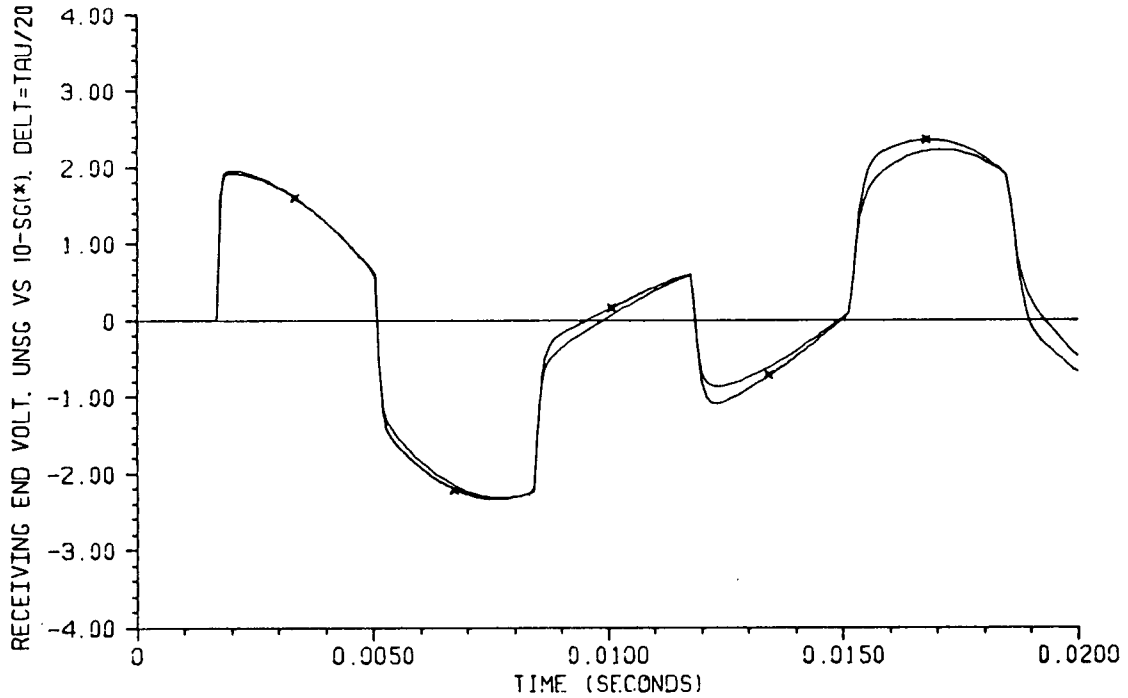

Graph 1.3: Receiving end voltage. Externally segmented vs unsegmented line.

Graphs 1.4 through 1.9 show the voltages at 450, 250, and 50 km from the receiving end, using both the profile and the 10-segment models.

Note that the error in the 10-segment model decreases with the distance from the sending end, while the profile presents a relatively constant error (see section 2.3). Also note that the profile model gives consistently better results than the 10-segment model.

Let us now consider truncation effects. Graph 1.10 shows the effect (on the unsegmented line) of using a time step that is not a submultiple of the travel time (in this case Δt = 0.1 ms, that is, $\tau_{50}/\Delta t$ = 1.68). The differences are not very large for the unsegmented line, but when the line is segmented into 10 sections the error is considerably larger (see Graph 1.11).

The profile model is not very sensitive to the external Δt; as a matter of fact it is only affected to the same extent the unsegmented line is affected (see Graphs 1.12 and 1.10; these graphs suggest that the truncation errors were introduced by the solution of the unsegmented line and not by the profile model). Graph 1.14, further illustrates that even when the external Δt is not a submultiple of τ (as it occurs in three-phase cases) the profile model performs adequately.

The running costs for the previous test are shown in Table 3.1 (based on UBC's rates of $1200 per hour of CPU time)

Number of variables requested in output	10 segments	Profile Model		
	(cc $)	Main Program (cc $)	Output Processing (cc $)	Total (cc $)
1	0.67	0.68	0.08	0.74
9	0.76	0.68	0.10	0.78
18	0.86	0.68	0.18	0.86

Table 3.1: Computing costs for the single-phase energization test.

Note that the profile calculations were only performed once (see appendix I-C) and all the voltages and currents were stored (written in free format) in an intermediate file. The desired amount of intermediate variables are read from this file and written in a manageable form with the aid of a post-processing program. Also note, that in the segmented case, a complete simulation has to be made every time the requested output changes. Also in the segmented case, the identification (and manipulation for later plotting) of the output variables becomes difficult (at best) when more than 10 variables are printed in the same run. When the number of lines (or branches) increases, the profile calculations are comparatively faster and the post-processing of the output almost becomes a necessity. The running costs for a two-phase, 10-section case are shown in Table 3.2 below.

Number of variables requested in output	10 segments (cc $)	Profile Model		
		Main Program (cc $)	Output Processing (cc $)	Total (cc $)
18	0.90	0.70	0.10	0.80
36	1.00	0.70	0.15	0.85

Table 3.2: Running costs for the energization of a two-phase line with 9 intermediate nodes.

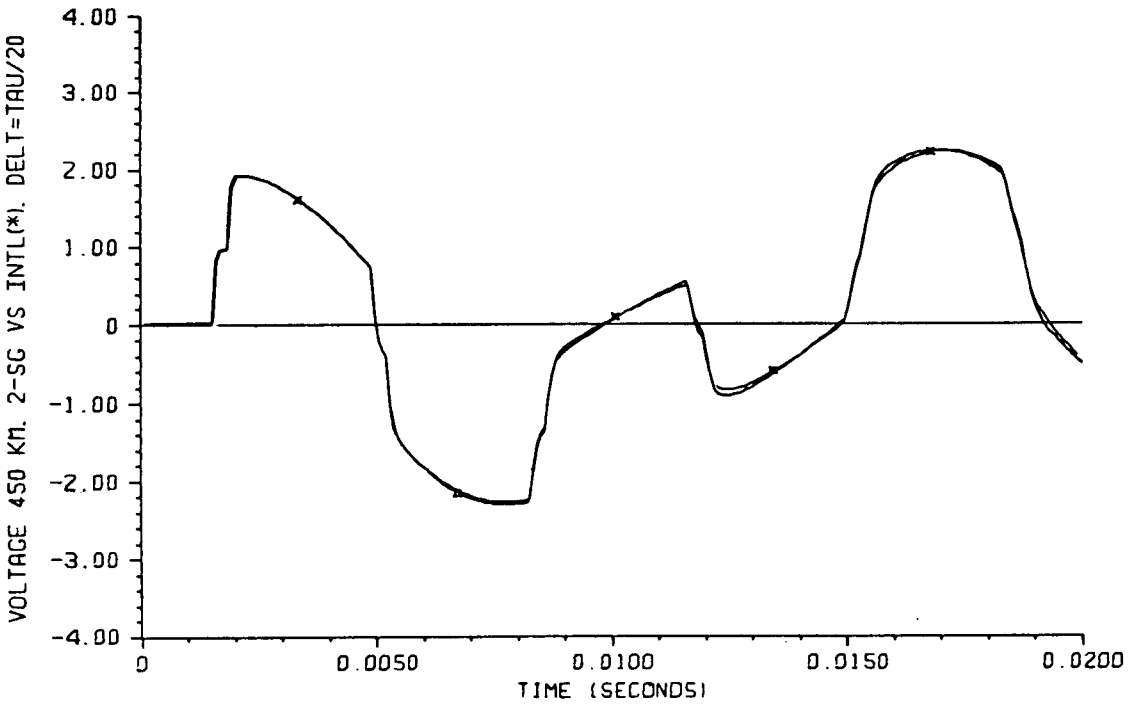

Graph 1.4: Voltage at 450 km from the sending end.
Two segments vs profile model; $\Delta t = \tau/20$.

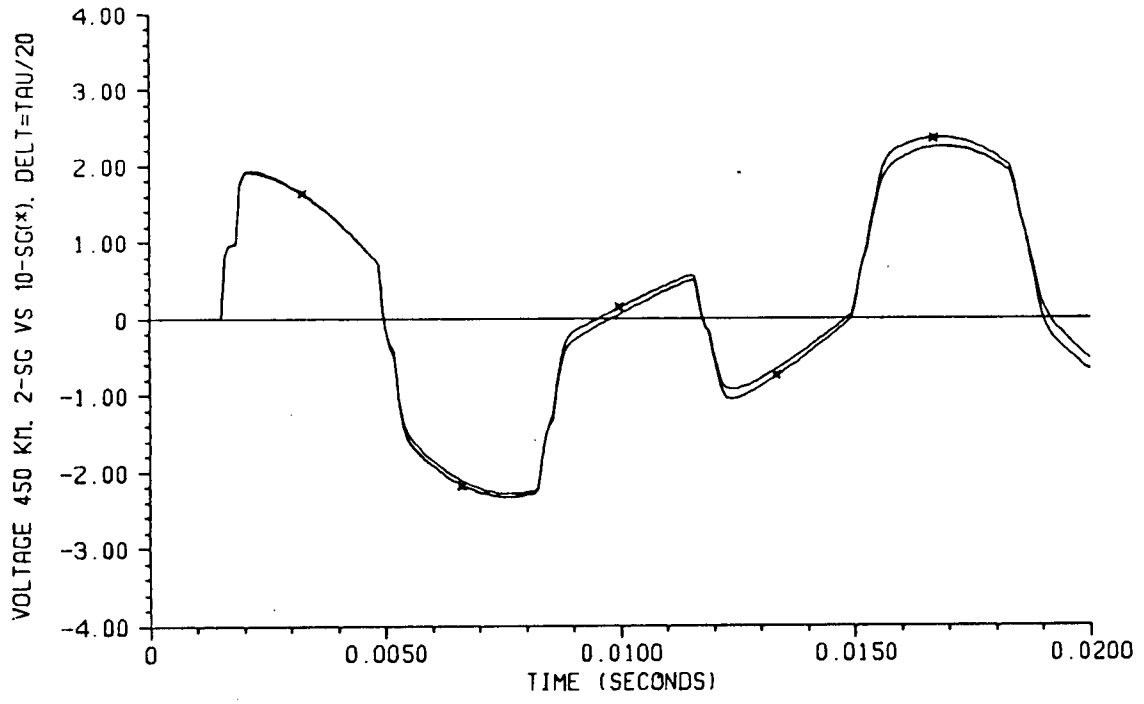

Graph 1.5: Voltage at 450 km from the sending end.
Two segments vs 10 segments; $\Delta t = \tau/20$.

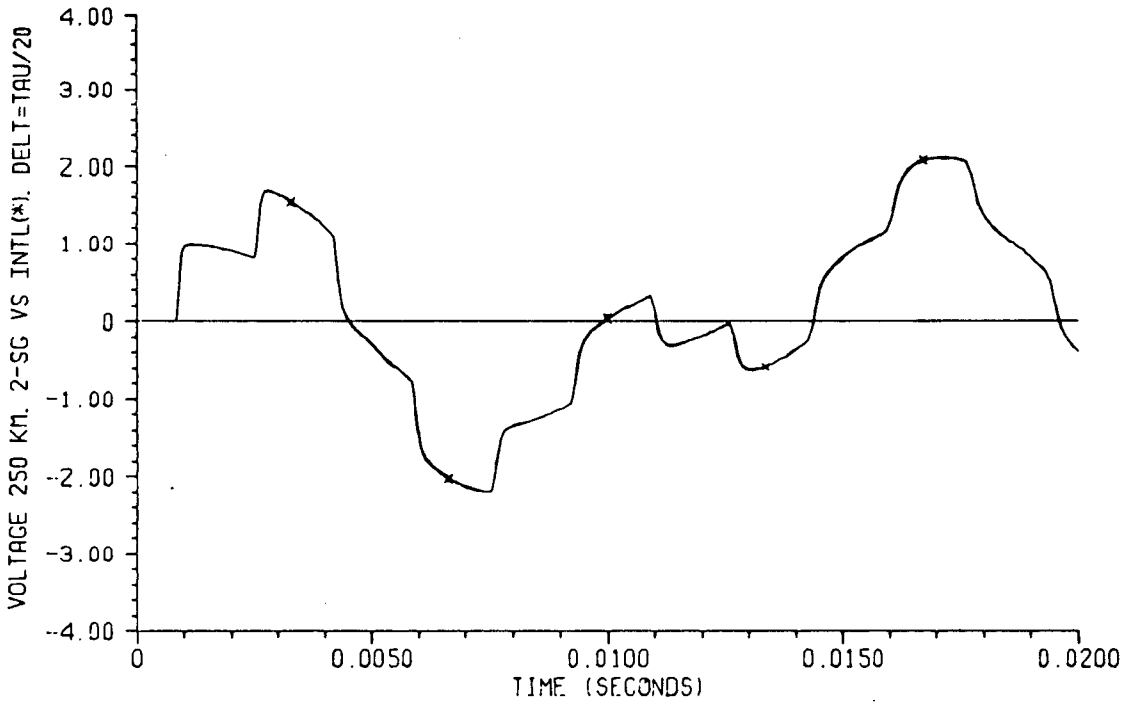

Graph 1.6: Voltage at 250 km from the sending end.
Two segments vs profile model; $\Delta t = \tau/20$.

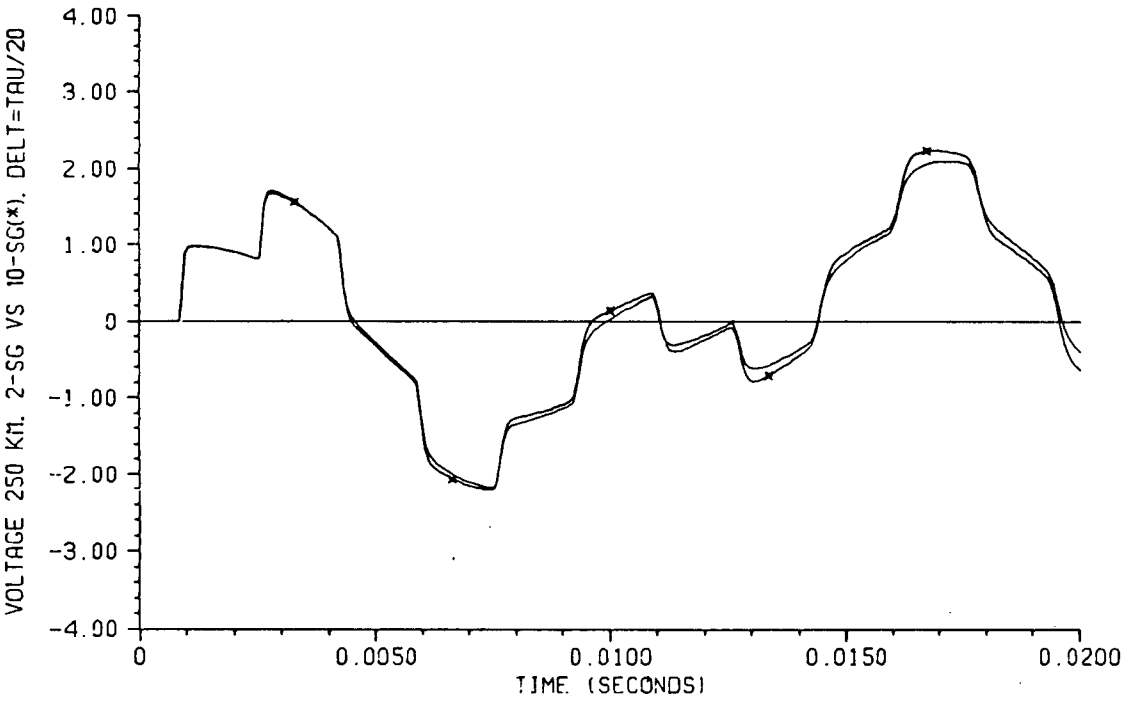

Graph 1.7: Voltage at 250 km from the sending end.
Two segments vs 10 segments; $\Delta t = \tau/20$.

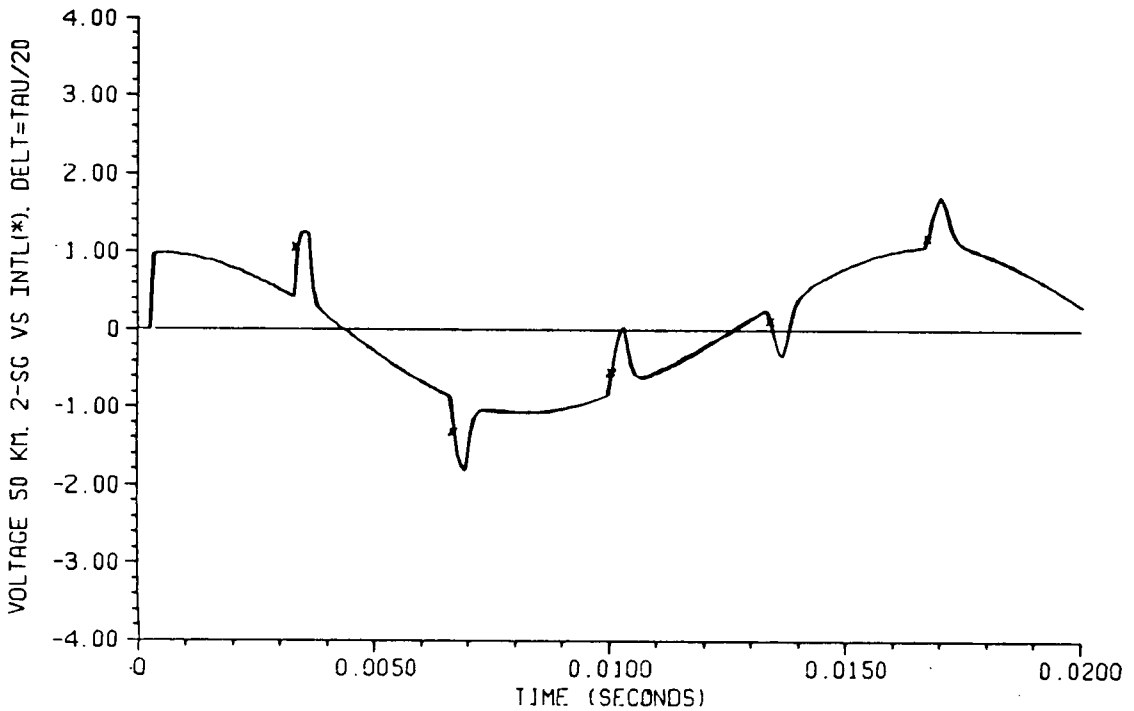

Graph 1.8: Voltage at 50 km from the sending end.
Two segments vs profile model; $\Delta t = \tau/20$.

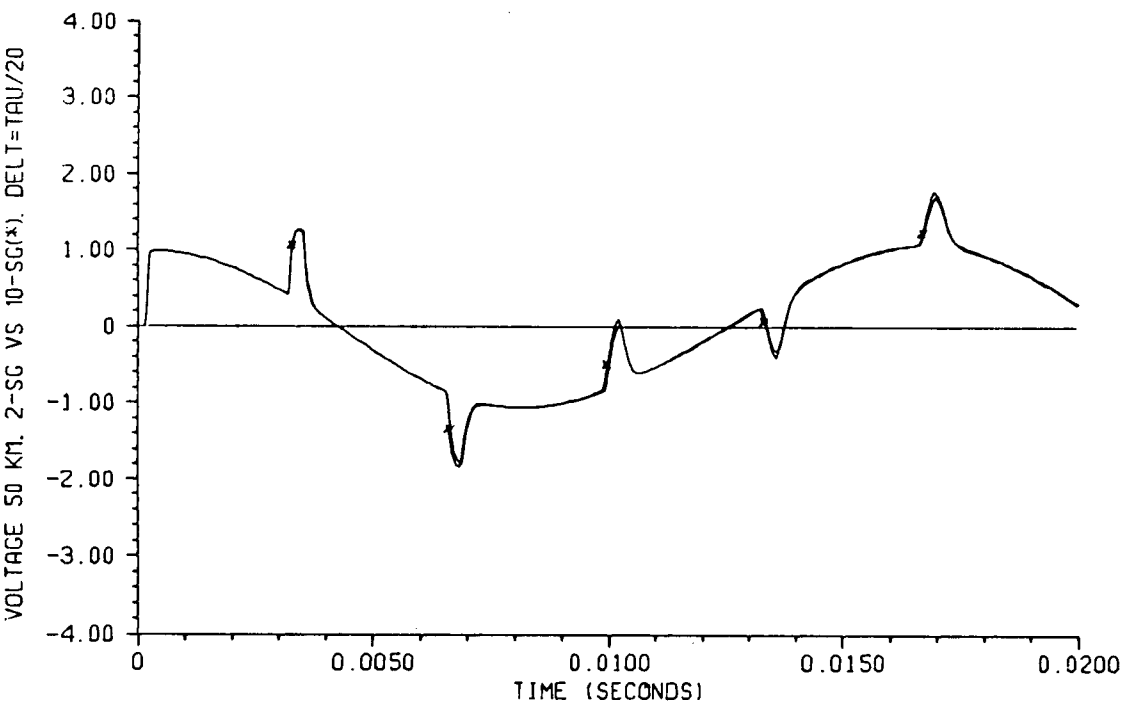

Graph 1.9: Voltage at 50 km from the sending end.
Two segments vs 10 segments; $\Delta t = \tau/20$.

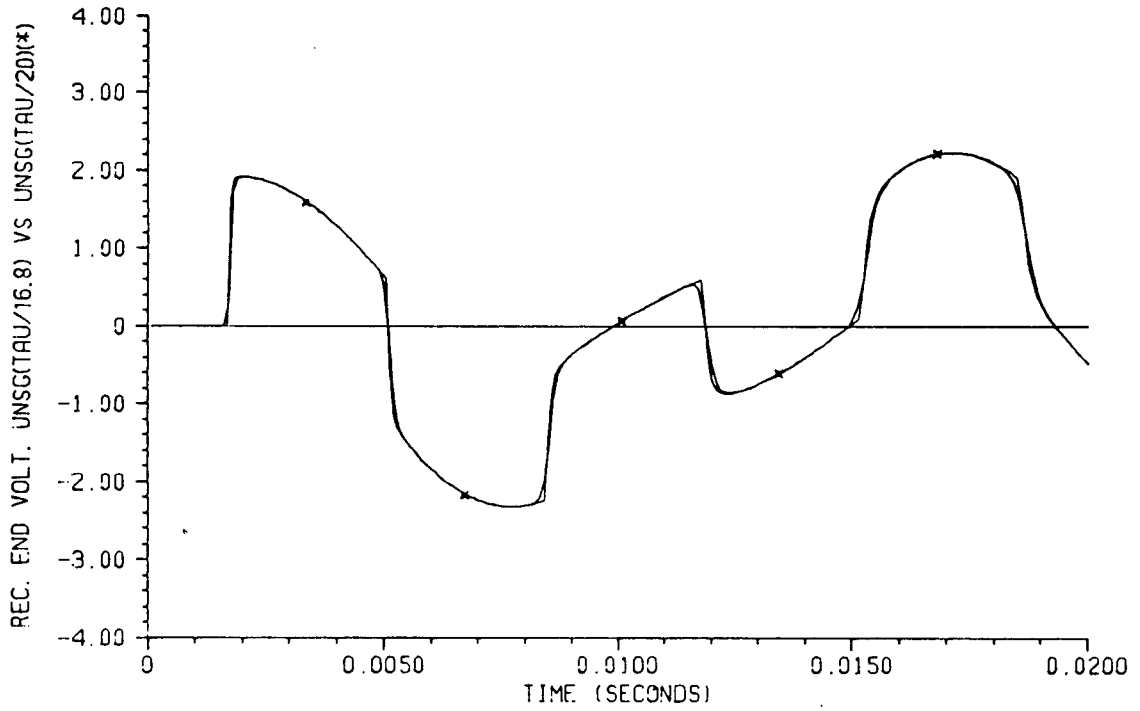

Graph 1.10: Receiving end voltage, unsegmented line.
$\Delta t = \tau/20$ vs $\Delta t = \tau/16.8$.

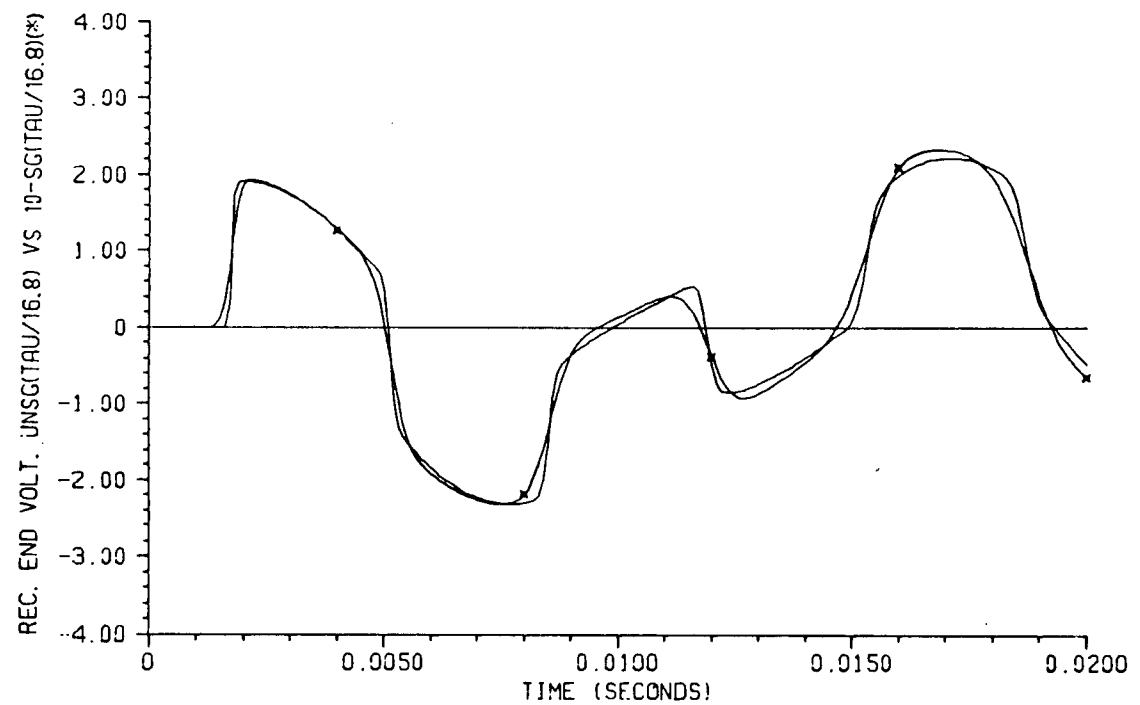

Graph 1.11: Receiving end voltage, 10 segments
vs unsegmented line ($\tau=\Delta t/16.8$).

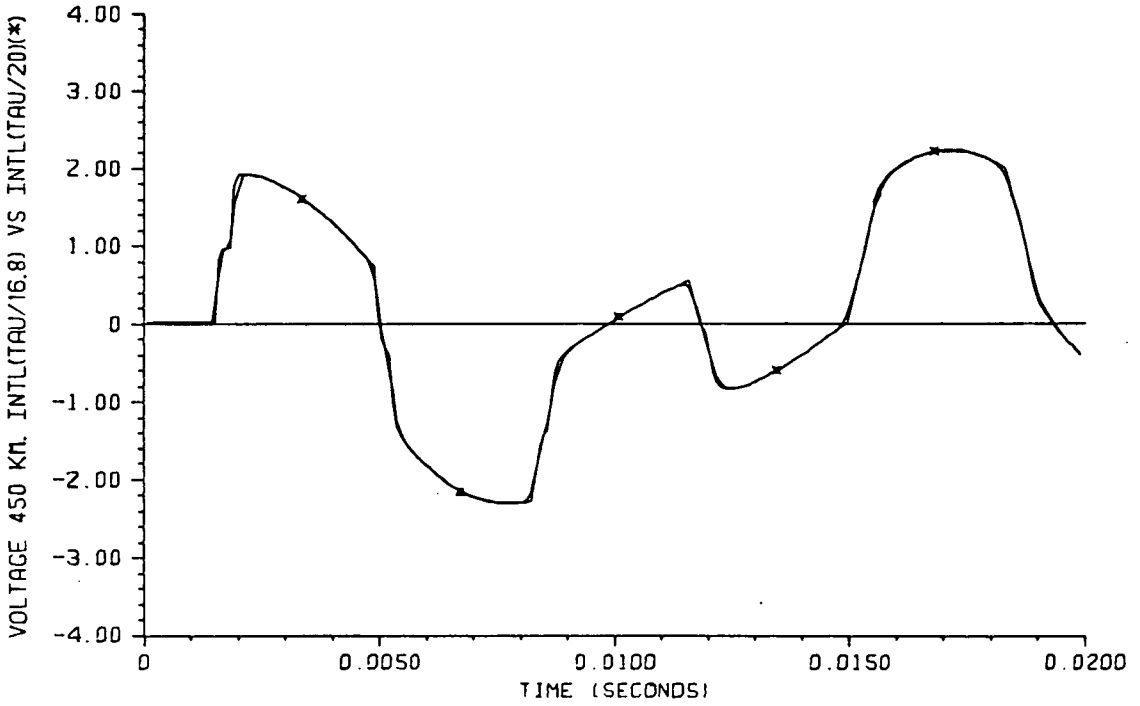

Graph 1.12: Voltage at 450 km from the sending end, profile model. $\Delta t = \tau/20$ vs $\Delta t = \tau/16.8$

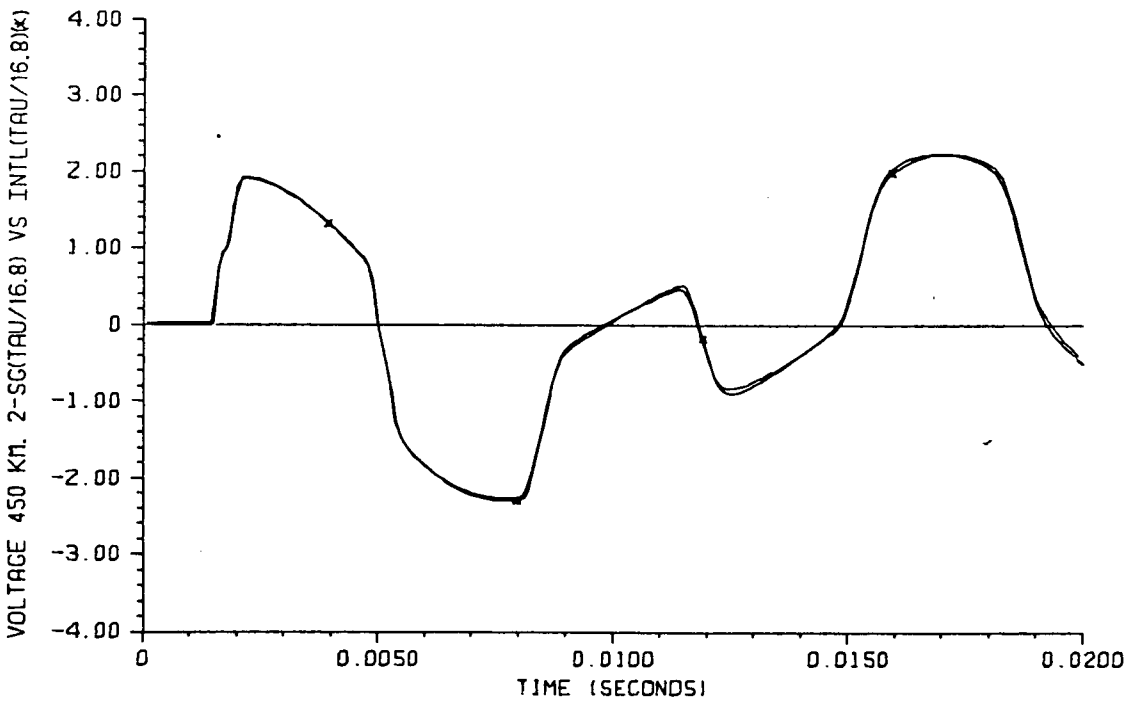

Graph 1.13: Voltage at 450 km from the sending end. Two segments vs profile model. $\Delta t = \tau/16.8$

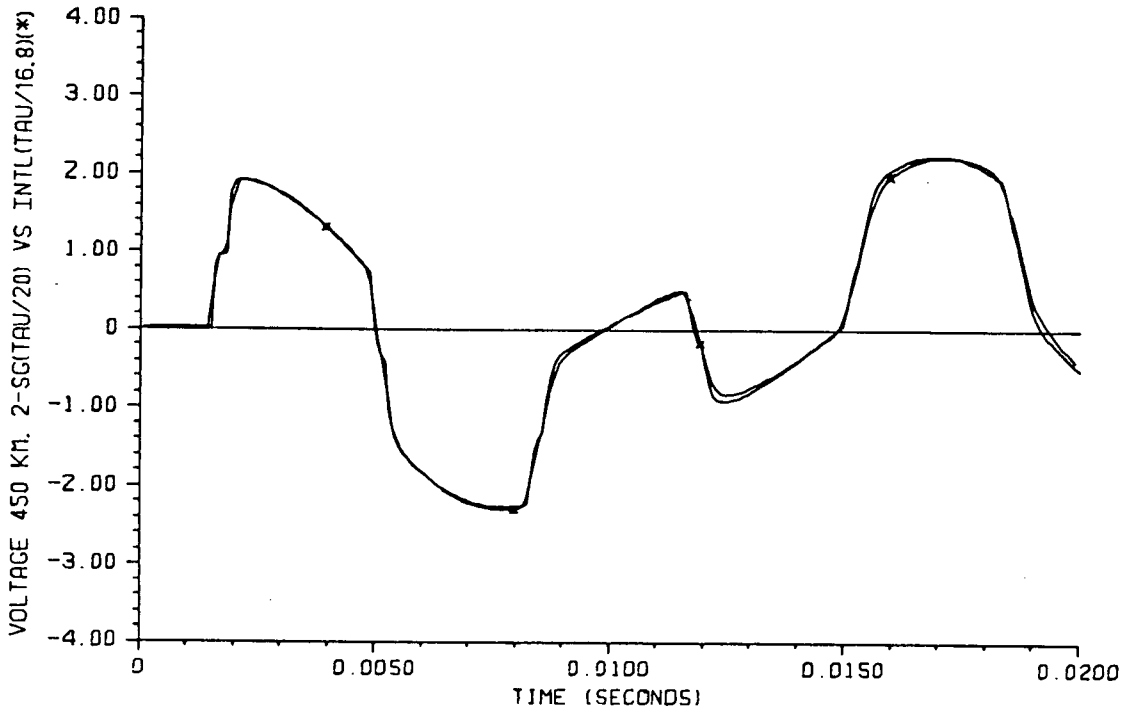

Graph 1.14: Voltage at 450 km from the sending end.
Two segments ($\Delta t = \tau/20$) vs profile model ($\Delta t = \tau/16.8$).

3.3 Energization of a Line Terminated With a Lightning Arrester

Occasionally, the information at the end points of the line gives insufficient insight into the overall performance of the line.

For example, it is sometimes assumed that the overvoltages at the receiving end are larger than at any intermediate point along the line. This is true as long as all the components in the system are linear. When a non-linear, voltage-limiting device such as a lightning arrester is connected at the end of the line, the voltages at the intermediate points can be substantially higher, and in some lines with little insulation margin, flashover at some intermediate towers could occur.

In this section, a situation where intermediate voltages are higher than the receiving end voltages will be simulated.

Consider the circuit shown in Figure 3.3

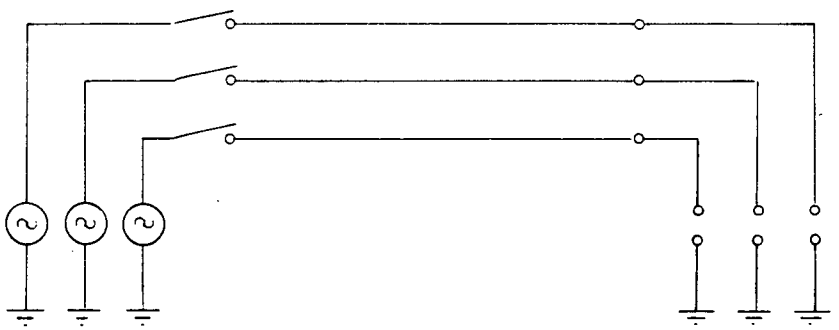

Fig. 3.3: Simulation of a three-phase line terminated with lightning arresters.

The simplified model used for the lightning arresters is shown in Figure 3.4

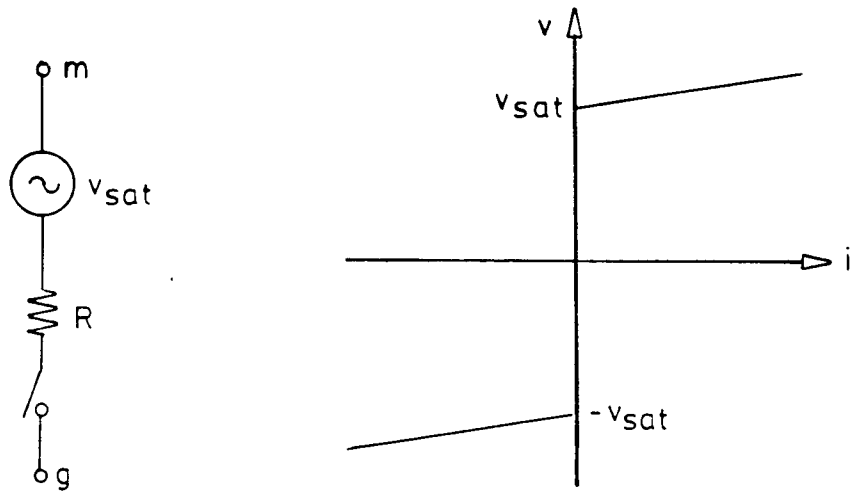

Figure 3.4: Lightning arrester model. (a) Equivalent circuit. (b) v-i characteristic.

The voltage-controlled switch of figure 3.4 (a) closes when the absolute value of the receiving end voltage exceeds v_{sat}, and opens again as soon as the current goes through zero.

For this test, the parameters of the lightning arrester were chosen so that under normal switching operations, without trapped charge, the overvoltages were below v_{sat} (i.e., v_{sat} = 2.6 p.u.). The voltage sources in Figure 3.3 were set to 1.0 p.u. (peak) and the slope of the arrester's characteristic (for $v>v_{sat}$) dv/di = 1.0 Ω; the line simulated is BPA's John Day to Lower Monumental for a length of 500 km.

Graph 1.15 shows the profile of maximum overvoltages (absolute values) when there is no trapped charge prior to line energization.

Graphs 1.16 to 1.18 show the receiving end voltages. Note that in this case the maximum overvoltage at the receiving end is larger than at any point along the line.

When the worst condition for trapped charge is simulated, the lightning arresters are triggered (see graphs 1.20 to 1.22). In this case the maximum overvoltages at several intermediate points along the line are higher than at the receiving end (see Graph 1.19). These voltages and the times at which they occur are listed in Table 3.3.

Distance from sending end (km)	Phase A		Phase B		Phase C	
	Vmax (p.u.)	Time (ms)	Vmax (p.u.)	Time (ms)	Vmax (p.u.)	Time (ms)
50	-2.38	7.39	1.89	7.12	-2.21	4.03
100	-2.79	7.36	2.05	6.94	-2.36	4.19
150	-2.87	7.53	2.20	6.78	-2.49	4.36
200	-2.92	7.51	2.37	6.60	-2.57	4.53
250	-2.92	7.56	2.51	6.53	-2.60	4.62
300	-2.90	7.40	2.61	6.27	-2.61	4.84
350	-2.84	7.21	2.65	6.10	-2.64	4.99
400	2.80	16.73	2.72	5.93	-2.51	5.15
450	2.74	16.51	2.79	5.75	-2.65	5.30
500	2.73	2.31	2.87	5.59	-2.71	5.38

Table 3.3: Maximum overvoltages with trapped charge prior to line energization.

Graphs 1.23 and 1.24 show the voltages at 50 and 300 km from the sending end when trapped charge is considered.

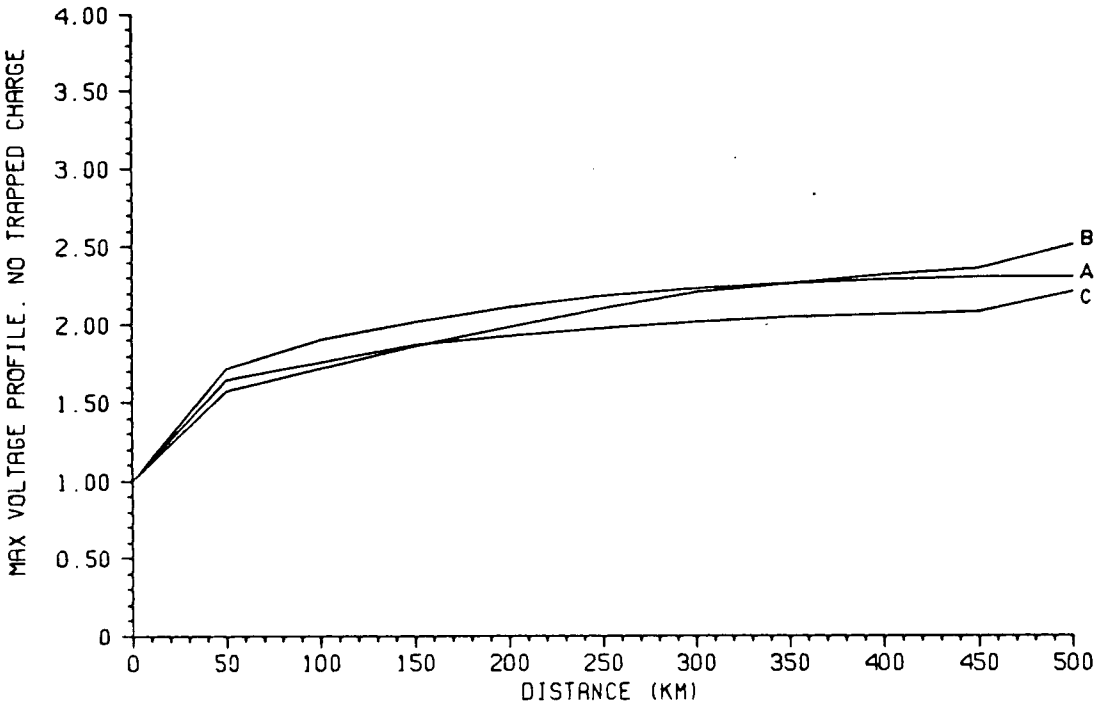

Graph 1.15: Profile of maximum overvoltages (absolute values). No trapped charge.

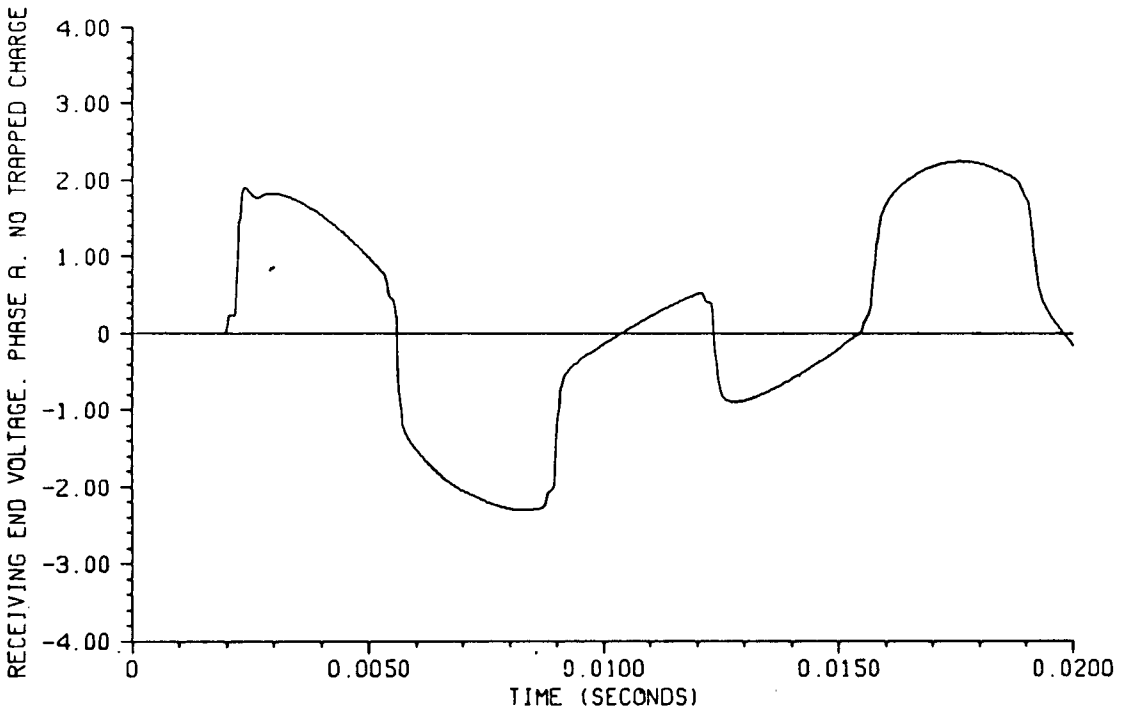

Graph 1.16: Receiving end voltage. Phase A, no trapped charge.

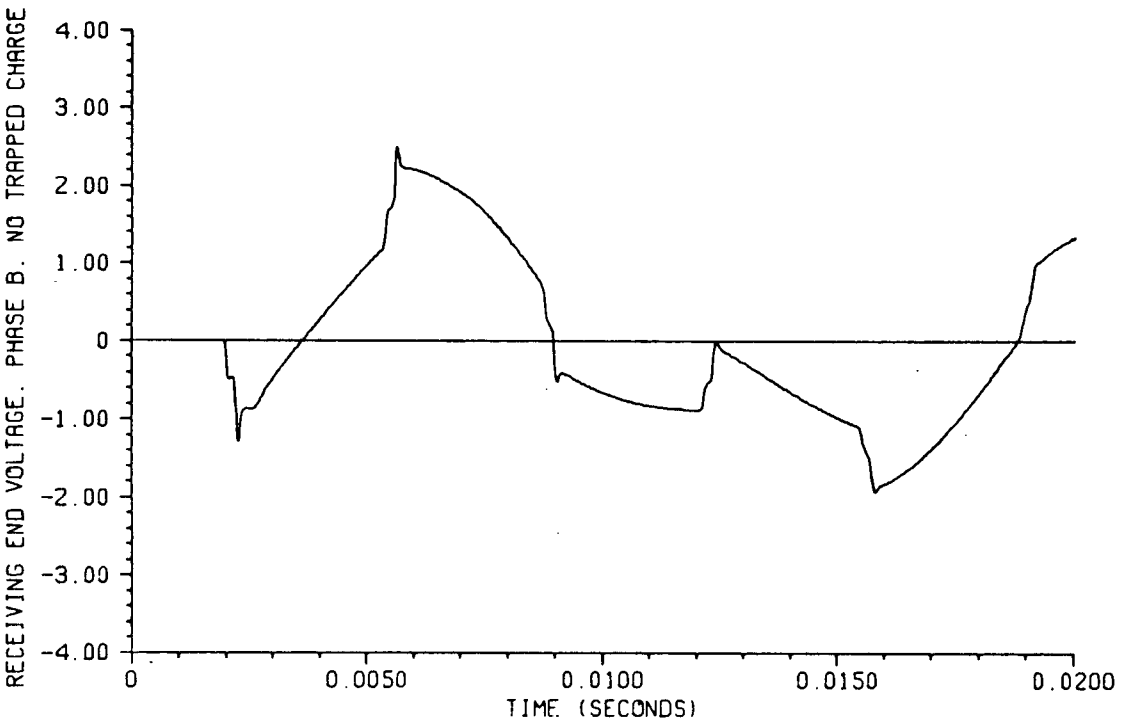

Graph 1.17: Receiving end voltage. Phase B, no trapped charge.

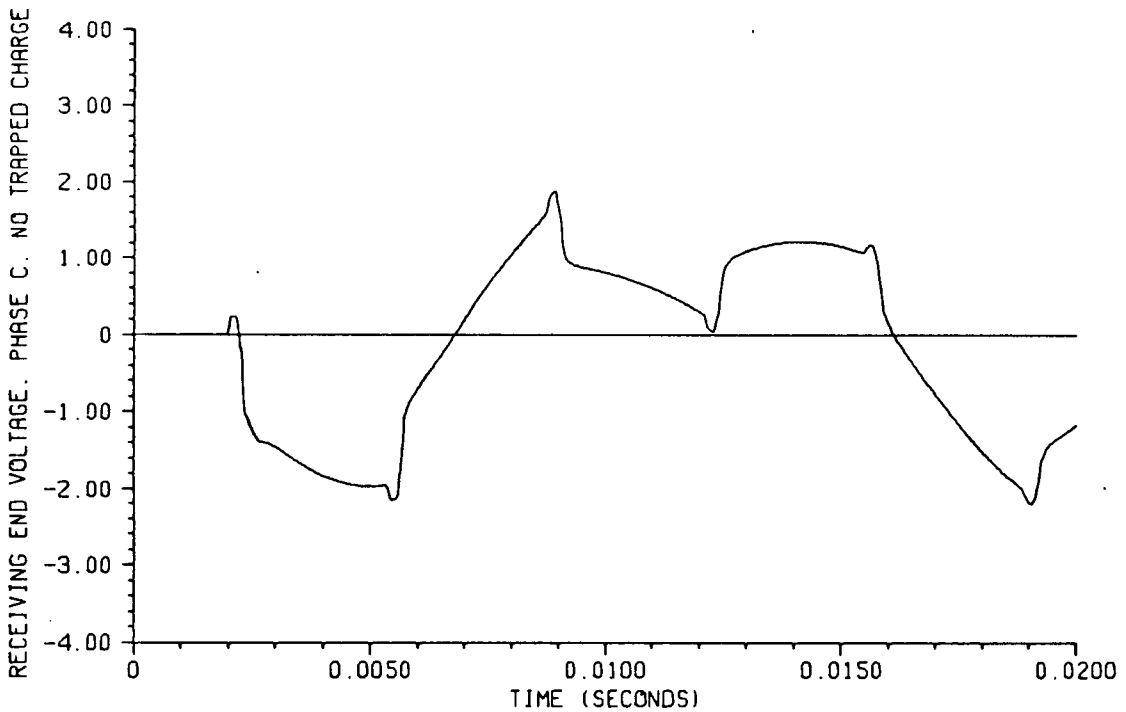

Graph 1.18: Receiving end voltage. Phase C, no trapped charge.

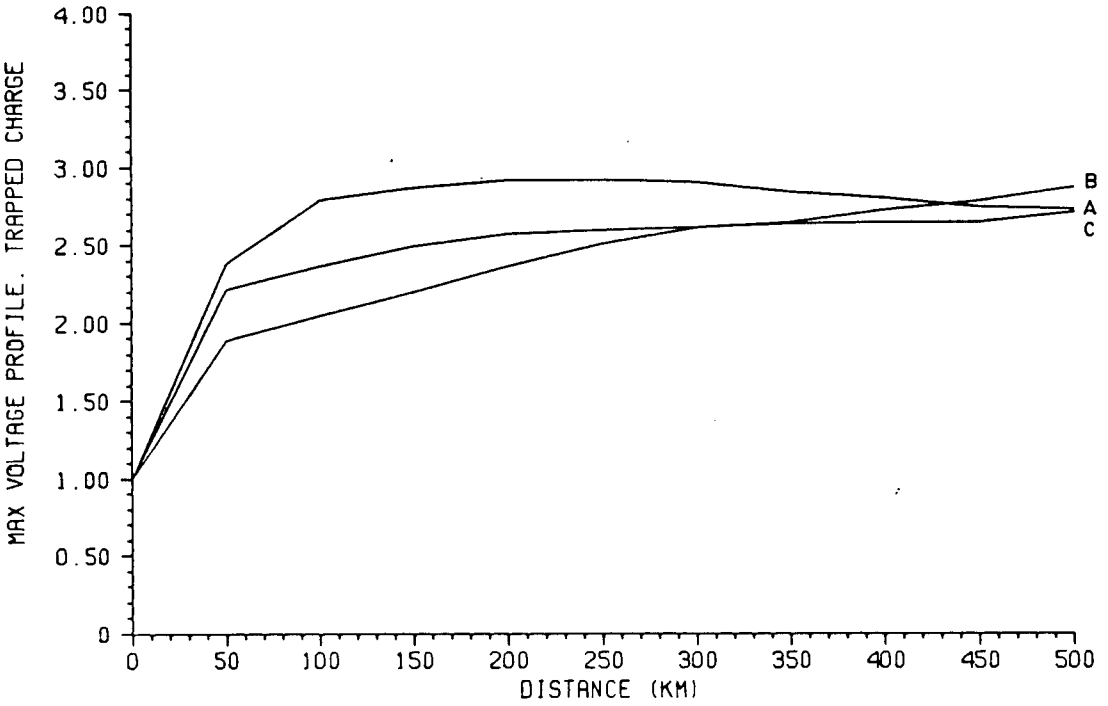

Graph 1.19: Profile of maximum overvoltages (absolute values). Trapped charge.

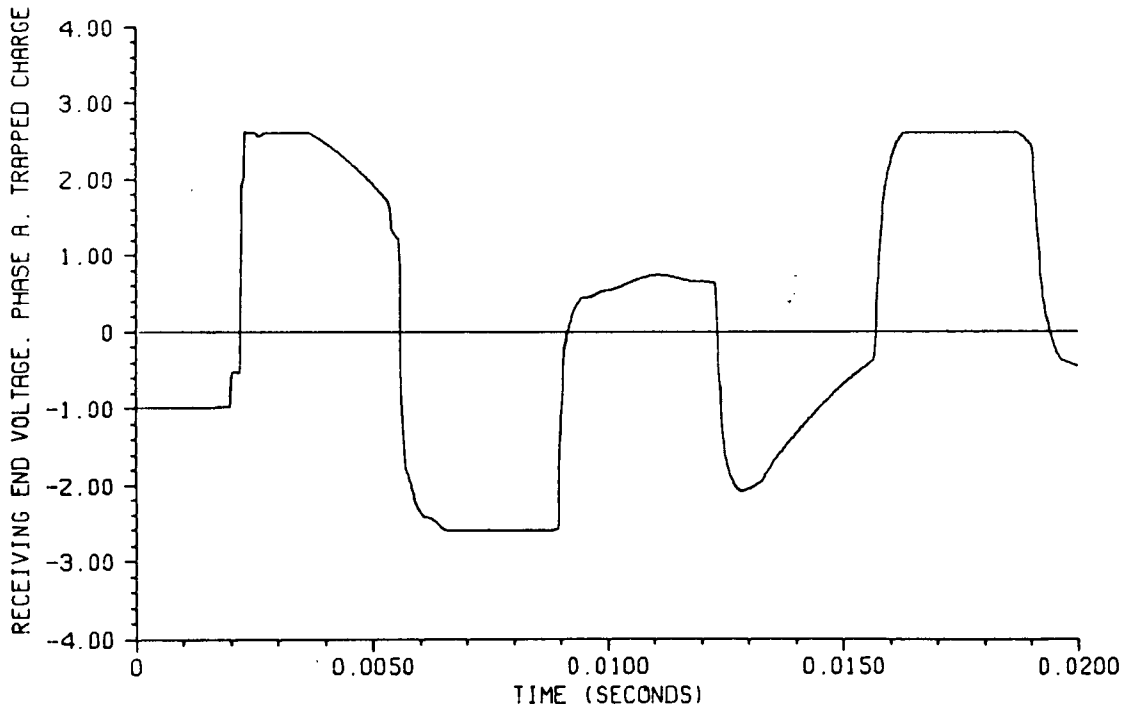

Graph 1.20: Receiving end voltage. Phase A, trapped charge.

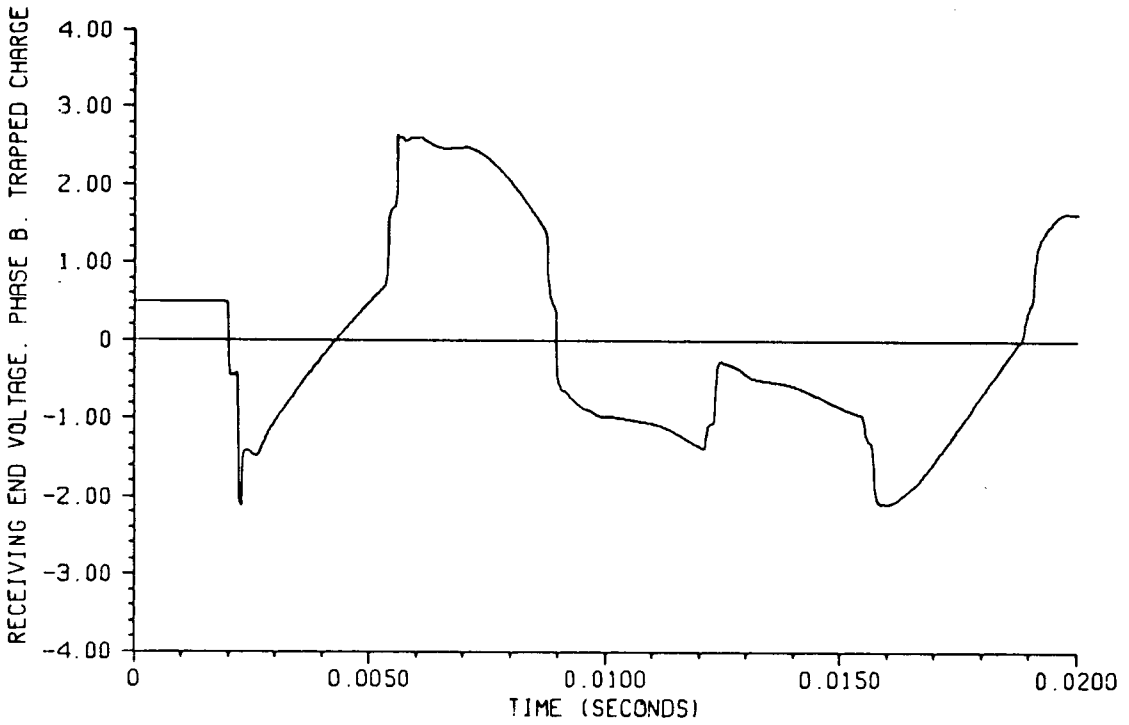

Graph 1.21: Receiving end voltage. Phase B, trapped charge.

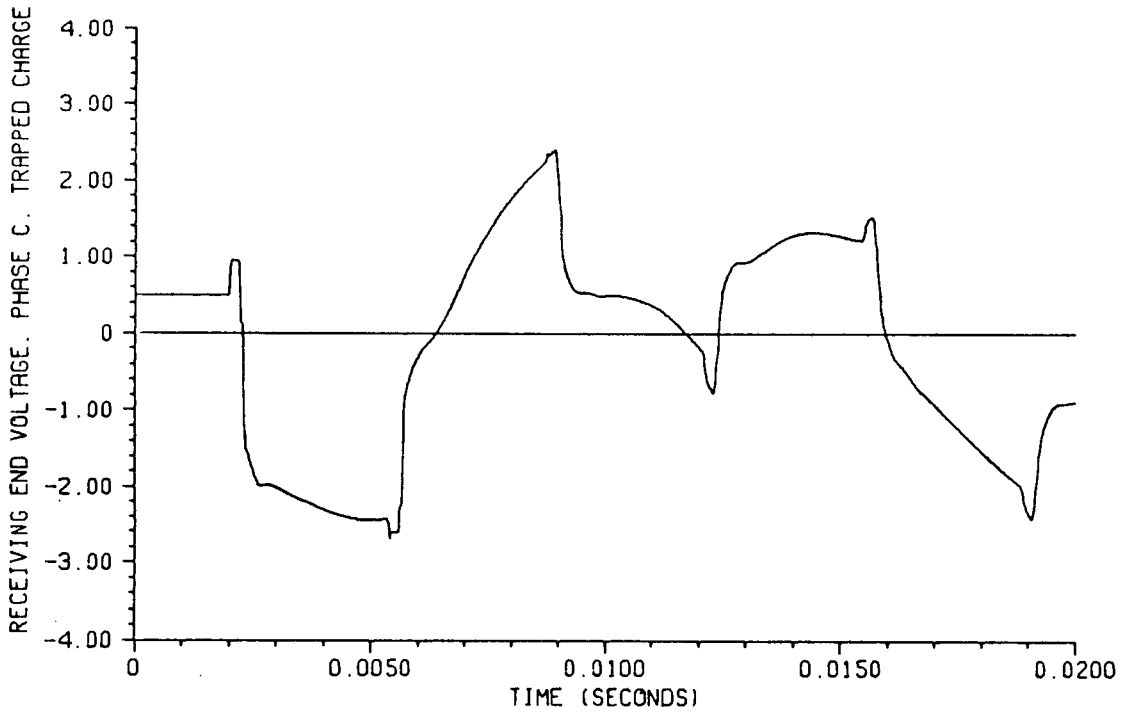

Graph 1.22: Receiving end voltage. Phase C, trapped charge.

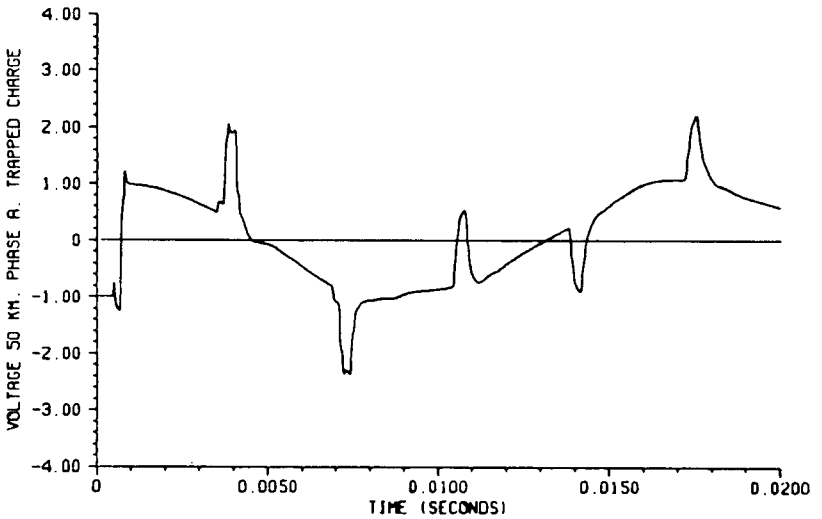

(a)

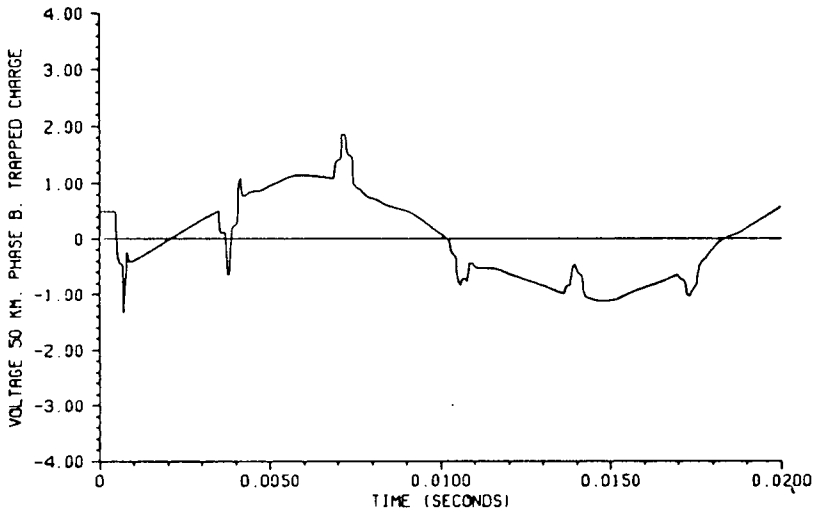

(b)

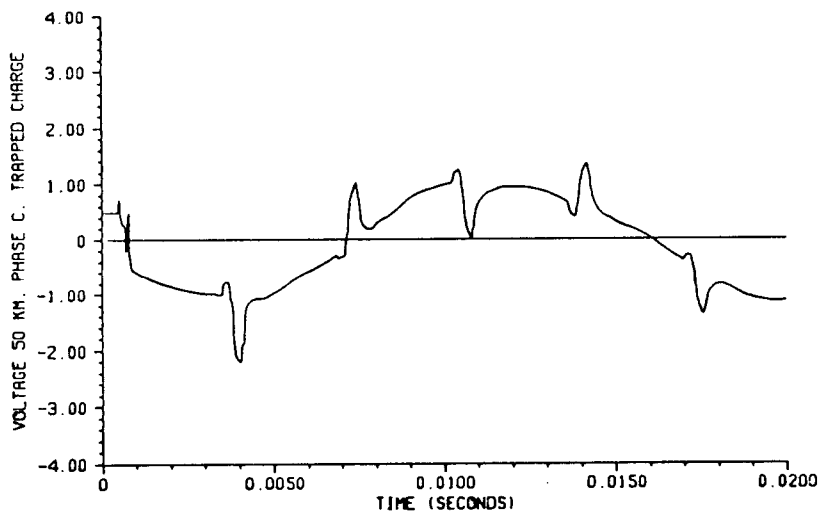

(c)

Graph 1.23: Voltage at 50 km from sending end.
(a) Phase A. (b) Phase B. (c) Phase C.

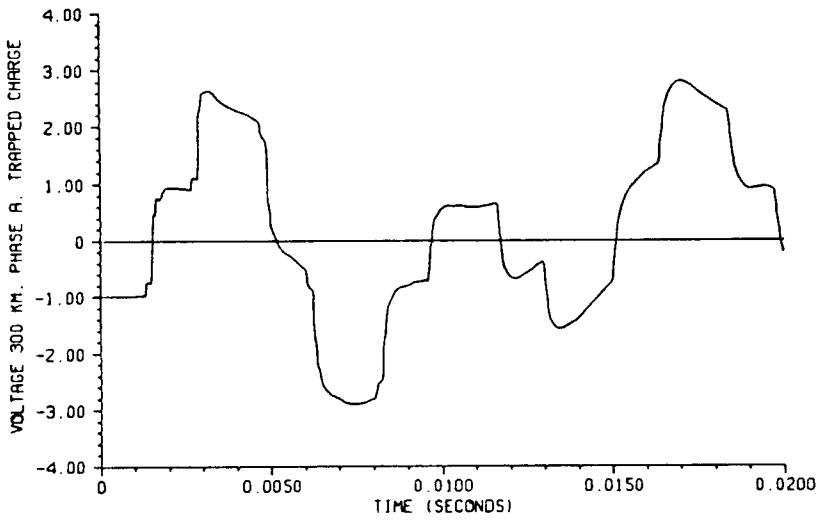

(a)

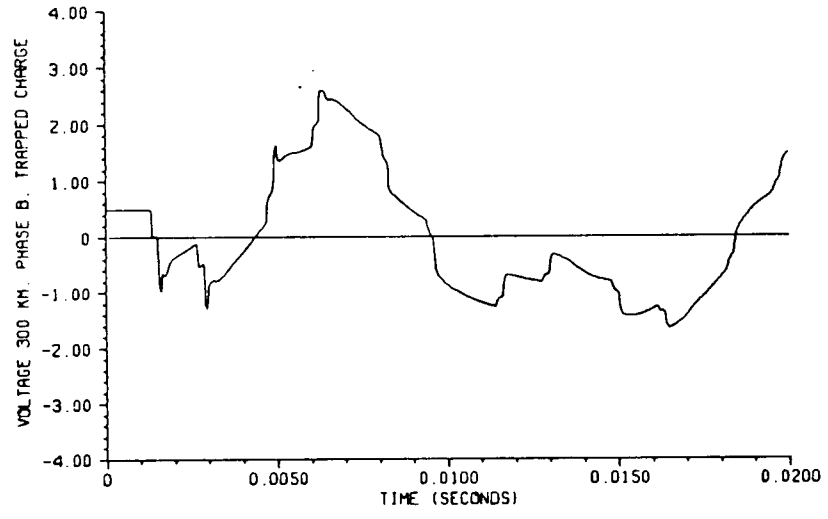

(b)

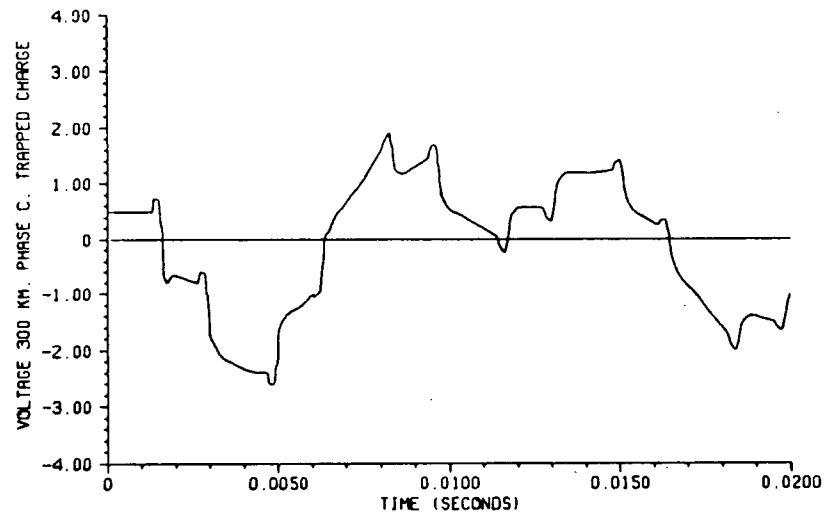

(c)

Graph 1.24: Voltage at 300 km from sending end.
(a) Phase A. (b) Phase B. (c) Phase C.

CONCLUDING REMARKS

In the first part of this thesis project a model for the evaluation of voltage and current profiles along a transmission line has been presented. The model and supporting routines have been designed to overcome the accuracy and data management difficulties encountered by standard segmentation methods for profile calculations.

The main advantages achieved can be summarized as follows:

i) The model and routines are general, and limited only by the capabilities of the main (host) program.

ii) Truncation errors are essentially eliminated, and segmentation errors are minimized.

iii) The routines are as fast or faster than standard segmentation procedures, and data management capabilities are clearly superior.

The possibility of routine profile calculations, is very useful in some practical applications (e.g., co-ordination of insulation and protection devices).

Profile related procedures such as the dynamic visual display of travelling waves could prove to be an excellent teaching aid and permit a better understanding of transient phenomena.

PART II

LOW-ORDER APPROXIMATION OF THE FREQUENCY DEPENDENCE OF TRANSMISSION LINE PARAMETERS

INTRODUCTION

Accurate models which take into account the frequency dependence of transmission line parameters, have become very important tools in the modern analysis of transient phenomena. Such accurate models usually require detailed information about tower configuration, earth resistivity, etc.; if many lines have to be modelled, the approximation of the line parameters becomes a tedious and time consuming process.

When the effect of one or more lines is not critical to the outcome of a particular study, the accurate modelling of these lines is neither justifiable nor desirable. In such cases, a faster and simpler line model would be preferred, if its accuracy were not seriously compromised.

A simplified line model should meet the following requirements:

a) It should be computationally faster, and easier to use than the existing accurate models.

b) It should be more accurate than models that do not take into account the frequency dependence of line parameters.

c) It should require less information (or input data) than the more accurate models.

d) It should be compatible with the host program of the more accurate models (in this case, the frequency-dependence version of UBC's EMTP code(*)).

(*) This and all future references to the frequency-dependence model and/or routines of the EMTP refer only to those developed by Jose R. Marti (as partial requirement for his Ph.D. degree at the University of British Columbia [7]). It is not intended to create the impression that this is the only frequency-dependence model available to EMTP users.

Such a simplified line model is developed in the second part of this thesis project, where the following assumptions have been made:

(1) The line is balanced or perfectly transposed, that is, only two distinct propagation modes are considered: zero sequence or ground mode, and positive sequence or sky mode.

(2) The capacitances and shunt conductance of the line are constant over the entire frequency range.

(3) The ground resistivity is constant, and its value, as well as the values of the electrical parameters R, L and C at power frequency, are known.

CHAPTER 1

THEORETICAL CONSIDERATIONS

1.1 Evaluation of the Transmission Line Parameters

1.1.1 Series Impedance Matrix

In the frequency domain, a transmission line can be described in terms of the following equations,

$$-\frac{d\,V_{ph}}{dx} = Z_{ph}\,I_{ph} \tag{1.1}$$

$$-\frac{d\,I_{ph}}{dx} = Y_{ph}\,V_{ph}\,, \tag{1.2}$$

where Z_{ph} and Y_{ph} are the series impedance and shunt admittance matrices, respectively (subscript $_{ph}$ stands for phase quantities). For an n-phase system (without ground wires),

$$Z_{ph}(\omega) = \begin{bmatrix} z_{1,1}(\omega) & z_{1,2}(\omega) & \cdots & z_{1,n}(\omega) \\ z_{2,1}(\omega) & & & \vdots \\ \vdots & & & \vdots \\ \vdots & & & \vdots \\ \vdots & & & \\ z_{n,1}(\omega) & \cdots\cdots & & z_{n,n}(\omega) \end{bmatrix} \tag{1.3}$$

$$Y_{ph}(\omega) = \begin{bmatrix} y_{1,1}(\omega) & y_{1,2}(\omega) & \cdots & y_{1,n}(\omega) \\ y_{2,1}(\omega) & & & \vdots \\ \vdots & & & \vdots \\ \vdots & & & \vdots \\ \vdots & & & \\ y_{n,1}(\omega) & \cdots\cdots & & y_{n,n}(\omega) \end{bmatrix} \tag{1.4}$$

The elements of $Z_{ph}(\omega)$ can be calculated from the physical characteristics of the conductors and tower configuration:

$$z_{k,k}(\omega) = R_k(\omega) + \Delta R_{k,k}(\omega) + j(\omega\, L_{int,k}(\omega) + \omega\, L_{ext,k} + \Delta X_{k,k}(\omega)) \quad \text{in } \Omega/\text{km} \tag{1.5}$$

$$z_{k,j}(\omega) = z_{j,k}(\omega) = \Delta R_{k,j}(\omega) + j(\omega L_{m,k,j} + \Delta X_{k,j}(\omega)) \quad \text{in } \Omega/km \tag{1.6}$$

where,

$R_k(\omega)$ is the ac resistance of conductor k. Its dependency on the frequency is due to skin effect (see appendix II-A)

$L_{int,k}(\omega)$ is the internal inductance of conductor k. Its value also depends on the frequency because of skin effect. If skin effect is ignored,

$$L_{int,k} = 2 \cdot 10^{-4} \ln \frac{r_k}{GMR_k} \quad \text{in H/km} \tag{1.7}$$

$L_{ext,k}$ is the external inductance. It only depends on the geometry of the tower, and it is given by,

$$L_{ext,k} = 2 \cdot 10^{-4} \ln \frac{2\, h_k}{r_k} \quad \text{in H/km} \tag{1.8}$$

$L_{m,k,j}$ is the mutual inductance between conductors k and j. It only depends on the geometry of the tower and it is given by,

$$L_{m,k,j} = 2 \cdot 10^{-4} \ln \frac{D_{k,j}}{d_{k,j}} \quad \text{in H/km} \tag{1.9}$$

h_k is the average height of conductor k in m.

GMR_k is the geometric mean radius of conductor k in m.

$D_{k,j}$ is the distance between conductor k and the image of conductor j in m. (see Fig.1.1)

$d_{k,j}$ is the distance between conductors k and j in m.

r_k is the radius of conductor k in m.

$\omega = 2 \pi f$ where f is the frequency in Hz.

$\Delta R_{k,k}(\omega)$, $\Delta R_{k,j}(\omega)$, $\Delta X_{k,k}(\omega)$, $\Delta X_{k,j}(\omega)$, are Carson's correction terms for earth return effects, in Ω/Km (see appendix II-B).

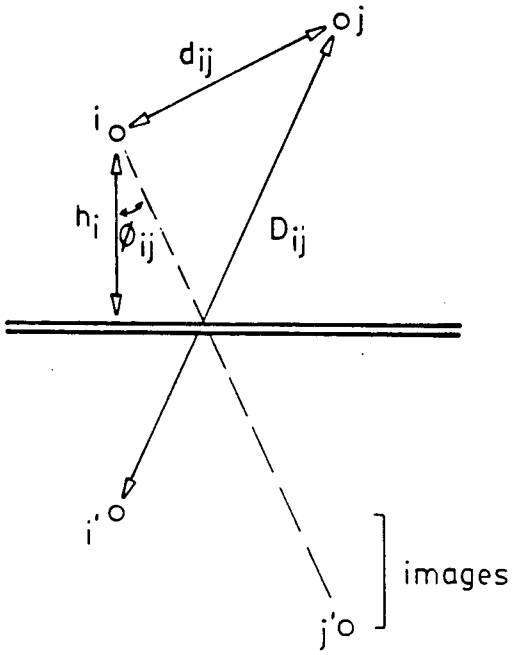

Fig. 1.1: Tower geometry.

In the case of bundled conductors (if the bundle is symmetrical, and if equal current distribution in the conductors of the bundle is assumed), the bundle can be treated as a single equivalent conductor by replacing the GMR_k and r_k in (1.7) and (1.8) by an equivalent GMR and an equivalent radius:

$$GMR_{eq,k} = \sqrt[N]{N \cdot GMR_k \cdot A^{N-1}} \qquad (1.10)$$

$$r_{eq,k} = \sqrt[N]{N \cdot r_k \cdot A^{N-1}} \qquad (1.11)$$

where N = number of conductors in the bundle.

GMR_k = geometric mean radius of the individual conductor in m.

A = radius of the bundle in m.

Note that equations (1.5) an (1.6) are general and account for the frequency dependence of the parameters. Let us now assume that all conductors are identical. It then follows that

$$r_{eq,k} = r_{eq,j} = r \tag{1.12}$$

$$GMR_{eq,k} = GMR_{eq,j} = GMR \tag{1.13}$$

$$R_k(\omega) = R_j(\omega) = R_s(\omega) \tag{1.14}.$$

If the line is perfectly transposed, we can assume that the impedance matrix Z_{ph} is the average of the impedance matrices of the different transposition sections. This is a particularly good approximation if the line is going to be studied at the end points only. This is illustrated, for a three-phase line transposed in two places, in Figure 1.2.

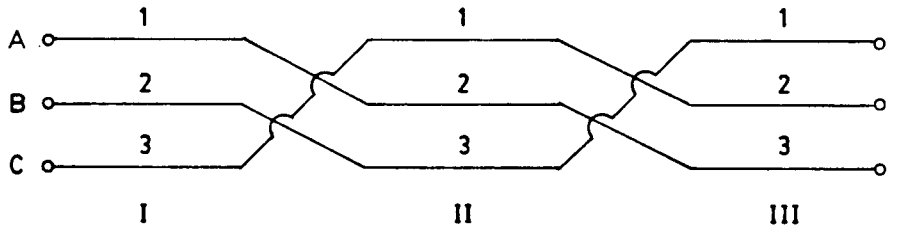

Fig. 1.2: Transposition for a single circuit.

The impedance matrix for the entire line is,

$$Z_{ph} = \frac{1}{3}([Z_{ph\ I}] + [Z_{ph\ II}] + [Z_{ph\ III}])$$

$$\frac{1}{3}\left[\begin{bmatrix} z_{11} & z_{12} & z_{13} \\ z_{21} & z_{22} & z_{23} \\ z_{31} & z_{32} & z_{33} \end{bmatrix} + \begin{bmatrix} z_{22} & z_{23} & z_{21} \\ z_{32} & z_{33} & z_{31} \\ z_{12} & z_{13} & z_{11} \end{bmatrix} + \begin{bmatrix} z_{33} & z_{31} & z_{32} \\ z_{13} & z_{11} & z_{12} \\ z_{23} & z_{21} & z_{22} \end{bmatrix}\right]$$

$$= \begin{bmatrix} z_s & z_m & z_m \\ z_m & z_s & z_m \\ z_m & z_m & z_s \end{bmatrix},$$

with,

$$z_s = \frac{1}{3}(z_{11} + z_{22} + z_{33})$$

$$z_m = \frac{1}{3}(z_{12} + z_{13} + z_{23})$$

In an n-phase system, z_s would be the average of all diagonal elements and z_m the average of all off-diagonal elements.

$$z_s = \frac{1}{n}\sum_{k=1}^{n} z_{kk} \tag{1.15}$$

$$z_m = \frac{2}{n(n-1)}\sum_{k=1}^{n-1}\sum_{j=2}^{n} z_{kk} \quad \text{for } k<j \tag{1.16}$$

Therefore, for a balanced (or perfectly transposed line),

$$Z_{ph}(\omega) = \begin{bmatrix} z_s(\omega) & z_m(\omega) & \cdots & z_m(\omega) \\ z_m(\omega) & z_s(\omega) & & \vdots \\ \vdots & & & \vdots \\ z_m(\omega) & \cdots & & z_s(\omega) \end{bmatrix} \tag{1.17}$$

where,

$$z_s(\omega) = R_s(\omega) + \Delta R_s(\omega) + j(\omega L_{int}(\omega) + \omega L_{ext} + \Delta X_s(\omega)) \tag{1.18}$$

$$z_m(\omega) = \Delta R_m(\omega) + j(\omega L_m + \Delta X_m(\omega)), \tag{1.19}$$

with,

$$L_{ext} = 2\cdot 10^{-4} \ln \frac{2h}{r} \tag{1.20}$$

$$L_m = 2\cdot 10^{-4} \ln \frac{D}{d} \tag{1.21}$$

$$L_{int} = 2\cdot 10^{-4} \ln \frac{r}{GMR} \qquad \text{(skin effect neglected)} \tag{1.22}$$

$$h = \left[\prod_{k=1}^{n} h_k\right]^{1/n} \qquad \text{(geometric mean height)} \tag{1.23}$$

$$D = \left[\prod_{k=1}^{n-1}\prod_{j=2}^{n} D_{k,j}\right]^{2/(n-1)n} \qquad k<j \text{ (geometric mean distance between k and and the image of j)} \tag{1.24}$$

$$d = \left[\prod_{k=1}^{n-1}\prod_{j=2}^{n} d_{k,j}\right]^{2/(n-1)n} \qquad k<j \text{ (geometric mean distance among the n conductors)} \tag{1.25}$$

$\Delta R_s(\omega)$, $\Delta R_m(\omega)$, $\Delta X_s(\omega)$ and $\Delta X_m(\omega)$, are the averages of Carson's correction terms,

$$\Delta R_s(\omega) = \frac{1}{n} \sum_{k=1}^{n} \Delta R_k(\omega)$$

$$\Delta X_s(\omega) = \frac{1}{n} \sum_{k=1}^{n} \Delta X_k(\omega)$$

$$\Delta R_m(\omega) = \frac{2}{n(n-1)} \sum_{k=1}^{n-1} \sum_{j=2}^{n} \Delta R_{k,j}(\omega) \qquad j>k$$

$$\Delta X_m(\omega) = \frac{2}{n(n-1)} \sum_{k=1}^{n} \sum_{j=2}^{n} \Delta X_{k,j}(\omega) \qquad j>k$$

The balanced matrix of equation (1.17) leads to only two distinct propagation modes (zero and positive sequence). Therefore the modal series impedance matrix has the form,

$$Z_m(\omega) = \begin{bmatrix} z_o(\omega) & & \cdots & \\ & z_1(\omega) & & \vdots \\ \vdots & & & \\ & \cdots & o & z_1(\omega) \end{bmatrix} \tag{1.26}$$

where

$$z_o(\omega) = z_s(\omega) + (n-1)\, z_m(\omega) \tag{1.27}$$

$$z_1(\omega) = z_s(\omega) - z_m(\omega) \tag{1.28}$$

To obtain the sequence impedances we introduce (1.18) and (1.19) into (1.27) and (1.28)

$$z_o(\omega) = R_s + \Delta R_s + (n-1)\Delta R_s(\omega) + j(\omega L_{int}(\omega) + \omega L_{ext} + (n-1)\omega L_m + \Delta X_s(\omega) + (n-1)\Delta X_m(\omega)), \tag{1.29}$$

$$z_1(\omega) = R_s(\omega) + \Delta R_s(\omega) - \Delta R_m(\omega) + j(\omega L_{int}(\omega) + \omega L_{ext}(\omega) - \omega L_m + \Delta X_s(\omega) - \Delta X_m(\omega)), \tag{1.30}$$

but,

$$z_o(\omega) = R_o(\omega) + jX_o(\omega)$$

$$z_1(\omega) = R_1(\omega) + jX_1(\omega),$$

then,

$$R_o(\omega) = R_s(\omega) + \Delta R_s(\omega) + (n-1)\Delta R_m(\omega) \tag{1.31}$$

$$X_o(\omega) = \omega \left(L_{int}(\omega) + L_{ext} + (n-1)\, L_m\right) + \Delta X_s(\omega) + (n-1)\, \Delta X_m(\omega) \tag{1.32}$$

$$R_1(\omega) = R_s(\omega) + \Delta R_s(\omega) - \Delta R_m(\omega) \tag{1.33}$$

$$X_1(\omega) = \omega \left(L_{int}(\omega) + L_{ext} - L_m\right) + \Delta X_s(\omega) - \Delta X_m(\omega). \tag{1.34}$$

1.1.2 Carson's Correction Terms

Carson's correction terms ΔR_s, ΔR_m, ΔX_s, and ΔX_m account for the earth return effect (see appendix II-B). These terms depend on the earth resistivity ρ, on the frequency f, and on the relative position of the conductors and earth plane.

At power frequency (50 or 60 Hz) the term a in equation (II-B.1) is small, so that only the first term in equation (II-B.2) needs to be retained.

If the line is perfectly transposed, the averaging procedure described in the previous section yields

$$\Delta R_s(\omega) = \Delta R_m(\omega) = \frac{\omega \pi \cdot 10^{-4}}{2} \quad \text{in } \Omega/\text{km} \tag{1.35}$$

$$\Delta X_s(\omega) = \omega \cdot 2 \cdot 10^{-4} \left[0.6159315 - \ell n \left(2\, h \cdot k \sqrt{\frac{f}{\rho}}\right)\right] \quad \text{in } \Omega/\text{km} \tag{1.36}$$

$$\Delta X_m(\omega) = \omega \cdot 2 \cdot 10^{-4} \left[0.6159315 - \ell n \left(D\, k \cdot \sqrt{\frac{f}{\rho}}\right)\right] \quad \text{in } \Omega/\text{km} \tag{1.37}$$

where $k = 4 \pi \sqrt{5} \cdot 10^{-4}$.

Introducing (1.35) into (1.31) and (1.33)

$$R_o(\omega) = R_s(\omega) + \frac{n \pi \cdot 10^{-4}}{2} \tag{1.38}$$

$$R_1(\omega) = R_s(\omega) \tag{1.39}$$

If we assume that the skin effect influence on the internal inductance at power frequencies is negligible, then from equation (1.22)

$$L_{int} = 2 \cdot 10^{-4} \ell n \frac{r}{GMR}$$

Introducing this value, and equations (1.36) and (1.37) into equation (1.32) we obtain, after some algebraic manipulations

$$X_o(\omega) = 2\, n\omega \cdot 10^{-4}\, \ell n\, \frac{b\sqrt{\rho/f}}{k\sqrt[n]{GMR\, d^{n-1}}} \qquad (1.40)$$

with

$$b = e^{0.6159315}$$

Similarly, introducing equations (1.36) and (1.37) into equation (1.34)

$$X_1(\omega) = 2\cdot\omega\cdot 10^{-4}\, \ell n\, \frac{d}{GMR} \qquad (1.41)$$

1.1.3 Shunt Admittance Matrix

To evaluate $Y_{ph}(\omega)$ it is convenient to evaluate first Maxwell's potential coefficient matrix P_{ph}

$$P_{ph} = \begin{bmatrix} p_{1,1} & p_{1,2} & \cdots & p_{1,n} \\ \vdots & & & \vdots \\ p_{n,1} & \cdots & & p_{n,n} \end{bmatrix}, \tag{1.42}$$

where

$$p_{k,k} = \frac{1}{2\pi\varepsilon_o} \ln \frac{2h_i}{r_i} \quad \text{in km/F} \tag{1.43}$$

$$p_{k,j} = p_{j,k} \quad \frac{1}{2\pi\varepsilon_o} \ln \frac{D_{k,j}}{d_{k,j}} \quad \text{in km/F} \tag{1.44}$$

If we assume that the shunt conductance matrix G is zero, the inverse of P_{ph} equals the capacitance matrix K_{ph}

$$P_{ph}^{-1} = K_{ph}$$

$$Y_{ph} = j\omega K_{ph}$$

If the line is perfectly transposed we can average out the diagonal and off-diagonal elements of P_{ph} to obtain a balanced matrix, whose elements are given by

$$p_s = \frac{1}{n} \left[\sum_{k=1}^{n} p_{k,k} \right] \tag{1.45}$$

$$p_m = \frac{1}{n(n-1)} \left[\sum_{k=1}^{n-1} \sum_{j=2}^{n} p_{k,j} \right] \qquad k<j \tag{1.46}$$

Introducing (1.43) and (1.44),

$$p_s = \frac{1}{2\pi\varepsilon_o} \ln \frac{2h}{r} \tag{1.47}$$

$$p_m = \frac{1}{2\pi\varepsilon_o} \ln \frac{D}{d} \tag{1.48}$$

with h, r, D and d defined as in the previous sections.

The modal potential coefficients are

$$p_o = p_s + (n-1)\, p_m$$

$$p_1 = p_s - p_m$$

Introducing equations (1.47) and (1.48), the modal, Maxwell's coefficients become,

$$p_o = \frac{1}{2\pi\varepsilon_o} \ln \frac{2h\, D^{n-1}}{r\, d^{n-1}} \tag{1.49}$$

$$p_1 = \frac{1}{2\pi\varepsilon_o} \ln \frac{2h\, d}{r\, D} \tag{1.50}$$

The inverse of P_{mode} is K_{mode}, and since P_{mode} is diagonal, the modal capacitances are simply the reciprocals of the modal potential coefficients,

$$C_o = \frac{2\pi\varepsilon_o}{\ln \frac{2h\, D^{n-1}}{r\, d^{n-1}}} \tag{1.51}$$

$$C_1 = \frac{2\pi\varepsilon_o}{\ln \frac{2h\, d}{r\, D}} \tag{1.52}$$

1.1.4 Comparison between Exact and Approximate Formulas

In order to illustrate the accuracy of the approximate formulas for the sequence quantities, a typical 500KV line design will be considered,

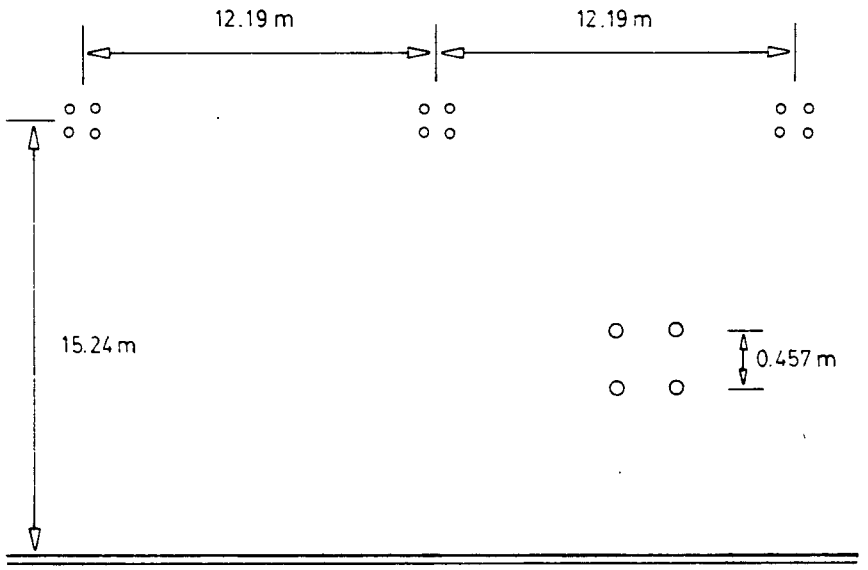

Fig. 1.3: Tower configuration of reference line.

where,

conductor diameter = 22.86 mm

conductor GMR = 9.32688 mm

conductor dc resistance = 0.104763 Ω/km.

Assuming that the line is perfectly transposed, and that the bundle is treated as a single equivalent conductor, we have

r = 198.253 mm

GMR = 188.427 mm

$d = 15.361$ m

$D = 34.78$ m

$R_{dc} = 0.02619$ Ω/km

Table 1.1 shows the results of introducing these quantities in the approximate formulas, compared to the "exact" parameters (at 60 Hz) obtained from the line's tower geometry using UBC's Line Constants Program.

	Exact Formulas	Approximate Formulas	Error (%)
R_1 (Ω/km)	0.02643	0.02643	-
L_1 (mH/km)	0.8801	0.8802	0.009
C_1 (μF/km)	0.0133	0.0132	0.84
R_o (Ω/km)	0.1974	0.2041	-3.38
L_o (mH/km)	3.307	3.289	0.55
C_o (μF/km)	0.008361	0.008341	0.24

Table 1.1: Comparison between exact and approximate parameters.

These results illustrate that the approximate formulas are accurate enough at power frequency. However, if the frequency were increased, these formulas would no longer be adequate.

1.2 Evaluation of an Equivalent Line Configuration From the Parameters at Power Frequency

In order to evaluate the line parameters over the frequency range of interest, the physical configuration of the line must be known. If L_1, C_1, L_o and C_o are known at a sufficiently low frequency (60 Hz, for instance), the approximate formulas developed in the previous sections can be used to find some of the physical parameters of the line, that is r, d, GMR, h, and D. These quantities define an equivalent line whose power frequency parameters are the same as those of the original line. If the physical parameters of the equivalent line are close to those of the original line, the frequency variation of its electrical parameters should also be close to that of the original line.

Consider the approximate equations for L_1, L_o, C_1 and C_o

$$L_1 = 2\cdot 10^{-4} \ln \frac{d}{GMR} \tag{1.53}$$

$$L_o = 2n\cdot 10^{-4} \ln \frac{b\sqrt{f/\rho}}{k \sqrt[n]{GMR \cdot d^{n-1}}} \tag{1.54}$$

$$C_1 = \frac{2\pi\varepsilon_o}{\ln \frac{2h\,d}{r\,D}} \tag{1.55}$$

$$C_o = \frac{2\pi\varepsilon_o}{\ln \frac{2h\,D^{n-1}}{r\,d^{n-1}}} \tag{1.56}$$

where $b = e^{0.6159315}$

$k = 4\pi\sqrt{5}\cdot 10^{-4}$

These are four equations and five unknowns. The additional equation needed is given by

$$D^2 = (2h)^2 + d^2. \tag{1.57}$$

The difference between D calculated from equation (1.57) and the value obtained by finding the geometric mean distance between the conductors and their images, is less than 2%.

Let us now define

$$a_1 = e^{(L_1/2\cdot 10^{-4})} \tag{1.58}$$

$$a_2 = \frac{b^n (\rho/f)^{n/2}}{k^n \, e^{(L_o/2\cdot 10^{-4})}} \tag{1.59}$$

$$a_3 = e^{(2\pi\varepsilon_o/C_1)} \tag{1.60}$$

$$a_4 = e^{(2\pi\varepsilon_o/C_o)} \tag{1.61}$$

Introducing these definitions into the equations above, we obtain

$$a_1 = \frac{d}{GMR} \tag{1.62}$$

$$a_2 = GMR \; d^{n-1} \tag{1.63}$$

$$a_3 = \frac{2\,h\,d}{r\,D} \tag{1.64}$$

$$a_4 = \frac{2\,h\,D^{n-1}}{r\,D^{n-1}} \tag{1.65}$$

$$D^2 = 4\,h^2 + d^2 \tag{1.57}$$

After some algebraic manipulations we finally obtain,

$$GMR = \frac{d}{a_1} \tag{1.68}$$

$$d = (a_1 \cdot a_2)^{1/n} \tag{1.69}$$

$$D = \left[\frac{a_4}{a_3}\right]^{1/n} \cdot d \tag{1.70}$$

$$h = \frac{1}{2}\sqrt{D^2 - d^2} \tag{1.71}$$

$$r = \frac{2\,h\,d}{a_3 D} \tag{1.72}$$

Equations (1.68) to (1.72) give the physical configuration of an equivalent line which has the same power frequency parameters as the line we wish to simulate.

A numerical example is given in table 1.2, where the tower configuration of the reference line is compared to the equivalent line configuration obtained from equations (1.68) to (1.72) using 60 Hz parameters.

	Reference Line (in m)	Equivalent Line (in m)	Error (%)
d	15.361	14.334	6.69
GMR	0.188427	0.175276	6.98
D	34.78	32.66	6.09
h	15.24	14.675	3.71
r	0.198253	0.196490	0.89

Table 1.2: Comparison between the actual line configuration and the equivalent line configuration.

Note that while the approximate equations for the electrical parameters were very accurate (less than 1% error) the physical configuration obtained from the same equations shows errors up to 7%. This is due to the logarithmic nature of the equations; small variations in L and C, produce relatively large changes in a_1, a_2, a_3, and a_4 (see equations (1.58) to (1.61)), which in turn reflect on the equivalent line configuration.

1.3 Skin Effect Correction Factor

With the equivalent line configuration obtained in the previous section, it is now possible to use the more exact formulas (1.32) and (1.34) to evaluate the sequence reactances. However, we have not yet accounted for the variation of $R_s(\omega)$ and $L_{int}(\omega)$ due to skin effect.

If we assume that the equivalent conductor is tubular, skin effect depends only on the conductor's dc resistance and on the correction factor s (see appendix II-A), which is defined as,

$$s = \frac{\text{internal radius}}{\text{external radius}} = \frac{q}{r}$$

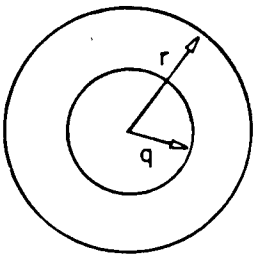

Fig. 1.4: Tubular conductor

Let us now recall equation (1.33)

$$R_1(\omega) = R_s(\omega) + \Delta R_s(\omega) - \Delta R_m(\omega)$$

Since $\Delta R_s(\omega)$ and $\Delta R_m(\omega)$ can now be evaluated from the equivalent line configuration, and $R_1(\omega)$ is assumed to be known, the self-resistance of the equivalent conductor can be determined,

$$R_s(\omega) = R_1(\omega) - \Delta R_s(\omega) + \Delta R_m(\omega) \qquad (1.73)$$

If the dc resistance of the conductor is also known, it is possible to find (numerically, using the skin effect subroutine) the value of s that makes the self-resistance vary from R_{dc} to $R_s(\omega)$. With s determined in this manner, all the information needed to evaluate the electrical parameters (over the entire frequency range) of the equivalent line is known.

If the dc resistance is not known, the value of s can be determined from the internal inductance $L_{int}(\omega)$.

From equation (1.34), $L_{int}(\omega)$ is given by

$$L_{int}(\omega) = \frac{1}{\omega}[X_1(\omega) - \Delta X_s(\omega) + \Delta X_m(\omega)] - L_{ext} + L_m \qquad (1.74)$$

where all the quantities in the right hand side can be evaluated with the equivalent line configuration. With $R_s(\omega)$ and $L_{int}(\omega)$ known, the values of R_{dc} and s can be determined numerically with the skin effect subroutine.

This alternative, although more desirable because less information needs to be known, is more inaccurate than the determination of s with R_{dc} given. The reason is that since $L_{int}(\omega)$ is a small fraction of the total inductance, the difference between the actual and equivalent physical parameters produce relatively large errors in the evaluation of $L_{int}(\omega)$. This can be illustrated with a numerical example using the reference line.

Let us assume that at 60 Hz $L_{int}(\omega)$ can be approximated using equation (1.22)

$$L_{int} = 2.10^{-4} \ln \frac{r}{GMR}$$

We now introduce the actual and equivalent line parameters into this equation. The results are shown below.

Reference Line (in mH/km)	Equivalent Line (in mH/km)	Error (%)
0.01016667	0.0221495	-117.86

These results illustrate that the relatively small error in GMR of 6.75% propagates exponentially because of the small magnitude of L_{int}.

It must be noted, however, that even though the relative error is large, the difference in magnitudes is not, and the actual errors in the determination of s and R_{dc} are considerably smaller. For the reference line, the values of s and R_{dc} calculated when R_{dc} is not given are only 23.2% and 16.9% smaller, respectively.

1.4 Correction of the Equivalent Line Configuration when R_{dc} is Known

As mentioned in the previous section, if the dc resistance is known, the value of s can be determined with good accuracy. The knowledge of an accurate value of s implies that an accurate value of the internal inductance is also known. With this additional piece of information, a finer approximation of the equivalent line can be obtained from the first estimate given by equations (1.68) through (1.72).

Consider equations (1.32) and (1.34),

$$L_o(\omega) = L_{int}(\omega) + L_{ext} + (n-1)\, L_m + (\Delta X_s(\omega) + (n-1)\, \Delta X_m(\omega))/\omega$$

$$L_1(\omega) = L_{int}(\omega) + L_{ext} - L_m + (\Delta X_s(\omega) - \Delta X_m(\omega))/\omega.$$

In these two equations $L_o(\omega)$ and $L_1(\omega)$ are the power frequency inductances and they are known data. The internal inductance $L_{int}(\omega)$ is given by the skin effect subroutine at power frequency. Carson's correction terms $\Delta X_s(\omega)$ and $\Delta X_m(\omega)$ are evaluated using the first approximation of the equivalent line parameters. Therefore L_{int} and L_m can be determined from equations (1.32) and (1.34) with a minimum (direct) knowledge of the tower configuration.

Let

$$a = L_1(\omega) - L_{int}(\omega) + (\Delta X_m(\omega) - \Delta X_s(\omega))/\omega \tag{1.75}$$

$$b = L_o(\omega) - L_{int}(\omega) - (\Delta X_s(\omega) + (n-1)\, \Delta X_m(\omega))/\omega \tag{1.76}$$

then

$$L_m = \frac{(b-a)}{n} \tag{1.77}$$

$$L_{ext} = a + L_m\ . \tag{1.78}$$

From equation (1.20)

$$L_{ext} = 2.10^{-4}\ \ell n\ \frac{2\,h}{r},$$

from which

$$h = \frac{r}{2} \; e^{(L_{ext}/2\cdot 10^{-4})} \tag{1.79}$$

where L_{ext} is calculated from equation (1.78) and r is the value obtained from equation (1.72).

From equation (1.22)

$$L_{int} = 2.10^{-4} \; \ell n \; \frac{r}{GMR}$$

from which

$$GMR = r \; e^{(L_{int}/2\cdot 10^{-4})} \tag{1.80}$$

And finally, d and D are obtained from equations (1.62) and (1.65)

$$d = a_1 \; GMR \tag{1.81}$$

$$D = \left[\frac{r \, a_4}{2 \, h}\right]^{1/(n-1)} \cdot d \tag{1.82}$$

The corrected tower configuration (for the reference line) is shown in table 1.3.

	Reference Line (in m)	Equivalent Line (in m)	Error (%)
d	15.361	15.058	1.97
GMR	0.188427	0.184440	2.12
D	34.78	34.01	2.22
h	15.24	14.99	1.64
r	0.198253	0.196490	0.89

Table 1.3: Second approximation of the tower configuration when R_{dc} is known.

This new equivalent line is a better approximation of the original line. The improvement obtained using this procedure depends on the accuracy of the initial estimate of the equivalent radius r. This initial estimate of r is usually very good because of the particular form of equations (1.68) through (1.72). It also depends on the value of

$L_{int}(\omega)$ obtained using the skin effect subroutine, which is also very accurate because little error is involved in the evaluation of s when R_{dc} is known.

This fine adjustment procedure can be interpreted as the iterative solution of equations (1.53) through (1.57) exchanging, after the first iteration, equation (1.57) with the equation that calculates skin effect. If the dc resistance is not known, the skin effect equation is not available (actually not reliable) and only the first iteration can be performed.

1.5 Evaluation of the Characteristic Impedance and Propagation Function

With the equivalent line configuration obtained in the previous section, the modal parameters of the line over the frequency range of interest can be evaluated, and with them, the characteristic impedance Z_c and propagation function A_1 for zero and positive sequence. These are defined as follows

$$Z_c(\omega) = \sqrt{\frac{R + j\omega L}{G + j\omega C}} \tag{1.83}$$

$$A_1(\omega) = e^{-\gamma(\omega)\ell} \tag{1.84}$$

$$\gamma(\omega) = \sqrt{(R + j\omega L)(G + j\omega C)}. \tag{1.85}$$

where R, L, C are the sequence parameters defined in the previous sections, ℓ is the line length, and G is the shunt conductance.

The modal resistances and inductances are evaluated over the frequency range, using equations (1.31) through (1.34), with the equivalent line configuration. The capacitances, since they are virtually constant over the frequency range of interest in transient analysis, are those given as input data [10].

The shunt conductance, up to this point, had been assumed to be zero. However, if G=0, the characteristic impedance goes to infinity as the frequency goes to zero (see equation (1.83)). This situation, apart from being physically impossible, is computationally undesirable. The approximation of $Z_c(\omega)$ by rational functions would require a superfluous amount of poles and zeros to simulate the low frequency region. Therefore, a finite value of G is assumed in the evaluation of $Z_c(\omega)$ (the same value of G is used in $A_1(\omega)$ for consistency). A typical value for a 500 KV line is $0.3 \cdot 10^{-7}$ S/km.

It is to be noted that the magnitude of G does not affect

significantly the results of transient simulations, however, past experience in the simulation of HVDC lines suggests that a finite value of G contributes to the numerical stability of the solution process during relatively long simulations (several seconds).

Up to this point the line under study has been assumed to have no ground wires. In general, ground wires are treated as normal conductors; in an n-phase system with m ground wires, $Z_{ph}(\omega)$ and $Y_{ph}(\omega)$ would then be (n + m) x (n + m) matrices. Using appropriate reduction techniques [11], $Z_{ph}(\omega)$ and $Y_{ph}(\omega)$ can be reduced to (n x n). The effect of the m ground wires is then implicit in these matrices, and equations (1.5) and (1.6) for $Z_{ph}(\omega)$, and (1.43) and (1.44) for the Maxwell's coefficient matrix are no longer true.

Although the overall effect of ground wires on the line parameters is small, the equivalent line configuration is noticeably affected. The accuracy of the approximation is therefore reduced, although not to the point of making it useless (see appendix II-C).

CHAPTER 2

RATIONAL FUNCTIONS APPROXIMATION OF THE CHARACTERISTIC IMPEDANCE AND PROPAGATION FUNCTION

2.1 Rational Functions. General Considerations

In the frequency-dependence version of the EMTP, $Z_c(\omega)$ and $A_1(\omega)$ must be approximated by rational functions in order to obtain closed mathematical forms which are compatible with the frequency-dependent solution algorithm. These rational functions have the general form

$$B(\omega) = k_o \frac{(s + z_1)(s + z_2) \ldots (s + z_m)}{(s + p_1)(s + p_2) \ldots (s + p_n)} \qquad (2.1)$$

where,

$s = j\omega$

z_i = zero of $B(\omega)$

p_i = pole of $B(\omega)$

k_o = positive, real constant

$n = m$ to approximate $Z_c(\omega)$

$n > m$ to approximate $A_1(\omega)$

All the zeros and poles in equation (2.1) are real and lie in the left-hand side of the complex plane. Under these conditions, $B(\omega)$ belongs to the class of minimum phase-shift functions, therefore, its magnitude function $|B(\omega)|$ uniquely determines its phase function arg $(B(\omega))$. This property reduces the approximating process to the localization of the poles and zeros of $B(\omega)$ so that the magnitudes of $B(\omega)$ and the function to be approximated are matched.

A very simple, and yet powerful, way to find the poles and zeros of $B(\omega)$ is the use of Bode's asymptotes. Consider the magnitude function of $B(\omega)$, and take its logarithm

$$\log |B(\omega)| = \log k_o + \log |s + z_1| + \log |s + z_2| + \ldots + \log |s + z_n| - \log |s + p_1| - \log |s + p_2| - \ldots - \log |s + p_m| . \quad (2.2)$$

For $s = j\omega$ each one of these terms has an asymptotic behaviour with respect to ω. Considering, for instance, the term

$$y = -\log |j\omega + p_1| ,$$

it follows that

$$\text{for } \omega << p_1 \qquad y = \log p_1 . \quad (2.3)$$

$$\text{for } \omega >> p_1 \qquad y = -\log \omega , \quad (2.4)$$

which, as a function of $\log \omega$, define two straight lines or asymptotes that intersect at $\omega = p_1$. These are shown in Figure 2.1.

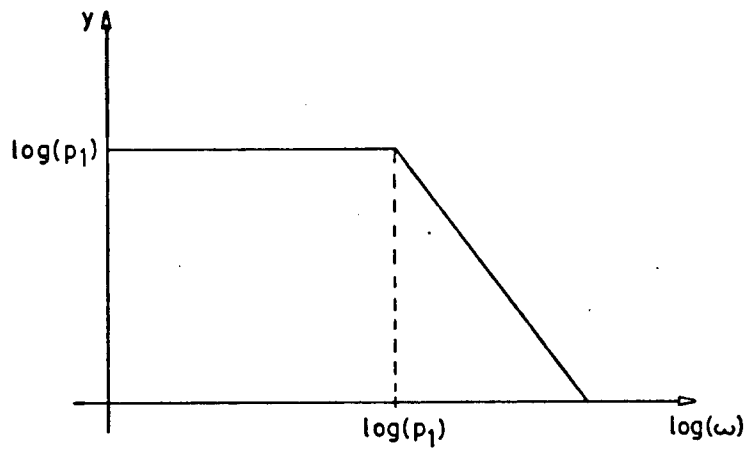

Fig. 2.1: Asymptotic behaviour of $y = -\log |s + p_1|$.

Equation (2.3) defines a horizontal line, and equation (2.4) defines a line of slope - 1 units/dec, that is, when $\omega_1/\omega_2 = 10$, y decreases by 1 unit.

Equation (2.2) can then be visualized as a set of building blocks or straight lines with which the function to be approximated can be traced. It should be noted that these line segments do not represent the actual form of $|B(\omega)|$, but an asymptotic guide or sketch that defines the boundaries where this function actually lies.

The routines of the frequency-dependence option of the EMTP use this principle to allocate the poles and zeros (corners) of the approximating function [7].

For the purposes of this thesis project, these routines are not adequate because the user has no direct control over the order of the approximation used. Furthermore, for approximations of very low order (e.g., two or three poles), these routines can give erratic results. Therefore, a simplified approach to the assignment of asymptotes has been developed in this thesis project. With this simplified method, the number of poles is fixed beforehand, and adequate approximations with very few corners are possible. The basic principles for this approach are discussed next.

2.2 Asymptotic Approximation when the Number of Poles is Fixed

Consider $H(\omega)$, whose magnitude function (shown in Figure 2.2) is bounded and monotonically decreasing over the frequency range of interest (0 to 10^6 Hz). (Note that $|H(\omega)|$ is plotted on a log-log scale)

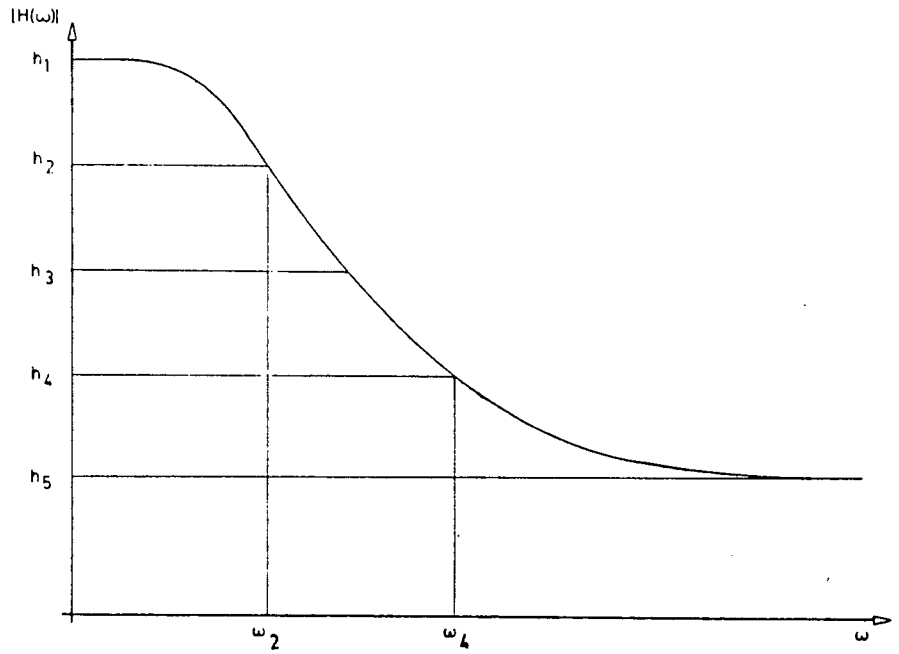

Fig. 2.2: Magnitude function of $H(\omega)$

As mentioned earlier, to approximate $H(\omega)$ with a rational function $B(\omega)$, it is sufficient to match their magnitude functions. Let $B(\omega)$ be of order two,

$$B(\omega) = k_o \frac{(s + z_1)(s + z_2)}{(s + p_1)(s + p_2)}. \tag{2.5}$$

Taking the logarithm of $|B(\omega)|$,

$$\log |B(\omega)| = \log k_o + \log |s + z_1| - \log |s + p_1| + \log |s + z_2| - \log |s + p_2| \tag{2.6}$$

Since $|H(\omega)|$ is bounded, it can be subdivided into four equally spaced sections. The horizontal asymptotes of $|B(\omega)|$ will pass through h_1, h_3 and h_5. The asymptotes with slope - 1 units/dec will pass through h_2 and h_4. The location of the corners of the asymptotic approximation will be at the intersection of the asymptotes (see Figure 2.3).

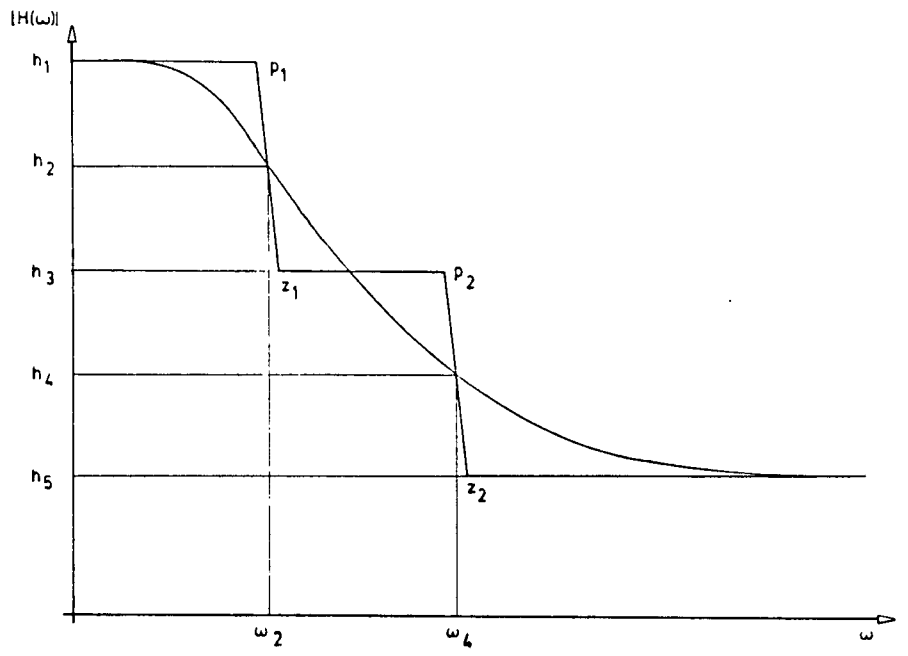

Fig. 2.3: Asymptotic approximation of $|H(\omega)|$.

For example, to find p_1 we intersect the straight lines

$$\log |H(\omega)| = \log h_1$$

$$\log |H(\omega)| = -\log \omega + \log h_2 + \log \omega_2.$$

Subtracting these equations

$$\log h_1 = -\log \omega + \log h_2 + \log \omega_2$$

$$\log (\omega) = -\log h_1 + \log h_2 + \log \omega_2$$

$$\omega = \frac{h_2}{h_1} \omega_2.$$

This is the value of ω at which the intersection occurs, therefore

$$p_1 = \frac{h_2}{h_1}\,\omega_2$$

Proceeding analogously with the other corners, we finally obtain

$$z_1 = \frac{h_2}{h_3}\,\omega_2$$

$$p_2 = \frac{h_4}{h_3}\,\omega_4$$

$$z_2 = \frac{h_4}{h_5}\,\omega_4$$

The value of k_o can be found by matching $|H(\omega)|$ and $|B(\omega)|$ at $\omega = 0$

$$|H(0)| = |B(0)| = k_o \frac{z_1\, z_2}{p_1\, p_2},$$

from which

$$k_o = |H(0)|\, \frac{p_1\, p_2}{z_1\, z_2}.$$

This procedure can be extended to an arbitrary number of poles and zeros n, by subdividing $|H(\omega)|$ into 2n segments and then finding the intersection of the horizontal asymptotes (which will pass through h_i, for i odd) with the non-horizontal asymptotes (which will pass through h_i, for i even). These intersections then define the positions of p_i and z_i.

$$p_i = \frac{h_{2i}}{h_{2i-1}}\,\omega_{2i} \tag{2.7}$$

$$z_i = \frac{h_{2i}}{h_{2i+1}}\,\omega_{2i} \tag{2.8}$$

where $i = 1,\ldots,n$

The constant k_o will then by given by

$$k_o = |H(0)| \prod_{i=1}^{n} \frac{p_i}{z_i}\,. \tag{2.9}$$

This method can be generalized to approximate functions with positive and negative slopes, provided they are single valued and can be broken down into segments of monotonically increasing and decreasing functions (see Figure 2.4).

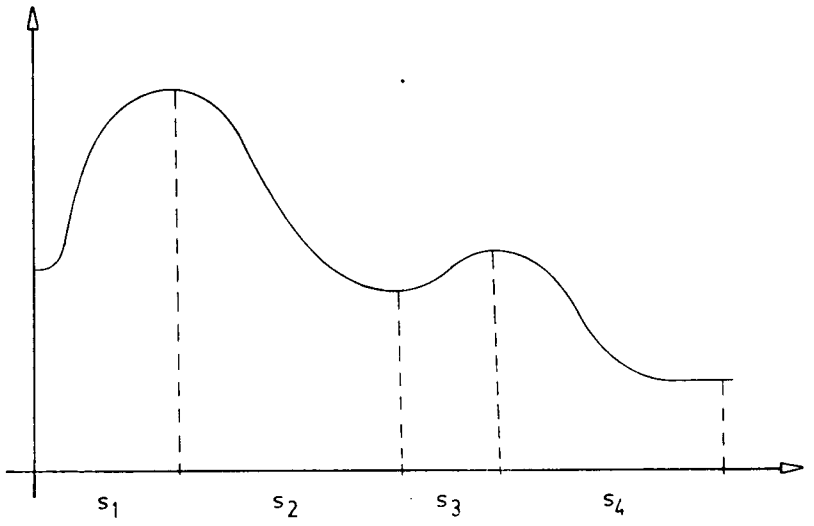

Fig. 2.4: Arbitrary function with positive and negative slopes.

2.3 Approximation of the Characteristic Impedance $Z_c(\omega)$

If G is assumed to be zero, the characteristic impedance is a monotonically decreasing function that becomes constant as ω tends to infinity. If G is non-zero, $|Z_c(\omega)|$ can show two regions: a segment with positive slope for low frequencies and a segment with negative slope for the rest of the function (see Figure 2.5).

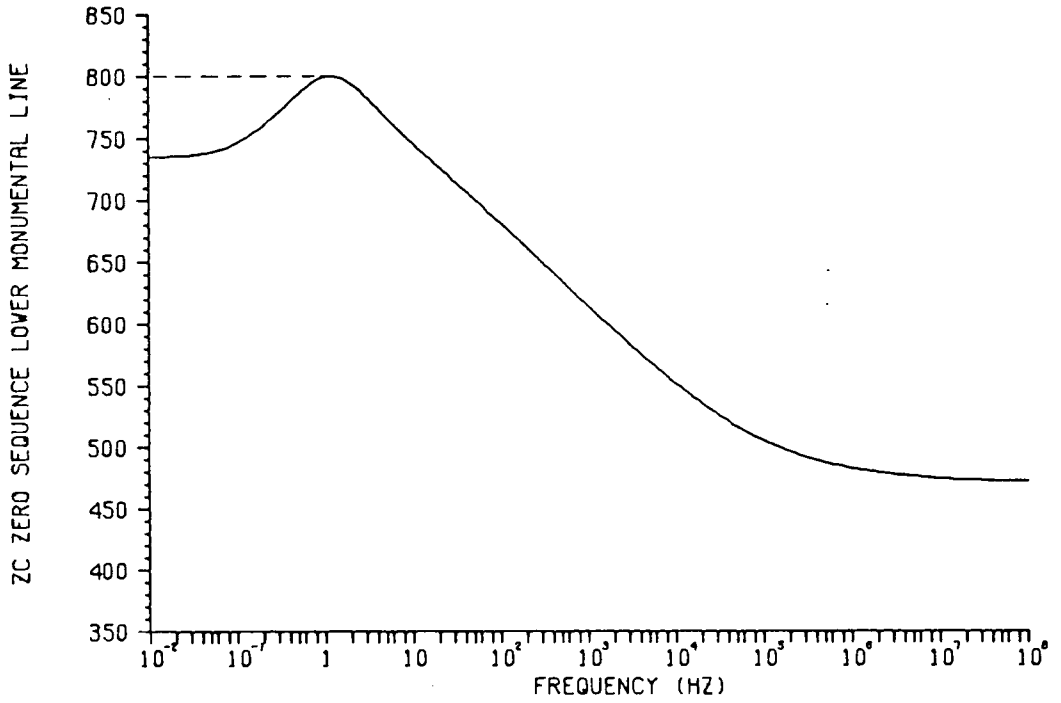

Fig. 2.5: $|Z_c(\omega)|$, zero sequence. From BPA's John Day-Lower Monumental 500 KV transmission line.

The presence of the peak in Figure 2.5 depends on the value of G. As mentioned earlier, the actual value of G does not affect significantly the results of a transient simulation, as long as it is non-zero.

In the approximating routines developed in this project, the peak in $|Z_c(\omega)|$ is eliminated, as shown by the dashed line in Figure 2.5 (this is approximately equivalent to decreasing G). Since the positive slope region is eliminated, fewer poles are needed in the approximation,

and the resulting monotonically decreasing function can be approximated with the method described in Section 2.2.

The overall accuracy of the approximation can be improved by shifting pole-zero pairs around their initial positions, until the area between $|Z_c(\omega)|$ and $|B(\omega)|$ is minimized.

When close matching at power frequency f_o is preferred to a good overall frequency response, the pole-zero pair that is closest to f_o can be shifted until the difference between $|B(\omega_o)|$ and $|Z_c(\omega_o)|$ is below an error level specified by the user. This procedure, however, may distort the overall frequency response when the specified number of poles is very small (e.g., two or three poles).

In the computer program developed as part of this thesis project, the use of either method (shifting or power frequency matching) is optional.

2.4 Approximation of the Propagation Function $A_1(\omega)$

The general shape of $|A_1(\omega)|$ is approximately the same for different line lengths and propagation modes. Three different regions can be observed:

I. A horizontal region for low frequencies (low attenuation).

II. An elbow or transition zone for mid-frequencies.

III. A high slope region for high frequencies (high attenuation).

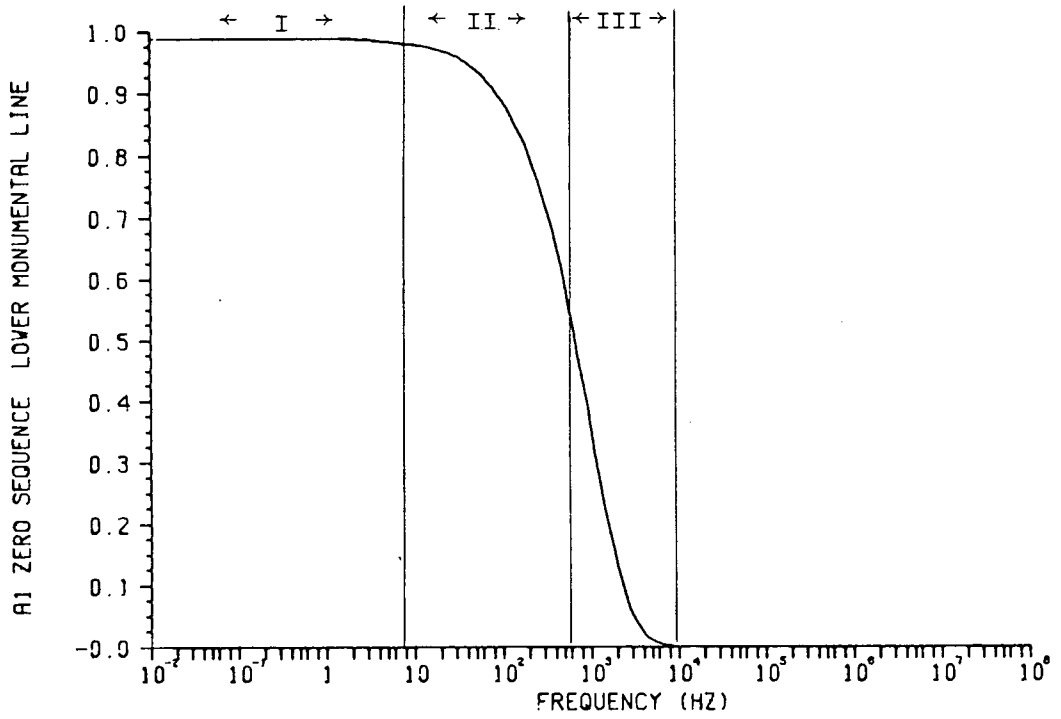

Fig. 2.6: $|A_1(\omega)|$ zero sequence.

The high attenuation region (see Figure 2.6) presents an almost constant slope of 1 unit/dec. This suggests that $|A_1(\omega)|$ could be approximated by a single-pole rational function $B_1(\omega)$,

$$B_1(\omega) = \frac{k_1}{(s + p_1)}.$$

Such a single-pole approximation is shown in Figure 2.7.

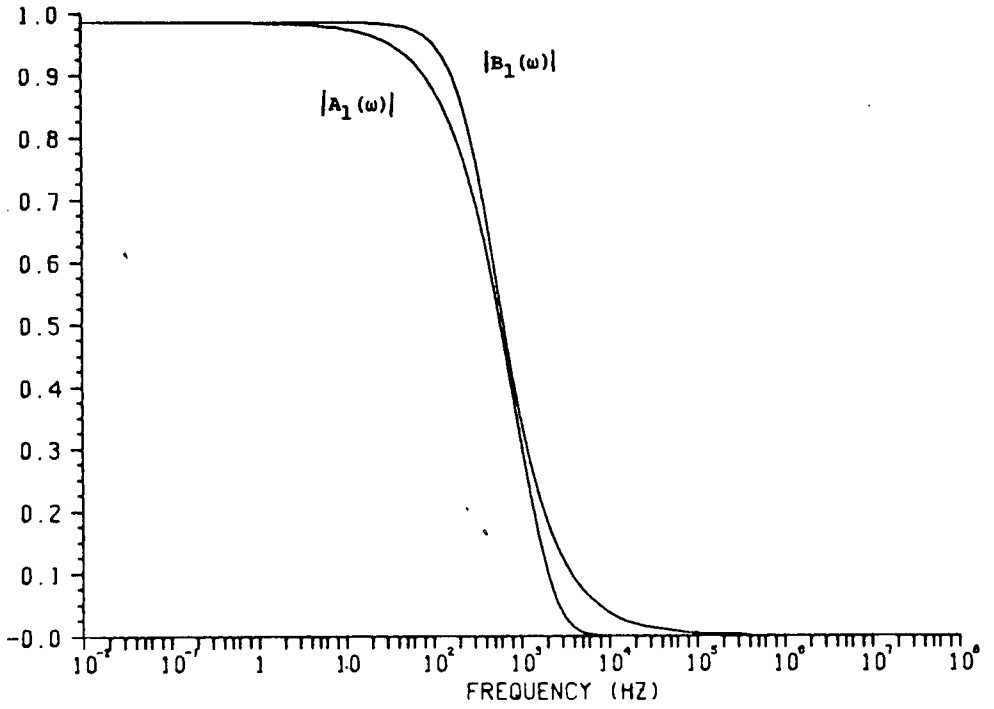

Fig. 2.7: Single-pole approximation of $|A_1(\omega)|$.

In this single-pole approximation, two large-error regions can be observed; one at very high frequencies, and the other, in the mid-frequency range.

The error in the high attenuation region is not critical. High frequencies in a typical transient case have relatively low magnitudes, and are rapidly attenuated by the line. Therefore, no additional poles will be used to improve the approximation for values of $|A_1(\omega)|$ below 0.4.

The other high-error region is in the transition zone. The accurate approximation of this zone is very important because it presents a relatively low attenuation and it usually lies close to the power frequency range, therefore, additional poles and zeros are needed to approximate this region.

One way to determine the allocation of these additional corners

is to examine the difference function between $|A_1(\omega)|$ and the single-pole approximation $|B_1(\omega)|$.

Consider the approximating function $B(\omega)$ with n poles and n-1 zeros,

$$B(\omega) = k_o \frac{(s + z_1) \ldots (s + z_n)}{(s + p_1) \ldots (s + p_{n-1}) (s + p_n)}. \tag{2.10}$$

Let $B_1(\omega)$ be the single-pole function that approximates $|A_1(\omega)|$

$$B_1(\omega) = \frac{k_1}{(s + p_n)}, \tag{2.11}$$

with $k_1 = |A_1(0)| \; p_n$.

The difference function $D(\omega)$ will be defined as,

$$\log |A_1(\omega)| - \log |B_1(\omega)| = \log |D(\omega)|$$

$$|D(\omega)| = \left| \frac{A_1(\omega)}{B_1(\omega)} \right| . \tag{2.12}$$

Introducing (2.11)

$$|D(\omega)| = \frac{1}{k_1} |A_1(\omega)| \; |s + p_n|$$

$$|D(\omega)| = p_n \frac{|A_1(\omega)| \; |s + p_n|}{|A_1(0)|}. \tag{2.13}$$

Let us now define $D_1(\omega)$ as the rational function that approximates $D(\omega)$ (substituting $A_1(\omega)$ by $B(\omega)$ in equation (2.12))

$$|D_1(\omega)| = \frac{|B(\omega)|}{|B_1(\omega)|} \tag{2.14}$$

Introducing equations (2.10) and (2.11), we finally obtain

$$|D_1(\omega)| = \frac{k_o}{k_1} \left| \frac{(s + z_1) \ldots (s + z_{n-1})}{(s + p_1) \ldots (s + p_{n-1})} \right| \tag{2.15}$$

The magnitude function of $D(\omega)$ is shown in Figure 2.9(a)

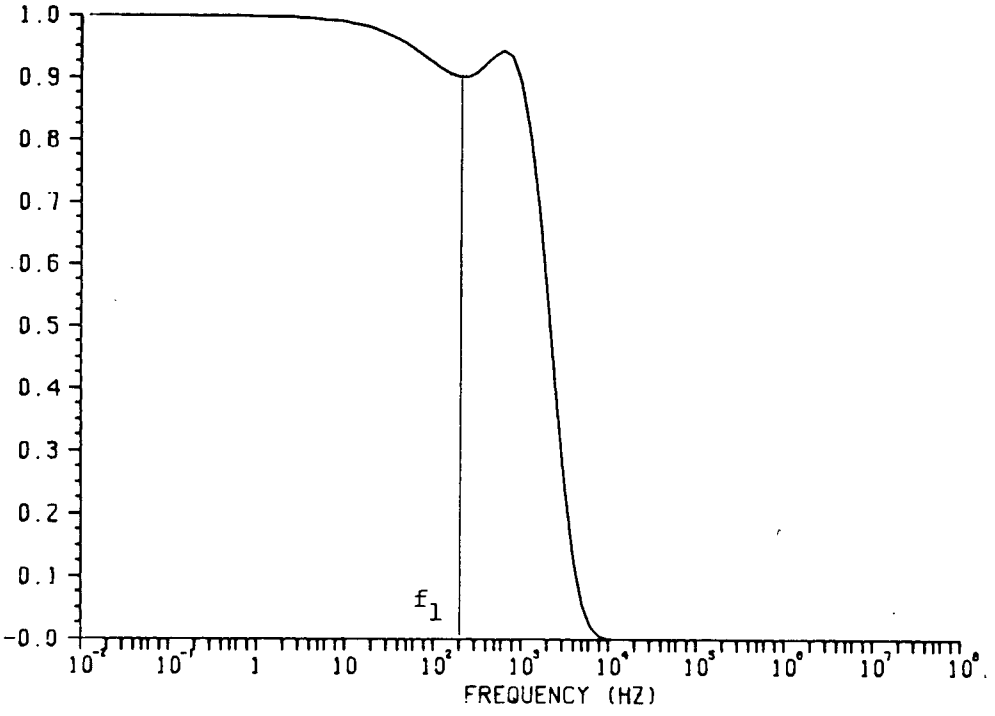

(a)

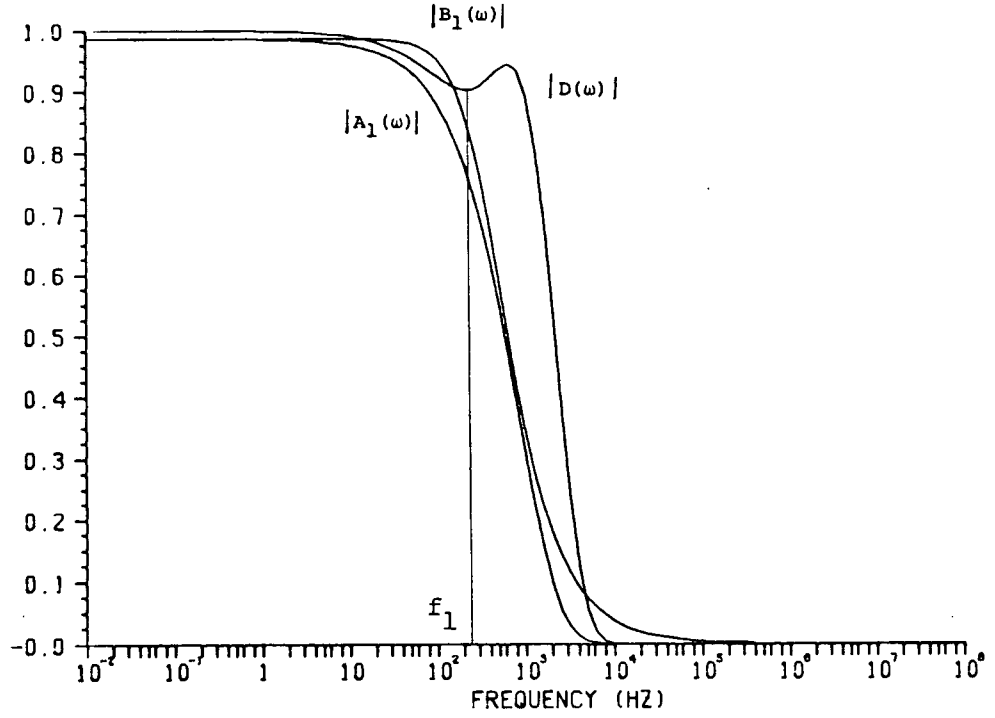

(b)

Fig. 2.9: Difference function $|D(\omega)|$. Zero sequence. Reference line (a) $|D(\omega)|$ (b) $|D(\omega)|$, $|B_1(\omega)|$ and $|A_1(\omega)|$.

The assignment of the additional corners of $|B(\omega)|$ is then reduced to the approximation of $|D(\omega)|$ by $|D_1(\omega)|$. Since we are interested in the accurate modelling of the transition zone, only the portion between $f = 0$ and $f = f_1$ will be approximated. This segment represents a monotonically decreasing function, and it is approximated with n-1 poles and zeros, using the procedure described in section 2.3.

The accuracy of a transient simulation depends strongly on the approximation of $A_1(\omega)$. If an accurate power frequency response is desired, an exact matching can be obtained by repositioning the closest pole-zero pair until the difference lies within a pre-specified range. However, shifting a single pole-zero pair may, in some instances, introduce distortion in the overall frequency response.

When overall accuracy is preferred to power frequency matching, all pole-zero pairs are shifted from their initial positions until the area between $|A_1(\omega)|$ and $|B_1(\omega)|$ is minimized.

2.5 Evaluation of τ

In the previous section the magnitude function of $A_1(\omega)$ has been approximated by a rational function $B_1(\omega)$. It is shown in appendix I-B that

$$A_1(\omega) = P(\omega)\, e^{-j\omega\tau} \tag{2.16}$$

Since $B(\omega)$ is a function of the class of minimum phase-shift, by approximating the magnitude function of $A_1(\omega)$ with $|B(\omega)|$, the phase function of $B(\omega)$ will coincide with the phase function of $P(\omega)$. To approximate both magnitude and phase of $A_1(\omega)$, τ must be evaluated so that

$$A_1(\omega) = B(\omega)\, e^{-j\omega\tau} \tag{2.17}$$

Taking the argument function of both sides of equation (2.17),

$$\arg(A_1(\omega)) = \arg(B(\omega)) - \omega\tau$$

from which,

$$\tau = \frac{1}{\omega}\left(\arg(B(\omega)) - \arg(A_1(\omega))\right). \tag{2.18}$$

Since $B(\omega)$ is not exactly equal to $P(\omega)$, the value of τ in equation (2.18) will vary with the frequency to a degree dictated by the accuracy of the approximation of the magnitude function.

The frequency dependence version of the EMTP evaluates τ by averaging the values obtained from equation (2.18) over a certain frequency range (i.e., for values of $|A_1(\omega)|$ between 0.9 and 0.7). When a high-order approximation is used, this procedure is justifiable because the differences between $|A_1(\omega)|$ and $|B(\omega)|$ are small. In this project, however, $A_1(\omega)$ is not known, but rather the propagation function of an equivalent line. Even if this equivalent line is a good estimate of the original line, the low number of poles and zeros in $B(\omega)$ only guarantees a good fit over a relatively limited frequency range. Because of these considerations, τ is evaluated at one point only, that is, at the power frequency.

2.6 Implementation of the Method

The evaluation of the equivalent line representation and the approximation of $A_1(\omega)$ and $Z_c(\omega)$, have been implemented in a FORTRAN computer program. This program (with approximately 1300 FORTRAN statements) has been designed so that a future interconnection with the existing EMTP code can be made with minimum effort.

A guide for its use is attached in appendix II-D.

CHAPTER 3

NUMERICAL RESULTS

3.1 Recapitulation

From the power frequency parameters (and dc resistance for higher accuracy) the physical configuration of an electrically equivalent line has been obtained. This permits the evaluation of $R(\omega)$ and $L(\omega)$, from which $Z_c(\omega)$ and $A_1(\omega)$ can be calculated over the entire frequency range.

The frequency-dependence version of the EMTP requires that $Z_c(\omega)$ and $A_1(\omega)$ be in a closed mathematical form. For this purpose, $Z_c(\omega)$and $A_1(\omega)$ are approximated by rational functions using approximating techniques that permit the use of a very low number of poles and zeros.

The transmission line described in Chapter 1 will be simulated using the techniques described in this thesis project. The results will be compared with those obtained using the frequency-dependence version of the EMTP.

3.2 Evaluation of the Line Parameters From the Equivalent Line Configuration

The input data necessary to otain the equivalent line configuration for the reference line (see Figure 1.3) is shown below:

Power frequency = 60 Hz

Line length = 500 km

Shunt conductance = $0.3 \cdot 10^{-7}$ S/km

Earth resistivity = 100 $\Omega \cdot$ m

dc resistance (R_{dc}) = 0.02619 Ω/km

The electrical parameters at 60 Hz (from the output of the Line Constants Program) are:

Positive sequence:

R_1 = 0.02643 Ω/km

L_1 = 0.8808 mH/km

C_1 = 0.0133 μF/km

Zero sequence:

R_o = 0.1974 Ω/km

L_o = 3.3308 mH/km

C_o = 0.008361 μF/km

The resulting equivalent line configuration is summarized below.

	Reference Line	Equivalent Line			
		R_{dc} given		R_{dc} not given	
	Parameters (in m)	Parameters (in m)	Error (%)	Parameters (in m)	Error (%)
d	15.361	15.058	1.97	14.334	6.69
GMR	0.18843	0.18444	2.12	0.17528	6.98
D	34.780	34.070	2.22	32.662	6.09
h	15.240	14.990	1.64	14.675	3.71
r	0.19825	0.196490	0.89	0.19649	0.89

The variation of R and L over the frequency range from 10^{-2} to 10^{8} Hz, is calculated from the equivalent line configurations (see graphs 2.1 through 2.4). The output from the Line Constants Program is used as reference.

From these graphs, the following observations can be made:

a) The estimated values of R and L are more accurate when R_{dc} is known.

b) Positive sequence parameters present larger error levels than zero sequence parameters.

c) The resistances present larger errors than the inductances.

When R_{dc} is known, the skin effect correction factor s is calculated from the increase in the self-resistance from its dc to its 60 Hz value

$$R_1(\omega) = R_s(\omega) + (\Delta R_s(\omega) - \Delta R_m(\omega)).$$

Since the term $(\Delta R_s(\omega)-\Delta R_m(\omega))$ is negligible at 60 Hz, the increase in $R_s(\omega)$ can be assumed to be caused by skin effect only. Therefore, the value of s estimated when R_{dc} is known is very accurate (see section 1.3).

When R_{dc} is not known, s cannot be estimated accurately because it is calculated from the increase in the internal inductance from its dc to its power frequency value; and as it was shown in section 1.3, the evaluation of L_{int} using the equivalent line configuration is very inaccurate. Also, when R_{dc} is not known, the finer adjustment of the line configuration explained in section 1.4 cannot be made, and the evaluation of Carson's correction terms becomes less accurate.

The positive sequence resistance is more sensitive to differences in ΔR_s and ΔR_m, than the zero sequence resistance. The reason is that R_1 depends on $(\Delta R_s-\Delta R_m)$, while R_o depends on $(\Delta R_s + (n-1)\,\Delta R_m)$;

since ΔR_s and ΔR_m are relatively large, and of comparable magnitudes (for mid to high frequencies), small errors in ΔR_s and ΔR_m produce relatively large errors in $(\Delta R_s - \Delta R_m)$, while $(\Delta R_s + (n-1)\Delta R_m)$ is affected to a lesser degree.

The evaluation of the inductances is more accurate than the evaluation of the resistances because skin effect only affects L_{int}, which is only a small fraction of L_1 and L_o. Furthermore, the magnitudes of Carson's correction terms are considerably smaller for the reactances. This can be easily visualized if we note that, for example, R_o increases over 10^4 times from its dc value, while L_o decreases only to $1/4^{th}$ of its dc value, when the frequency is in the MHz range.

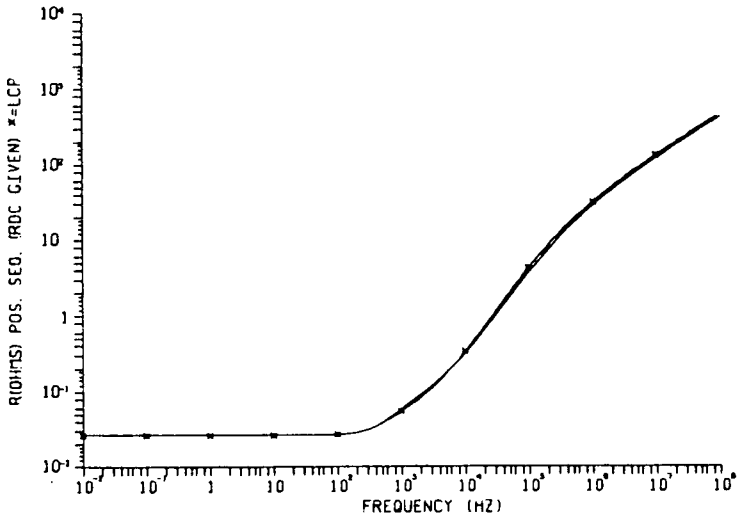

(a)

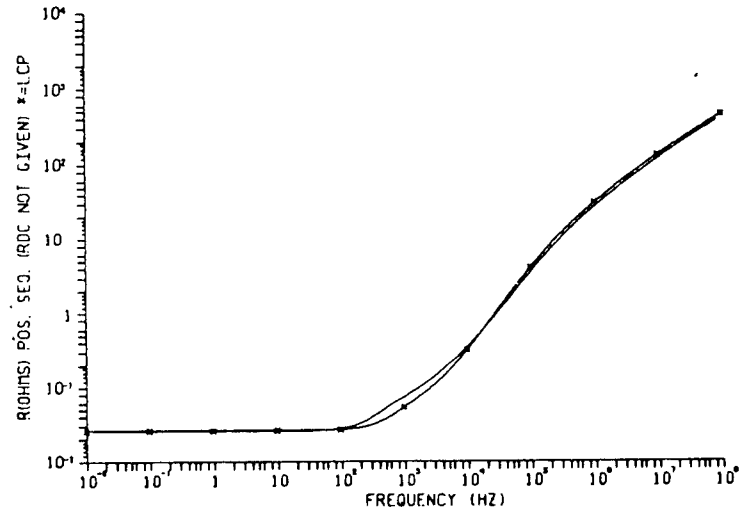

(b)

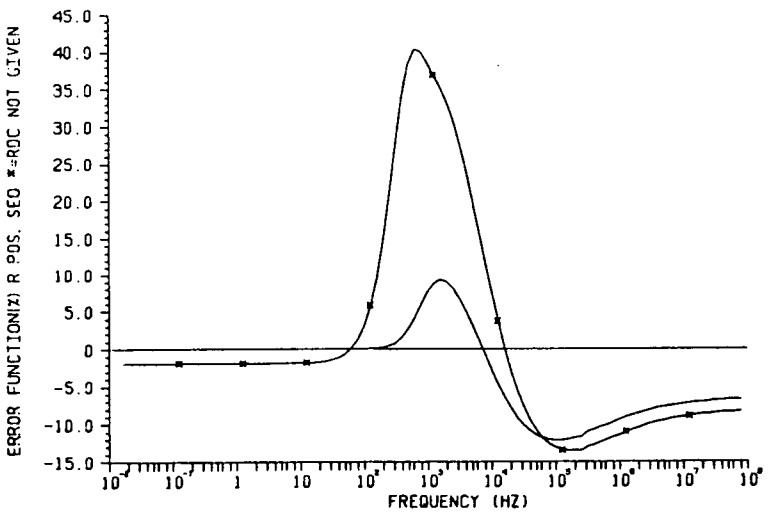

(c)

Graph 2.1: Positive sequence resistance. (a) R_{dc} given (b) R_{dc} not given (c) Error function.

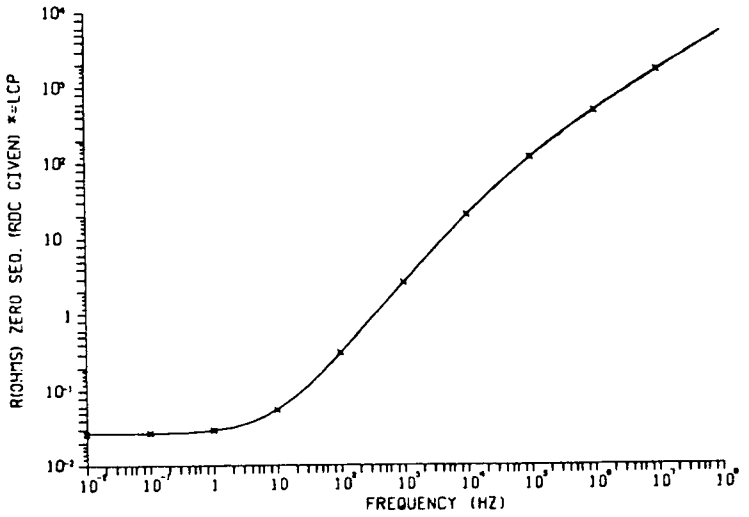

(a)

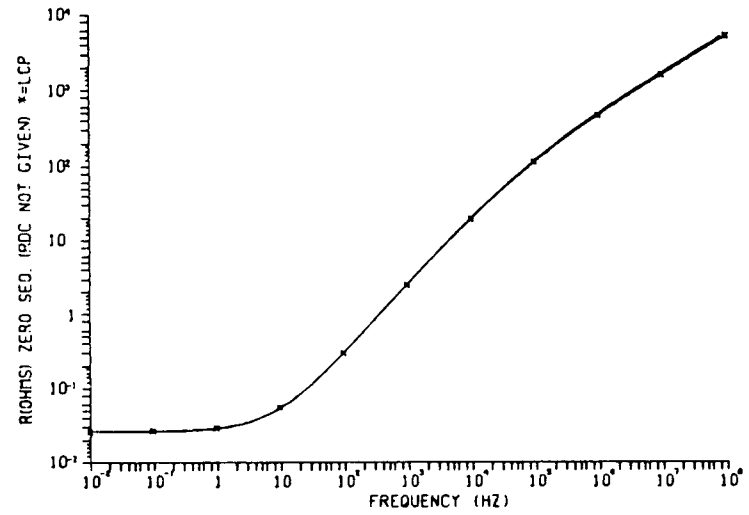

(b)

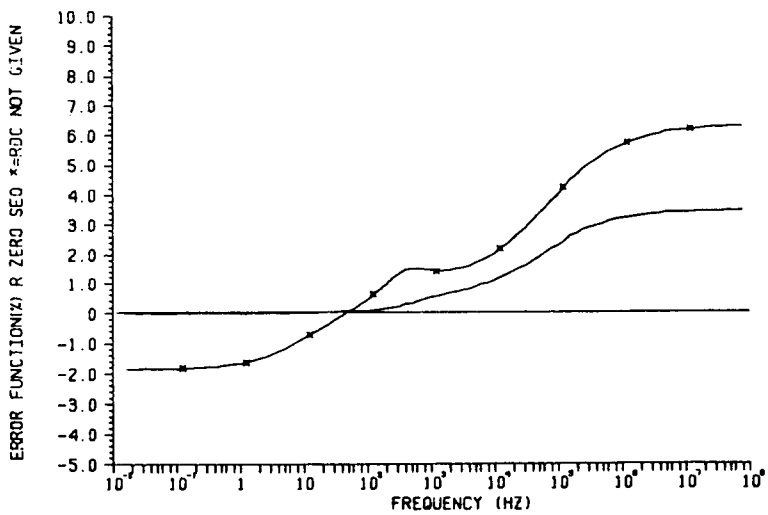

(c)

Graph 2.2: Zero sequence resistance. (a) R_{dc} given
(b) R_{dc} not given (c) Error function.

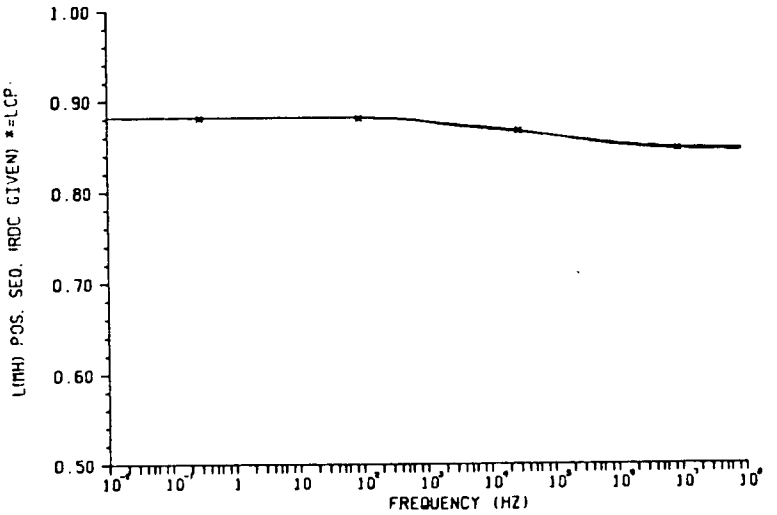

(a)

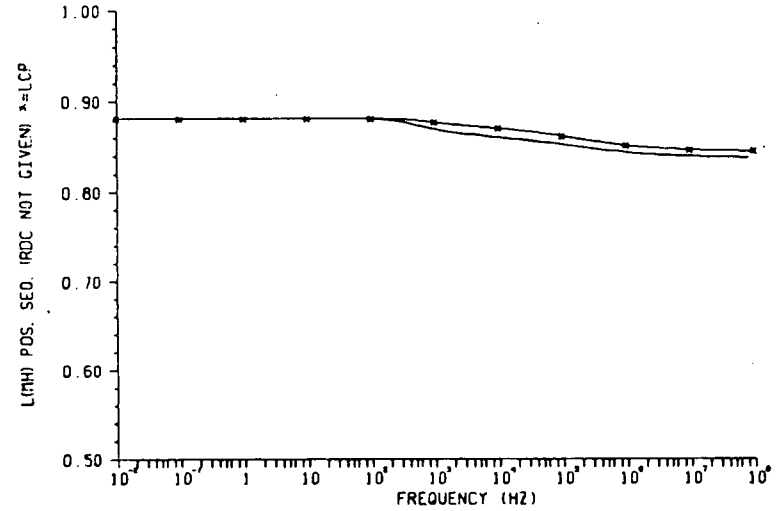

(b)

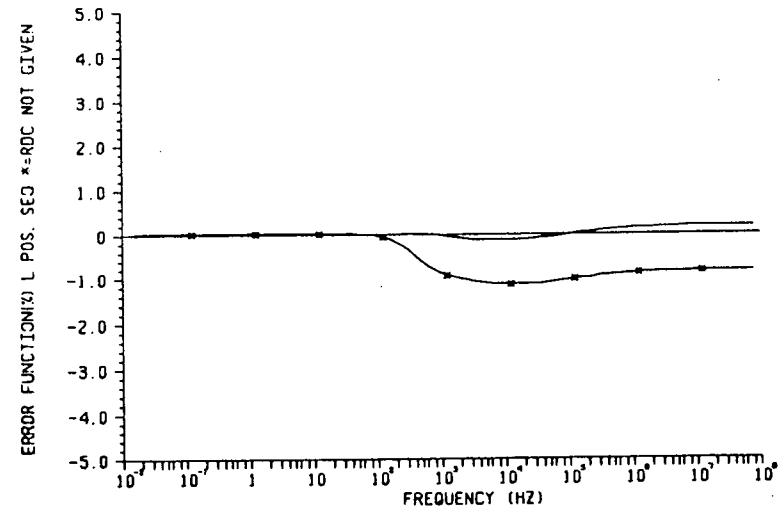

(c)

Graph 2.3: Positive sequence inductance. (a) R_{dc} given (b) R_{dc} not given (c) Error function.

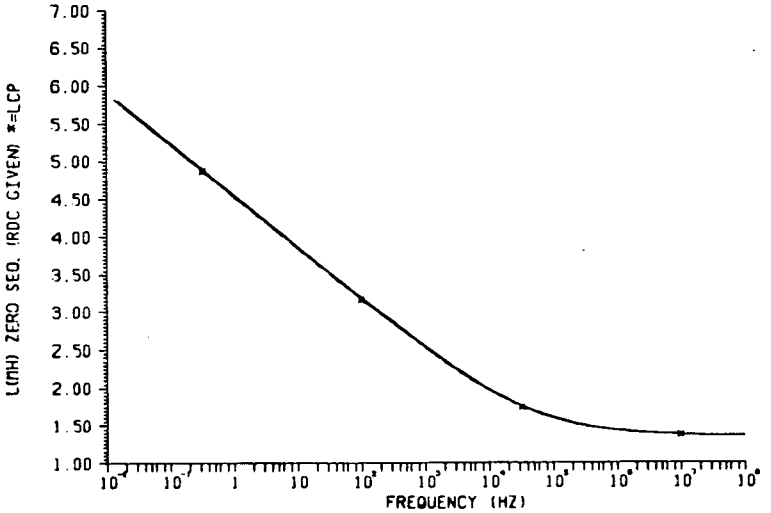

(a)

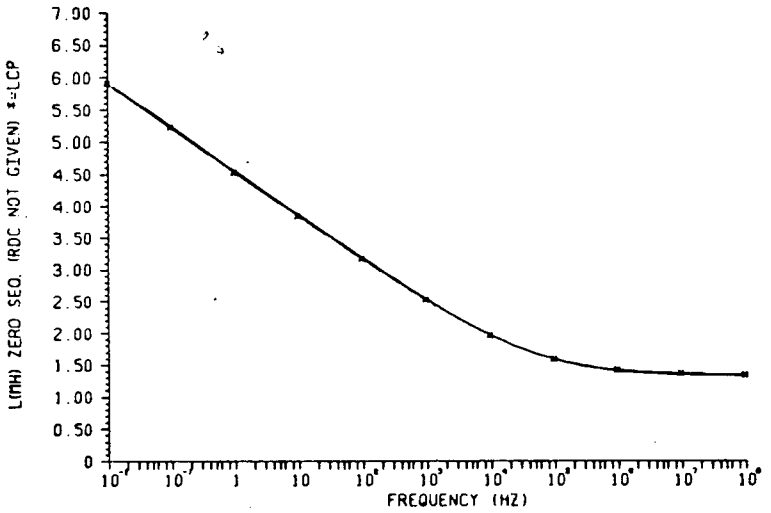

(b)

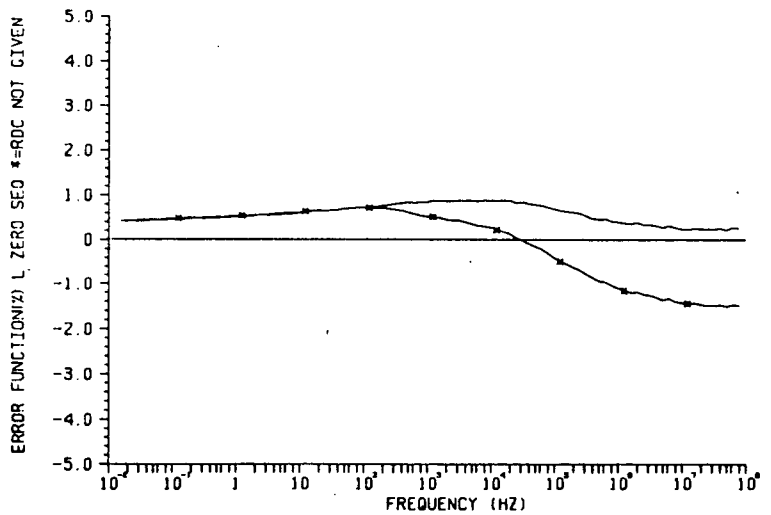

(c)

Graph 2.4: Zero sequence inductance. (a) R_{dc} given
(b) R_{dc} not given (c) Error function.

3.3 Evaluation of $A_1(\omega)$ and $Z_c(\omega)$

The magnitude and phase functions of $A_1(\omega)$ and $Z_c(\omega)$ are shown in graphs 2.5 through 2.12.

Note that the error levels in the evaluation of the positive sequence resistance, are also reflected in $Z_c(\omega)$ and $A_1(\omega)$. Also note that the high error region in the phase function of $Z_c(\omega)$, positive sequence (for frequencies above 100 Hz), is not very significant because the phase angle is very close to zero, and small differences between the phase angles of the real function and the approximation, appear as large relative errors (see graph 2.9).

Similarly, when the magnitude of $A_1(\omega)$ is below 0.05 times its dc value, large relative errors lose their significance. In graph 2.5 the error function for $|A_1(\omega)| < 0.05$ has been omitted.

Note that the phase functions of $Z_c(\omega)$ have been plotted in degrees, while the phase functions of $A_1(\omega)$ have been plotted in radians (allowing arg $(A_1(\omega)) > \pi$).

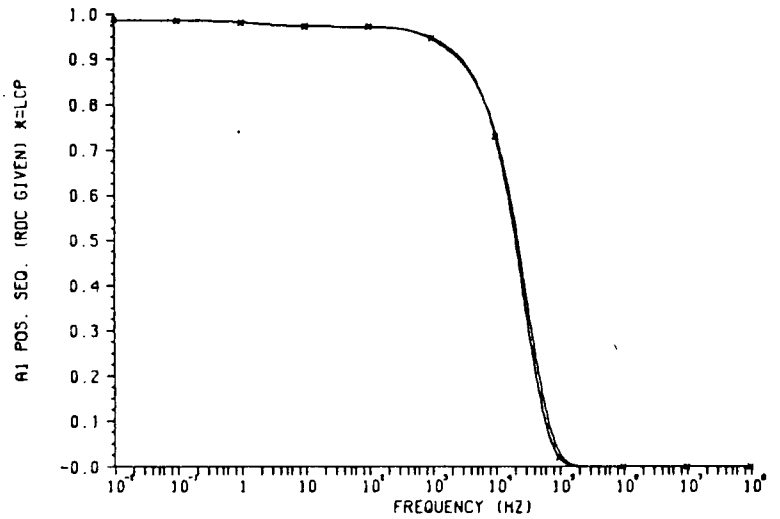

(a)

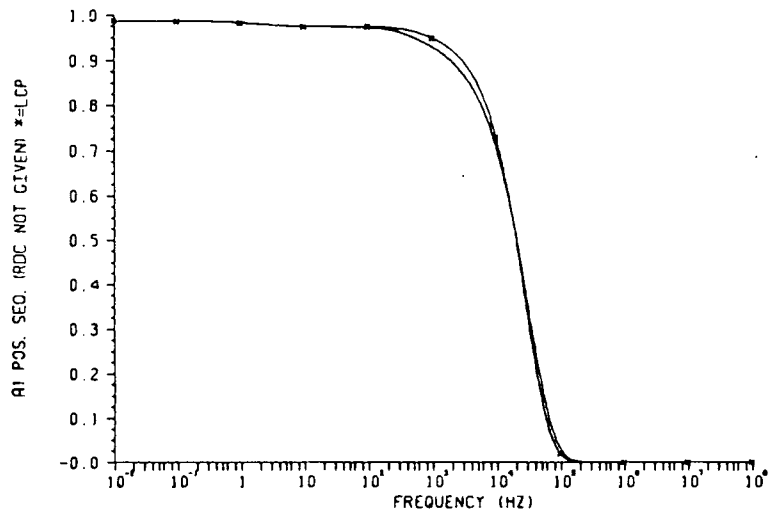

(b)

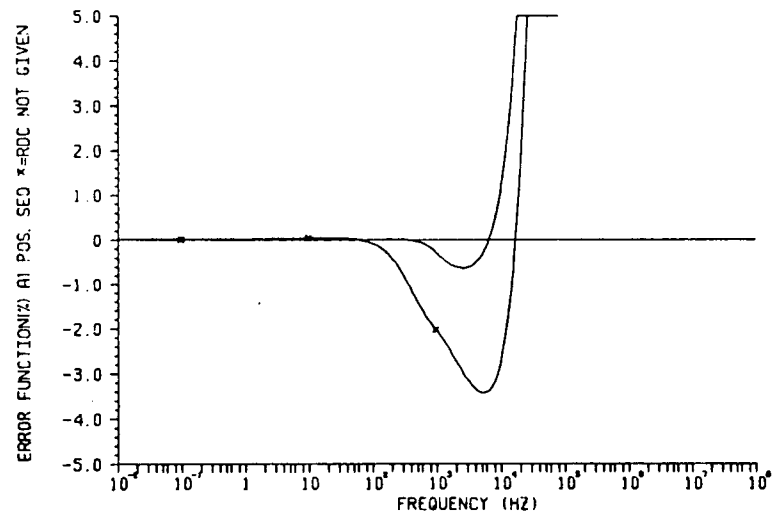

(c)

Graph 2.5: A_1 magnitude function, positive sequence.
(a) R_{dc} given (b) R_{dc} not given (c) Error function.

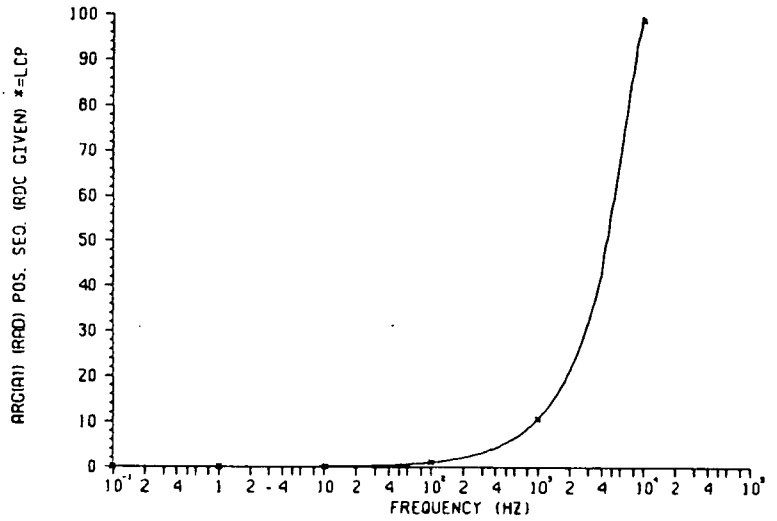

(a)

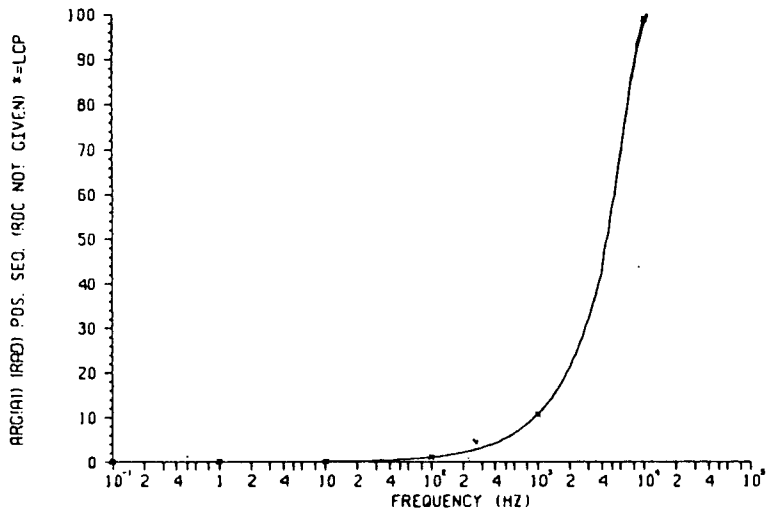

(b)

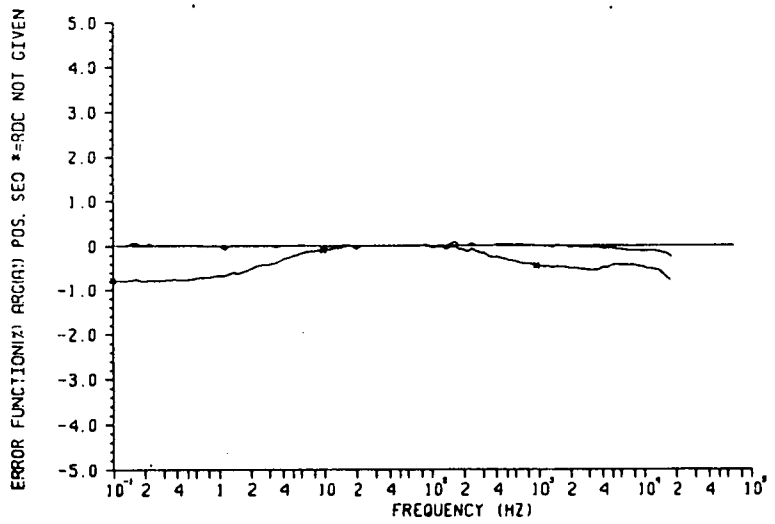

(c)

Graph 2.6: A_1 phase function, positive sequence.
(a) R_{dc} given (b) R_{dc} not given (c) Error function.

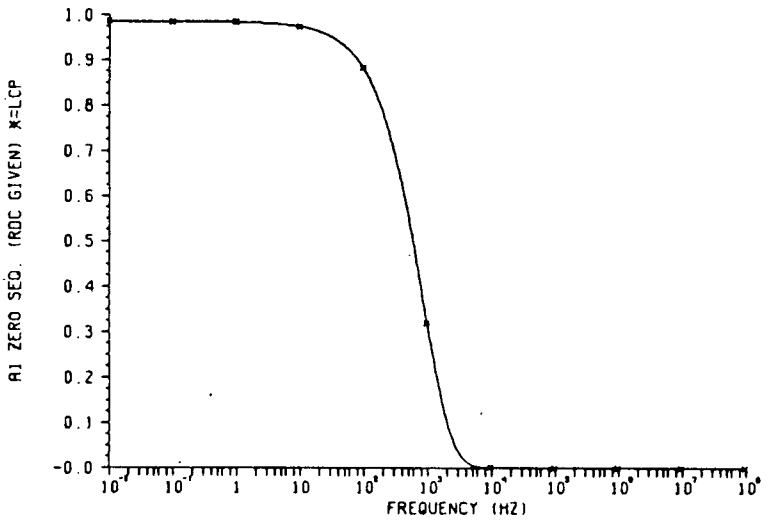

(a)

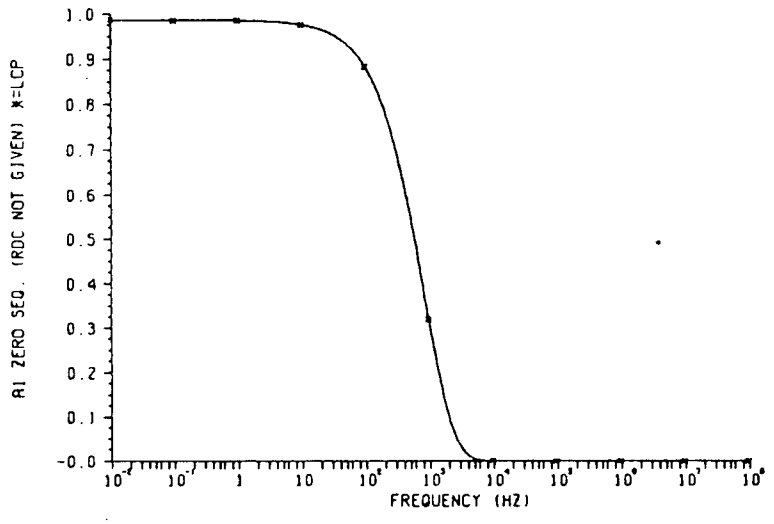

(b)

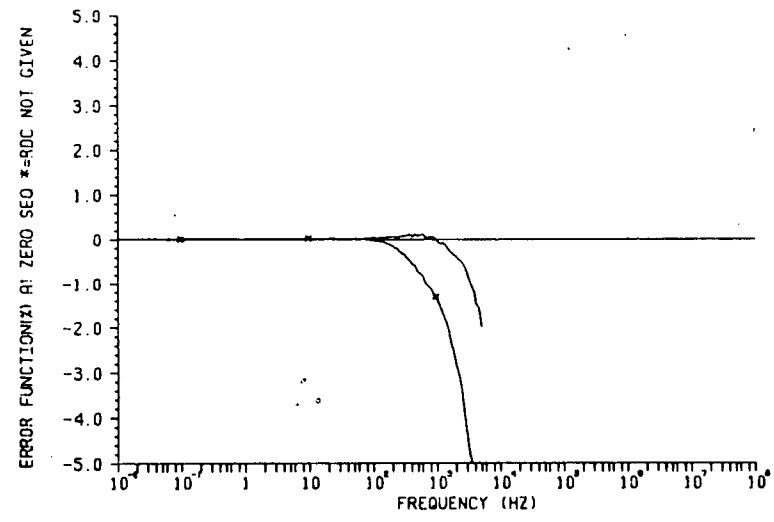

(c)

Graph 2.7: A_1 magnitude function, zero sequence.
(a) R_{dc} given (b) R_{dc} not given (c) Error function.

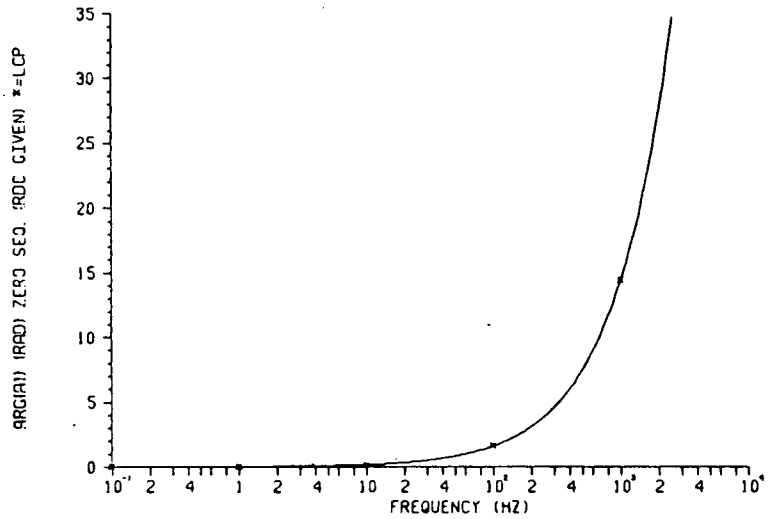

(a)

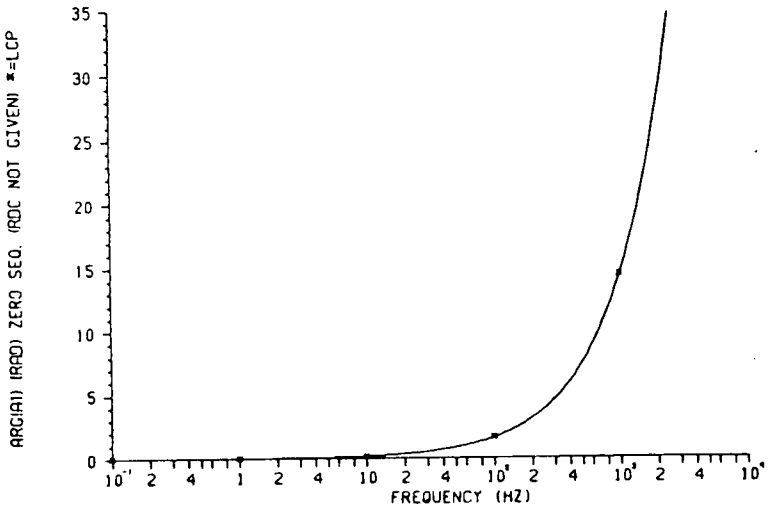

(b)

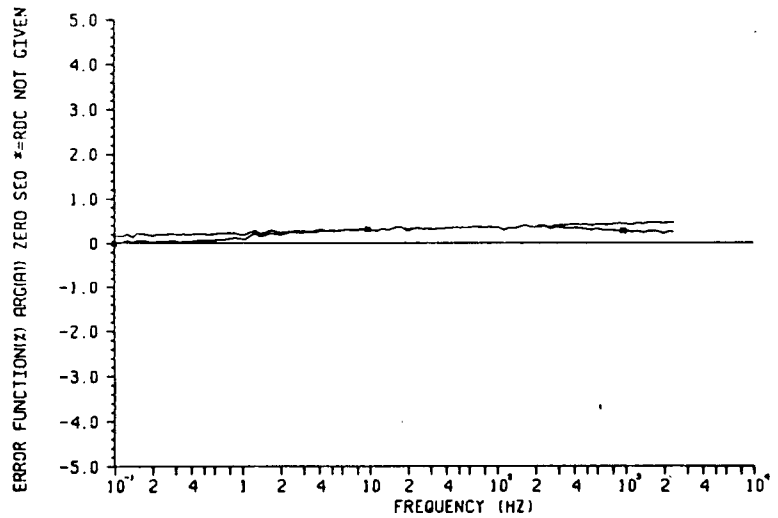

(c)

Graph 2.8: A_1 phase function, zero sequence.
(a) R_{dc} given (b) R_{dc} not given (c) Error function.

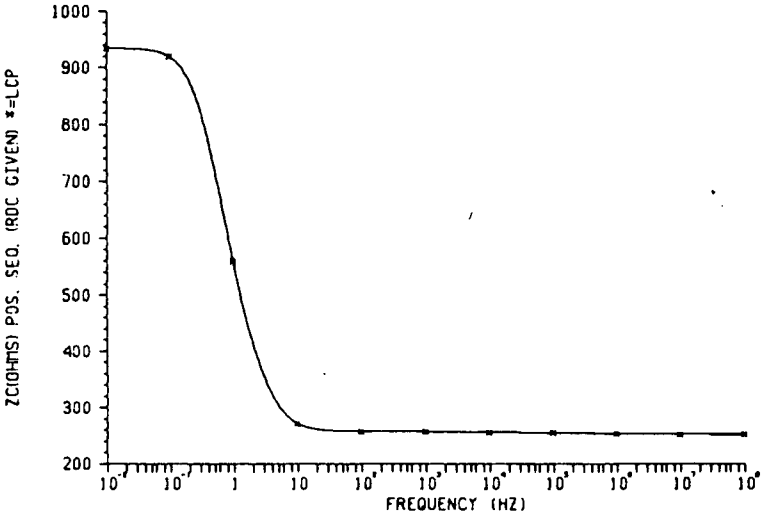

(a)

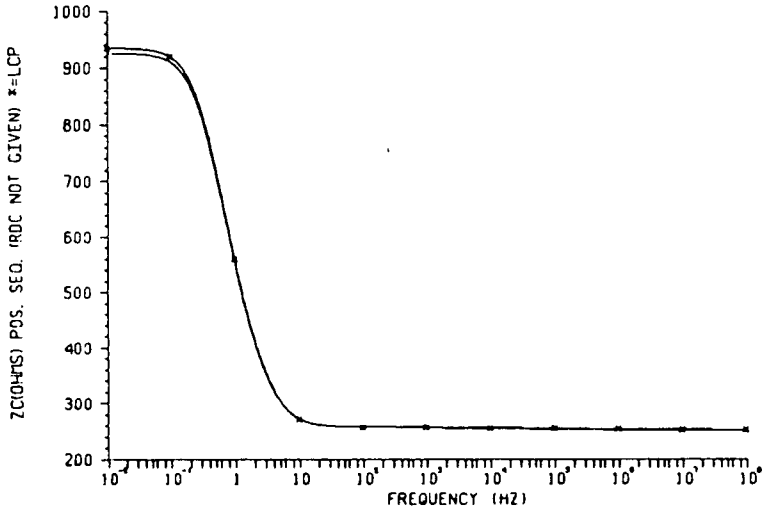

(b)

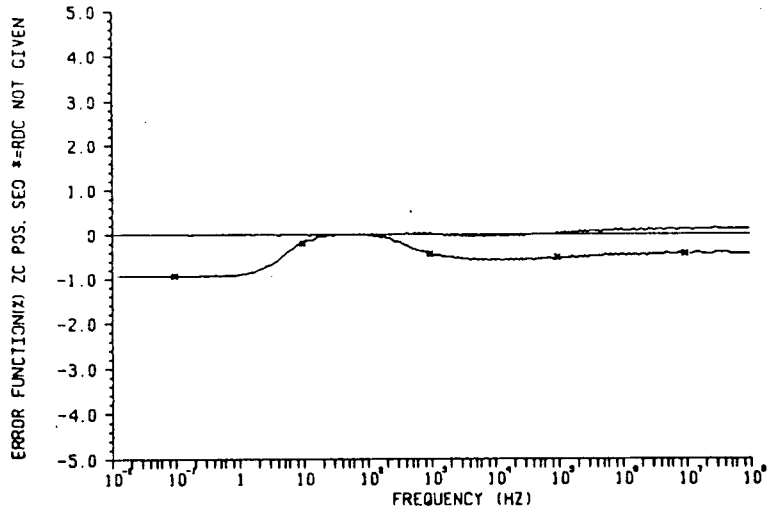

(c)

Graph 2.9: Z_c magnitude function, positive sequence.
(a) R_{dc} given (b) R_{dc} not given (c) Error function.

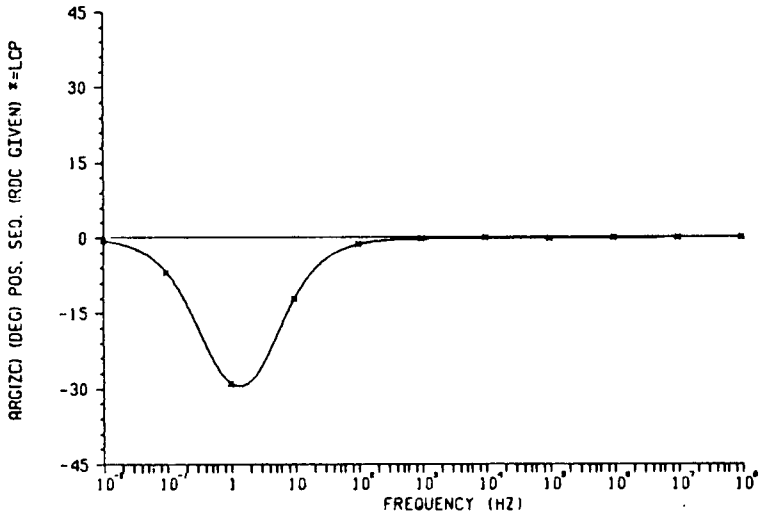

(a)

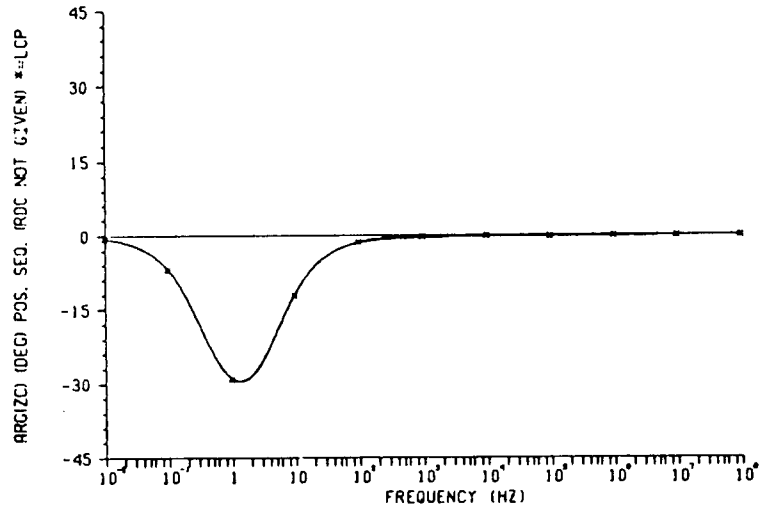

(b)

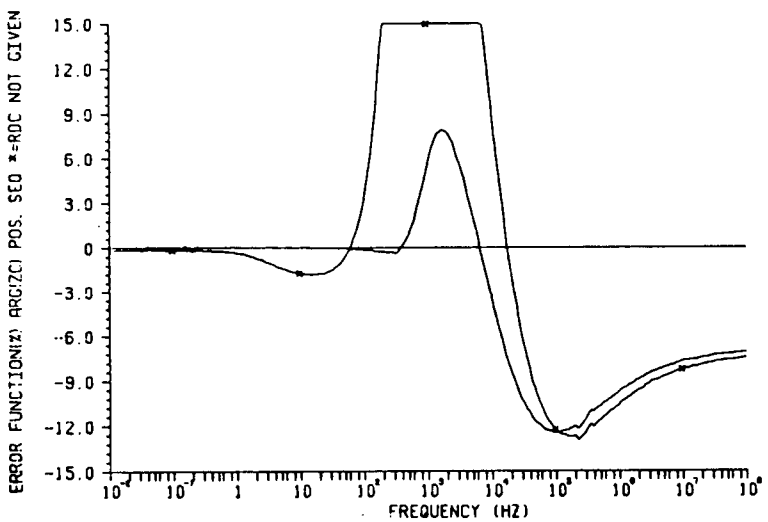

(c)

Graph 2.10: Z_c phase function, positive sequence.
(a) R_{dc} given (b) R_{dc} not given (c) Error function.

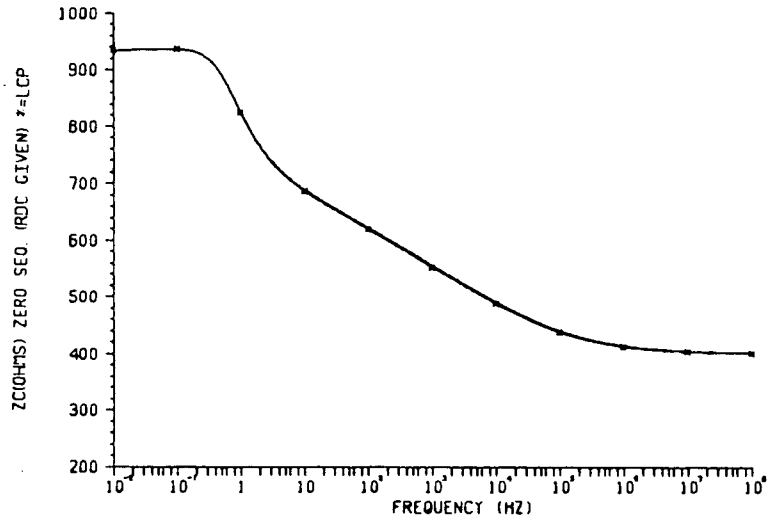

(a)

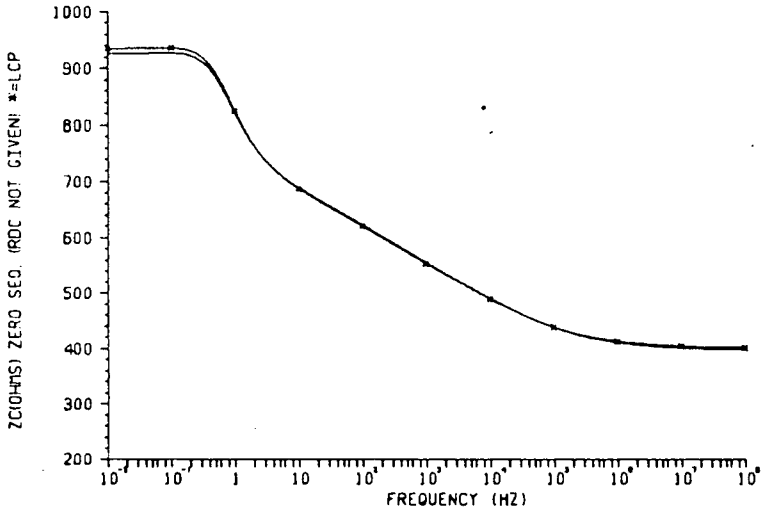

(b)

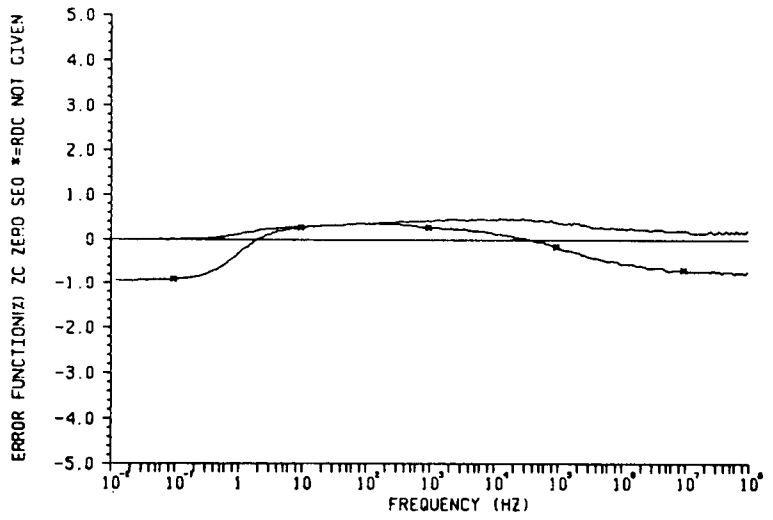

(c)

Graph 2.11: Z_c magnitude function, zero sequence.
(a) R_{dc} given (b) R_{dc} not given (c) Error function.

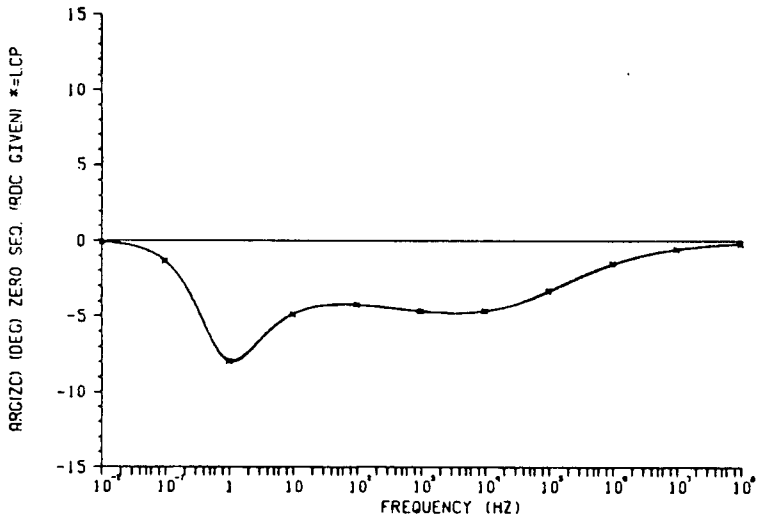

(a)

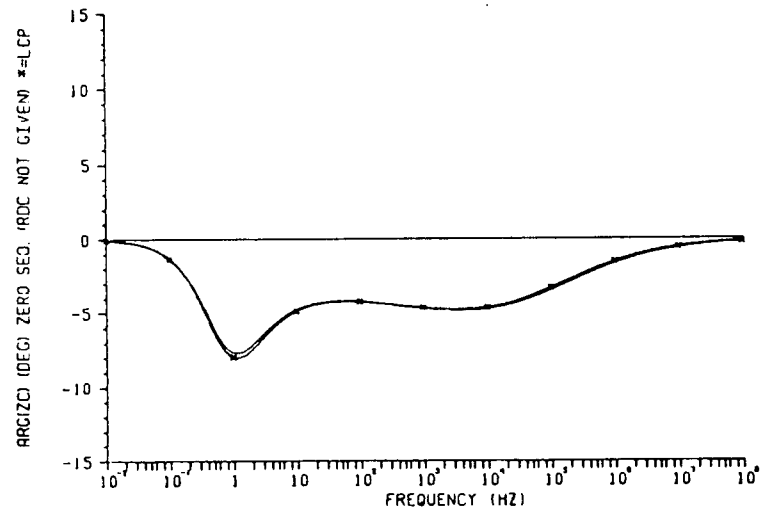

(b)

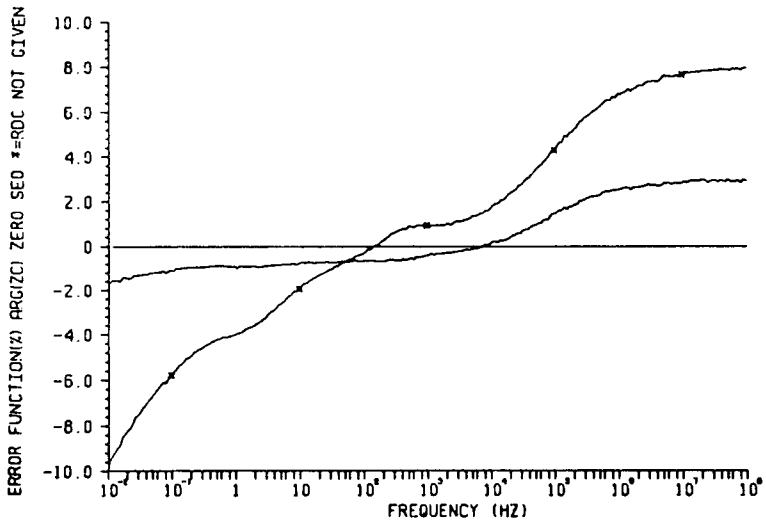

(c)

Graph 2.12: Z_c phase function, zero sequence.
(a) R_{dc} given (b) R_{dc} not given (c) Error function.

3.4 Low-Order Rational-Functions Approximations

In order to assess the performance of the rational-functions approximating routines, $A_1(\omega)$ and $Z_c(\omega)$ calculated from the equivalent line configuration (of the reference line) will be approximated with various numbers of poles and zeros. For these approximations R_{dc} is assumed to be known.

Graphs 2.13 to 2.16 show the error functions of these approximations with and without the pole-zero shifting procedure explained in Chapter 2. When no shifting is used, the error at 60 Hz has not been allowed to exceed 0.5%.

The number of poles needed to approximate a given function depends on its particular shape and the accuracy desired. In the magnitude of the zero sequence propagation function, for instance, there is little improvement when the number of poles is increased beyond five. Note that for frequencies above 300 Hz, the error remains unchanged regardless the number of poles used because no additional poles are added to model this region. For frequencies above 1 KHz, that is, for the high attenuation region ($|A_1(\omega)| < 0.1$) the error exceeds 5%, but as mentioned in Chapter 2 the accurate approximation of this region is not important.

Also note that the shifting procedure reduces the overall error, but slows considerably the fitting process (see table 3.1) as compared to the simple power frequency matching process.

The approximation of $A_1(\omega)$ for positive sequence, is particularly difficult in this line because of the small depression in $|A_1(\omega)|$ in the 1 to 100 Hz region (see graphs 2.13 and 2.17). This irregularity, usually present for lengths of 500 km or more, is responsible for the increase in the error of the 5-pole approximation over the 4-pole one. However, as the number of poles increases beyond 5, the overall error

decreases as expected. It should be noted that the number of shifting loops for these calculations was limited to four (to decrease costs).

If the shifting process had been allowed to continue automatically (until the improvement between iterations were less than 1%), a better approximation would have been obtained.

The approximation of $Z_c(\omega)$ for zero sequence is comparatively more difficult because a large number of poles is necessary to approximate the endpoints (see graphs 2.16 and 2.20). The EMTP routines needed 17 poles to accurately approximate the whole frequency range. However, errors in excess of 1% only occur for frequencies above 20 KHz, therefore, a number of poles larger than eight is not justifiable in the context of this project. Note that in this case, if the shifting process had been allowed to proceed beyond four iterations, the error in the low to mid frequencies would have increased slightly to decrease the error at high frequencies.

The approximation of $Z_c(\omega)$ for positive sequence, is an interesting case where the pole-zero shifting procedure is very important for the accurate matching of the function. When no shifting is used, an increase in the order of the approximation just accumulates the additional poles in the low frequency region, distorting the approximation rather than improving it.

In graphs 2.17 through 2.20, three sets of approximations are shown: a very low-order approximation (2 poles), a more accurate approximation (10 poles), and a compromise between accuracy and number of poles (4 poles for $Z_c(\omega)$ and $A_1(\omega)$ positive sequence, 5 poles for $A_1(\omega)$ zero sequence, and 6 poles for $Z_c(\omega)$ zero sequence).

One of the main advantages of the low-order approximation routines, is that they are very inexpensive computationally. A high-

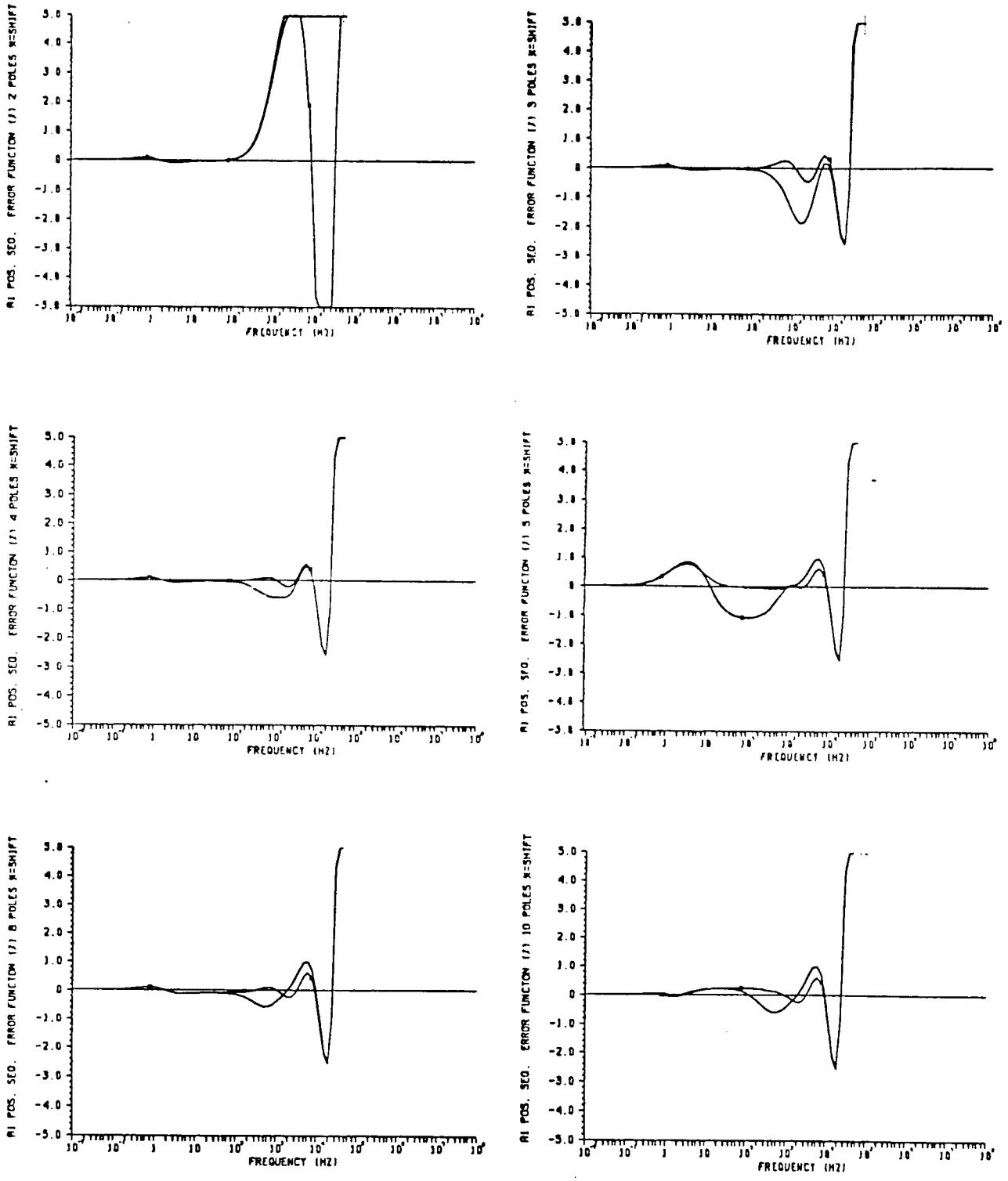

Graph 2.13: Error functions. Low-order approximation of A_1, positive sequence.

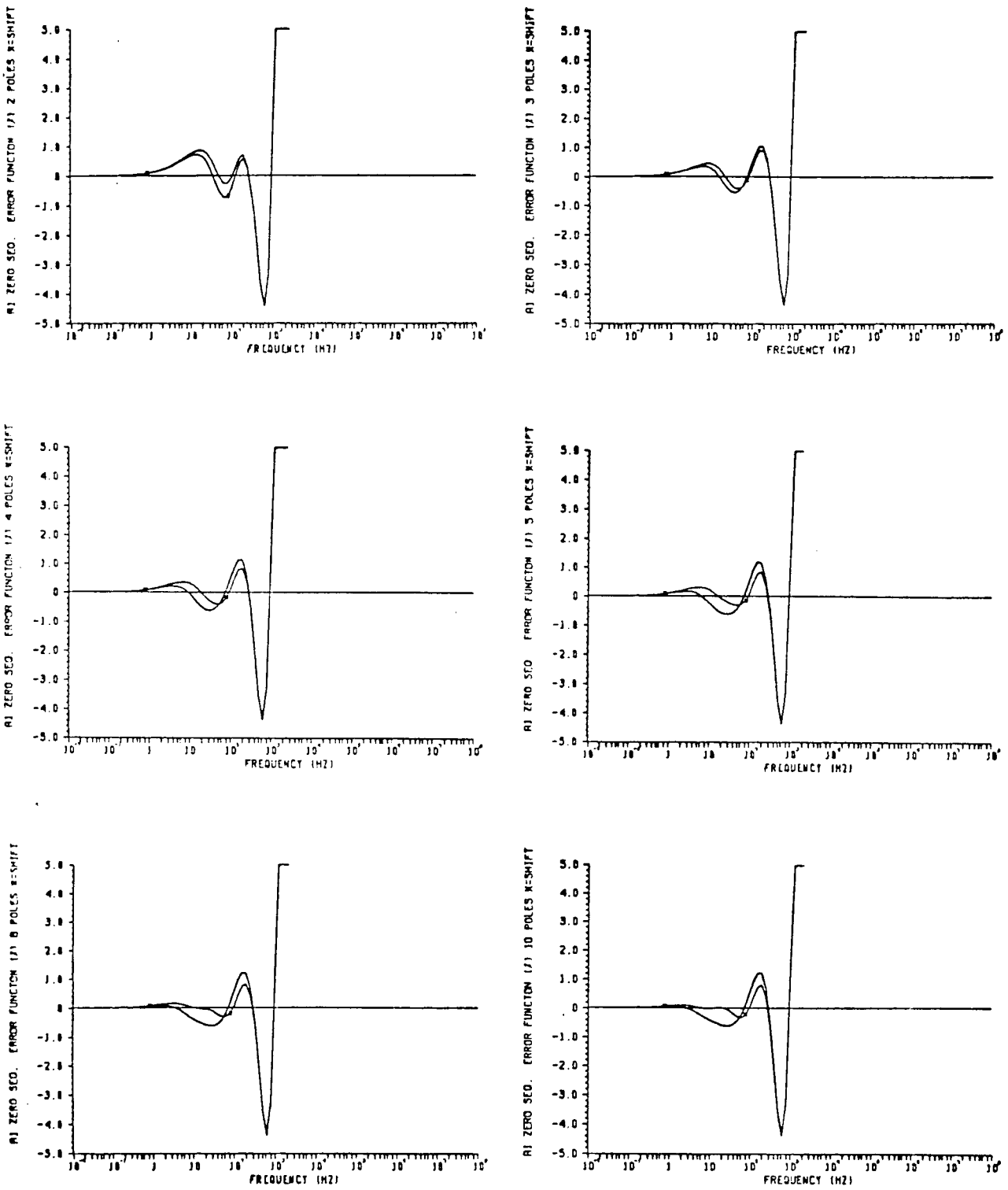

Graph 2.14: Error functions. Low-order approximation of A_1, zero sequence.

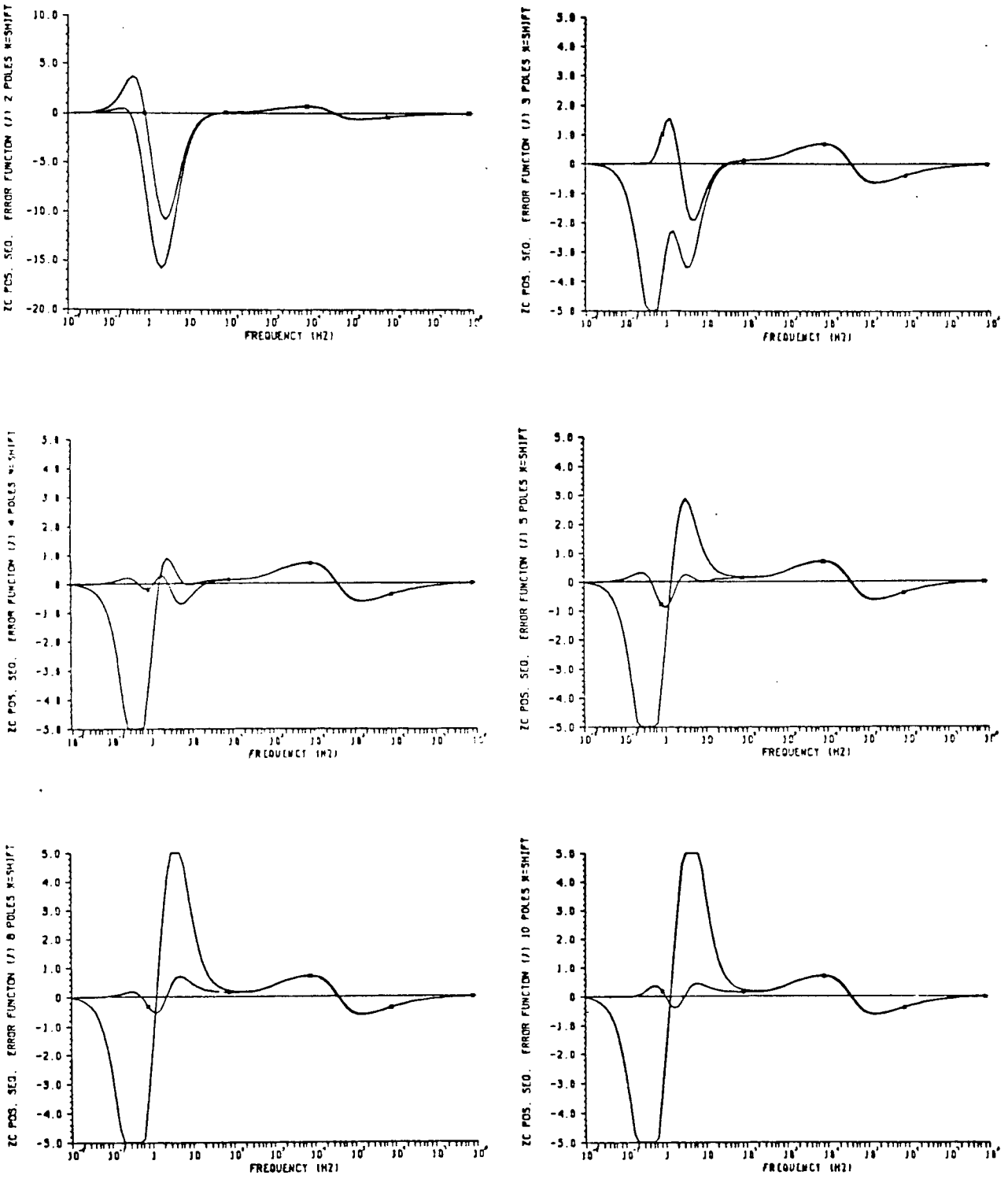

Graph 2.15: Error functions. Low-order approximation of Z_C, positive sequence.

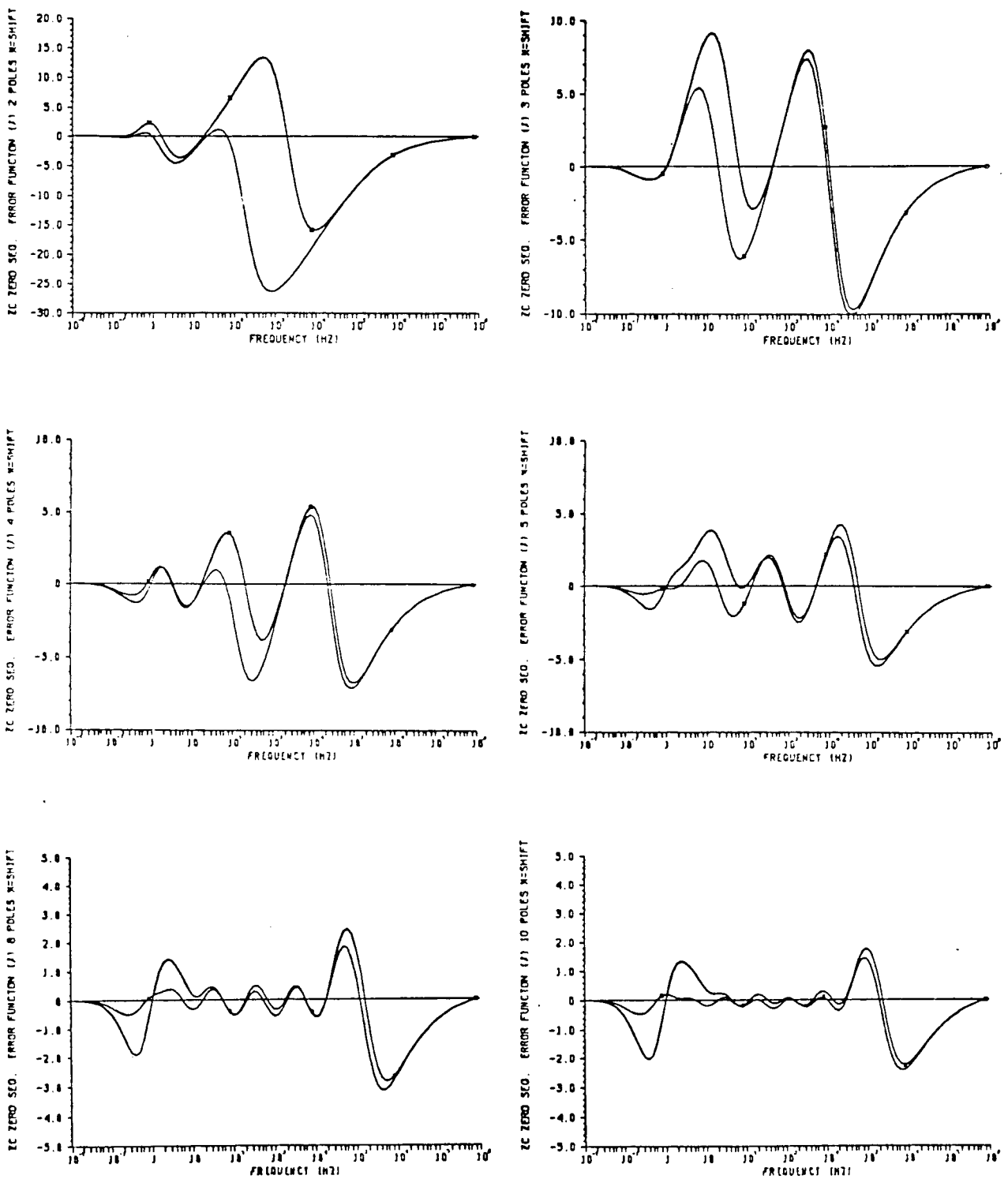

Graph 2.16: Error functions. Low-order approximation of Z_c, zero sequence.

accuracy approximation produced with the EMTP routines can cost over $10.00, while low-order approximation costs are usually under $3.00 (using 10 poles in $Z_c(\omega)$ and $A_1(\omega)$, and 4 shifting loops). These running costs are based on UBC's rates of $1,200.00 per hour of CPU time under Terminal use.

Table 3.1 shows the cost of a high accuracy simulation of the reference line using the EMPT routines. The corresponding approximations are shown in graphs 2.21 to 2.24, where the output from the Line Constants Program is used as reference.

UBC's line constants program	$ 4.50
TRANFLIN.0	
(Calculation of $Z_c(\omega)$ and $A_1(\omega)$)	$ 0.24
TRANA1.0	
(approximation of $A_1(\omega)$)	
Positive sequence (18 poles, 12 zeros)	$ 1.23
Zero sequence (21 poles, 15 zeros)	$ 1.11
TRANZC.0	
(approximation of $Z_c(\omega)$)	
Positive sequence (9 poles, 9 zeros)	$ 1.18
Zero sequence (17 poles, 17 zeros)	$ 1.75
Total	$ 10.01

Table 3.1: Costs in $cc of the frequency-dependence routines of the EMTP.

Table 3.2 shows the running costs of the low-approximation program for various numbers of poles and zeros.

Number of Poles				Cost $cc	
$Z_c(\omega)$		$A_1(\omega)$			
Positive Sequence	Zero Sequence	Positive Sequence	Zero Sequence	Shifting	No shifting
2	2	2	2	0.25	0.16
3	3	3	3	0.34	0.16
4	4	4	4	0.51	0.16
5	5	5	5	0.93	0.15
6	6	6	6	1.27	0.17
7	7	7	7	1.63	0.20
8	8	8	8	2.04	0.12
9	9	9	9	2.53	0.17
10	10	10	10	3.05	0.17
4	6	4	5	0.79	--

Table 3.2: Costs in $cc of the low-approximation program.

It is interesting to note that high and low-order approximations of $A_1(\omega)$ have comparable error levels when $|A_1(\omega)|$ is greater than 0.4. Therefore the higher computational effort in the high-order approximation can be attributed to the modelling of the high attenuation region of $A_1(\omega)$.

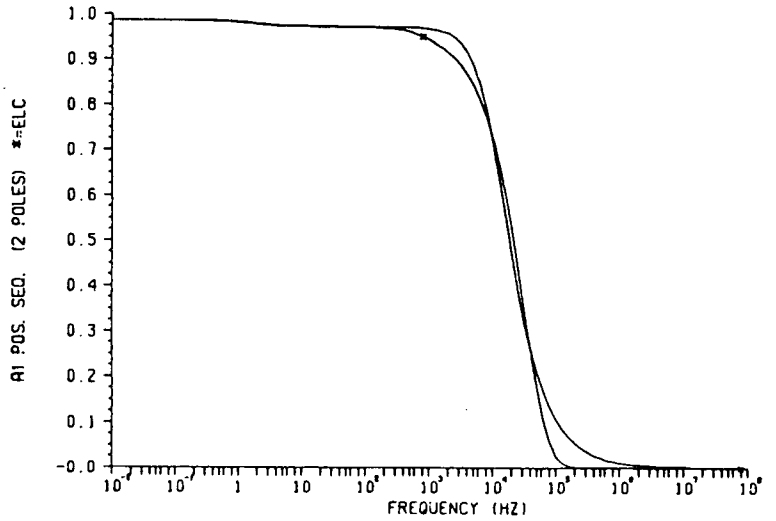

(a)

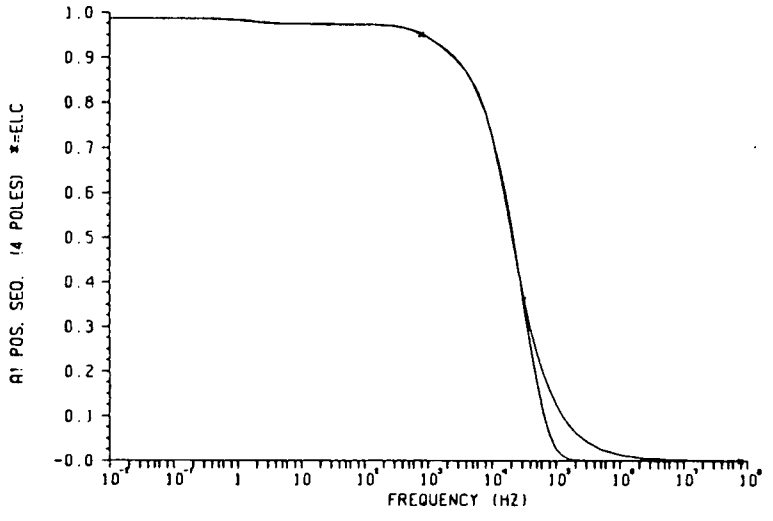

(b)

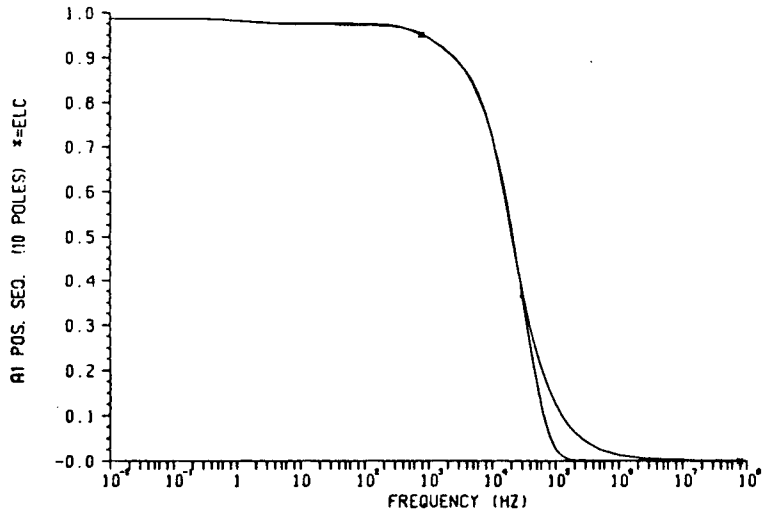

(c)

Graph 2.17: Approximation of A_1, positive sequence.
(a) 2 poles (b) 4 poles (c) 10 poles

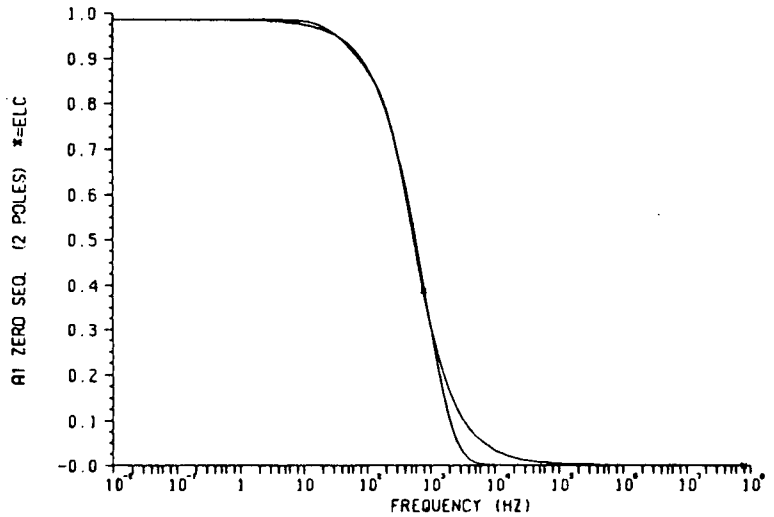

(a)

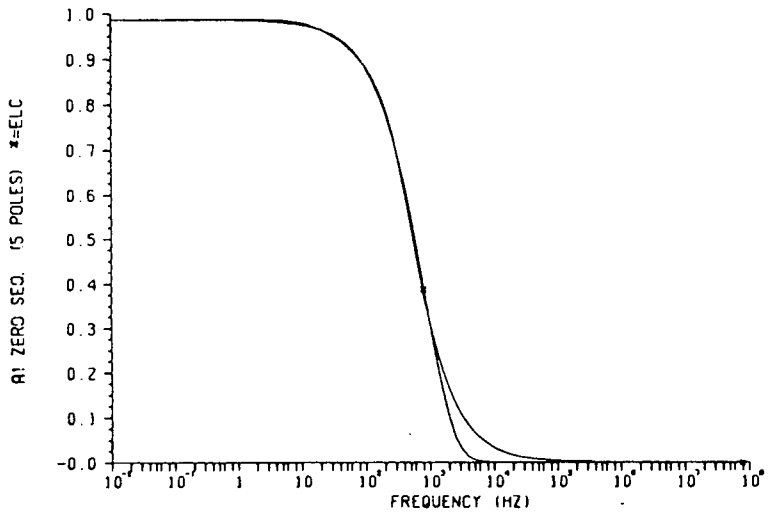

(b)

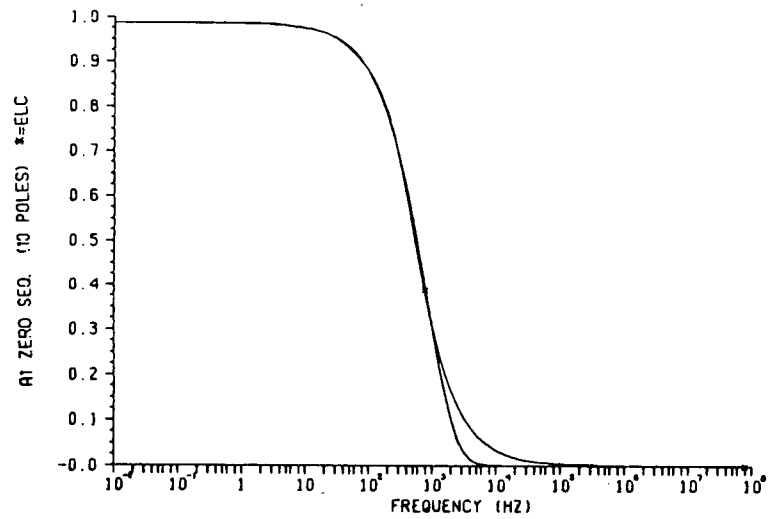

(c)

Graph 2.18: Approximation of A_1, zero sequence.
(a) 2 poles (b) 5 poles (c) 10 poles

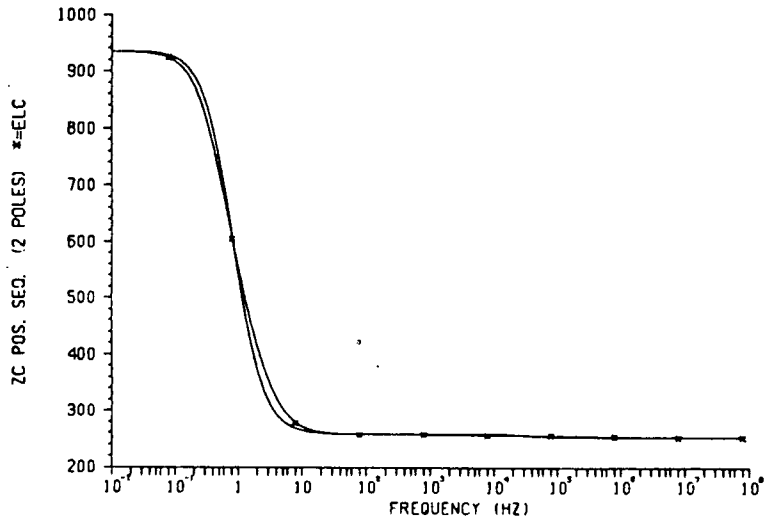

(a)

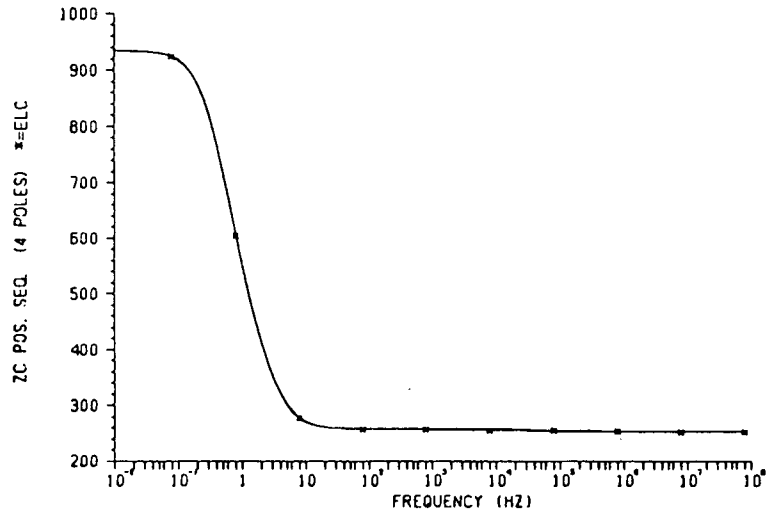

(b)

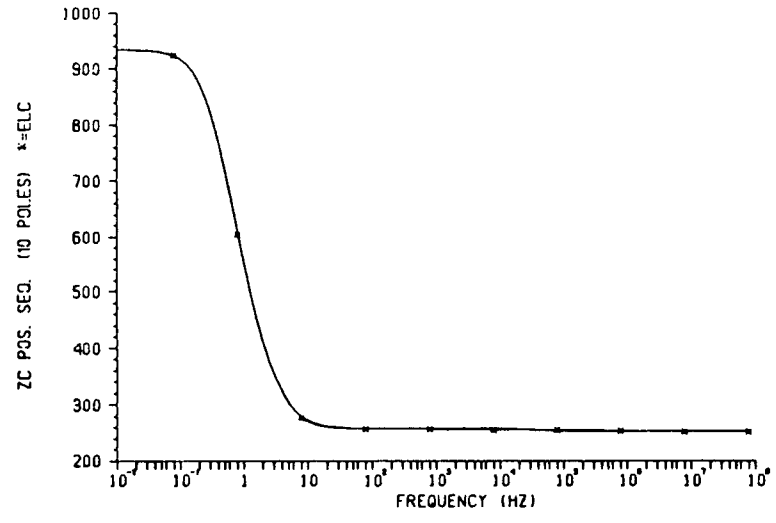

(c)

Graph 2.19: Approximation of Z_C, positive sequence.
(a) 2 poles (b) 4 poles (c) 10 poles

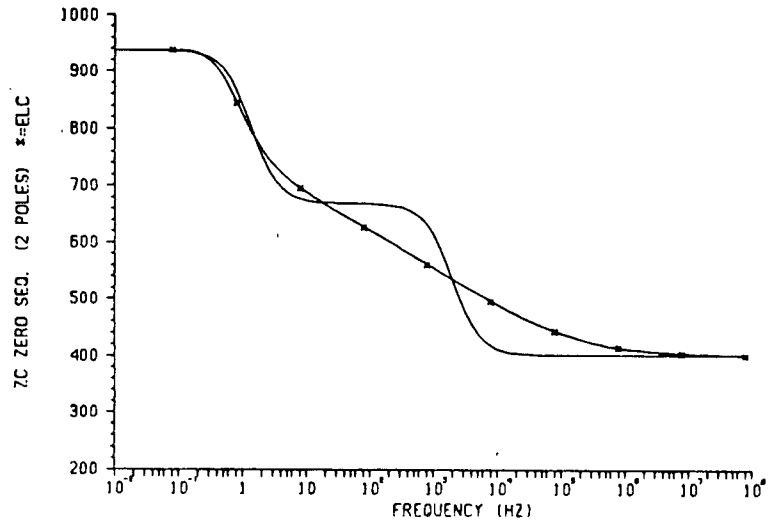

(a)

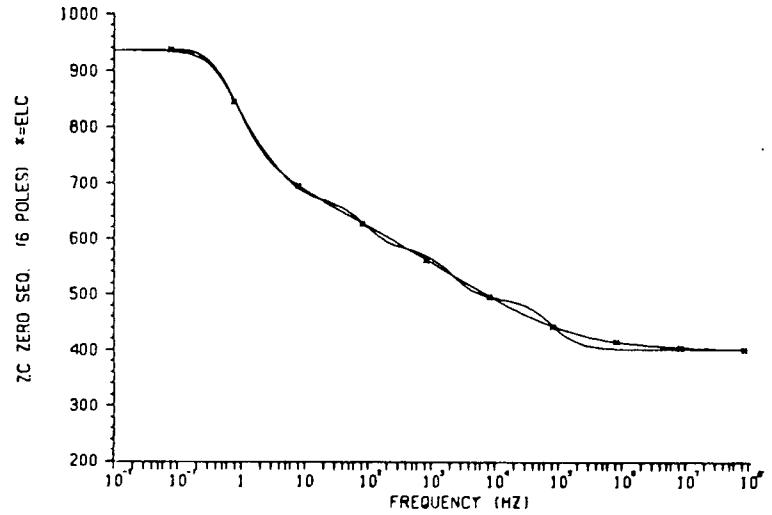

(b)

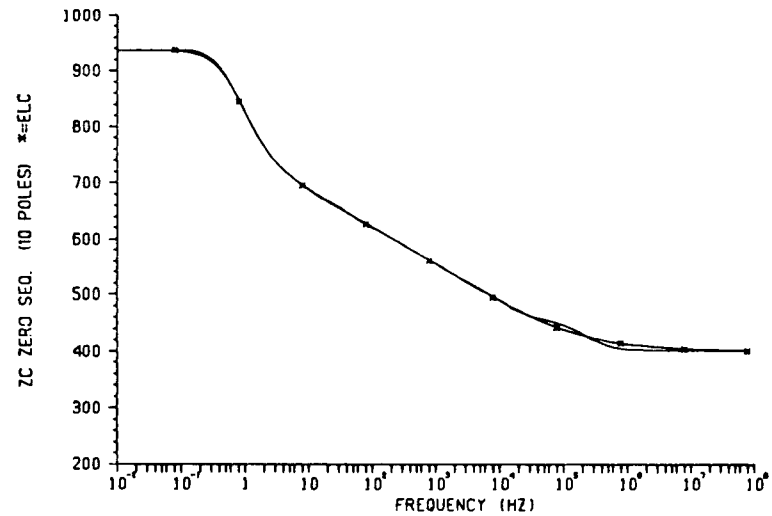

(c)

Graph 2.20: Approximation of Z_C, zero sequence.
(a) 2 poles (b) 6 poles (c) 10 poles

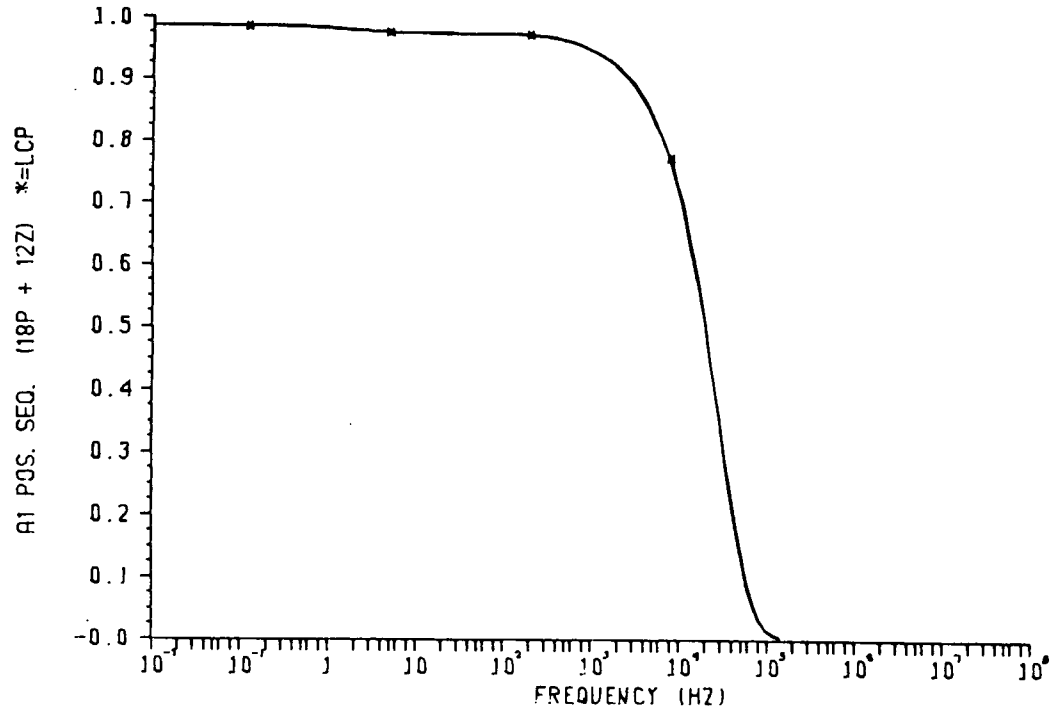

(a)

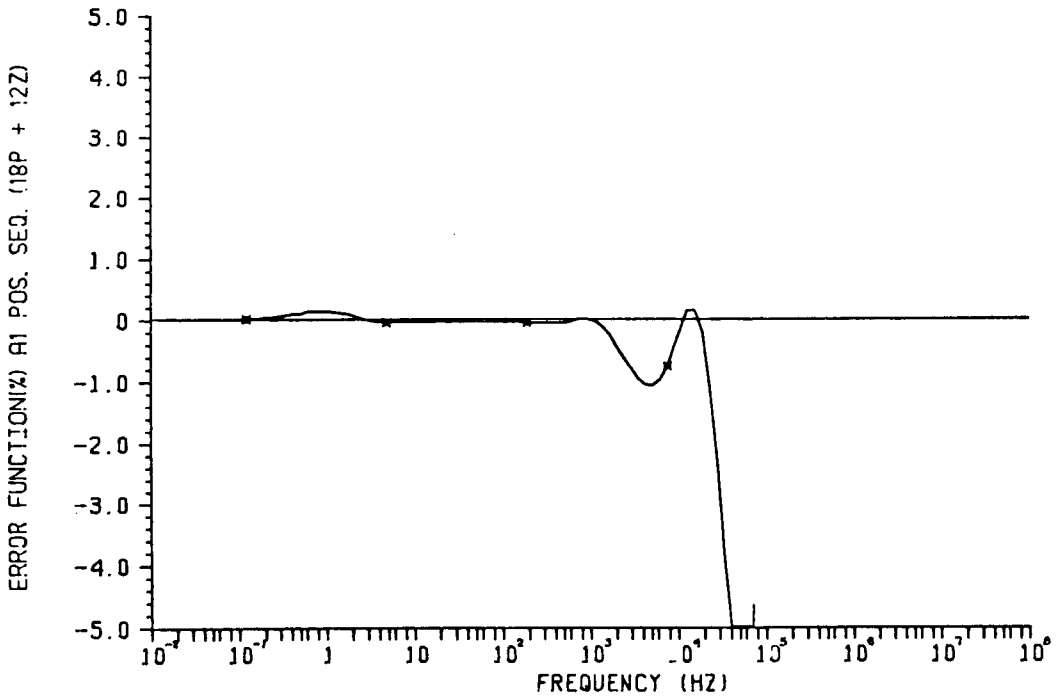

(b)

Graph 2.21: A_1 positive sequence, high-order approximation.
(a) Magnitude function (b) Error function

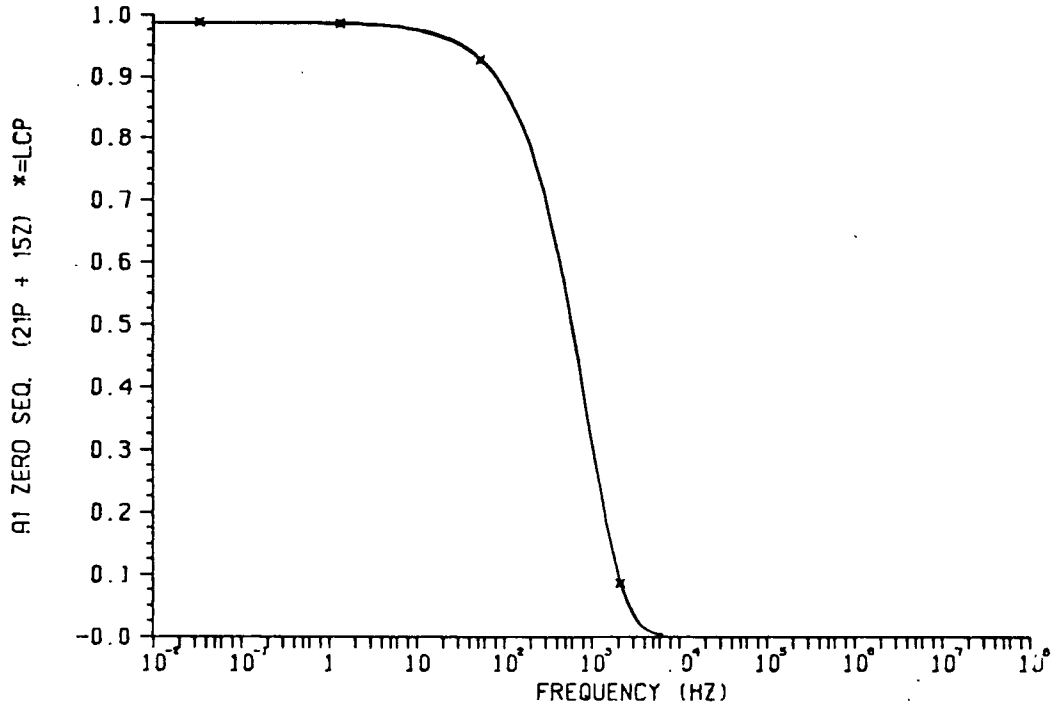

(a)

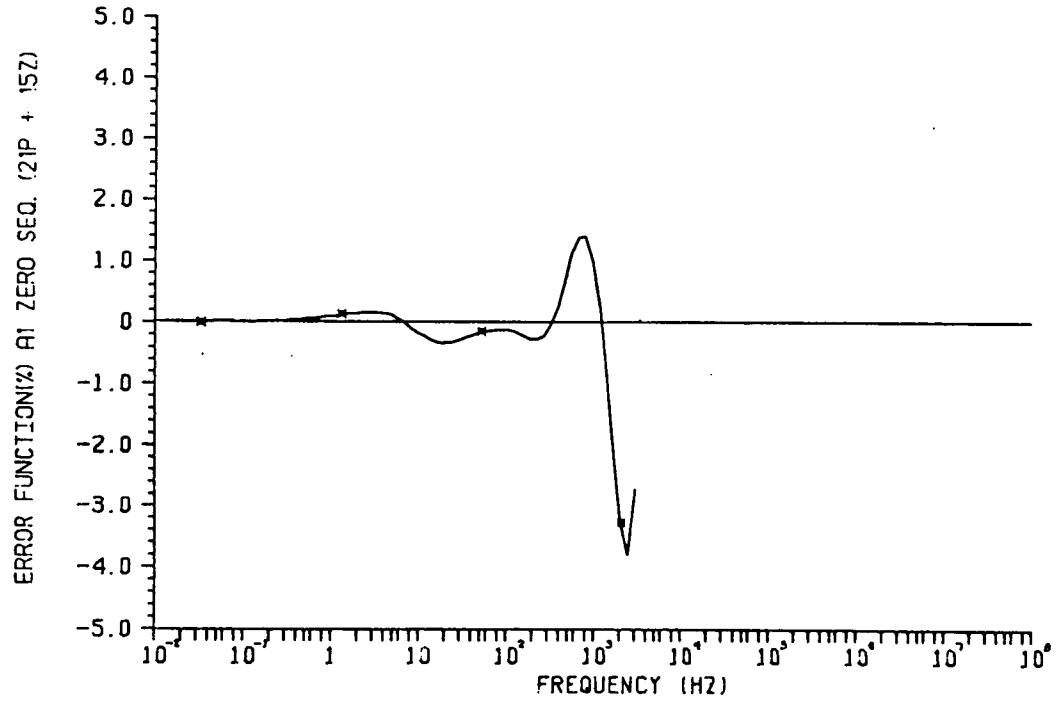

(b)

Graph 2.22: A_1 zero sequence, high-order approximation.
(a) Magnitude function (b) Error function

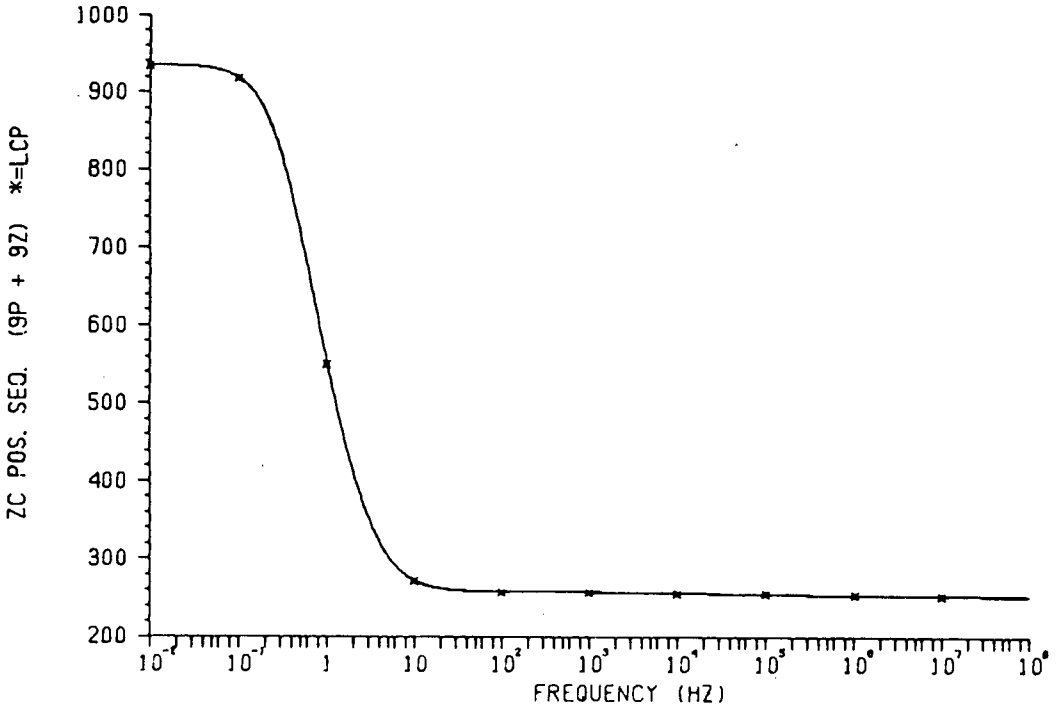

(a)

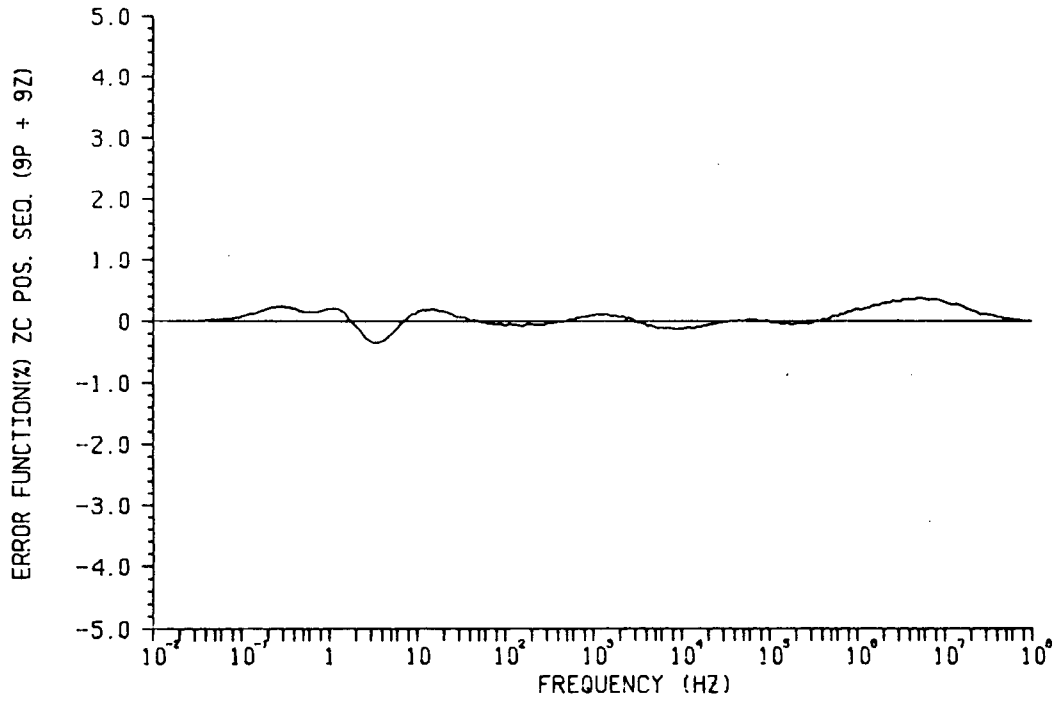

(b)

Graph 2.23: Z_C positive sequence, high-order approximation.
(a) Magnitude function (b) Error function

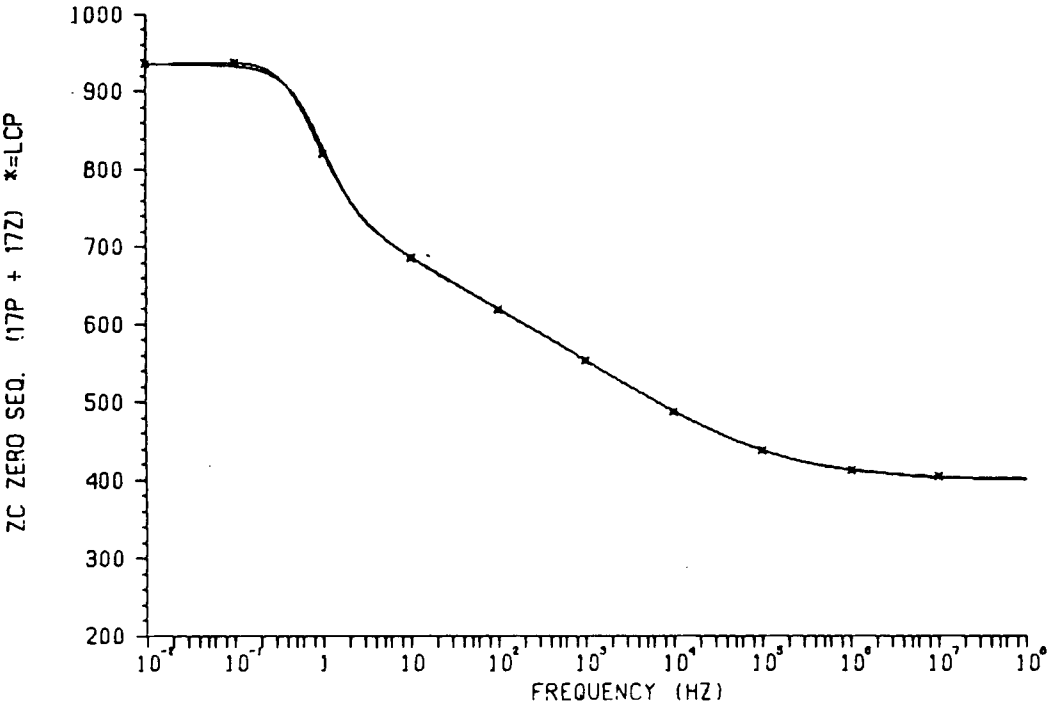

(a)

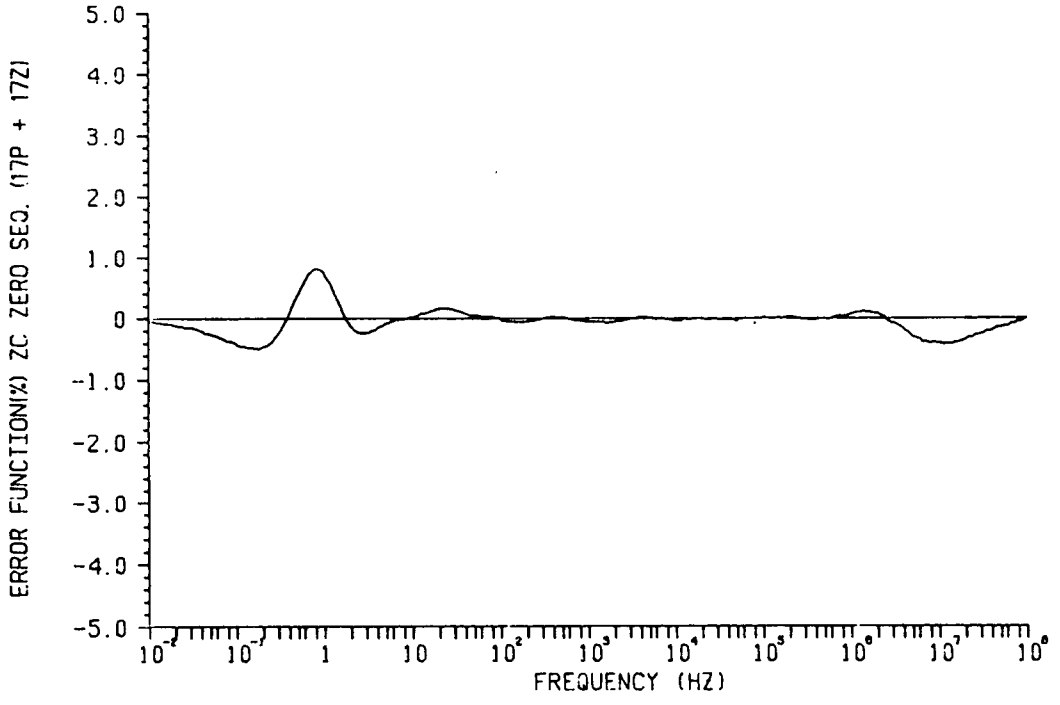

(b)

Graph 2.24: Z_C zero sequence, high-order approximation.
(a) Magnitude function (b) Error function

3.5 Frequency Domain Response

3.5.1 Introduction

The best test for the validity of the approximating techniques described in this project, is to simulate transient phenomena in the EMTP, and to compare the results with those obtained using the available high-accuracy models. Unfortunately, the number of possible simulations is very large and it would not be practical to present a large number of results here. However, a small but wisely chosen number of tests can give a good idea of the relative accuracy of the models. Two such tests are the steady-state, open and short circuit responses to sinusoidal excitation at one frequency; with the frequency varied over the frequency range of interest.

From the solution of the line equations in the frequency domain (see appendix I-A), the open circuit response (see Figure 3.1), is given by

$$V_m(\omega) = \frac{2\ V_o\ A_1(\omega)}{1 + A_1^2(\omega)} \tag{3.1}$$

where V_o is the peak magnitude of the voltage source, and V_m is the receiving end voltage.

Similarly, the short circuit response, or receiving end current when the line is shorted, is given by

$$I_m(\omega) = \frac{2\ V_o\ A_1(\omega)}{Z_c(\omega)\ (1 - A_1^2(\omega))} \tag{3.2}$$

These two tests present several advantages:

(a) Open and short circuit terminations are extreme and trying cases for a line model; if the response is good for these two cases, it is reasonable to assume that the response for any other termination will also be good.

(b) The behaviour of the models over the whole frequency range can be readily observed.

(c) The results of the different rational-functions approximations can be compared to theoretical results since $A_1(\omega)$ and $Z_c(\omega)$ in equations (3.1) and (3.2) can be evaluated at any given frequency from the output of UBC's Line Constants Program.

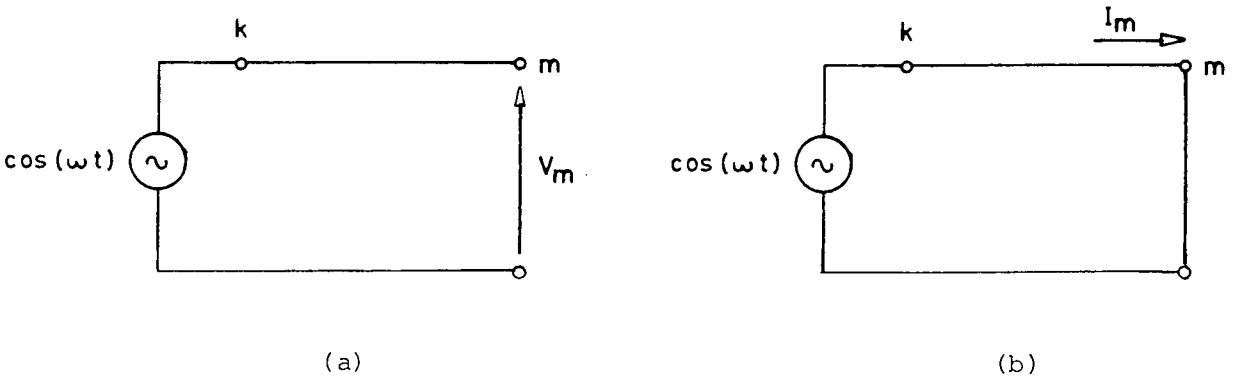

Fig. 3.1: (a) Open circuit and (b) Short circuit tests.

In these tests, the line will be assumed to be single-phase, with positive or zero sequence parameters, in order to isolate the effects of the approximations involved in each propagation mode.

The following models have been tested:

Model 1. - High-order approximation using the parameters calculated from UBC's Line Constants Program.

Model 2. - High-order approximation using the parameters calculated from the equivalent line representation with R_{dc} given.

Model 3. - High-order approximation using the parameters calculated from the equivalent line representation with R_{dc} not given.

Model 4. - Low-order approximation (2 poles, R_{dc} given).

Model 5. - Low-order approximation (10 poles, R_{dc} given).

Model 6. - Low-order approximation (4,5 and 6 poles, R_{dc} given).

Model 7. - Constant parameters option of the EMTP.

Table 3.3 shows the number of poles and zeros used in the different approximations.

	$Z_c(\omega)$				$A_1(\omega)$			
	Zero sequence		Positive sequence		Zero sequence		Positive sequence	
Model	Poles	Zeros	Poles	Zeros	Poles	Zeros	Poles	Zeros
1	17	17	9	9	21	15	18	12
2	17	17	9	9	21	15	18	12
3	18	18	9	9	25	19	17	11
4	2	2	2	2	2	1	2	1
5	10	10	10	10	10	9	10	9
6	6	6	4	4	5	4	4	3

Table 3.3: Number of poles and zeros used in the different models tested in this section.

Models 2 and 3 are used to isolate the effect of the rational-functions approximation from the effect of the estimation of the line parameters (from the equivalent line configuration). Models 4, 5 and 6 show the effects of the order of the approximation in the response of the line.

3.5.2 Open Circuit Response

The open circuit response for the different line models described above, is shown in graphs 2.25 through 2.31. Note that $V_m(\omega)$ depends on $A_1(\omega)$ only (see equation (3.1)), therefore the effects of the approximation of $Z_c(\omega)$ are not present in this test.

The response of model 2 for zero sequence is virtually identical to the theoretical response; the positive sequence response of the same model shows significant errors only for frequencies above 10 KHz.

When R_{dc} is not known (model 3), the response is still good for zero sequence, but presents considerable errors for positive sequence, reflecting the errors in the simulation of $A_1(\omega)$ (see graph 2.5).

It is interesting to note that the differences between the responses of models 5 and 6 are relatively small, although the order of the approximation in model 6 is almost twice that of model 5.

The response of the 2-pole approximation (model 4) is reasonably good in the low to mid frequencies range, and offers a definite overall improvement over the constant parameters model (model 7).

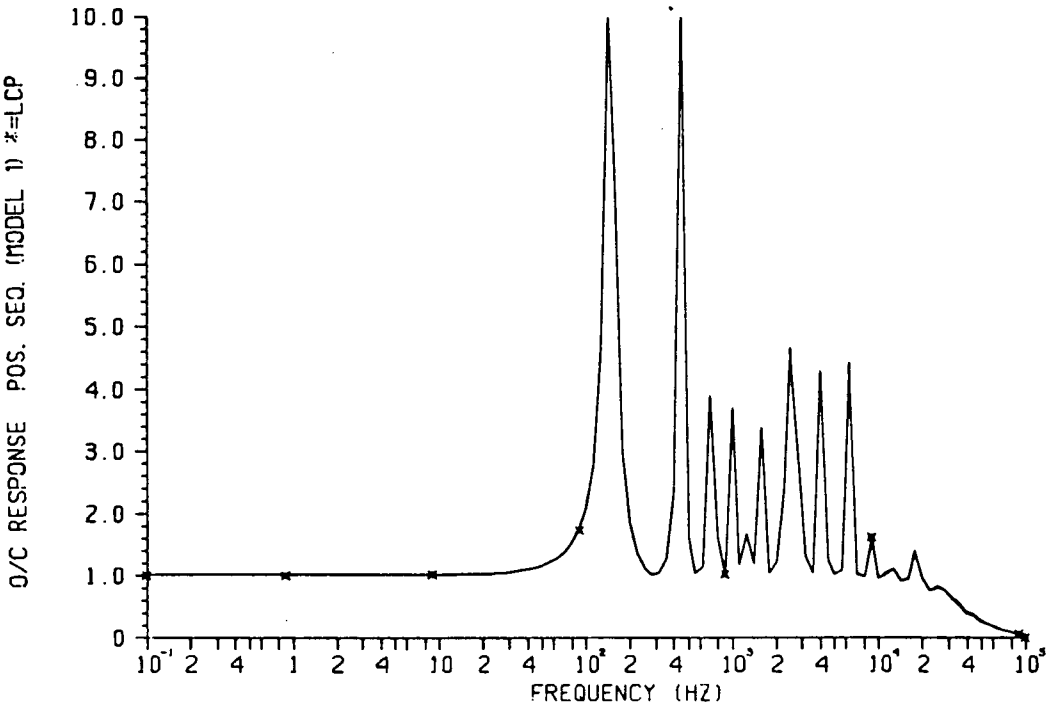

(a)

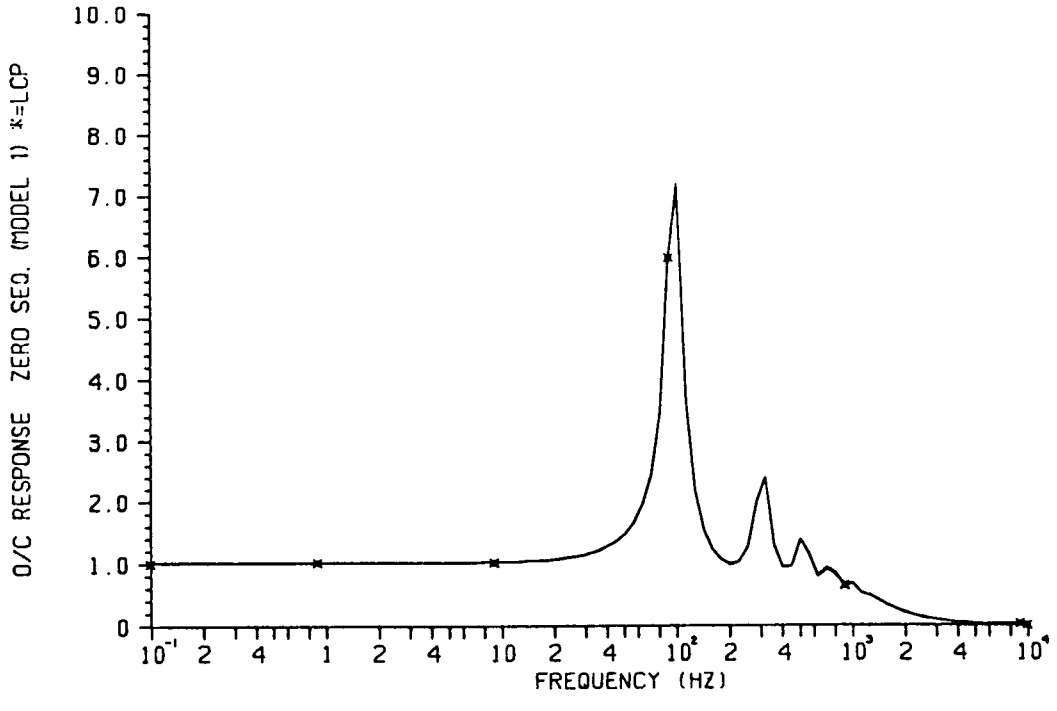

(b)

Fig. 2.25: O/C response, model 1.
(a) Positive sequence (b) Zero sequence

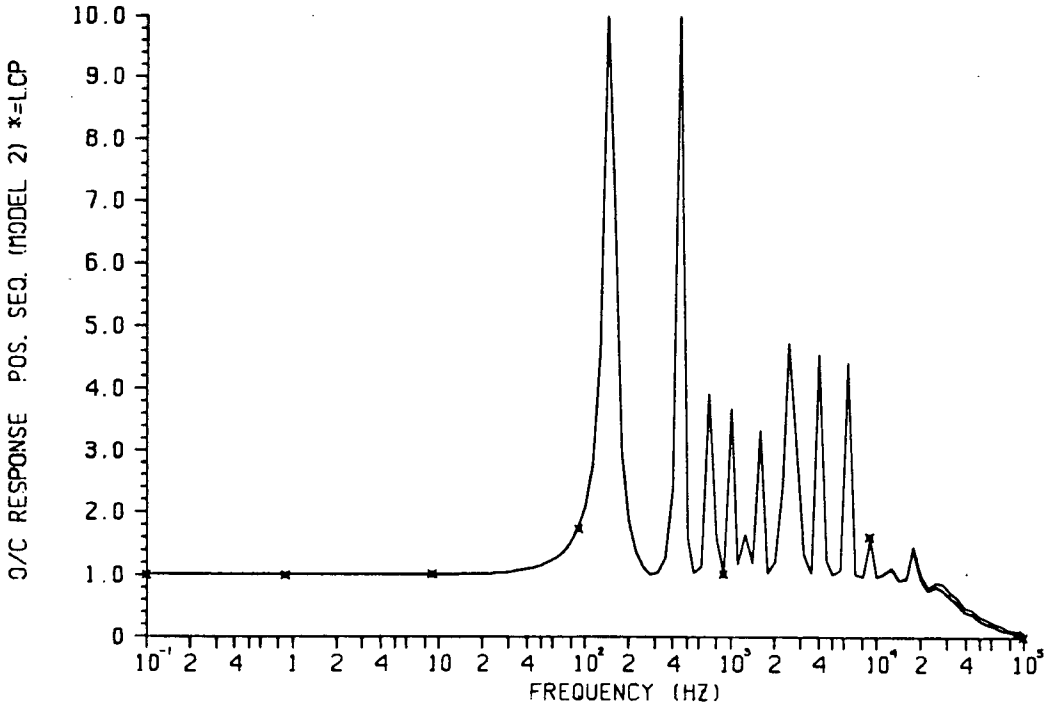

(a)

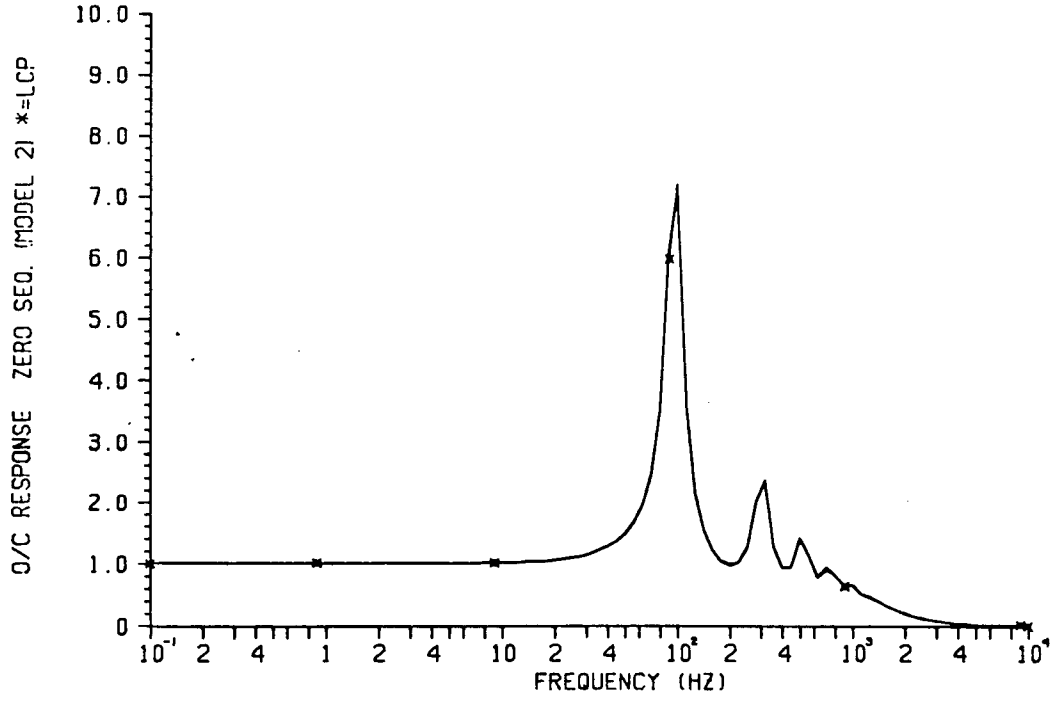

(b)

Fig. 2.26: O/C response, model 2.
(a) Positive sequence (b) Zero sequence

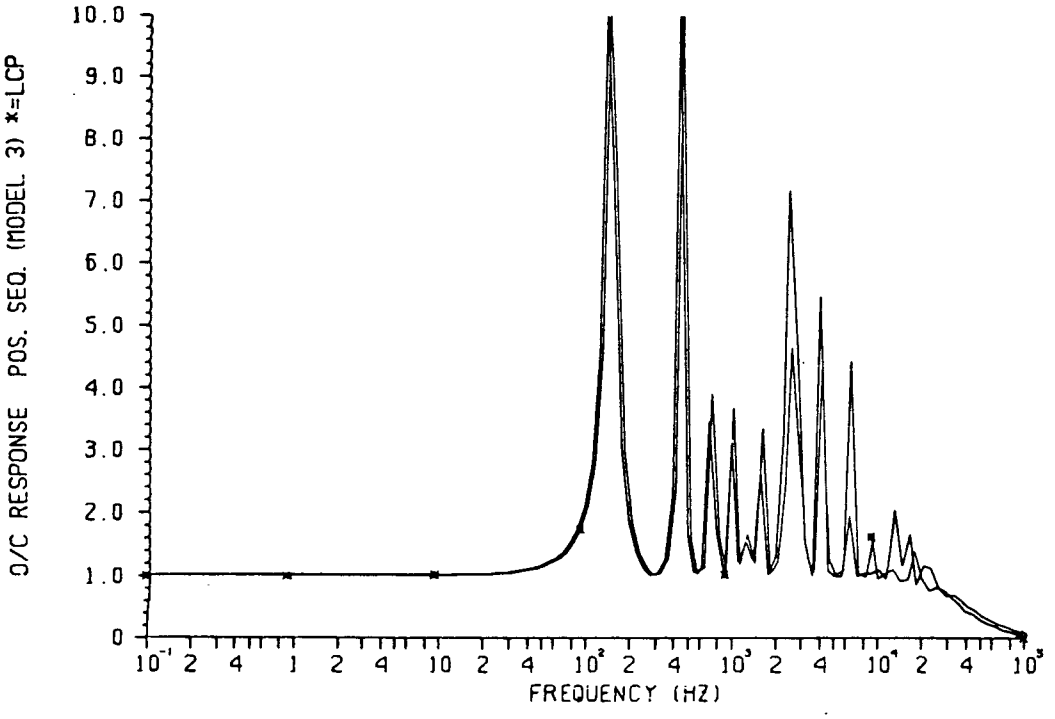

(a)

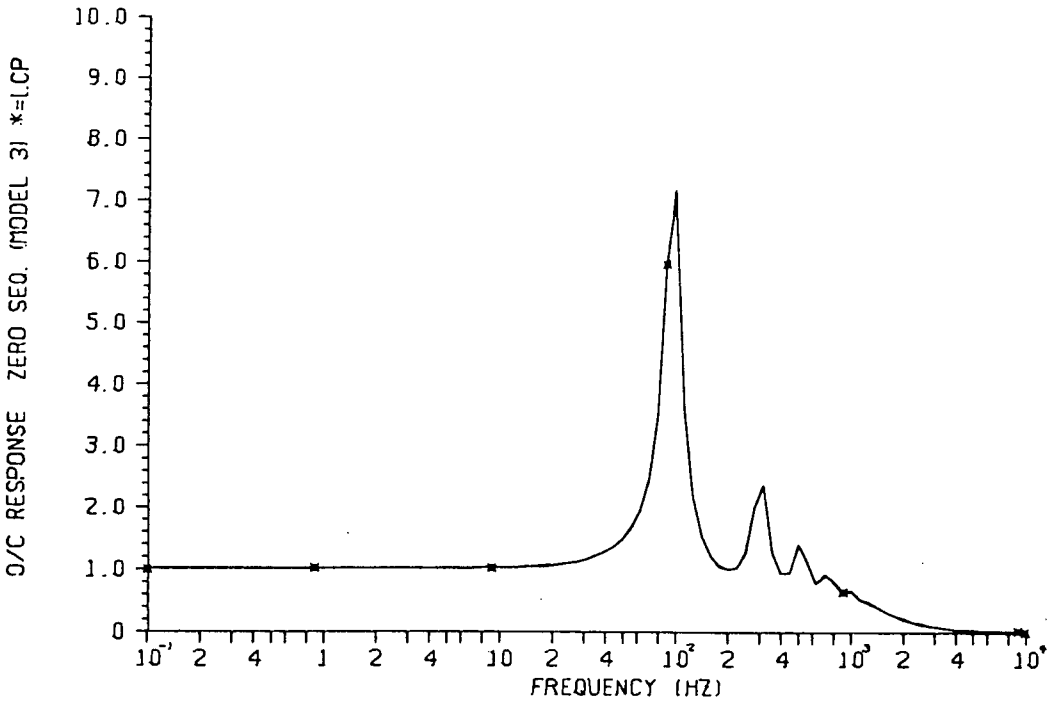

(b)

Fig. 2.27: O/C response, model 3.
(a) Positive sequence (b) Zero sequence

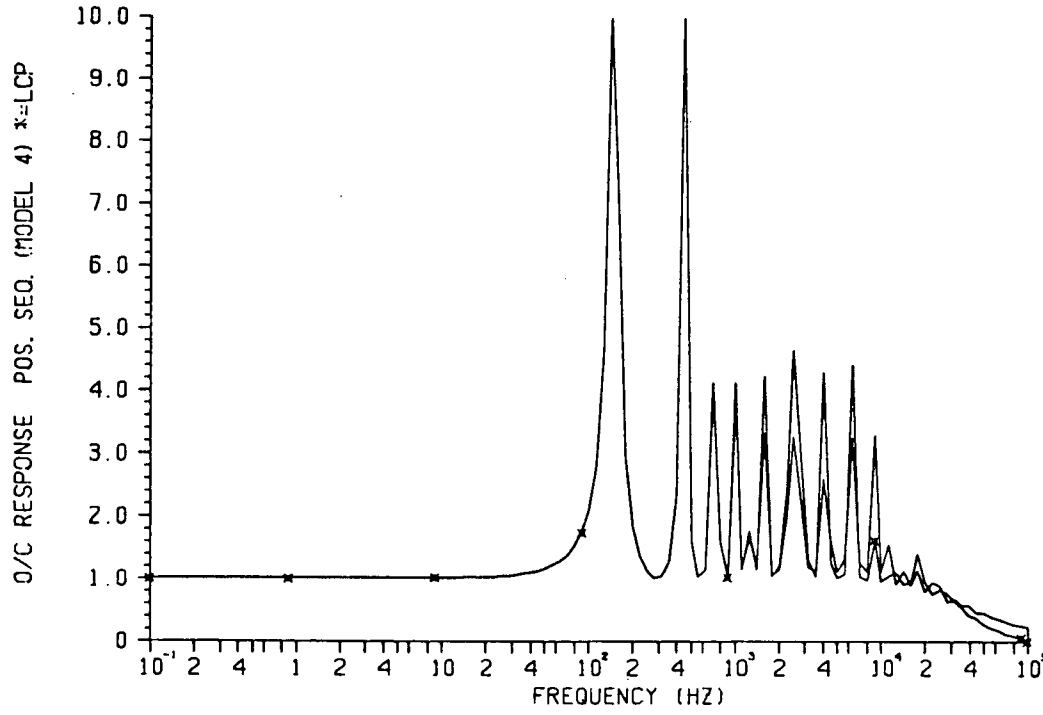

(a)

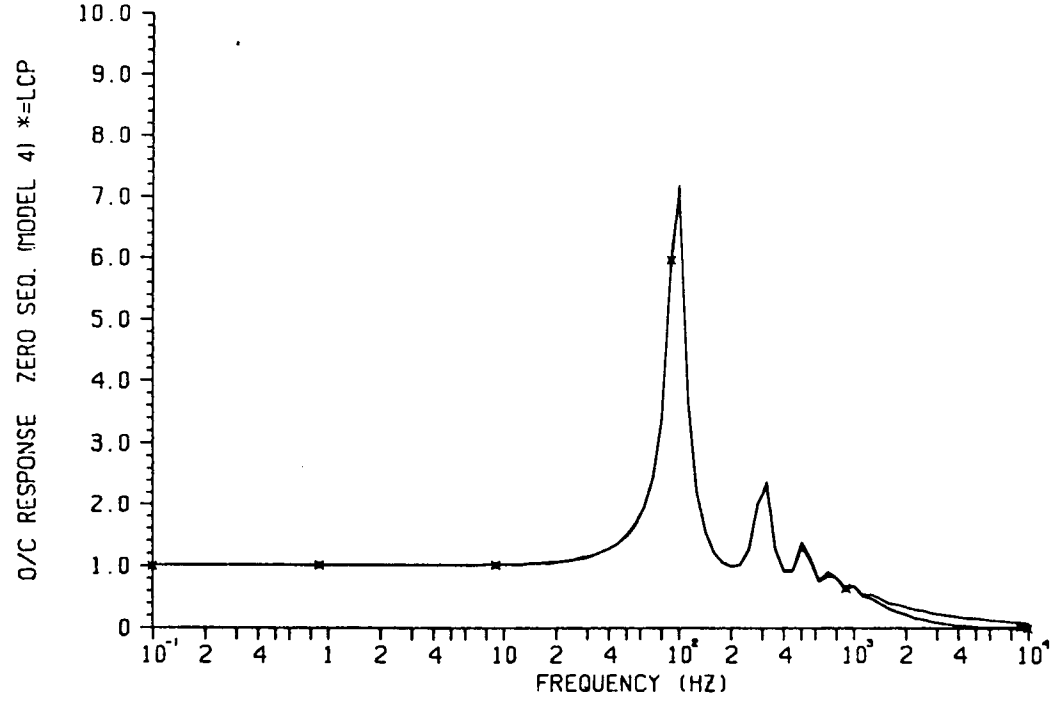

(b)

Fig. 2.28: O/C response, model 4.
(a) Positive sequence (b) Zero sequence

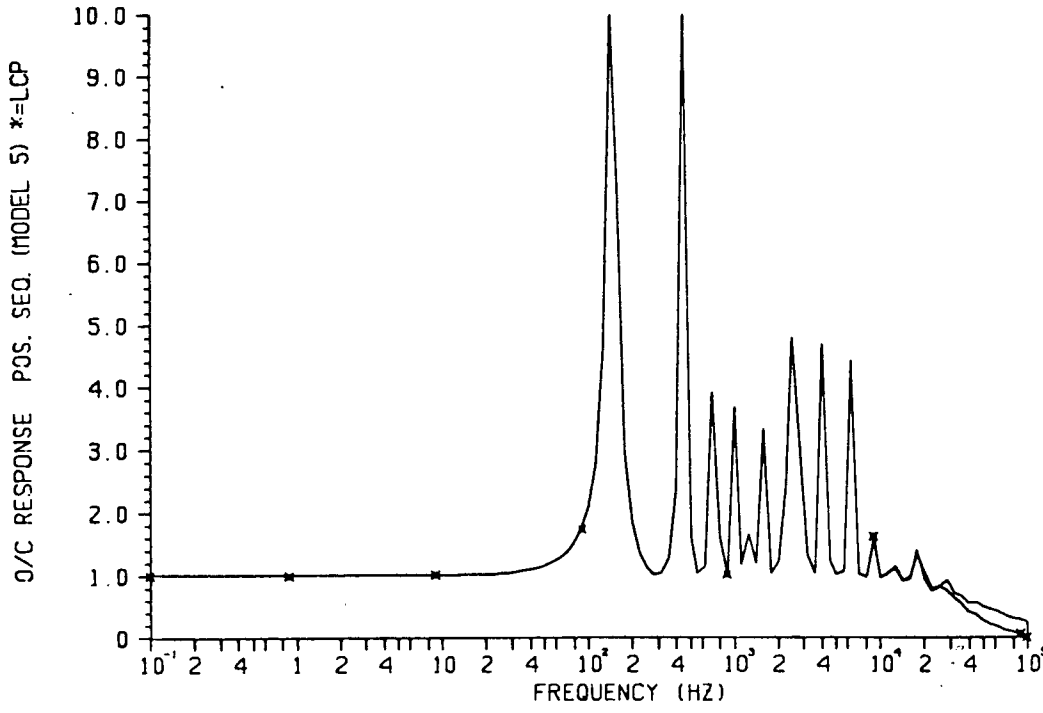

(a)

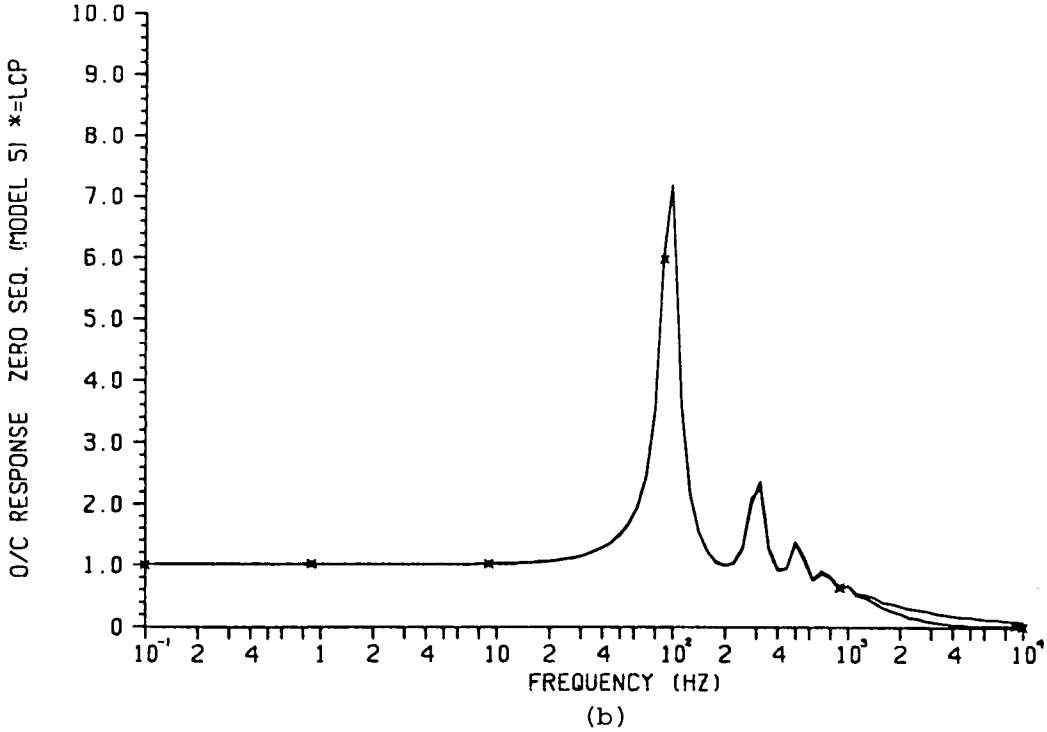

(b)

Fig. 2.29: O/C response, model 5.
(a) Positive sequence (b) Zero sequence

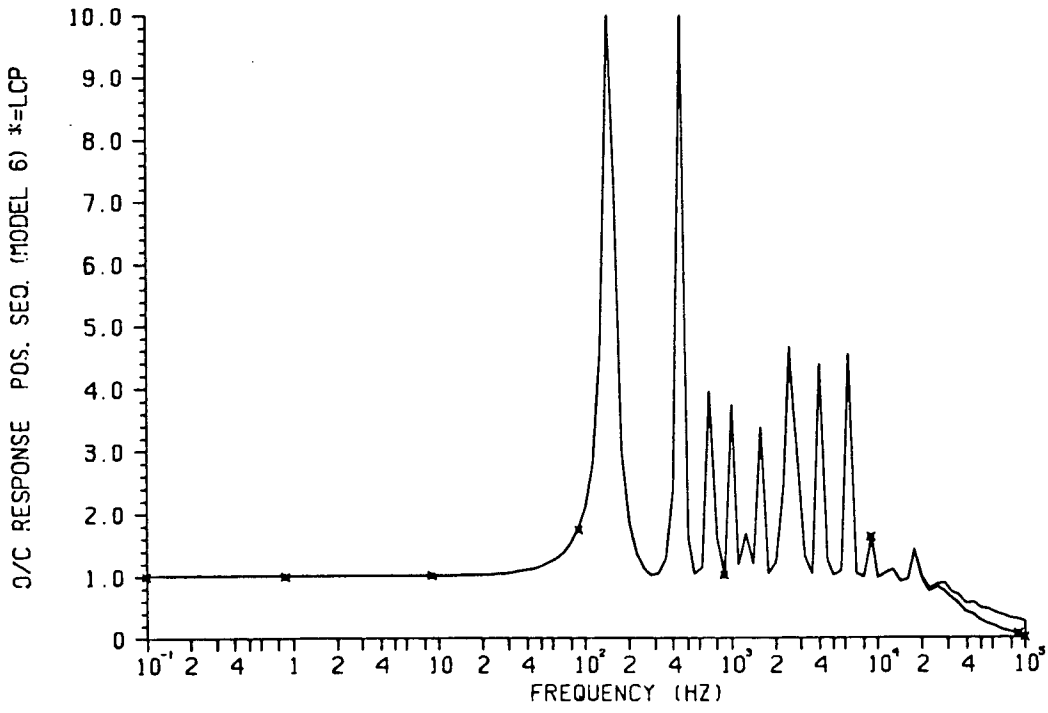

(a)

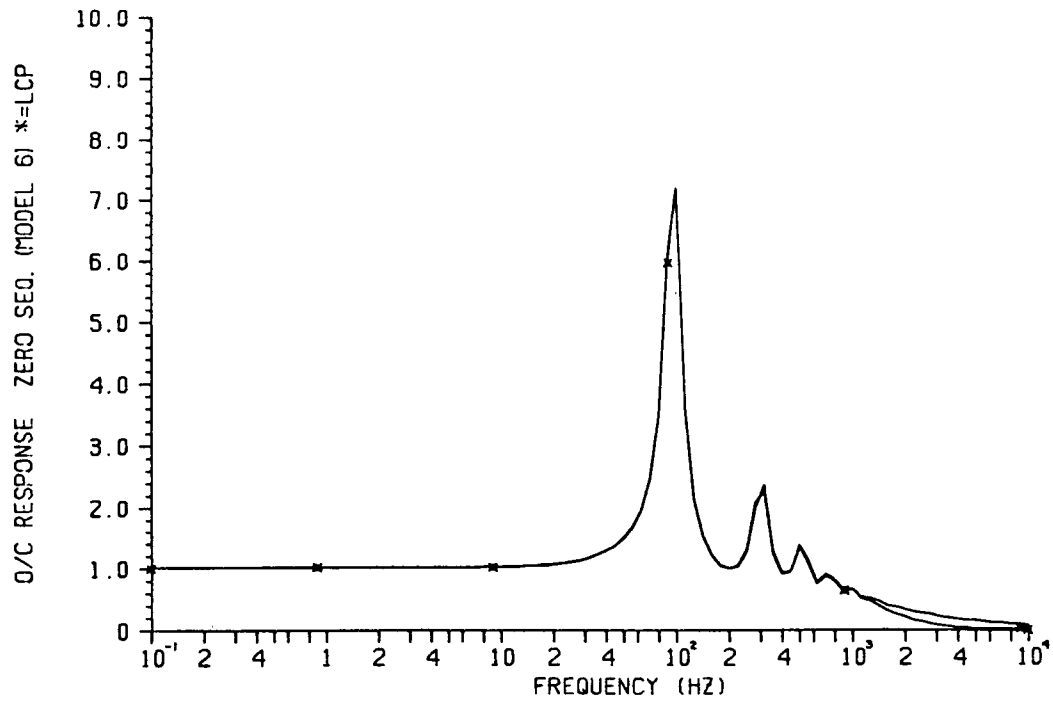

(b)

Fig. 2.30: O/C response, model 6.
(a) Positive sequence (b) Zero sequence

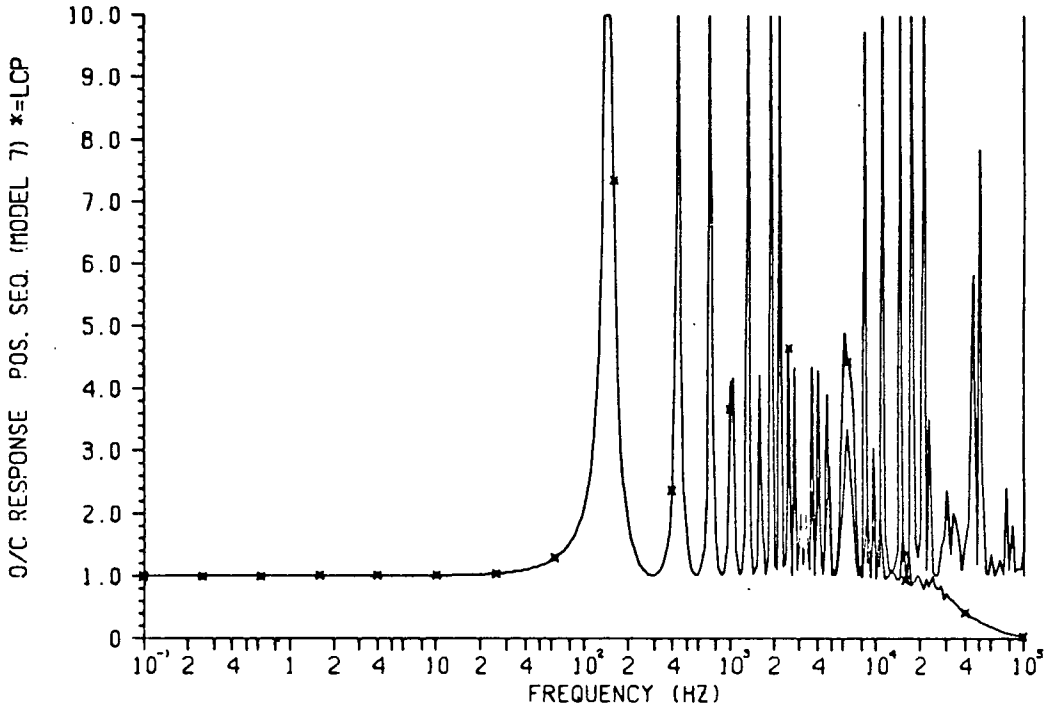

(a)

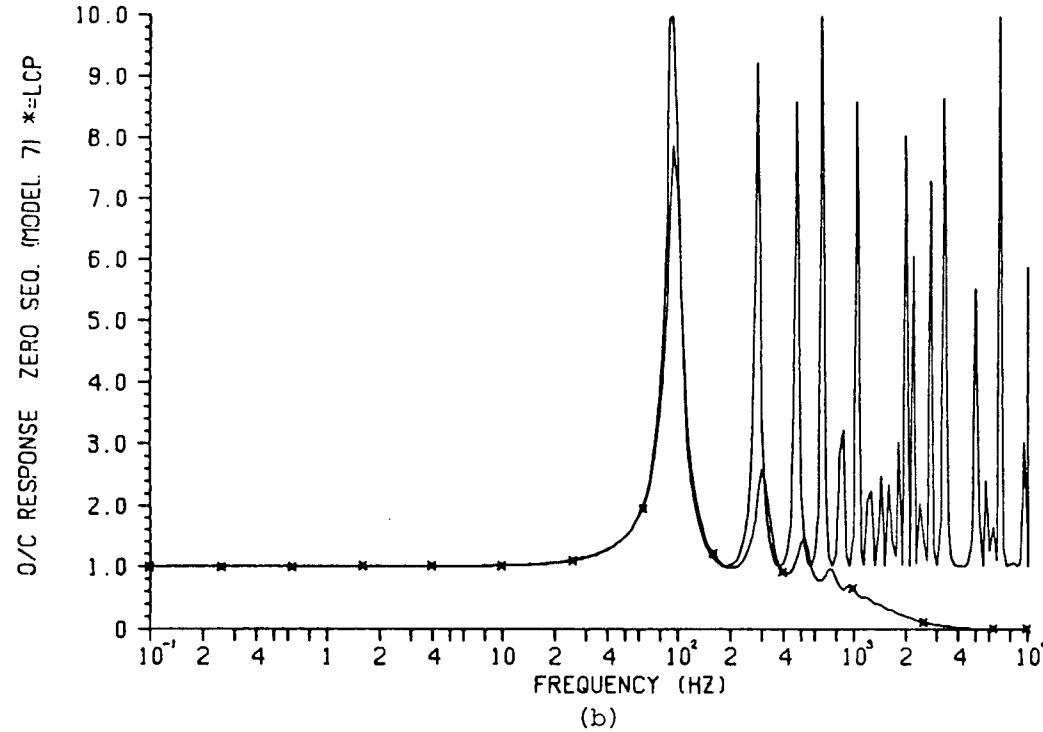

(b)

Fig. 2.31: O/C response, model 7.
(a) Positive sequence (b) Zero sequence

3.5.3 Short Circuit Response

The short circuit responses of the different models are shown in graphs 2.32 through 2.45.

In this test, the results are influenced by the approximation of $Z_c(\omega)$ (see equation (3.2)), and the errors in the approximation of $A_1(\omega)$ now combine (usually disfavourably) with the errors in $Z_c(\omega)$.

The relatively large errors in the low frequency range are due to the numerical sensitivity of the factor $A_1/(1 - A_1^2)$ in equation (3.2) at low frequencies, where the magnitude of $A_1(\omega)$ is very close to 1.0. For example, a difference of 0.01% in the approximation of $A_1(\omega)$ can produce errors up to 100% in the short circuit response [9]. These errors, however, are not very important as long as the dc response is matched identically, which is the case when R_{dc} is known.

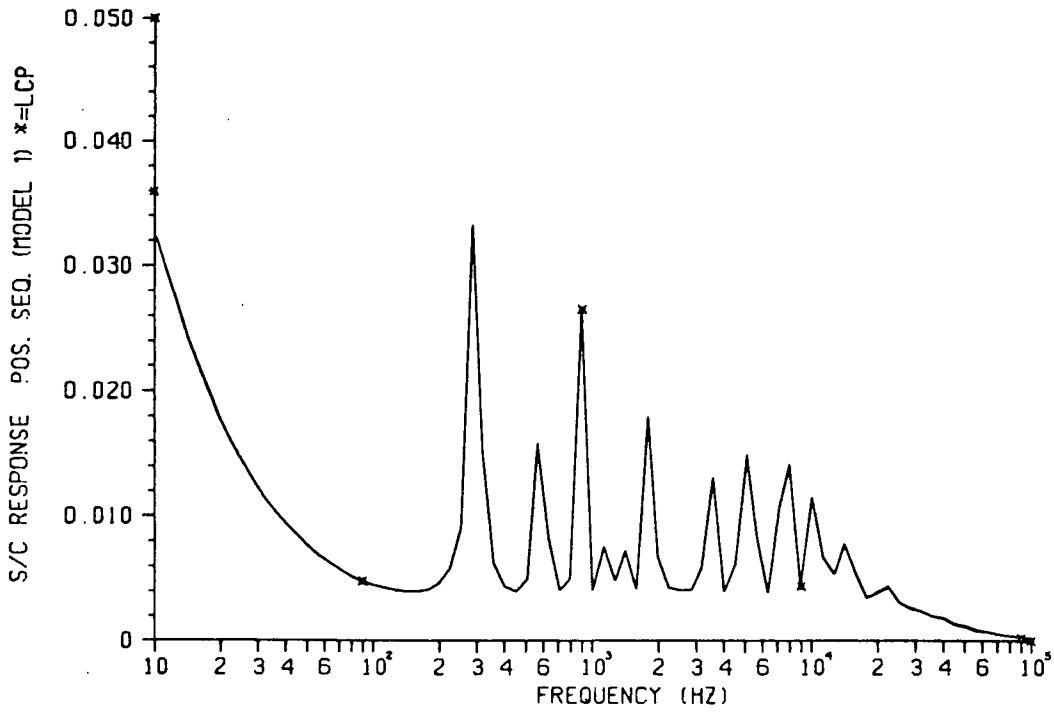

(a)

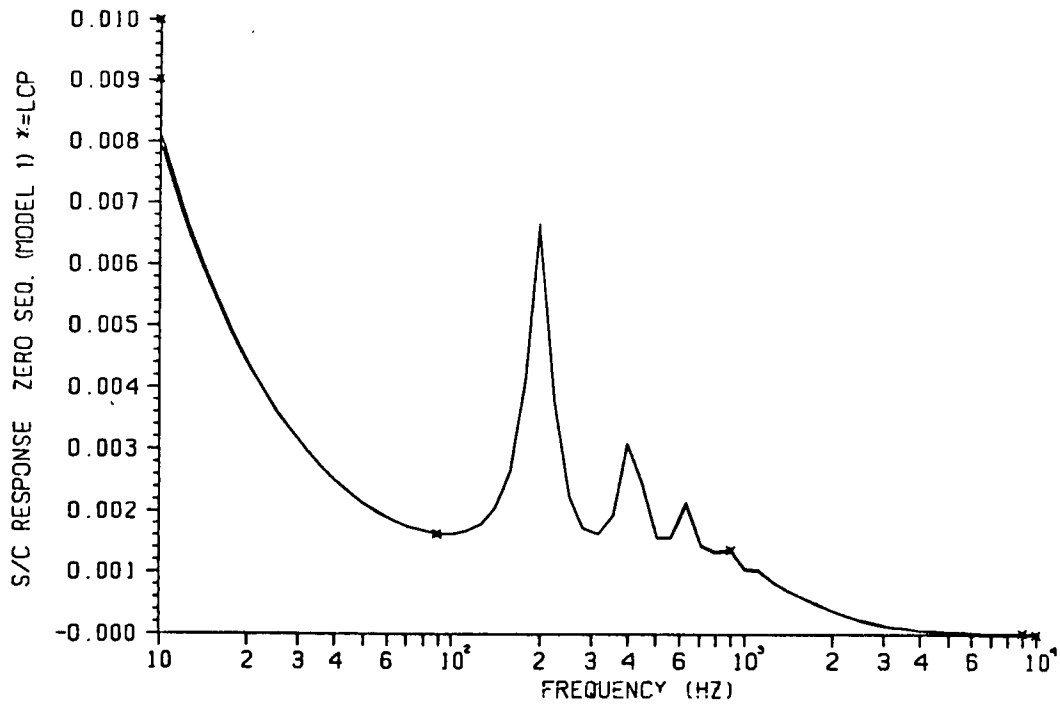

(b)

Graph 2.32: S/C response, model 1. Mid to high frequencies.
(a) Positive sequence (b) Zero sequence

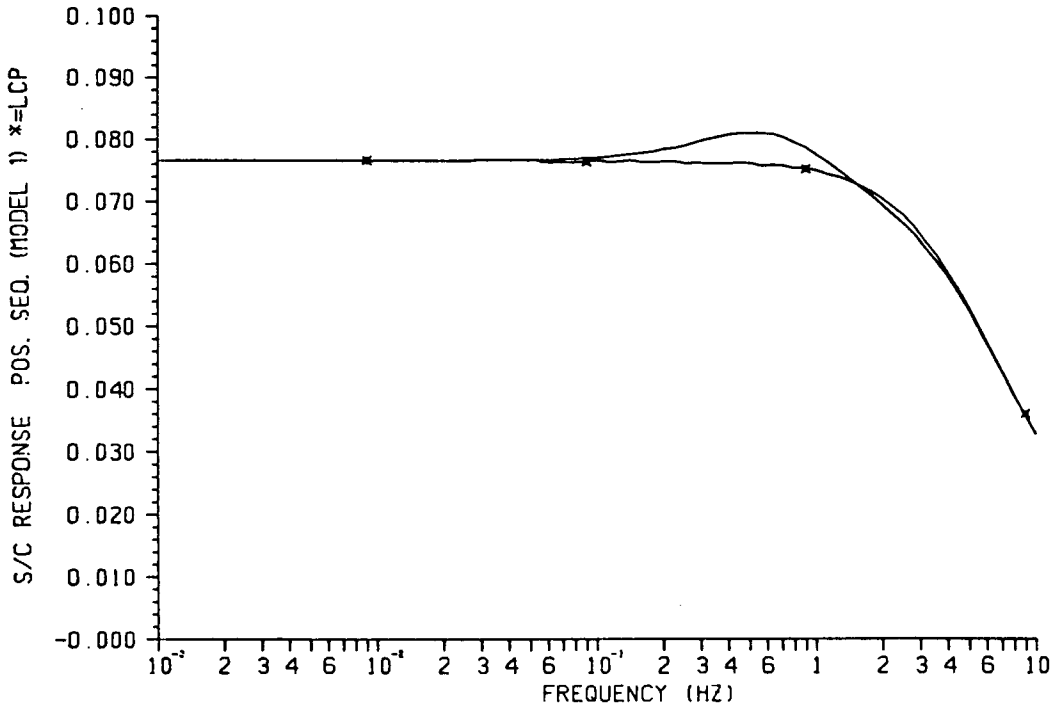

(a)

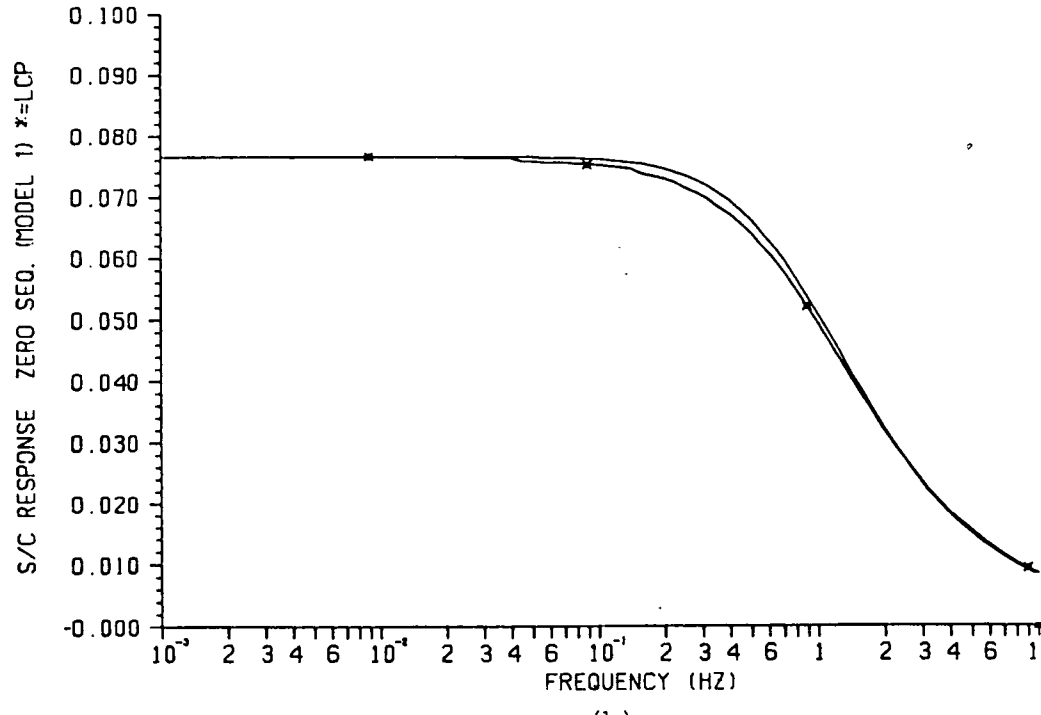

(b)

Graph 2.33: S/C response, model 1. Low frequencies.
(a) Positive sequence (b) Zero sequence

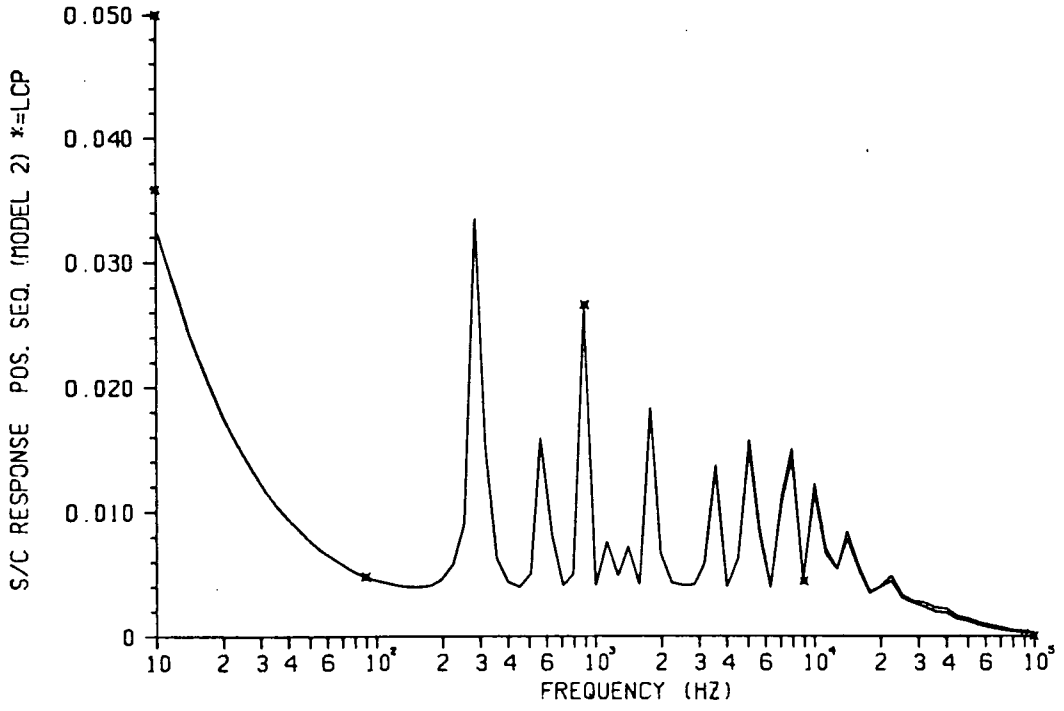

(a)

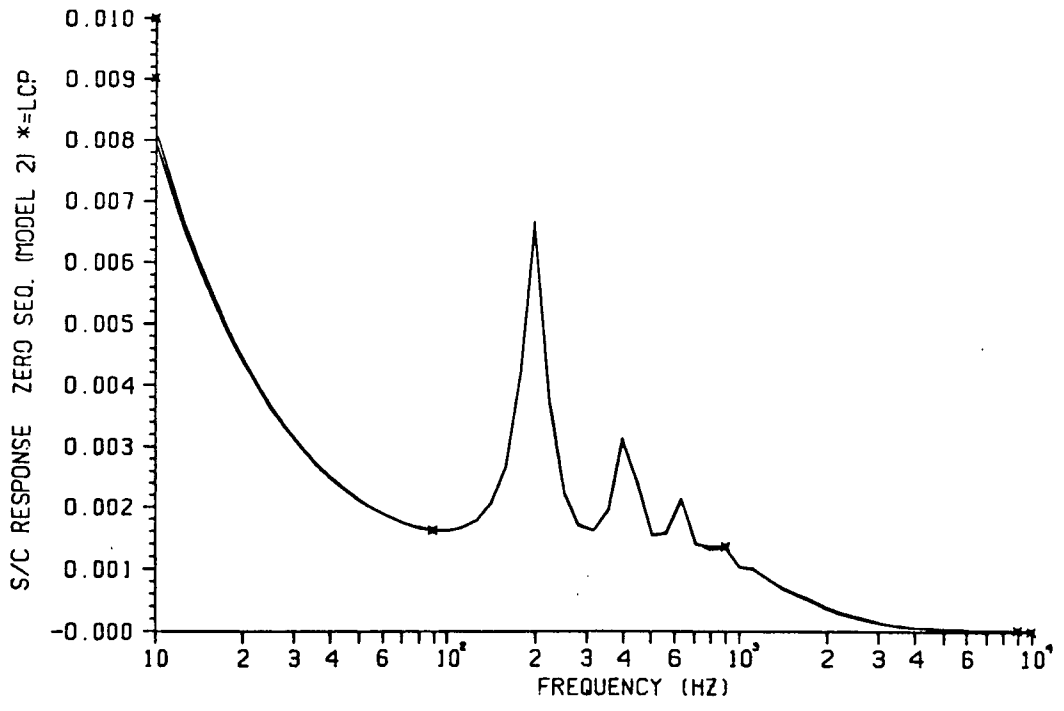

(b)

Graph 2.34: S/C response, model 2. Mid to high frequencies.
(a) Positive sequence (b) Zero sequence

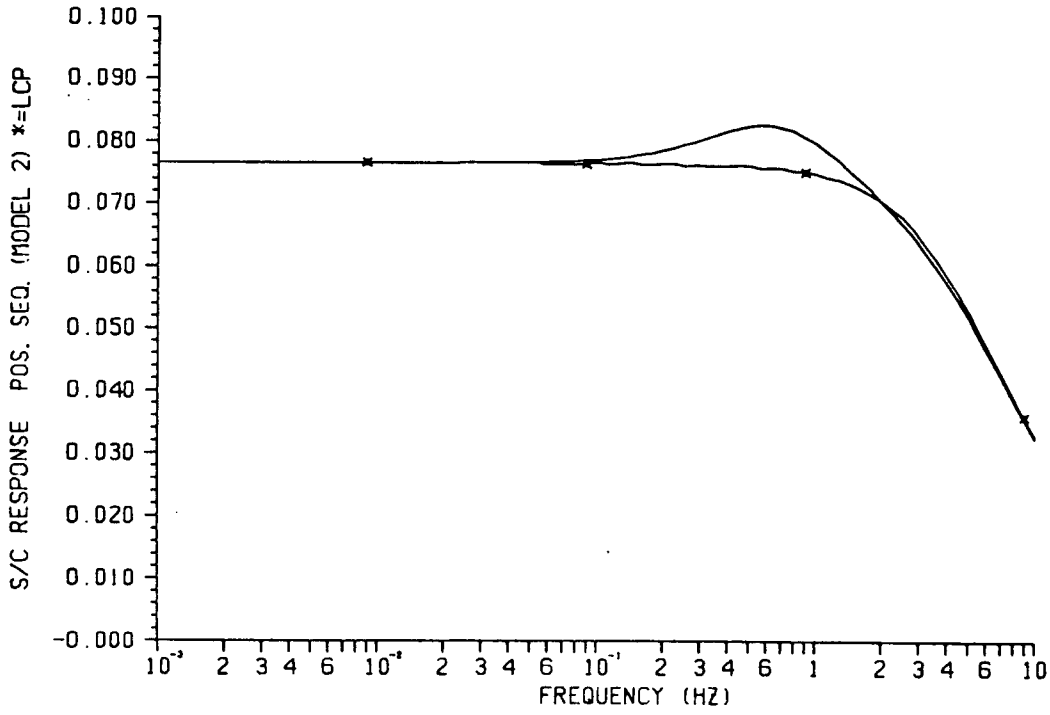

(a)

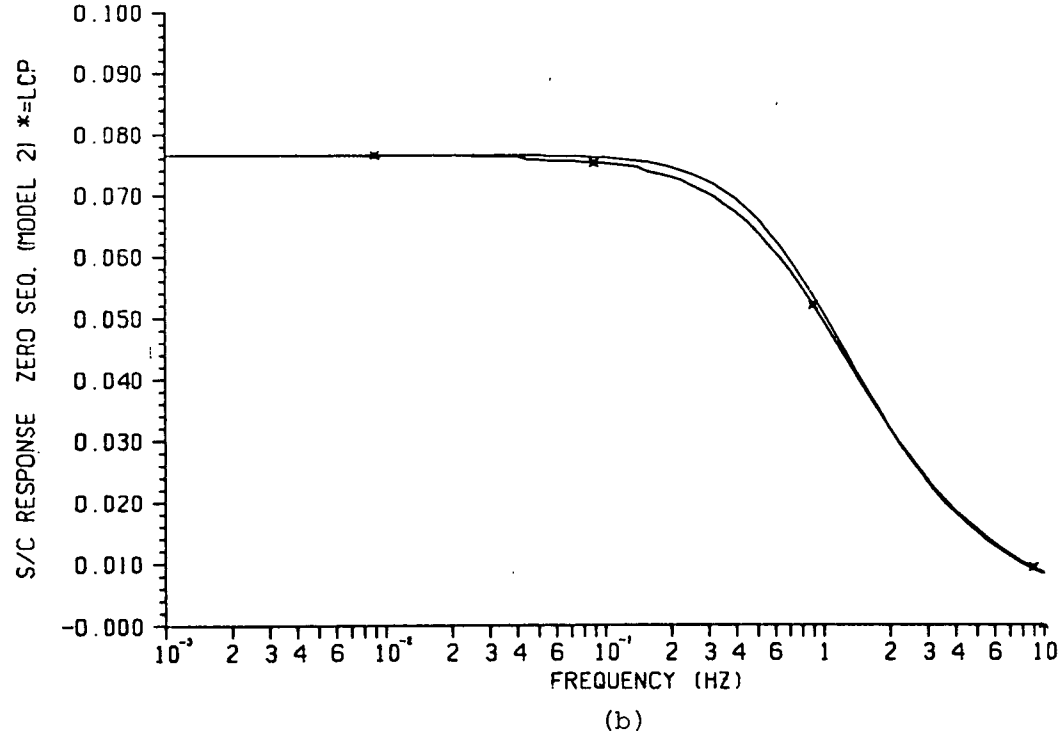

(b)

Graph 2.35: S/C response, model 2. Low frequencies.
(a) Positive sequence (b) Zero sequence

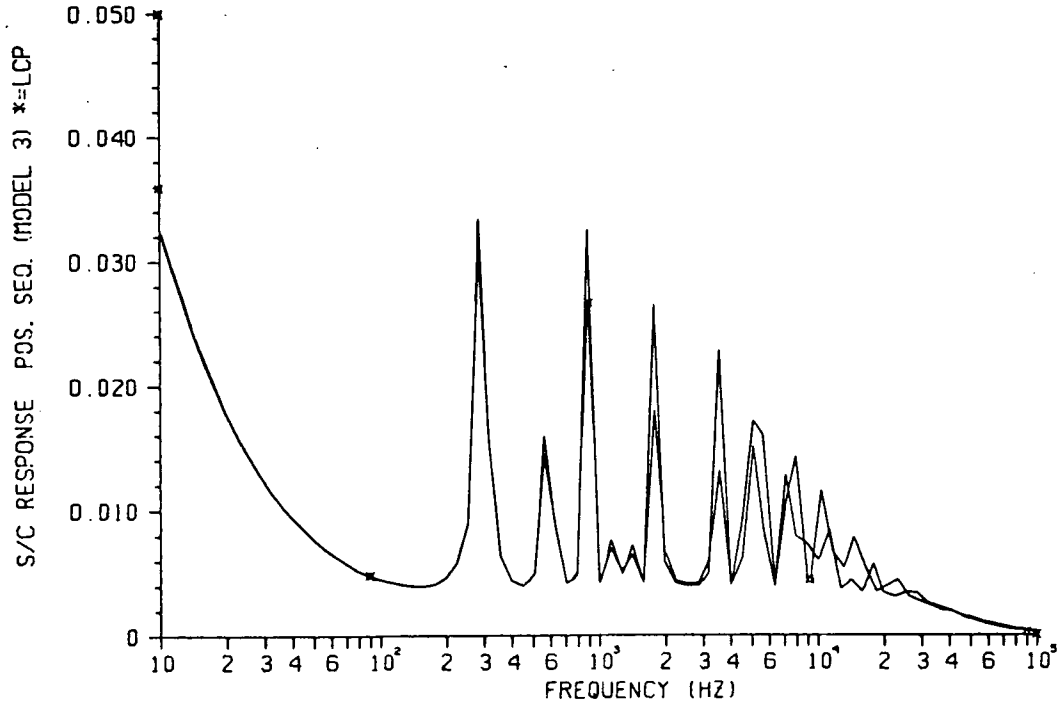

(a)

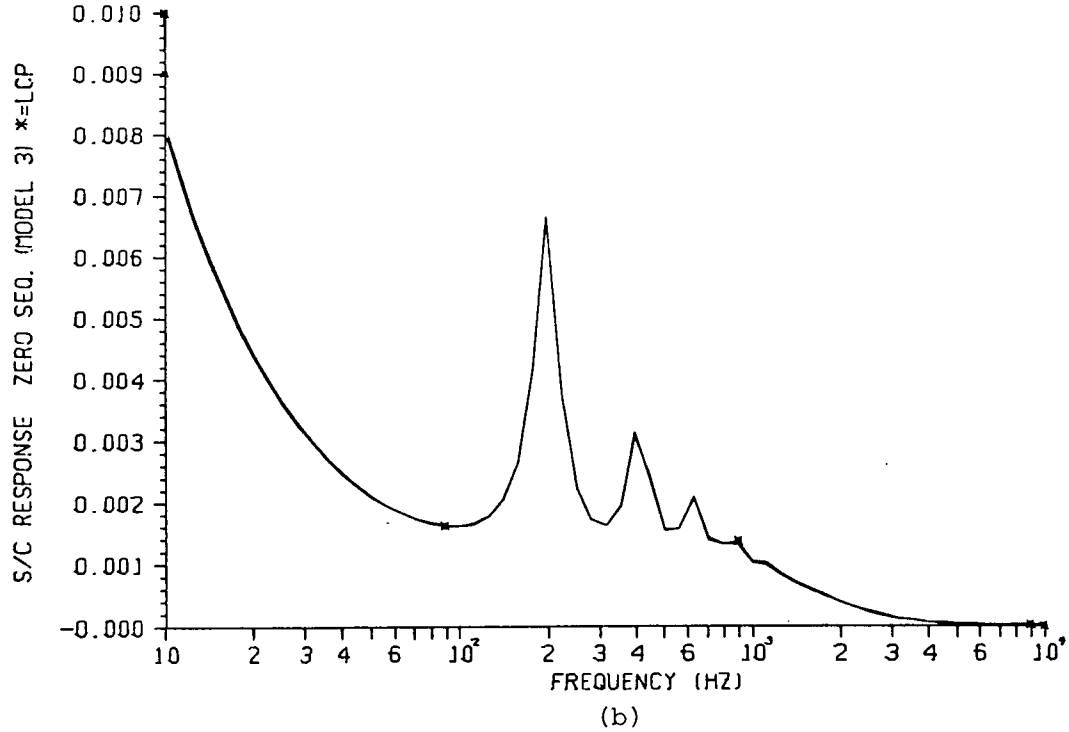

(b)

Graph 2.36: S/C response, model 3. Mid to high frequencies.
(a) Positive sequence (b) Zero sequence

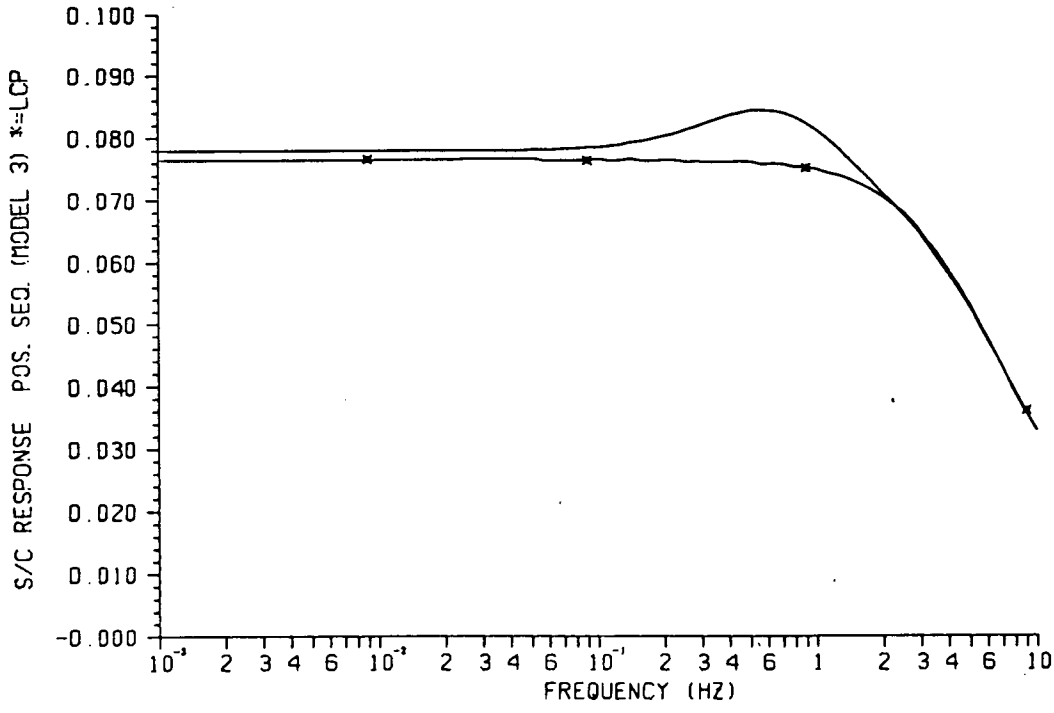

(a)

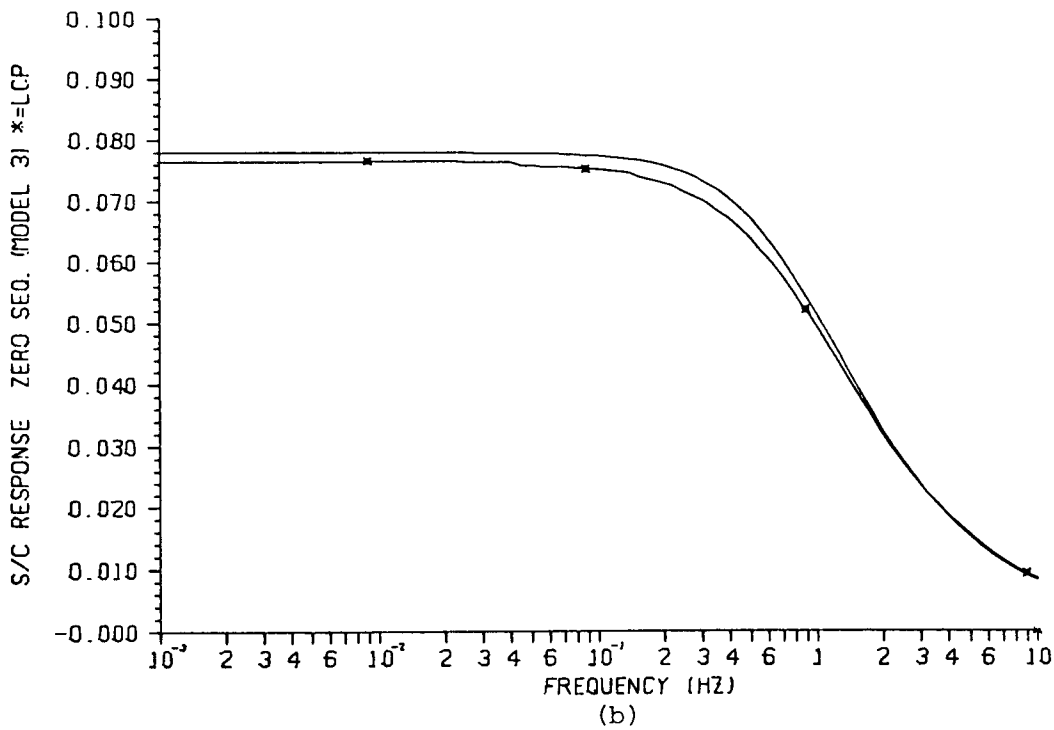

(b)

Graph 2.37: S/C response, model 3. Low frequencies.
(a) Positive sequence (b) Zero sequence

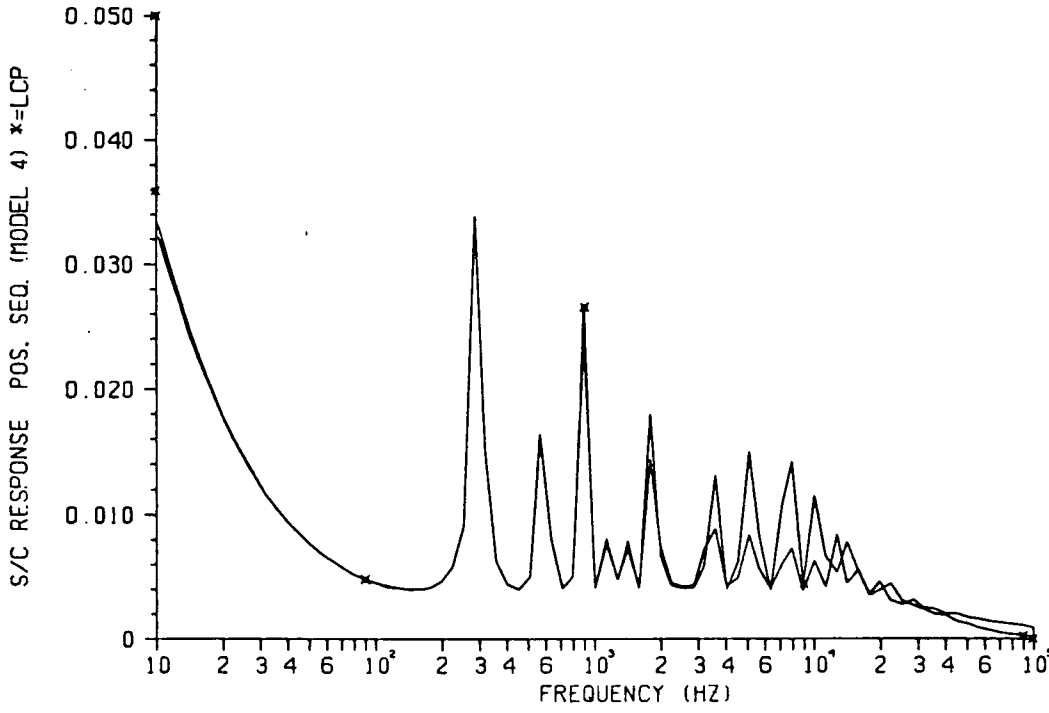

(a)

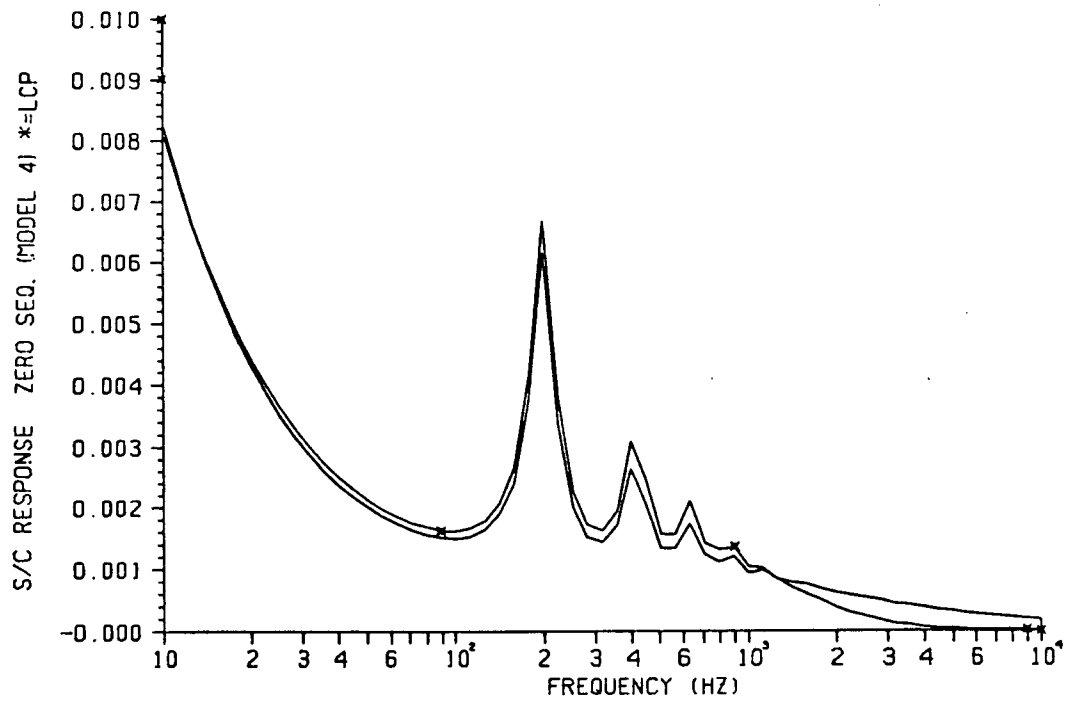

(b)

Graph 2.38: S/C response, model 4. Mid to high frequencies.
(a) Positive sequence (b) Zero sequence

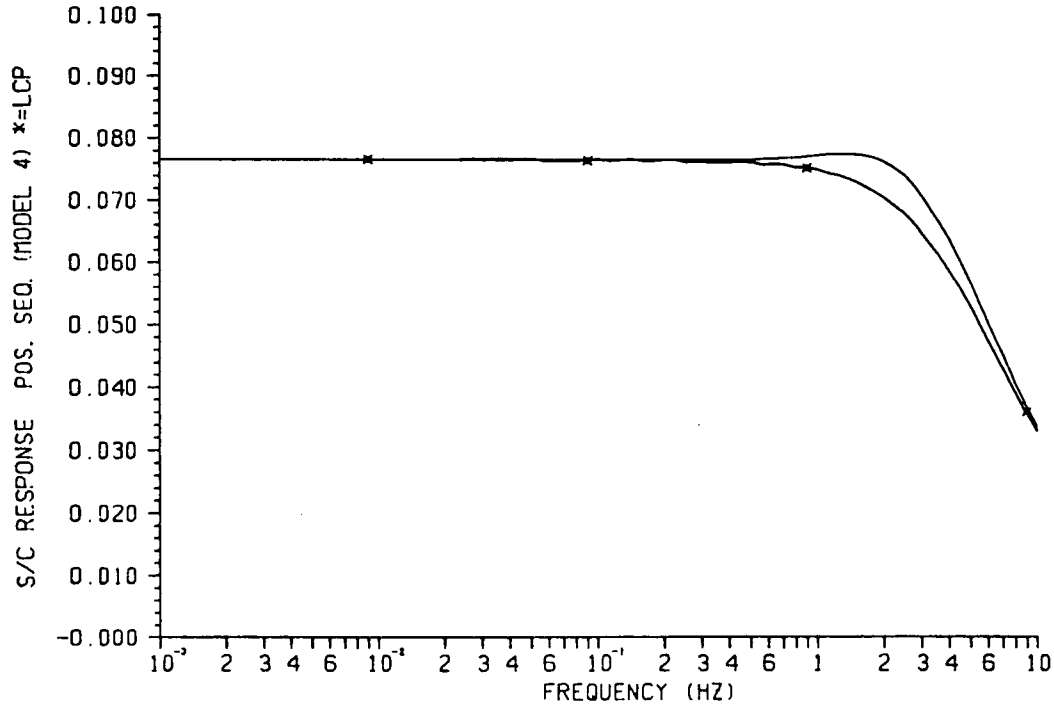

(a)

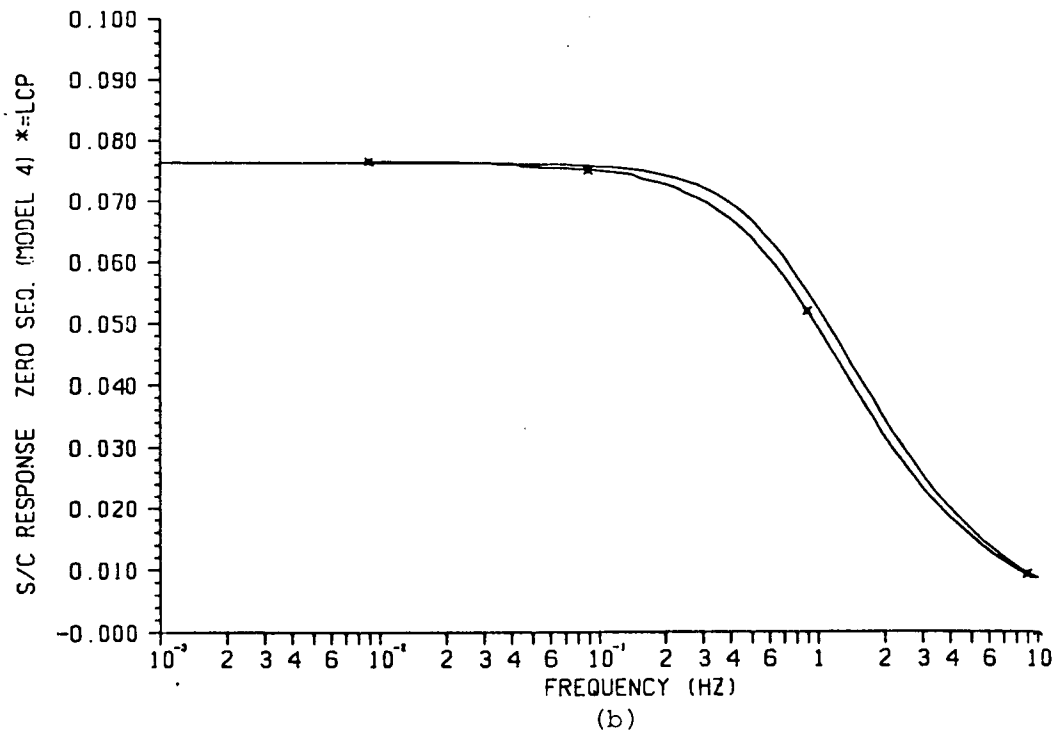

(b)

Graph 2.39: S/C response, model 4. Low frequencies.
(a) Positive sequence (b) Zero sequence

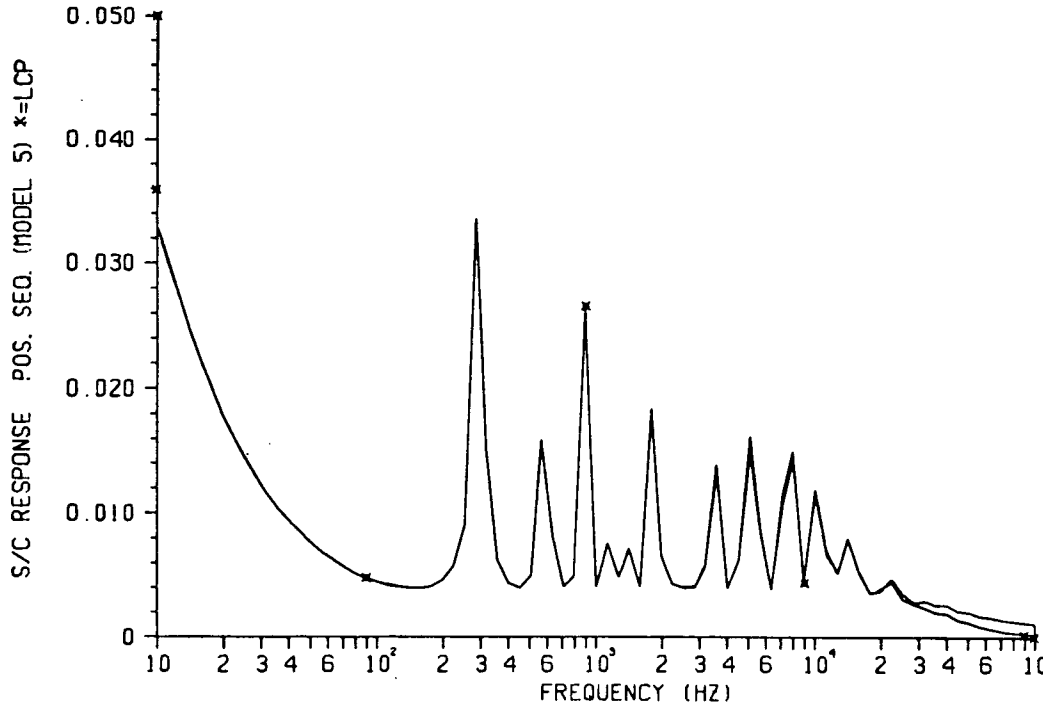

(a)

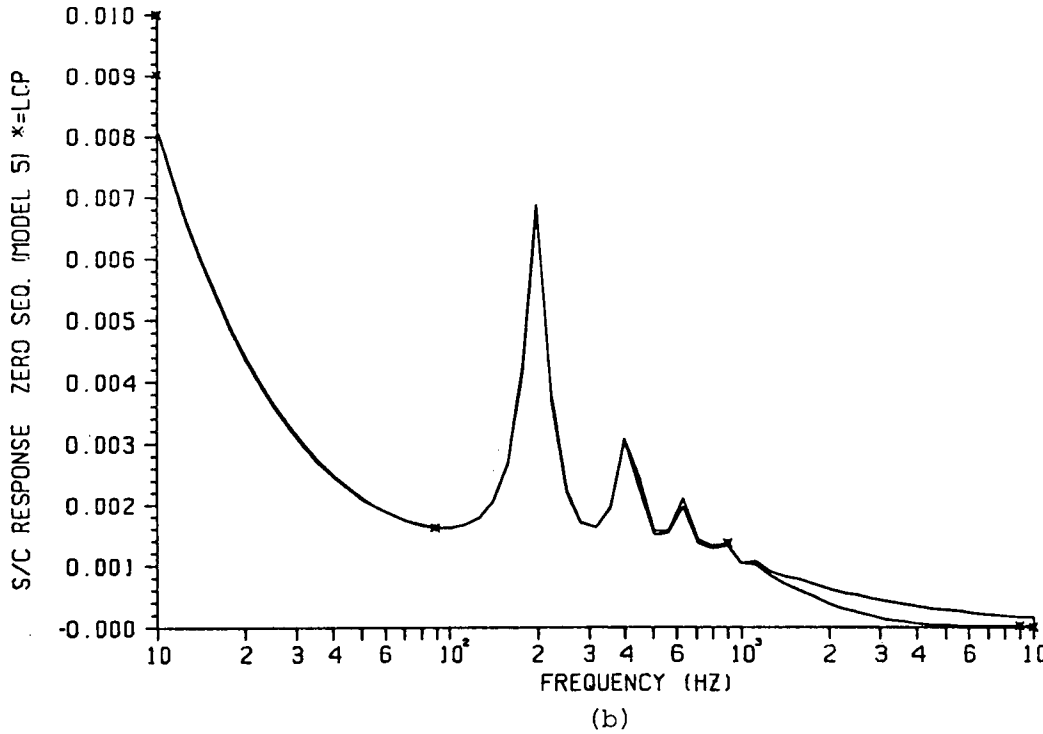

(b)

Graph 2.40: S/C response, model 5. Mid to high frequencies.
(a) Positive sequence (b) Zero sequence

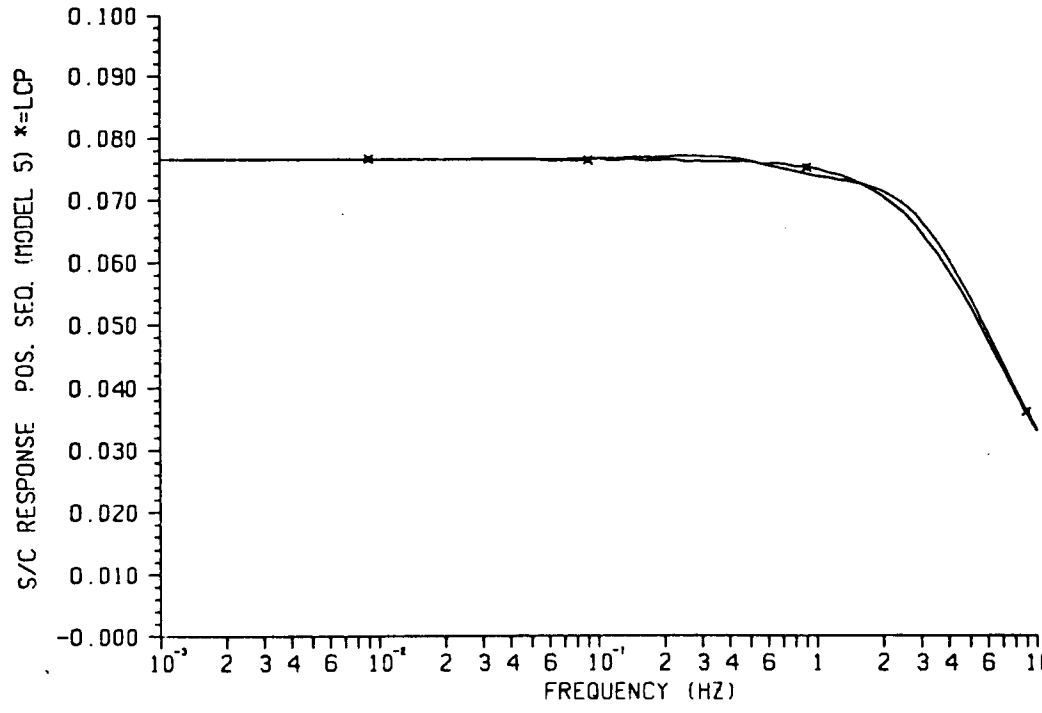

(a)

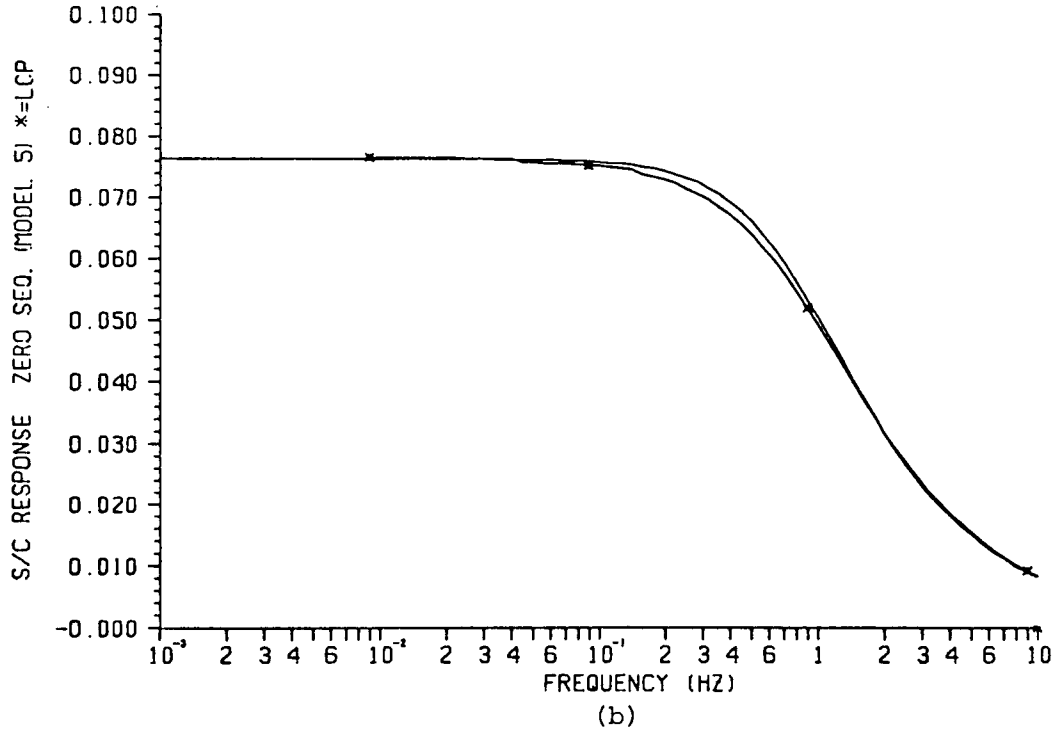

(b)

Graph 2.41: S/C response, model 5. Low frequencies.
(a) Positive sequence (b) Zero sequence

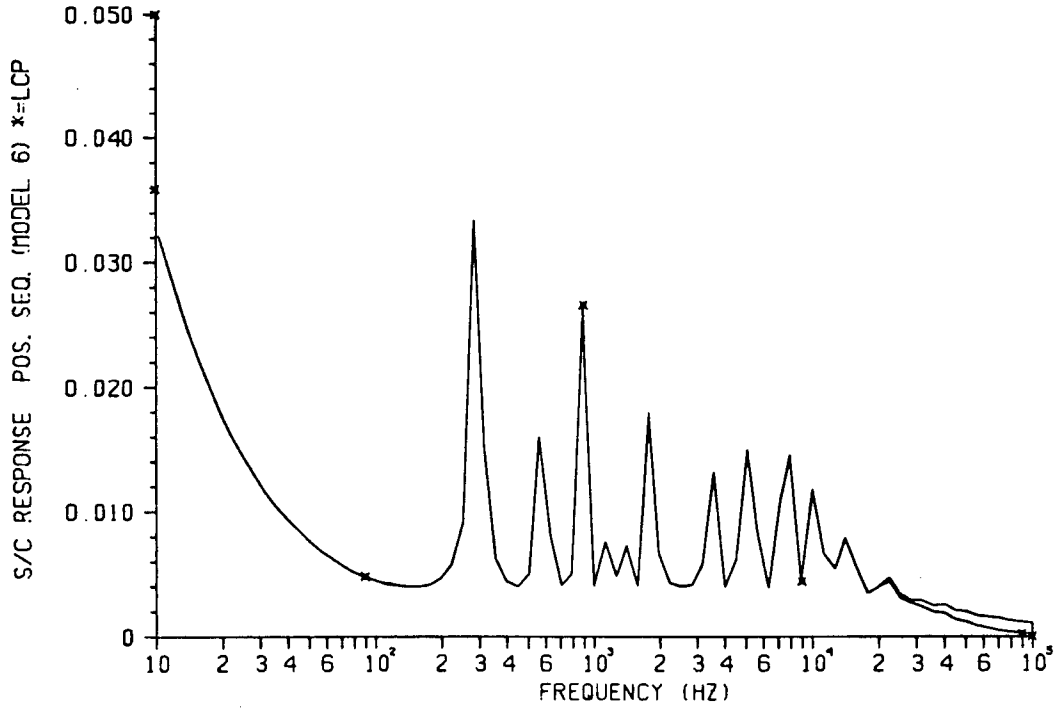

(a)

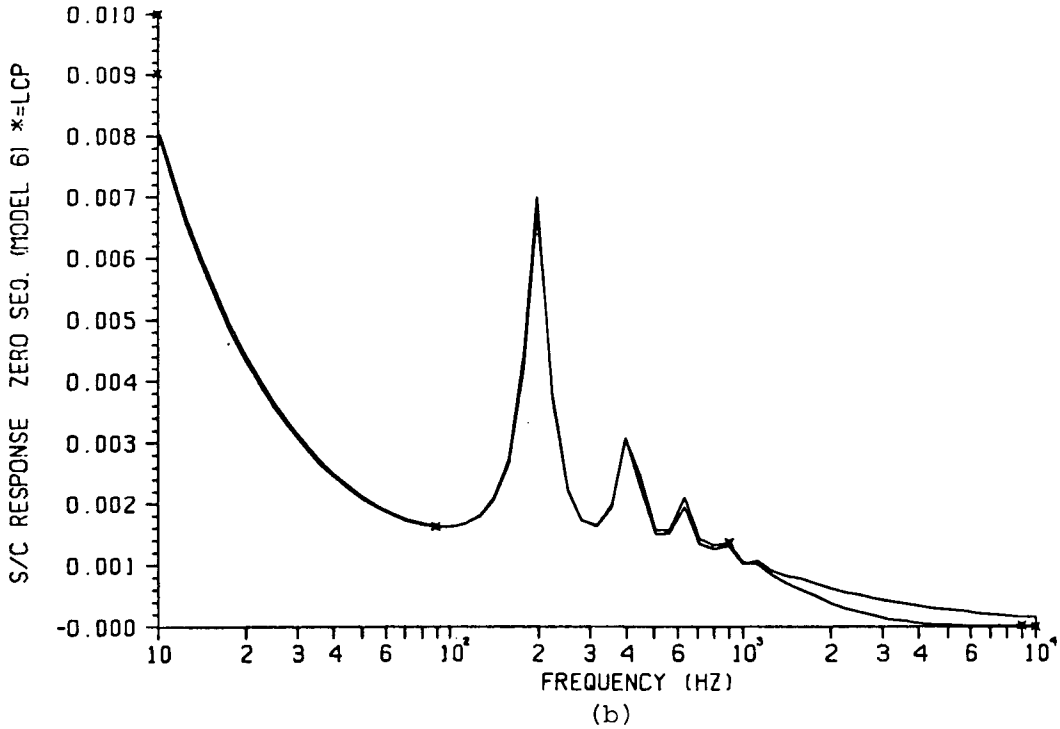

(b)

Graph 2.42: S/C response, model 6. Mid to high frequencies.
(a) Positive sequence (b) Zero sequence

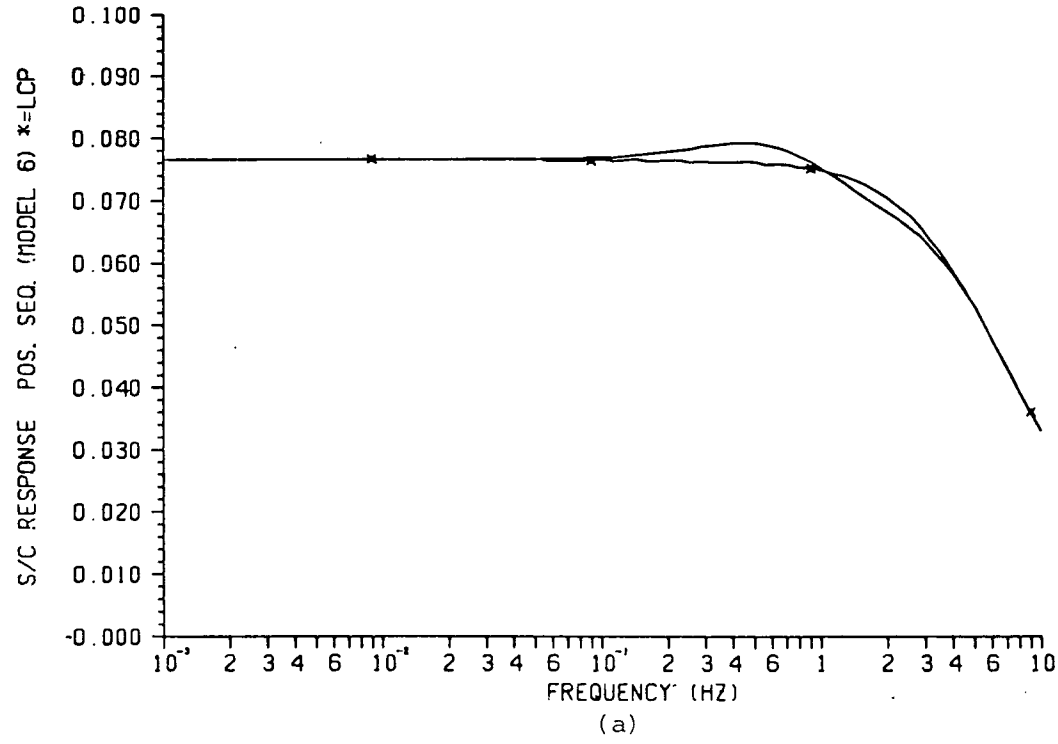

(a)

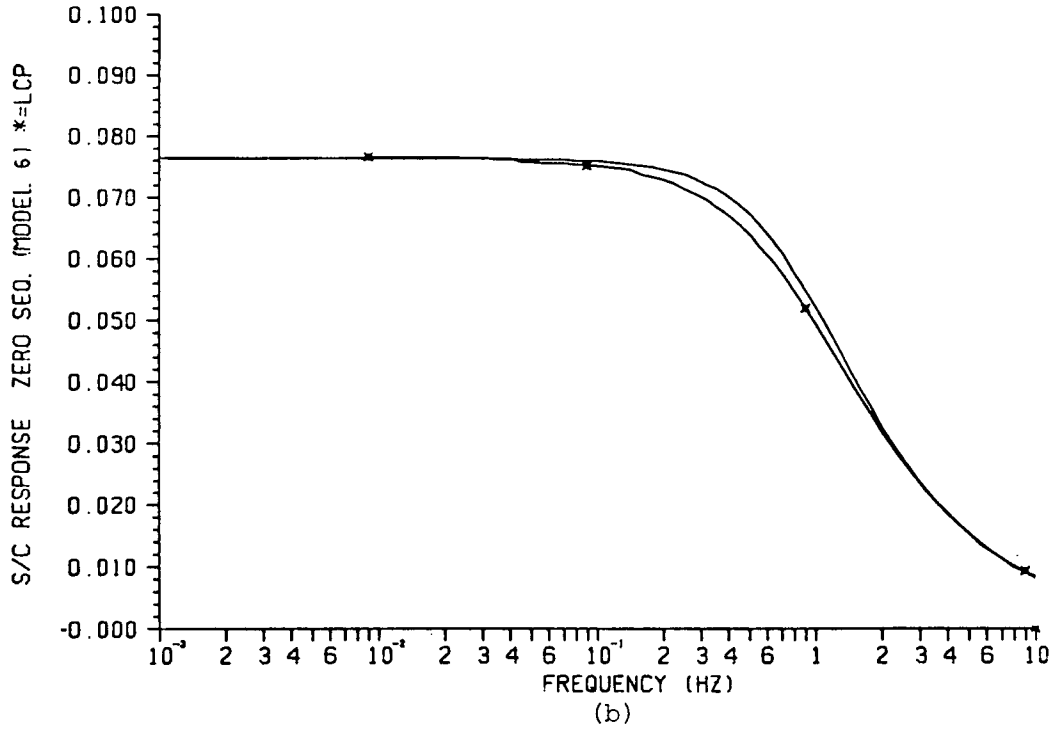

(b)

Graph 2.43: S/C response, model 6. Low frequencies.
(a) Positive sequence (b) Zero sequence

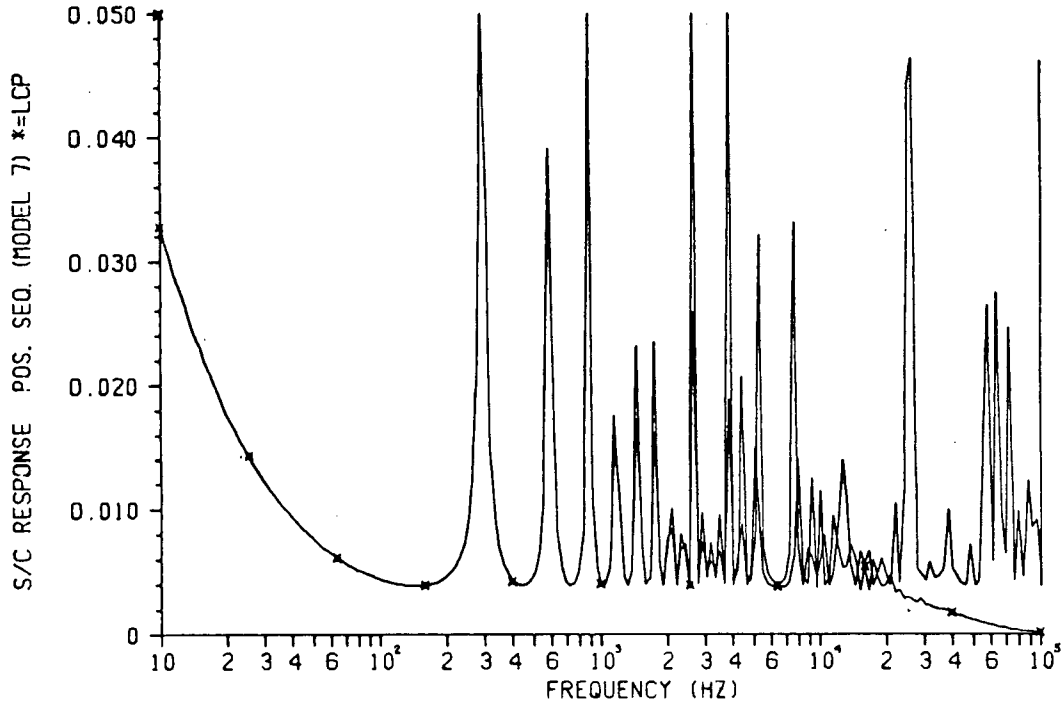

(a)

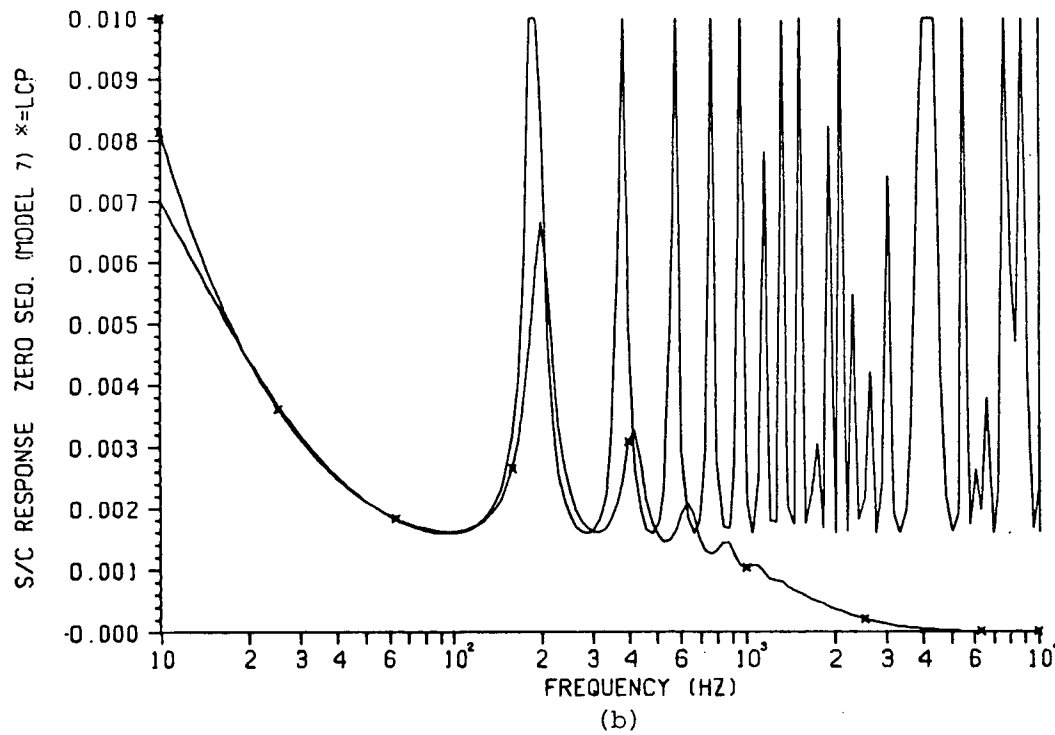

(b)

Graph 2.44: S/C response, model 7. Mid to high frequencies.
(a) Positive sequence (b) Zero sequence

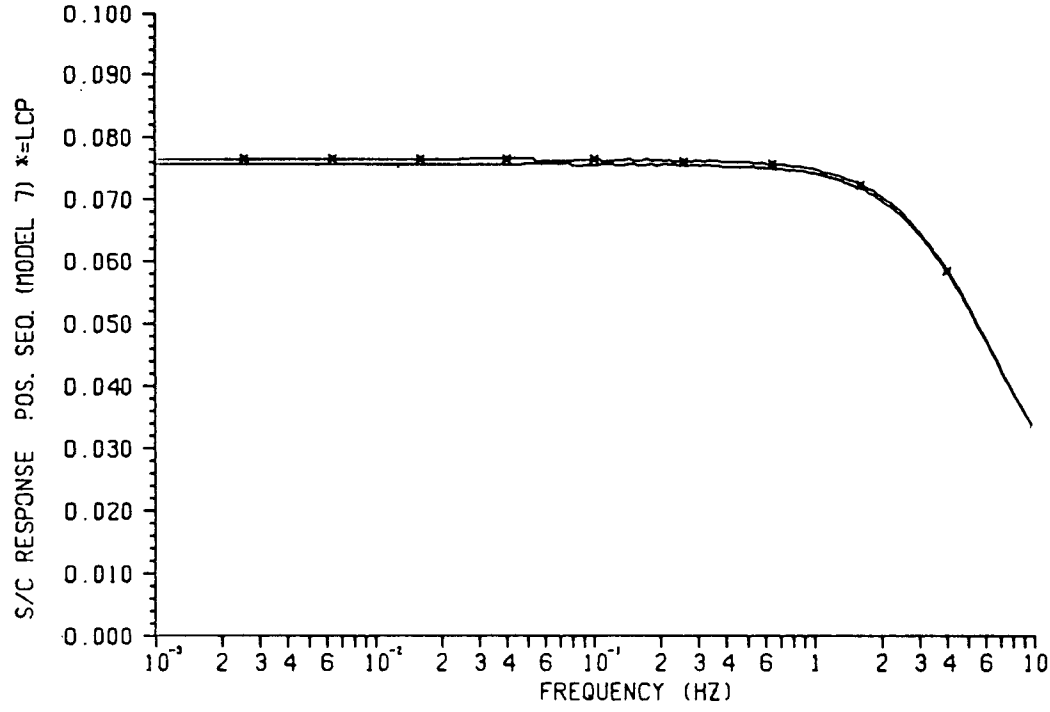

(a)

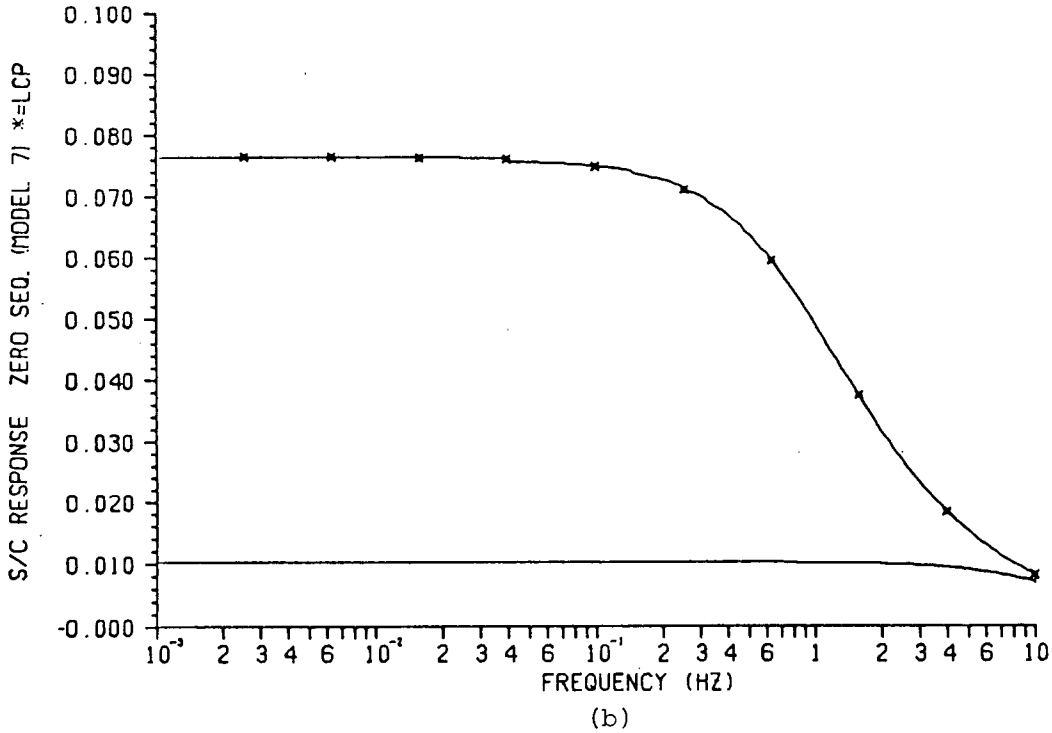

(b)

Graph 2.45: S/C response, model 7. Low frequencies.
(a) Positive sequence (b) Zero sequence

3.6 Transient Simulation in the EMTP

To complement the tests in section 3.5, a transient simulation using the EMTP, will be shown in this section. Consider the circuit in Figure 3.2.

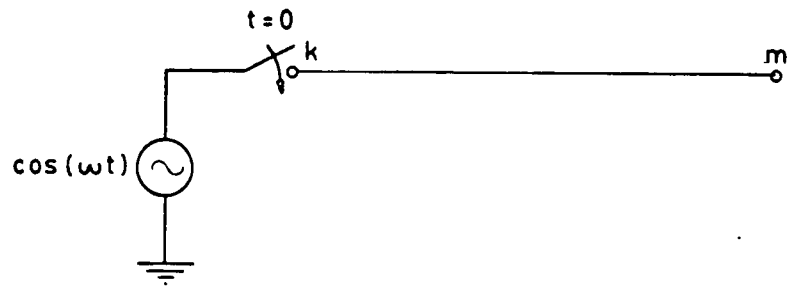

Fig. 3.2: Line energization test.

The line will be assumed to be single-phase with positive or zero sequence parameters. The 60 Hz sinusoidal voltage source (1.0 p.u. peak) is connected to the circuit at t = 0, and the receiving end is open. The receiving end voltages for the different models used in section 3.5 are shown in graphs 2.46 to 2.51. Note that the results from the high order approximation, obtained with the frequency-dependence routines of the EMTP (model 1), are used as a reference.

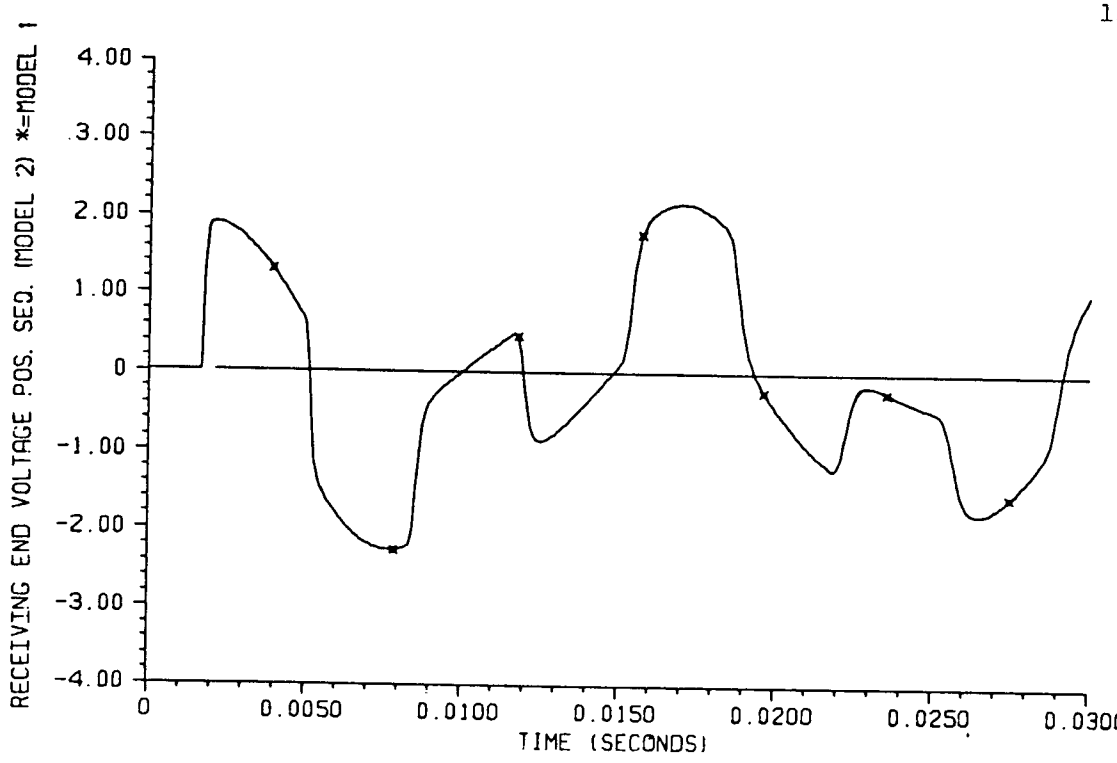

(a)

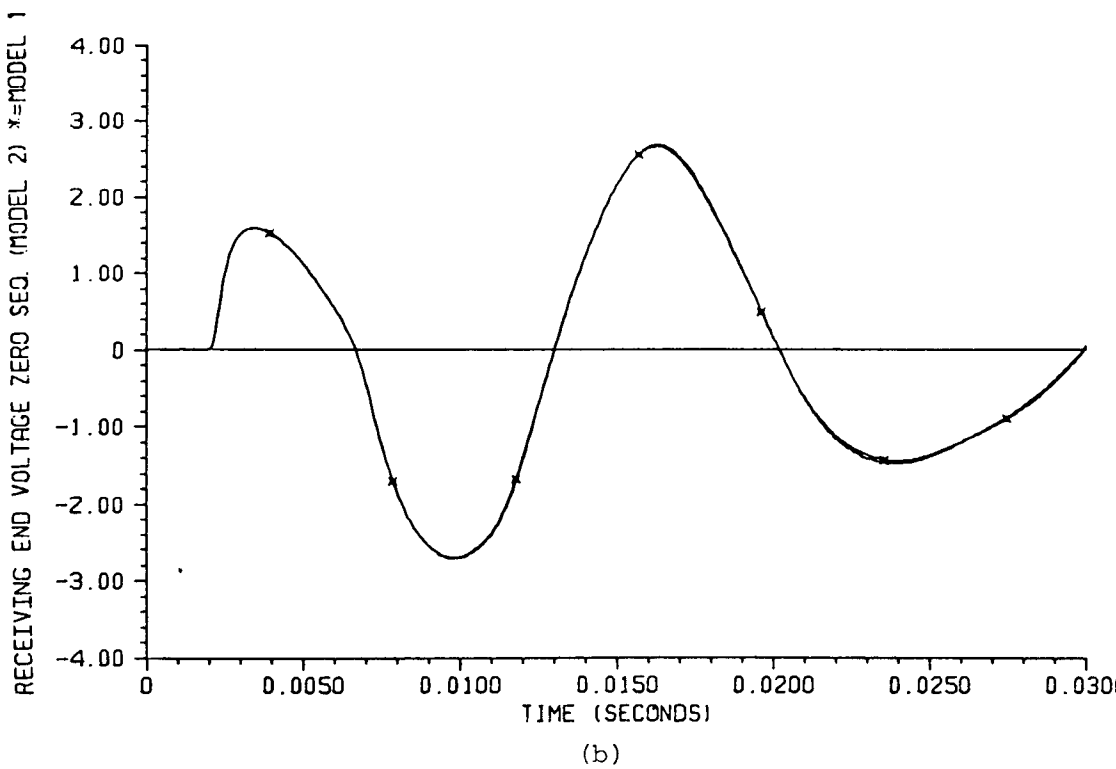

(b)

Graph 2.46: Energization test, receiving end voltage. Model 2.
(a) Positive sequence (b) Zero sequence

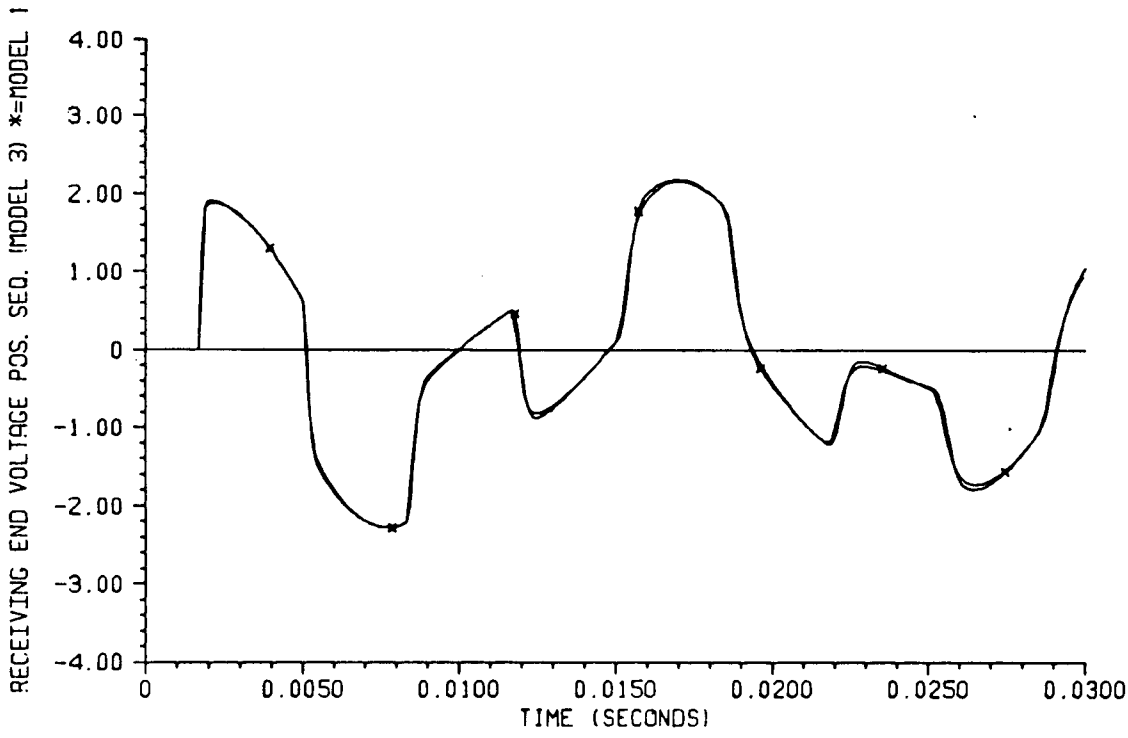

(a)

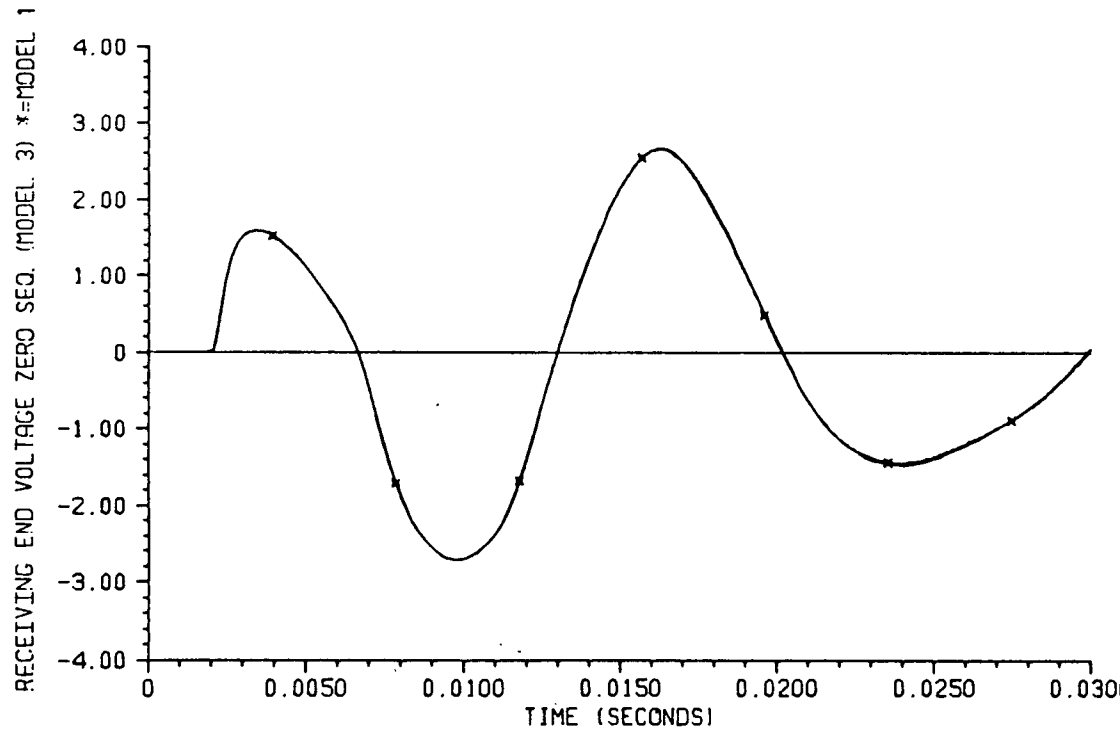

(b)

Graph 2.47: Energization test, receiving end voltage. Model 3.
(a) Positive sequence (b) Zero sequence

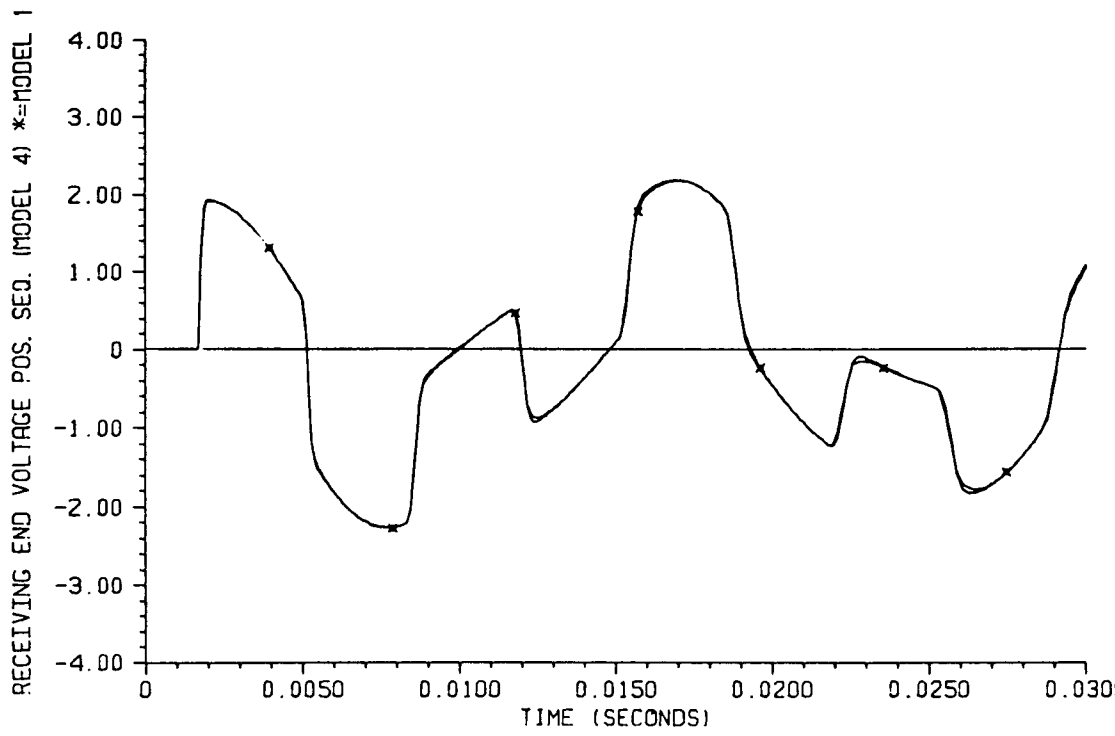

(a)

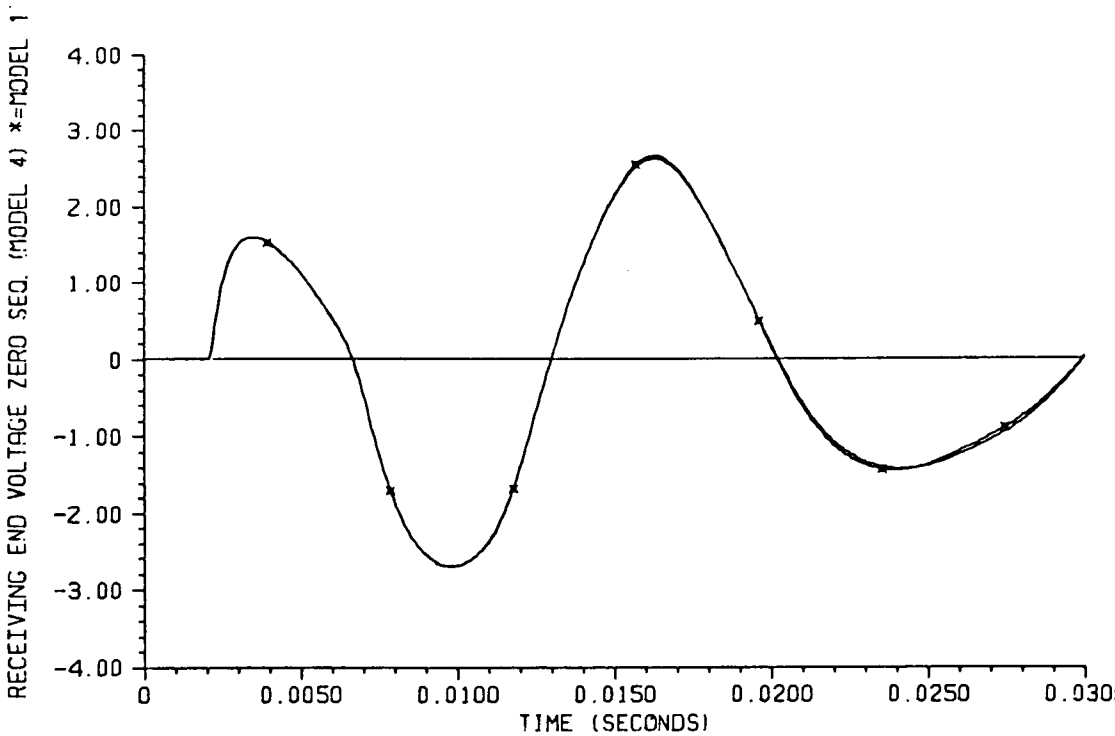

(b)

Graph 2.48: Energization test, receiving end voltage. Model 4.
(a) Positive sequence (b) Zero sequence

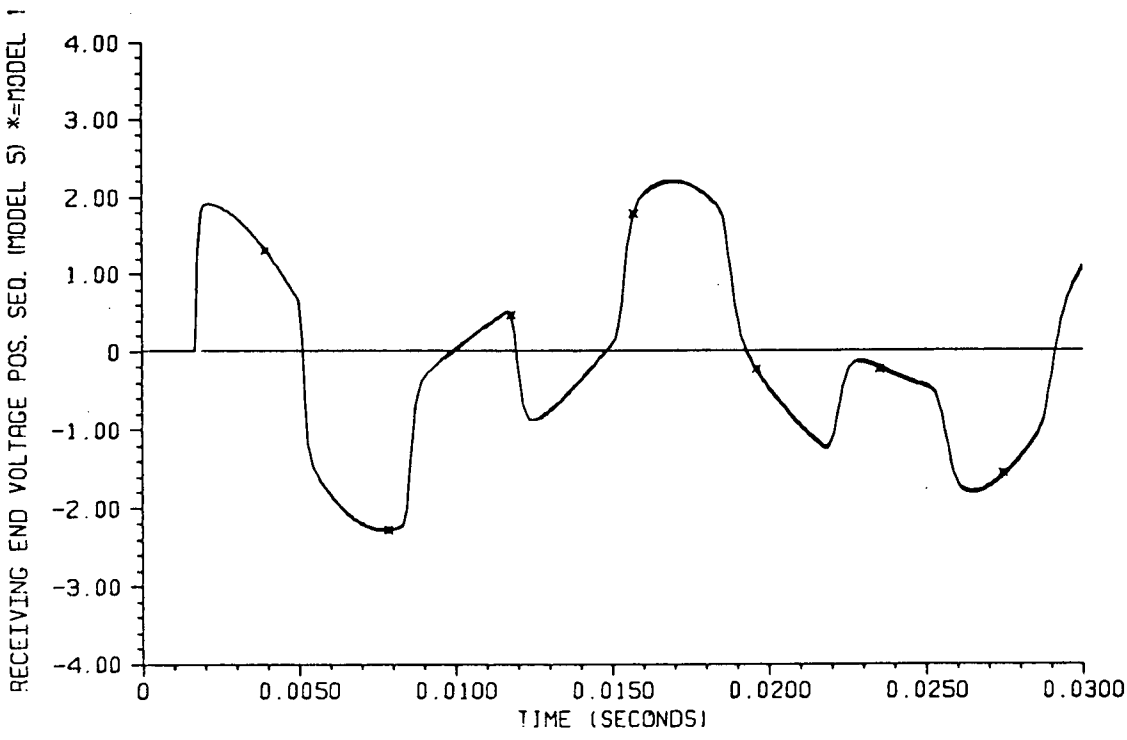

(a)

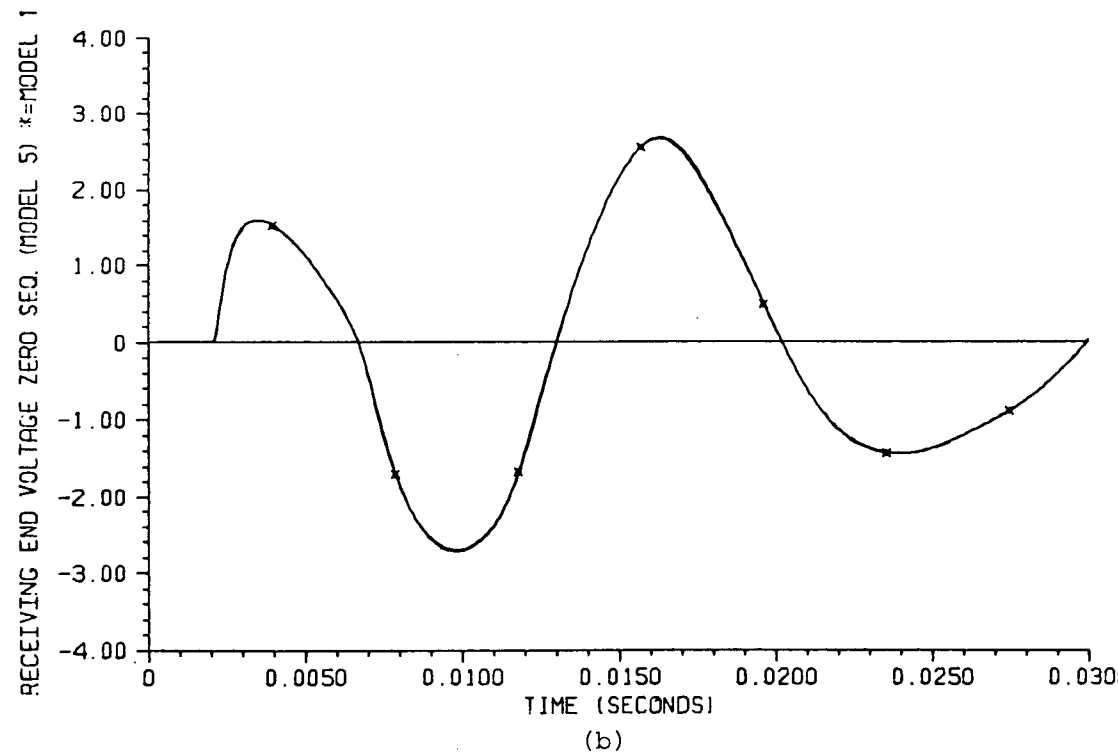

(b)

Graph 2.49: Energization test, receiving end voltage. Model 5.
(a) Positive sequence (b) Zero sequence

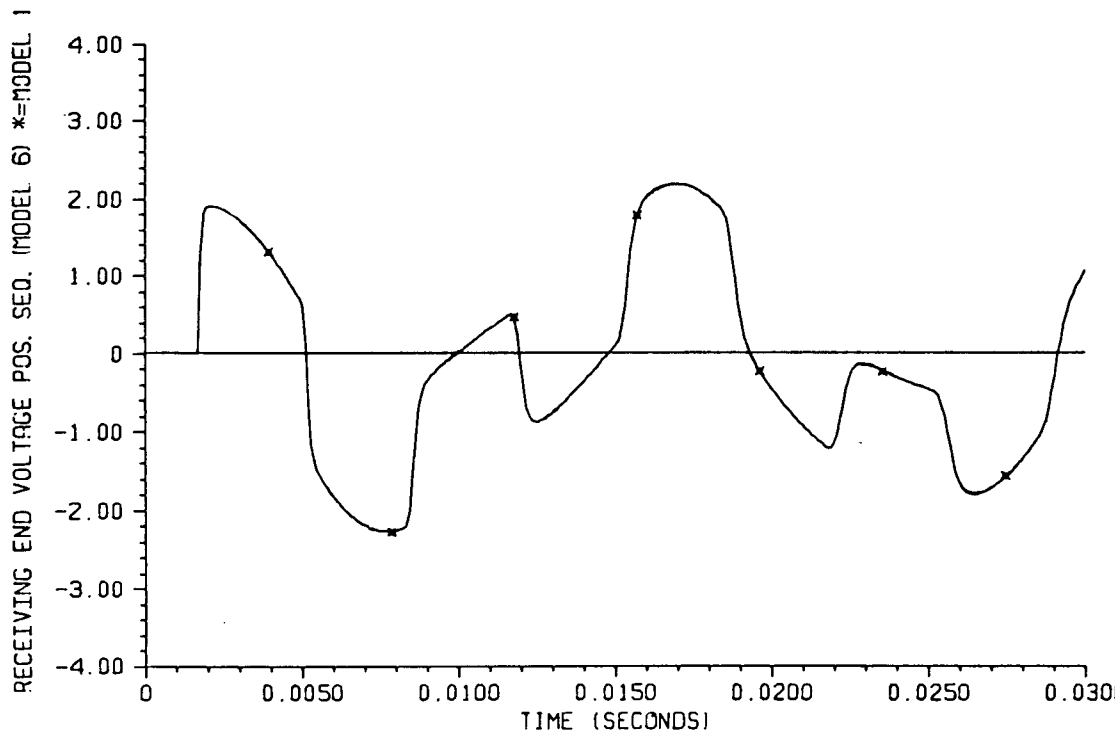

(a)

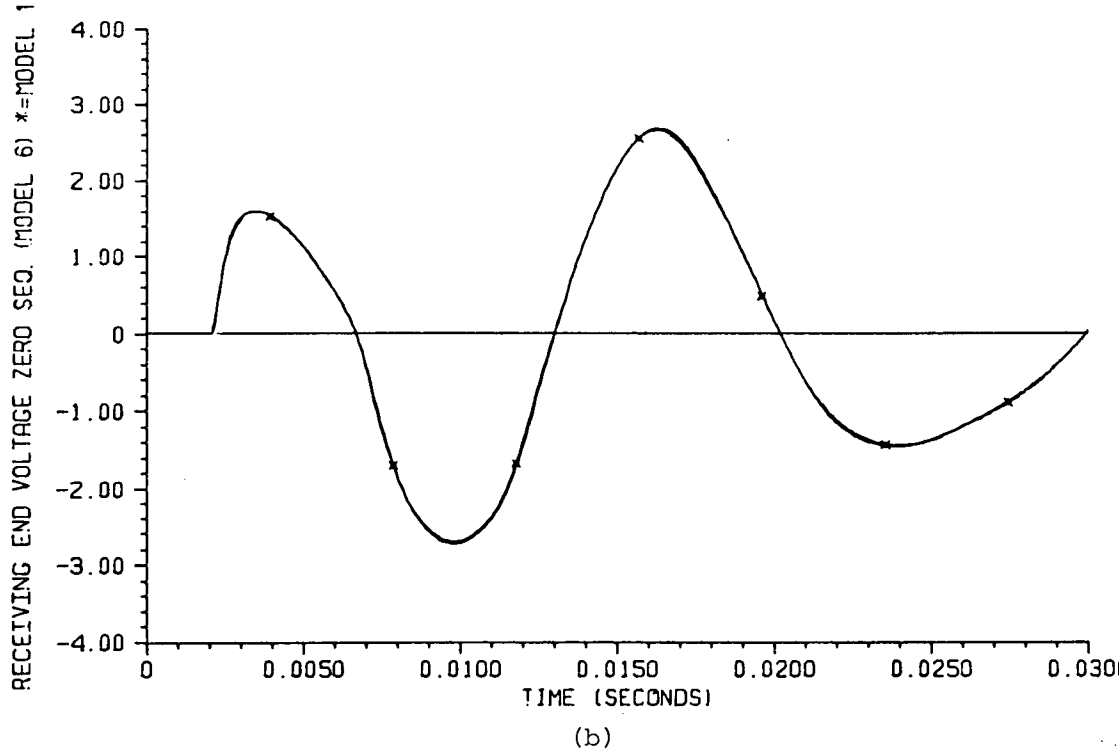

(b)

Graph 2.50: Energization test, receiving end voltage. Model 6.
(a) Positive sequence (b) Zero sequence

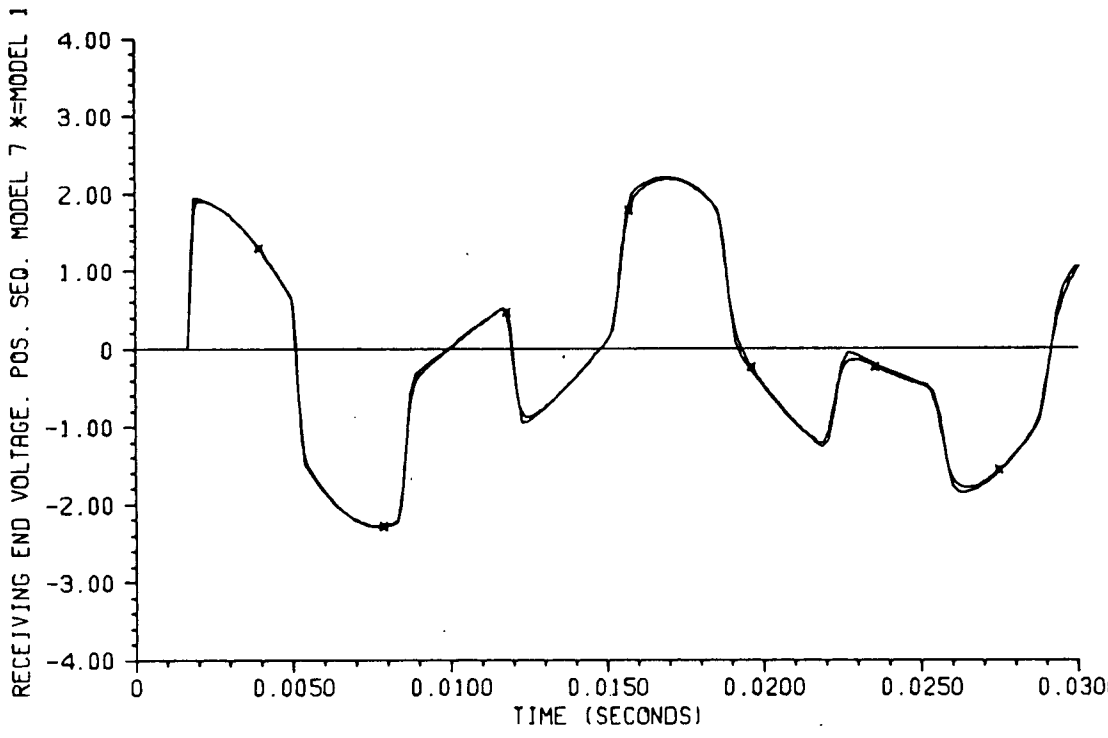

(a)

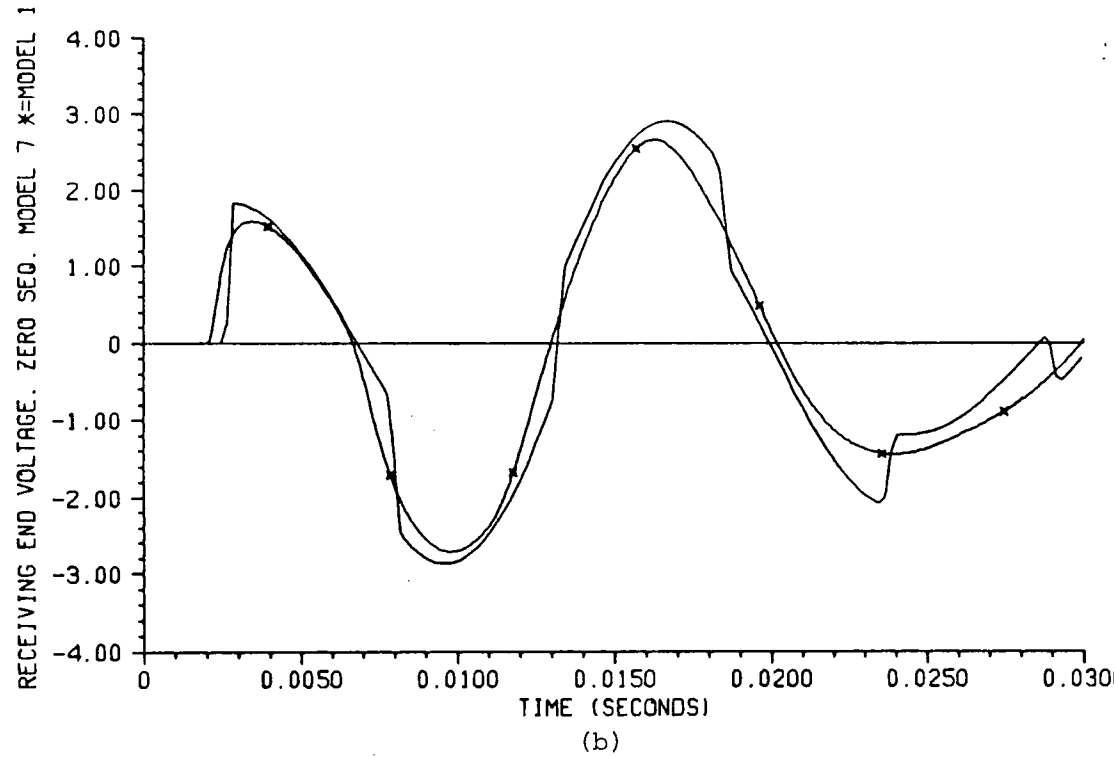

(b)

Graph 2.51: Energization test, receiving end voltage. Model 7.
(a) Positive sequence (b) Zero sequence

CONCLUSIONS

A low-order approximation for the frequency-dependent parameters of a transposed, overhead transmission line, has been obtained in the second part of this thesis project.

The amount of information required for such an approximation is relatively small. Compared to the constant parameters option of the EMTP, the only additional parameters needed to approximate the frequency-dependent behaviour of the line, are the earth resistivity and the dc resistance of the conductors.

The main advantages of this approximation can be summarized as follows:

i) It is computationally faster than the existing frequency-dependence routines of the EMTP, both in the line parameters approximating process and during transient simulations.

ii) It is more accurate than the constant parameters model.

iii) It gives very accurate results over the low to mid frequencies range.

Two main disadvantages can be pointed out:

i) The equivalent line configuration is only accurate when the transmission line can be assumed to be perfectly transposed.

ii) It loses accuracy when very fast transients are considered.

APPENDIX I-A

GENERAL SOLUTION OF THE LINE EQUATIONS IN THE FREQUENCY DOMAIN

The equations relating voltages and currents in the frequency domain are

$$-\frac{d\,V_{ph}}{dx} = Z_{ph}\ I_{ph} \quad \text{(series voltage drop equation)} \qquad \text{(I-A.1)}$$

$$-\frac{d\,I_{ph}}{dx} = Y_{ph}\ V_{ph} \quad \text{(shunt current drop equation).} \qquad \text{(I-A.2)}$$

Where Z_{ph} and Y_{ph} are the series impedance and shunt admittance matrices, respectively, and the subscript $_{ph}$ stands for phase quantities. Differentiating (I-A.1) and (I-A.2) we obtain

$$\frac{d^2\,V_{ph}}{d\,x^2} = (Z_{ph}\ Y_{ph})\ V_{ph} \qquad \text{(I-A.3)}$$

$$\frac{d^2\,I_{ph}}{d\,x^2} = (Y_{ph}\ Z_{ph})\ I_{ph} \qquad \text{(I-A.4)}$$

To proceed with the solution of equations (I-A.3) and (I-A.4), it is convenient to diagonalize $(Z_{ph}\ Y_{ph})$ and $(Y_{ph}\ Z_{ph})$ in order to obtain a decoupled set of differential equations.

Let P and Q be the matrices that diagonalize $(Z_{ph}\ Y_{ph})$ and $(Y_{ph}Z_{ph})$, respectively. Then

$$P^{-1}\ Z_{ph}\ Y_{ph}\ P = D_{zy} \quad \text{(diagonal)} \qquad \text{(I-A.5)}$$

$$Q^{-1}\ Y_{ph}\ Z_{ph}\ Q = D_{yz} \quad \text{(diagonal).} \qquad \text{(I-A.6)}$$

Let us now define

$$P^{-1}\ V_{ph} = V_m \qquad \text{(I-A.7)}$$

$$Q^{-1}\ I_{ph} = I_m. \qquad \text{(I-A.8)}$$

Introducing these definitions and equations (I-A.5) and (I-A.6) into (I-A.3) and (I-A.4). we obtain

$$\frac{d^2 V_m}{d x^2} = D_{zy} V_m \qquad \text{(I-A.7)}$$

$$\frac{d^2 I_m}{d x^2} = D_{yz} I_m \qquad \text{(I-A.8)}$$

Introducing the above definitions into equations (I-A.1) and (I-A.2)

$$- \frac{d V_m}{d x} = D_z I_m \qquad \text{(I-A.9)}$$

$$- \frac{d I_m}{d x} = D_y V_m, \qquad \text{(I-A.10)}$$

where,

$$D_z = P^{-1} Z_{ph} Q = Z_m \qquad \text{(diagonal)} \qquad \text{(I-A.11)}$$

$$D_y = Q^{-1} Y_{ph} P = Y_m \qquad \text{(diagonal)}, \qquad \text{(I-A.12)}$$

and,

Z_m = modal impedance matrix

Y_m = modal admittance matrix

$D_{zy} = D_{yz} = \gamma^2$.

Equations (I-A.7) to (I-A.10) can now be rewritten,

$$\frac{d^2 V_m}{d x^2} = \gamma^2 V_m \qquad \text{(I-A.13)}$$

$$\frac{d^2 I_m}{d x^2} = \gamma^2 I_m \qquad \text{(I-A.14)}$$

$$- \frac{d V_m}{d x} = Z_m I_m \qquad \text{(I-A.15)}$$

$$-\frac{d\, I_m}{d\, x} = Y_m\, V_m \qquad \text{(I-A.16)}$$

These equations define the behaviour of the line in the modal domain. Since they are uncoupled, the solution is relatively simple and given by

$$V_m(x,\omega) = A\, e^{-\gamma(\omega)\, x} + B\, e^{\gamma(\omega)\, x} \qquad \text{(I-A.17)}$$

$$I_m(x,\omega) = \frac{A}{Z_c}\, e^{-\gamma(\omega)\, x} - \frac{B}{Z_c}\, e^{\gamma(\omega)\, x}\,, \qquad \text{(I-A.18)}$$

where,

$$\gamma = \sqrt{Z_m\, Y_m} \qquad \text{(propagation constant)}$$

$$Z_c = \sqrt{\frac{Z_m}{Y_m}} \qquad \text{(surge impedance)}$$

Note that Z_c and γ are diagonal matrices; this implies that equations (I-A.17) and (I-A.18) have the same form when Z_c and γ are either matrices or scalars (i.e., when only one propagation mode is under consideration). A and B are also diagonal matrices and they are defined by boundary conditions.

Consider, for example, the line below

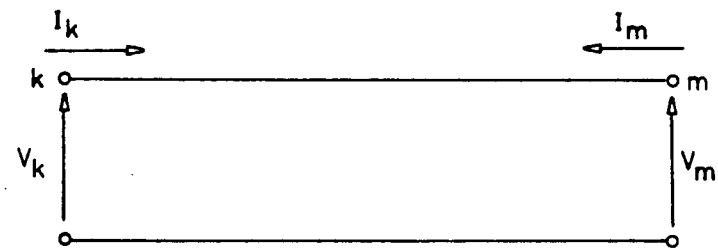

where only one propagation mode will be considered, and subscripts k and m now denote sending and receiving ends, respectively.

Taking, for instance, $x = \ell$

$$V_m = A\, e^{-\gamma\ell} + B\, e^{\gamma\ell}$$

$$-I_m = \frac{A}{Z_c} e^{-\gamma\ell} - \frac{B}{Z_c} e^{\gamma\ell}$$

give

$$A = \frac{V_m - Z_c I_m}{2} e^{\gamma\ell}$$

$$B = \frac{V_m + Z_c I_m}{2} e^{-\gamma\ell}.$$

Therefore the voltage and current at the sending end become

$$V_k = V_m \frac{e^{\gamma\ell} + e^{-\gamma\ell}}{2} - Z_c\, I_m \frac{e^{\gamma\ell} - e^{-\gamma\ell}}{2}$$

$$I_k = \frac{V_m}{Z_c} \frac{e^{\gamma\ell} - e^{-\gamma\ell}}{2} - I_m \frac{e^{\gamma\ell} + e^{-\gamma\ell}}{2}$$

which in terms of hyperbolic functions, give

$$V_k = V_m \cosh(\gamma\ell) - Z_c\, I_m \sinh(\gamma\ell) \qquad \text{(I-A.19)}$$

$$I_k = \frac{V_m}{Z_c} \sinh(\gamma\ell) - I_m \cosh(\gamma\ell) \qquad \text{(I-A.20)}$$

These represent the "classical" solution for a single phase line in the frequency domain. For detailed proof of the matrix relationships stated here, the reader should refer to [8].

APPENDIX I-B

JOSE MARTI'S FREQUENCY-DEPENDENCE MODEL

What follows is only a brief overview of the basic concepts upon which the frequency-dependence model used in this thesis project is based. Obvious space limitations do not permit a detailed explanation of the model, but rather a reference guide for the reader who is somewhat familiar with the model. For a more complete explanation of the model the reader should refer to [3] and [7].

Consider the line represented (for a given mode) in Figure I-B.1 below

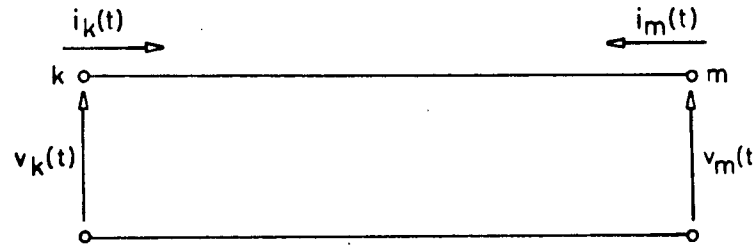

Fig. I-B.1: Modal representation in the time domain.

The associated model for this line in the frequency domain is shown in Figure I-B.2.

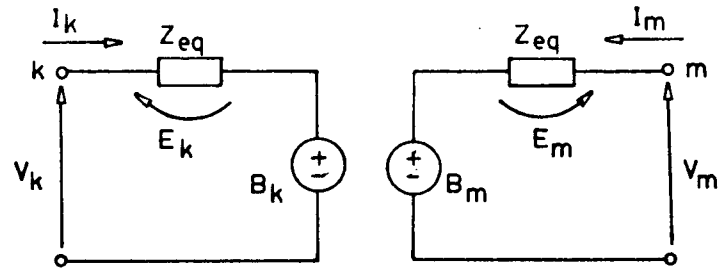

Fig. I-B.2: Line model in the frequency domain.

$Z_{eq}(\omega)$ is approximated as an R-C network which has, essentially, the same response as the surge impedance $Z_c(\omega)$. The backward propagation

functions $B_k(\omega)$ and $B_m(\omega)$ are defined as follows

$$B_k(\omega) = V_k(\omega) - Z_{eq}(\omega)\, I_k(\omega) \qquad \text{(I-B.1)}$$

$$B_m(\omega) = V_m(\omega) - Z_{eq}(\omega)\, I_m(\omega). \qquad \text{(I-B.2)}$$

Let us now define the forward propagation functions $F_k(\omega)$ and $F_m(\omega)$,

$$F_k(\omega) = V_k(\omega) + Z_{eq}(\omega)\, I_k(\omega) \qquad \text{(I-B.3)}$$

$$F_m(\omega) = V_m(\omega) + Z_{eq}(\omega)\, I_m(\omega). \qquad \text{(I-B.4)}$$

The general solution of the line in the frequency domain (see appendix I-A) is given by

$$V_k = \cosh(\gamma\ell)\, V_m - Z_c \sinh(\gamma\ell)\, I_m \qquad \text{(I-B.5)}$$

$$I_k = \frac{1}{Z_c} \sinh(\gamma\ell)\, V_m - \cosh(\gamma\ell)\, I_m. \qquad \text{(I-B.6)}$$

The relationship between $B_k(\omega)$ and $F_k(\omega)$ is found by combining equations (I-B.1) to (I-B.6). After some algebraic manipulations, and taking into account that $Z_{eq}(\omega) = Z_c(\omega)$, we obtain,

$$B_k(\omega) = e^{-\gamma\ell}\, F_m(\omega) \qquad \text{(I-B.7)}$$

$$B_m(\omega) = e^{-\gamma\ell}\, F_k(\omega). \qquad \text{(I-B.8)}$$

Let us now define the propagation function $A_1(\omega)$ as

$$A_1(\omega) = e^{-\gamma\ell}, \qquad \text{(I-B.9)}$$

where ℓ is the line length and $\gamma = \sqrt{Z'Y'}$ (see appendix I-A).

Equations (I-B.1) to (I-B.4) can now be rewritten as

$$B_k(\omega) = V_k(\omega) - E_k(\omega) = A_1 F_m(\omega) \qquad \text{(I-B.10)}$$

$$B_m(\omega) = V_m(\omega) - E_m(\omega) = A_1 F_k(\omega) \qquad \text{(I-B.11)}$$

$$F_k(\omega) = V_k(\omega) + E_k(\omega) \qquad \text{(I-B.12)}$$

$$F_m(\omega) = V_m(\omega) + E_m(\omega), \qquad \text{(I-B.13)}$$

where,

$$E_k(\omega) = I_k(\omega)\, Z_{eq}(\omega) \qquad \text{(I-B.14)}$$

$$E_m(\omega) = I_m(\omega)\, Z_{eq}(\omega). \qquad \text{(I-B.15)}$$

Since $Z_{eq}(\omega)$ is the response of a linear R-C network, the time domain representation of equations (I-B.10) through (I-B.15) can be found by means of the Inverse Fourier Transform, that is,

$$b_k(t) = v_k(t) - e_k(t) = a_1(t)*f_m(t) \qquad \text{(I-B.16)}$$

$$b_m(t) = v_m(t) - e_m(t) = a_1(t)*f_k(t), \qquad \text{(I-B.17)}$$

where

$$e_k(t) = z_{eq}(t)*i_k(t) \qquad \text{(I-B.18)}$$

$$e_m(t) = z_{eq}(t)*i_m(t). \qquad \text{(I-B.19)}$$

(lower case letters are used to indicate time domain quantities, while upper case is used in the frequency domain)

These equations define the equivalent circuit of Figure II-B.3

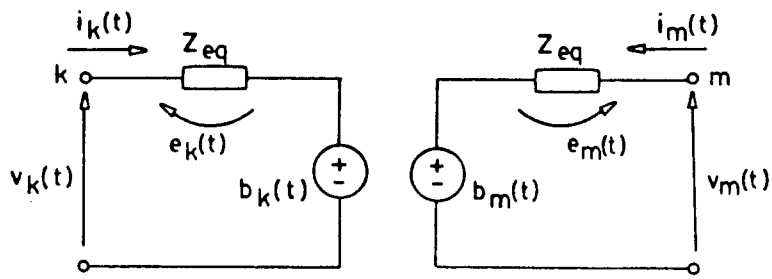

Fig. II-B.3: Frequency dependence model in the time domain.

Note that in the time domain, $e_k(t)$ is the voltage across the equivalent R-C network that simulates $Z_c(\omega)$.

The propagation function $a_1(t)$ in the time domain can be expressed as

$$a_1(t) = p(t-\tau), \qquad \text{(I-B.20)}$$

where p(t) has the same shape as $a_1(t)$ but displaced τ time units from the origin.

In the frequency domain $A_1(\omega)$ can then be expressed as

$$A_1(\omega) = P(\omega)\, e^{-j\omega\tau} \qquad \text{(I-B.21)}$$

The function $P(\omega)$ can be approximated by rational functions of the form

$$P(s) = H\, \frac{(s + z_1)\,(s + z_2) \ldots (s + z_n)}{(s + p_1)\,(s + p_2) \ldots (s + p_m)},$$

where z_i and p_i are the zeros and poles of P(s) in the complex plane; these singularities are real and lie in the left-hand side of the complex plane (m>n). P(s) can be expanded in partial fractions

$$P(s) = \frac{k_1}{s + p_1} + \frac{k_2}{s + p_2} + \ldots + \frac{k_m}{s + p_m}. \qquad \text{(I-B.22)}$$

Therefore, in the time domain p(t) becomes

$$p(t) = [k_1\, e^{-p_1 t} + k_2\, e^{-p_2 t} + \ldots + k_m\, e^{-p_m t}]\, u(t).$$

From equation (I-B.20) we now obtain $a_1(t)$

$$a_1(t) = [k_1\, e^{-p_1 (t-\tau)} + k_2\, e^{-p_2 (t-\tau)} + \ldots + k_m\, e^{-p_m (t-\tau)}]\, u(t-\tau) \qquad \text{(I-B.23)}$$

With $a_1(t)$ in the form of equation (I-B.23), the convolutions in equations (I-B.16) and (I-B.17) can be solved by recursive integration methods. Consider, for instance, the convolution integral of equation (I-B.16)

$$b_k(t) = \int_{-\infty}^{\infty} f_m(t-u)\, a_1(u)\, du,$$

since $a_1(t) = 0$ for $t<\tau$ this integral becomes

$$b_k(t) = \int_{\tau}^{\infty} f_m(t-u)\, a_1(u)\, du. \qquad \text{(I-B.24)}$$

Introducing equation (I-B.23) into (I-B.24),

$$b_k(t) = \sum_{i=1}^{m} b_{k,i}(t) \qquad \text{(I-B.25)}$$

where

$$b_{k,i}(t) = \int_{\tau}^{\infty} f_m(t-u)\ k_i\ e^{-\beta_i(u-\tau)}\ du \qquad \text{(I-B.26)}$$

Note that in equation (I-B.26) p_i has been substituted by β_i to avoid future confusion in notation. The integral in equation (I-B.26) can be broken into two parts,

$$b_{k,i}(t) = \int_{\tau}^{\tau+\Delta t} f_m(t-u)\ k_i\ e^{-\beta_i(u-\tau)}du + \int_{\tau+\Delta t}^{\infty} f_m(t-u)\ k_i\ e^{-\beta_i(u-\tau)}du, \qquad \text{(I-B.27)}$$

but the second integral in equation (I-B.27) is $e^{-\beta_i\Delta t}\ b_{ki}(t-\Delta t)$, and the first integral can be evaluated numerically using the trapezoidal rule. After some algebraic manipulations,

$$b_{k,i}(t) = g_i\ b_{k,i}(t-\Delta t) + c_i\ f_m(t-\tau) + d_i\ f_m(t-\tau-\Delta t), \qquad \text{(I-B.28)}$$

where,

$$g_i = e^{-\beta_i\Delta t}$$

$$h_i = \frac{1 - g_i}{\beta_i \Delta t}$$

$$c_i = \frac{k_i}{\beta_i}(1 - h_i)$$

$$d_i = -\frac{k_i}{\beta_i}(g_i - h_i)$$

and

$$b_k(t) = \sum_{i=1}^{m} b_{k,i}(t)$$

From equations (I-B.11) and (I-B.13) it can be seen that

$$f_m(t) = 2\ v_m(t) - b_m(t),$$

therefore, $b_{k,i}(t)$ in equation (I-B.28) depends only on past history values of $b_{k,i}$, b_m and v_m.

The evaluation of $e_k(t) = i_k(t) * z_{eq}(t)$ proceeds in a

similar fashion as the evaluation of $b_k(t)$. The rational fractions that approximate $Z_{eq}(\omega)$ are given by,

$$Z_{eq}(s) = H \frac{(s + z_1)(s + z_2) \ldots (s + z_n)}{(s + p_1)(s + p_2) \ldots (s + p_m)},$$

where, as in the case of $A_1(\omega)$ the poles are real and lie in the left-hand side of the complex plane, but in this case n = m.

Expanding in partial fractions,

$$Z_{eq}(s) = k_o + \frac{k_1}{s + p_1} + \ldots + \frac{k_m}{s + p_m} \qquad \text{(I-B.29)},$$

therefore,

$$z_{eq}(t) = [k_o\, \delta(t) + k_1\, e^{-\alpha_1 t} + \ldots + k_m\, e^{-\alpha_m t}]\, u(t), \qquad \text{(I-B.30)}$$

where p_i has been substituted by α_i to avoid ambiguity in the notation.

From equation (I-B.18)

$$e_k = \int_o^\infty i_k(t-u)\, z_{eq}(u)\, du, \qquad \text{(I-B.31)}$$

where the lower limit in the integral is zero because $z_{eq}(t) = 0$ for $t<0$.

Introducing equation (I-B.30) into (I-B.31),

$$e_k(t) = e_{k,o}(t) + \sum_{i=1}^{m} e_{k,i}(t), \qquad \text{(I-B.32)}$$

where,

$$e_{k,o}(t) = i_k(t)\, k_o = R_o\, i_k(t) \qquad \text{(I-B.33)}$$

$$e_{k,i}(t) = \int_o^\infty i_k(t-u)\, k_i\, e^{-\alpha_i u}\, du. \qquad \text{(I-B.34}$$

Noting that the integral in equation (I-B.34) is analogous to the integral in equation (I-B.24) with $\tau = 0$,

$$e_{k,i}(t) = m_i\, e_{k,i}(t-\Delta t) + p_i\, i_k(t) + q_i\, i_k(t-\Delta t) \qquad \text{(I-B.35)}$$

where,

$$m_i = e^{-\alpha_i \Delta t}$$

$$h_i = \frac{1 - m_i}{\alpha_i \Delta t}$$

$$p_i = \frac{k_i}{\alpha_i}(1-h_i)$$

$$q_i = -\frac{k_i}{\alpha_i}(m_i - h_i).$$

Introducing equations (I-B.33) and (I-B.35) into (I-B.32)

$$e_k(t) = R_k\, i_k(t) + e_{k,e}(t-\Delta t) + e_{k,c}(t-\Delta t), \qquad \text{(I-B.36)}$$

where,

$R_k = R_o + \sum_{i=1}^{m} p_i$ (equivalent constant resistance)

$e_{k,c}(t-\Delta t) = \left[\sum_{i=1}^{m} q_i\right] i_k(t-\Delta t)$ (history of currents)

$e_{k,e}(t-\Delta t) = \sum_{i=1}^{m} m_i\, e_{k,i}(t-\Delta t)$ (history of partial voltages $e_{k,i}$).

With equations (I-B.28) and (I-B.36), the equivalent circuit of Figure I-B.3 can be simplified as shown in Figure I-B.4

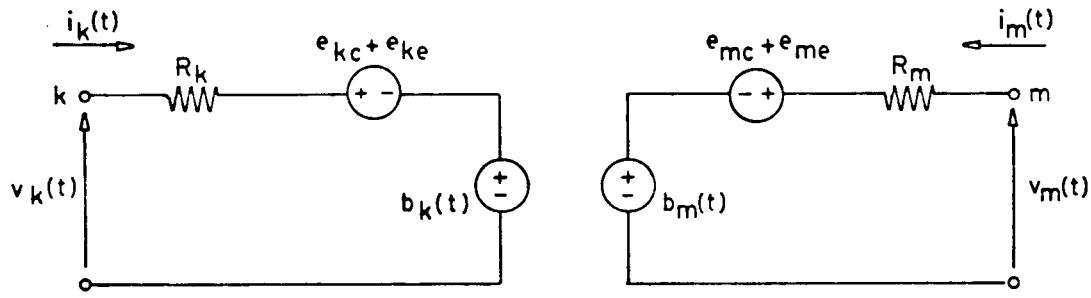

Fig. I-B.4: Equivalent circuit in the time domain

This equivalent circuit (using elementary circuit transformations) can be transformed into the circuit of Figure I-B.5, which is compatible with the EMTP;

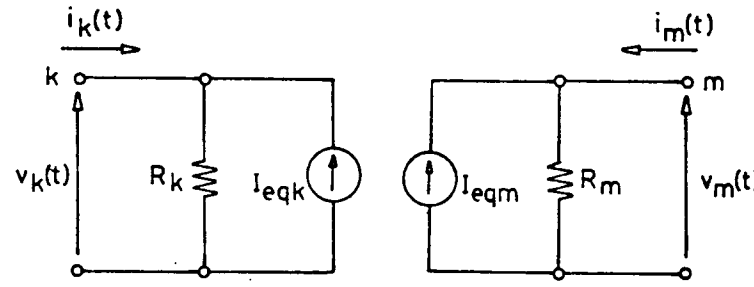

Fig. I-B.5: Simplifed circuit in the time domain.

where $i_{eq,k}$ is a past history current source, and R_k is an equivalent constant resistance,

$$i_{eq,k} = [e_{k,c}(t-\Delta t) + e_{k,e}(t-\Delta t) + b_k(t)]/R_k \qquad \text{(I-B.37)}$$

The equivalent circuit in Figure I-B.5 can be solved recording the past history values of equation (I-B.37). At the beginning of the process these are zero if the initial conditions at the ends of the line are zero.

If these initial conditions are not zero, that is, if they are given by pre-transient steady-state, or user-supplied dc initial conditions (i.e., trapped charge), the past history current sources can be determined as follows.

The equivalent circuit for steady-state conditions is shown in Figure I-B.6

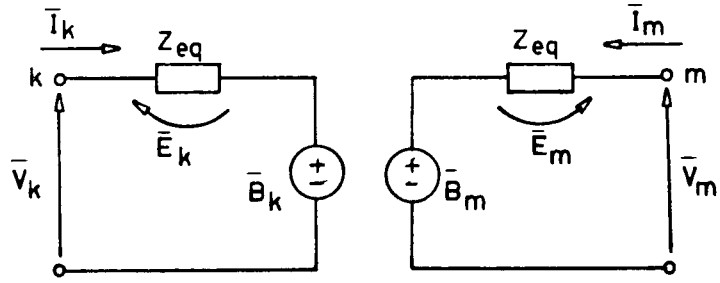

Fig. I-B.6: Equivalent circuit for steady-state conditions.

Consider for example node k. $\bar{V}_k$ and $\bar{I}_k$ are the phasor voltages and currents known from the initial steady-state solution of the system. We must now find the steady-state equivalents of

$$e_{k,i} \longleftrightarrow \bar{E}_{k,i}$$
$$b_{k,i} \longleftrightarrow \bar{B}_{k,i}$$
$$f_m \longleftrightarrow \bar{F}_m$$

From equation (I-B.14)

$$\bar{E}_k = \bar{I}_k Z_{eq}$$

but from equation (I-B.29)

$$Z_{eq} = Z_o + Z_1 + \ldots + Z_m, \tag{I-B.38}$$

where,

$$Z_o = k_o \tag{I-B.39}$$

$$Z_i = \frac{k_i}{j\omega + p_i} \cdot \tag{I-B.40}$$

Introducing (I-B.39) and (I-B.40) into (I-B.14)

$$\bar{E}_k = Z_o \bar{I}_k + \left(\sum_{i=1}^{m} Z_i \right) \bar{I}_k$$

therefore,

$$\bar{E}_{k,i} = Z_i \bar{I}_k$$

Partial history sources $B_{k,i}$ are obtained as follows:

From equation (I-B.10)

$$\bar{B}_k = A_1 \bar{F}_m ,$$

but from equations (I-B.21) and (I-B.22)

$$A_1 = A_{1,1} + A_{1,2} + \cdots + A_{1,n}$$

where,

$$A_{1,i} = \frac{k_i}{j\omega + p_i} e^{-j\omega\tau}$$

Introducing (I-B.42) into (I-B.10),

$$\bar{B}_k = \bar{F}_m \left(\sum_{i=1}^{m} A_{1,i} \right) ,$$

and,

$$\bar{B}_{k,i} = \bar{F}_m A_{1,i}$$

Finally, $\bar{F}_m$ is obtained from equation (I-B.4)

$$\bar{F}_m = \bar{V}_m + Z_{eq} \bar{I}_m$$

The phasor quantities in the time domain are given by

$$e_{k,i}(t) = |\bar{E}_{k,i}| \cos(\omega t + \arg(\bar{E}_{k,i}))$$

$$b_{k,i}(t) = |\bar{B}_{k,i}| \cos(\omega t + \arg(\bar{B}_{k,i}))$$

$$f_m(t) = |\bar{F}_m| \cos(\omega t + \arg(\bar{F}_m)) .$$

When the initial conditions are supplied by the user, i.e., trapped charge, the initial values of $e_{k,i}$, $b_{k,i}$ and f_m can be obtained as before by setting $\omega = 0$.

A similar procedure is followed for node m.

APPENDIX I-C

USER'S GUIDE FOR THE VOLTAGE AND CURRENT PROFILE OPTION OF THE EMTP, AND FOR THE OUTPUT DISPLAY PROGRAM

The routines that evaluate the electrical profile of a line have been implemented as part of the frequency-dependence version of UBC's EMTP The object code of this version is available to UBC users under the name LUI:MDTRAN3.0. The interconnection with the EMTP required approximately 90 FORTRAN statements, and the supporting subroutines required slightly less than 660 FORTRAN statements.

A typical call to this version of the EMTP is shown below

```
$ RUN LUI:MDTRAN3.O 0=PAR.INT  1=PAR  2=-2  3=-3  4=-4  5=TRAN.DA 6=-X
```

The only differences between this command and the standard frequency-dependence command are logical units 0 and 3.

Logical unit 0 contains the constants k_i and β_i from the rational-functions approximation of $A_1(\omega)$ for the length of one of the segments into which the line has been subdivided. File PAR.INT does not include the approximation for $z_c(\omega)$ since it is the same used for the complete line (logical unit 1 still contains the same parameters whether the profile is requested or not).

The currents and voltages are written in free format (to save computer costs and to ease the manipulation of the large amounts of data involved) into logical unit 3.

To invoke the "profile" option, the following modifications have been introduced into the line card (frequency-dependence option) in file TRAN.DA (logical unit 5)

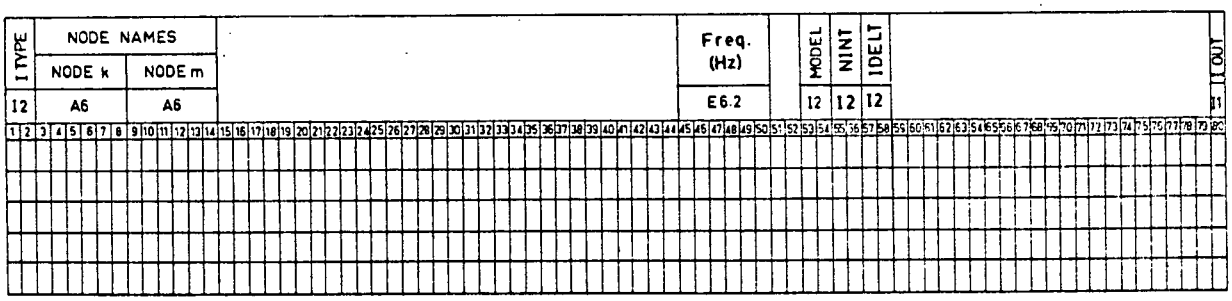

The additional parameters are explained below:

NINT > 0 number of intermediate voltages and currents. The minimum is 1 and the maximum is 99.

= 0 disables "profile" option.

IDELT > 0 number of times the internal Δt is to be segmented. For example, IDELT=2 reduces the internal time step $\Delta t'$ to $\Delta t'/2$.

IDELT = 0 the internal Δt is determined automatically by the program.

(Note that even if IDELT > 0, the voltages and currents will still be printed with the same number of time steps defined in the main program).

A time saving option has been included in the time card,

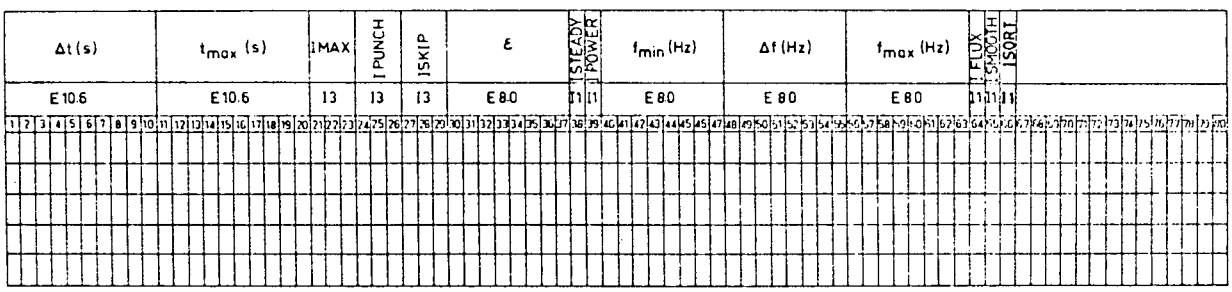

ISORT = 0 or 1 All voltages and currents will be written on logical unit 3.

ISORT = 2 Only the intermediate voltages will be written on logical unit 3.

ISORT = 3 Only the intermediate currents will be written on logical unit 3.

A sample of the different input files is shown below for the John Day - Lower Monumental line. Only the intermediate voltages are requested, the line will be segmented into 9 sections, and the internal

time step will be made two times smaller than the internally calculated time step.

```
 1     INTERMEDIATE PARAMETERS  ARRESTER TEST. 3PHASE MON LINE
 2     .93322E-05.020                        0                      2
 3     -1SWIA  TWOA                                 60.00  -1 9
 4     -2SWIB  TWOB                                 60.00  -1 9
 5     -3SWIC  TWOC                                 60.00  -1 9
 6
 7       ONEA  SWIA   .0005     1.0
 8       ONEB  SWIB   .0003     1.0
 9       ONEC  SWIC   .0006     1.0
10     92TWOA        1.0              2.6       2.0
11     92TWOB        1.0              2.6       2.0
12     92TWOC        1.0              2.6       2.0
13
14     14ONEA   1 1.0      60.      -10.8                          0.0
15     14ONEB   1 1.0      60.      -130.8                         0.0
16     14ONEC   1 1.0      60.      109.2                          0.0
17
18       TWOA  TWOB  TWOC
19
20
21
End of File
```

Sample input parameters file of the profile option of the EMTP

To ease the manipulation of the large amounts of output generated during profile calculations, a separate program reads the output data from logical unit 3 (originally written in free format and thus meaningless under MTS LIST OR COPY commands) and writes only the part of the output requested by the user. The object code of this auxiliary program is available under the name LUI:OUTINTL.0.

A typical run command is shown below

```
$ RUN LUI:OUTINTL.0  3=-3  5=PAR.OUT  6=-A  7=-B
```

The requested voltages are written on logical unit 6 and the currents on logical unit 7.

File PAR.OUT contains the output control parameters. An example

is shown below (a sample control file is also available on "READ ONLY" basis under the name LUI:PAR.OUT).

```
      1      +0                          IALLV
      2      -1                          IALLI
      3       1  1                       (BRANCH,SECTION) (VOLTAGES)
      4       2  1                       (BRANCH,SECTION) (VOLTAGES)
      5       3  1                       (BRANCH,SECTION) (VOLTAGES)
      6       2  9                       (BRANCH,SECTION) (VOLTAGES)
      7                                  (BLANK CARD) (VOLTAGES)
      8                                  (BLANK CARD) (CURRENTS)
End of File
```

Sample control parameters file

The parameter IALLV controls the output mode:

IALLV < 0 No voltages will be printed.

IALLV = 1 All intermediate voltages will be printed.

IALLV = 0 Only the voltages specified by the user will be printed.

When IALLV = 0, the output is selected by indicating the branch(es) and intermediate section(s) for which the voltages are desired. The branch number is determined by the order in which the frequency dependent lines were specified in the input file for the EMTP (TRAN.DA in this example). If, for example, two three-phase lines are studied, phase B of line 1 will be branch number 2. If phase C of line two is desired, the branch number would be 6. The maximum number of voltages that can be specified this way is 300. A blank card signals the end of the specified voltages. If IALLV is less than zero or 1, a blank card must also be inserted, to signal the end of user specified voltages.

IALLI is analogous to IALLV, but used for the output of currents. Note that if, for example IALLV = IALLI = 1, two blank cards must be inserted after IALLI.

A sample output from logical units 6 and 7, using the control file shown above, is listed below. Note that a reference table with the names of the line nodes (as used in TRAN.DA), and the code number of each branch is printed for easy reference (also useful to verify that the output requested is the output obtained).

```
VOLTAGES     (BRANCH,SECTION)

REFERENCE TABLE

LINE 1   FROM BUS   SWIA     TO BUS   TWOA

LINE 2   FROM BUS   SWIB     TO BUS   TWOB

LINE 3   FROM BUS   SWIC     TO BUS   TWOC
     TIME              1   1           2   1           3   1           2   9
0.0              0.0            -0.0            -0.0            -0.0
0.90589439E-05-0.67144878E-76-0.67144878E-76-0.67144878E-76-0.67144878E-76
0.18117888E-04-0.20728855E-76-0.20728855E-76-0.20728855E-76-0.20728855E-76
0.27176832E-04-0.71533231E-77-0.71533231E-77-0.71533231E-77-0.71533231E-77
0.36235776E-04-0.20253559E-77-0.20253559E-77-0.20253559E-77-0.20253559E-77
0.45294720E-04-0.83561079E-78-0.83561079E-78-0.83561079E-78-0.83561079E-78
0.54353664E-04 0.0             -0.0            -0.0            -0.0
0.63412607E-04 0.0             -0.0            -0.0            -0.0
0.72471551E-04 0.0             -0.0            -0.0            -0.0
0.81530495E-04 0.0             -0.0            -0.0            -0.0
0.90589439E-04 0.0             -0.0            -0.0            -0.0
0.99648383E-04 0.0             -0.0            -0.0            -0.0
0.10870733E-03 0.0             -0.0            -0.0            -0.0


0.45294720E-03 0.0             -0.0            -0.0            -0.0
0.46200614E-03 0.0             -0.0            -0.0            -0.0
0.47106508E-03 0.64531823E-01-0.12906365E+00 0.64531823E-01-0.0
0.48012403E-03 0.13092492E+00-0.26216827E+00 0.13092492E+00-0.0
0.48918297E-03 0.13217002E+00-0.27711089E+00 0.13217002E+00-0.0
0.49824192E-03 0.97277730E-01-0.30802471E+00 0.97277730E-01-0.0
0.50730086E-03 0.44892915E-01-0.35641999E+00 0.44892915E-01-0.0
0.51635980E-03 0.11844803E-02-0.39645930E+00 0.11844803E-02-0.0

0.17574351E-02 0.91578177E+00-0.11345900E+00-0.80320761E+00-0.0
0.17664941E-02 0.91442024E+00-0.11006518E+00-0.80522853E+00-0.0
0.17755530E-02 0.91304797E+00-0.10667015E+00-0.80724016E+00-0.0
0.17846120E-02 0.91166498E+00-0.10327395E+00-0.80924245E+00-0.0
0.17936709E-02 0.91027129E+00-0.99876626E-01-0.81123540E+00-0.0
0.18027298E-02 0.90886692E+00-0.96478212E-01-0.81321896E+00-0.0
0.18117888E-02 0.90745188E+00-0.93078746E-01-0.81519312E+00-0.28648792E-01
0.18208477E-02 0.90602620E+00-0.89678265E-01-0.81715785E+00-0.12252582E+00
0.18299067E-02 0.90458989E+00-0.86276807E-01-0.81911312E+00-0.19735267E+00
0.18389656E-02 0.90314298E+00-0.82874410E-01-0.82105892E+00-0.23084061E+00
0.18557322E-02 0.90043776E+00-0.76574874E-01-0.82463582E+00-0.24633897E+00
0.18650575E-02 0.89891700E+00-0.73069876E-01-0.82661063E+00-0.24802598E+00
0.18743827E-02 0.89738506E+00-0.69564040E-01-0.82857528E+00-0.24856349E+00
0.18837080E-02 0.89584197E+00-0.66057407E-01-0.83052975E+00-0.24852947E+00
```

Sample output from logical unit 6. Output display program.

```
CURRENTS     (BRANCH,SECTION)

REFERENCE TABLE

LINE 1   FROM BUS   SWIA     TO BUS   TWOA

LINE 2   FROM BUS   SWIB     TO BUS   TWOB

LINE 3   FROM BUS   SWIC     TO BUS   TWOC
NO CURRENT OUTPUT REQUESTED
```

Sample output from logical unit 7. Output display program.

APPENDIX II-A

SKIN EFFECT CORRECTION

FOR ROUND CYLINDRICAL CONDUCTORS

As the frequency of the current circulating in a conductor increases, the current density increases near the surface of the conductor. This phenomenon is known as skin effect and it affects the resistance and internal inductance in large power conductors. The resistance increases with the frequency while the internal inductance decreases.

The formulas shown below permit the calculation of skin effect for tubular conductors. Stranded conductors can be approximated as solid conductors of the same cross-sectional area. Steel reinforced conductors can be approximated as tubular conductors when the influence of the steel core is negligible (note that solid conductors are only a particular case of tubular conductors).

The formula used for the calculation of skin effect is

$$\frac{R_s + j\omega L_{int}}{R_{dc}} = j\frac{1}{2}\, mr(1-s^2)\, \frac{(ber\ mr + jbei\ mr) + \emptyset\,(ker\ mr + jkei\ mr)}{(ber'\ mr + jbei'\ mr) + \emptyset\,(ker'\ mr + jkei'\ mr)}$$

with

$$\emptyset = \frac{ber'\ mq + jbei'\ mq}{ker'\ mq + jkei'\ mq},$$

and,

R_s = ac resistance (skin effect included) in Ω/km

R_{dc} = dc resistance in Ω/km

L_{int} = internal inductance (skin effect included) in H/km

r = outside radius of conductor

q = inside radius of conductor

$s = \frac{q}{r}$

and,

$$(mr)^2 = k\,\frac{1}{1 - s^2}$$

$$(mq)^2 = k \frac{s^2}{1 - s^2}$$

with

$$k = \frac{8 \cdot 10^{-4} \pi f \mu_r}{R_{dc}}$$

and μ_r = relative permeability

f = frequency in Hz.

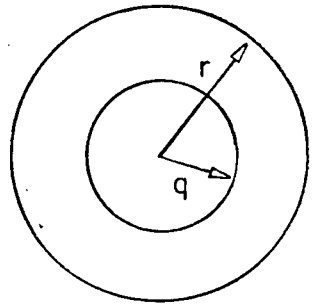

Fig. II-A.1: Tubular conductor.

The modified Bessel functions can be calculated with polynomial approximations. A subroutine that uses the above formulas is used in the Line Constants Program. The same subroutine is used for all the skin effect calculations in this thesis. A typical call to this subroutine has the form

CALL SKIN (S, RDC, F, RS, XI)

where

S = q/r

RDC = dc resistance in Ω/km

F = frequency in Hz

RS = ac resistance in Ω/km

XI = ac reactance in Ω/km

A sample calculation of R/R_{dc} and $L_{int}/L_{int,dc}$ for s = 0.5 and R_{dc} = 0.01 Ω/km is shown in Figure II-A.2

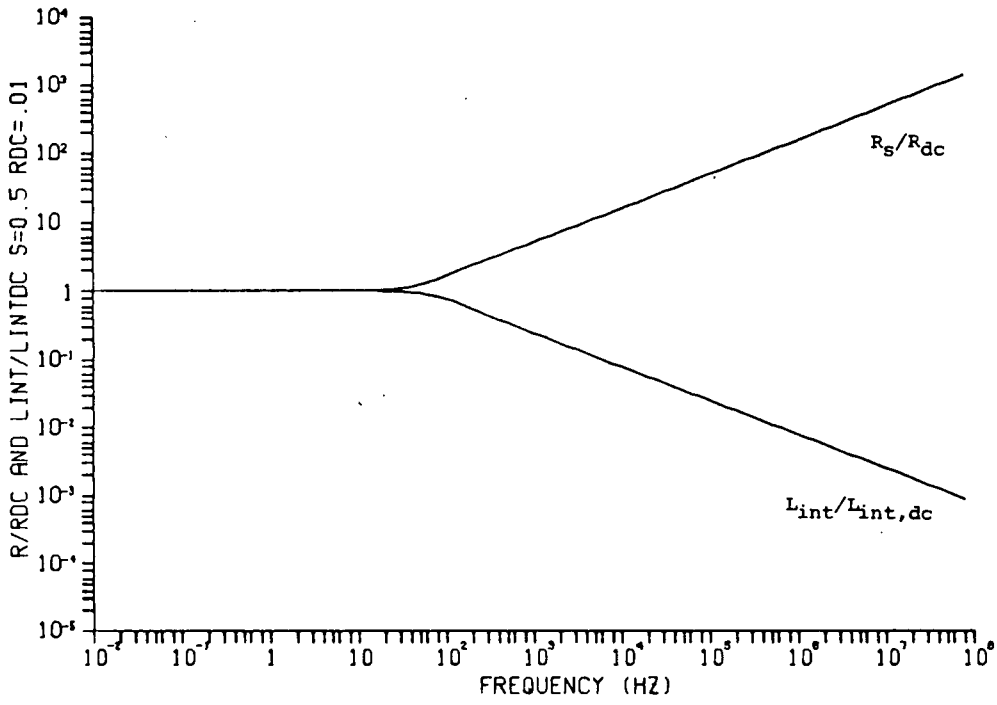

Fig. II-A.2: Variation of the resistance and internal inductance due to skin effect.

APPENDIX II-B

CARSON'S CORRECTION TERMS

FOR EARTH RETURN EFFECT

Carson's correction terms account for the fact that the earth does not behave as an infinite and perfectly conducting plane for ground return currents. Carson's formula is normally accurate enough for power systems studies. It is based on the following assumptions:

(a) The conductors are long enough so that three dimensional end-effects can be neglected (this permits the solution of the field problem on a plane perpendicular to the conductors).

(b) The earth has uniform conductivity and can be represented as an infinite plane, to which the conductors are parallel.

(c) The spacing between the conductors is much larger than their radius, so that proximity effects can be ignored.

Carson's correction terms depend on the angle Φ ($\Phi = 0$ for self impedance and $\Phi = \Phi_{i,k}$ for mutual impedance), and on the parameter a, where

$$a = 4\pi\sqrt{5}\cdot 10^{-4} D\sqrt{\frac{f}{\rho}} \qquad \text{(II-B.1)}$$

with

$D = 2 h_i$ (in m) for self impedance

$D = D_{i,k}$ (in m) for mutual impedance

f = frequency in Hz

ρ = earth resistivity in $\Omega\cdot$m.

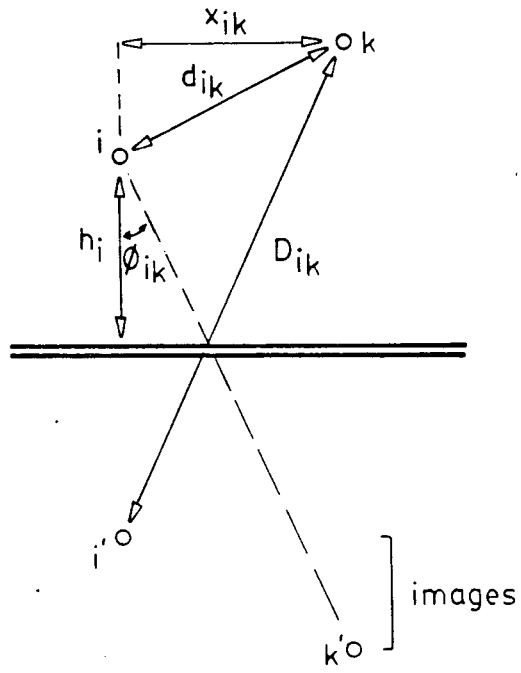

Fig. II-B.1: Tower geometry.

The correction term for the resistance ΔR becomes infinite when $f \to \infty$, while $\Delta X/\omega = \Delta L$ goes to zero. If the earth resistivity is very low and f is finite, ΔR and ΔX are very small. In the limit, if earth is a perfect conductor ($\rho = 0$), ΔR and ΔX become zero.

Carson's infinite series when $a \leq 5$ can be written as,

$$\begin{aligned}\Delta R = {} & 4\omega\cdot 10^{-4}\{\tfrac{\pi}{8} \\ & -b_1 a\cdot\cos\phi \\ & +b_2[(c_2-\ln a)a^2\cos 2\phi+\phi a^2\sin 2\phi] \\ & +b_3 a^3\cos 3\phi \\ & -d_4 a^4\cos 4\phi \\ & -b_5 a^5\cos 5\phi \\ & +b_6[(c_6-\ln a)a^6\cos 6\phi+\phi a^6\sin 6\phi] \\ & +b_7 a^7\cos 7\phi \\ & -d_8 a^8\cos 8\phi \\ & -\ldots\} \end{aligned} \qquad \text{(II-B.3)}$$

$$\begin{aligned}\Delta X = {} & 4\omega\cdot 10^{-4}\{\tfrac{1}{2}(0.6159315-\ln a) \\ & +b_1 a\cdot\cos\phi \\ & -d_2 a^2\cos 2\phi \\ & +b_3 a^3\cos\phi \\ & -b_4[(c_4-\ln a)a^4\cos 4\phi+\phi a^4\sin 4\phi] \\ & +b_5 a^5\cos 5\phi \\ & -d_6 a^6\cos 6\phi \\ & +b_7 a^7\cos 7\phi \\ & -b_8[(c_8-\ln a)a^8\cos 8\phi+\phi a^8\sin 8\phi] \\ & +\ldots\} \end{aligned} \qquad \text{(II-B.4)}$$

Each 4 successive terms form a repetitive pattern. The coefficients b_i, c_i and d_i are constants, which are obtained from the recursive formulas:

$$b_i = b_{i-2} \frac{\text{sign}}{i(i+2)} \text{ with the starting value } \begin{cases} b_1 = \frac{\sqrt{2}}{6} & \text{for odd subscripts.} \\ b_2 = \frac{1}{16} & \text{for even subscripts.} \end{cases}$$

$$c_i = c_{i-2} + \frac{1}{i} + \frac{1}{i+2} \text{ with the starting value } c = 1.3659315,$$

$$d_i = \frac{\pi}{4} \cdot b_i ,$$

with sign = ±1 changing after each 4 successive terms (sign = +1 for i = 1,2,3,4; sign = -1 for i = 5,6,7,8, etc.,).

For a > 5, the following finite series is used:

$$\Delta R' = \left[\frac{\cos\phi}{a} - \frac{2\cos 2\phi}{a^2} + \frac{\cos 3\phi}{a^3} + \frac{3\cos 5\phi}{a^5} - \frac{45\cos 7\phi}{a^7}\right] \cdot \frac{4\omega \cdot 10^{-4}}{\sqrt{2}} \qquad \text{(II-B.4)}$$

$$\Delta X' = \left[\frac{\cos\phi}{a} - \frac{\cos 3\phi}{a^3} + \frac{3\cos 5\phi}{a^5} + \frac{45\cos 7\phi}{a^7}\right] \cdot \frac{4\omega \cdot 10^{-4}}{\sqrt{2}} \qquad \text{(II-B.5)}$$

The trigonometric functions are calculated directly from the geometry,

$$\cos\phi_{ik} = \frac{h_i + h_k}{D_{ik}} \quad \text{and} \quad \sin\phi_{ik} = \frac{x_{ik}}{D_{ik}}$$

and for higher terms in the series, from the recursive formulas

$$a^i\cos(i\phi) = [a^{i-1}\cos(i-1)\phi \cdot \cos\phi - a^{i-1}\sin(i-1)\phi \cdot \sin\phi] \cdot a$$

$$a^i\cos(i\phi) = [a^{i-1}\cos(i-1)\phi \cdot \sin\phi + a^{i-1}\sin(i-1)\phi \cdot \cos\phi] \cdot a$$

For power circuits at power frequency, a reasonable approximation can be obtained if only two terms in equation (II-B.2) are used. For higher frequencies, low resistivity, and wider spacings, more terms need to be taken into account as the parameter a becomes larger. The Line Constants Program uses these formulas to account for ground return effects.

For the purposes of this thesis project, the section of the Line Constants Program that calculates Carson's terms has been rewritten as a subroutine. A typical call to this subroutine has the form

CALL CARSON (HAV, DM, F, RHO, DRS, DRM, DXS, DXM)

where,

HAV = average height in m.

DM = geometric mean distance between conductors

RHO = earth resistivity in $\Omega \cdot m$.

F = frequency in Hz.

DRS, DRM, DXS, DXM are the resulting self and mutual correction terms in Ω/km.

APPENDIX II-C

SIMULATION OF THE

JOHN DAY-LOWER MONUMENTAL TRANSMISSION LINE

USING THE LOW-ORDER APPROXIMATION PROGRAM

BPA's John Day to Lower Monumental 500 KV transmission line (see Figure 3.1, part I) has been modeled with the low-order approximation routines developed in part II of this thesis project.

In order to illustrate the effect of ground wires in the evaluation of the equivalent line configuration, $|A_1(\omega)|$ and $|Z_c(\omega)|$ with segmented or T connected ground wires (see footnote, page 28) are shown in graphs II-C.1 and II-C.2. Graph II-C.3 and II-C.4 show $|A_1(\omega)|$ and $|Z_c(\omega)|$ when the ground wires have been removed.

It is interesting to note in graphs II-C.3 and II-C.4, that the slightly better approximation obtained for the reference line (see Figure 1.3, part II) is probably due to the fact that the tower configuration of the reference line is horizontal, while the configuration of BPA's line is triangular. This would affect the accuracy of the estimation of Carson's correction terms at high frequencies, where the difference between considering an average height or the height of the individual conductors is more marked.

Graphs II-C.5 to II-C.7 show the open and short circuit responses of this line when there are no ground wires.

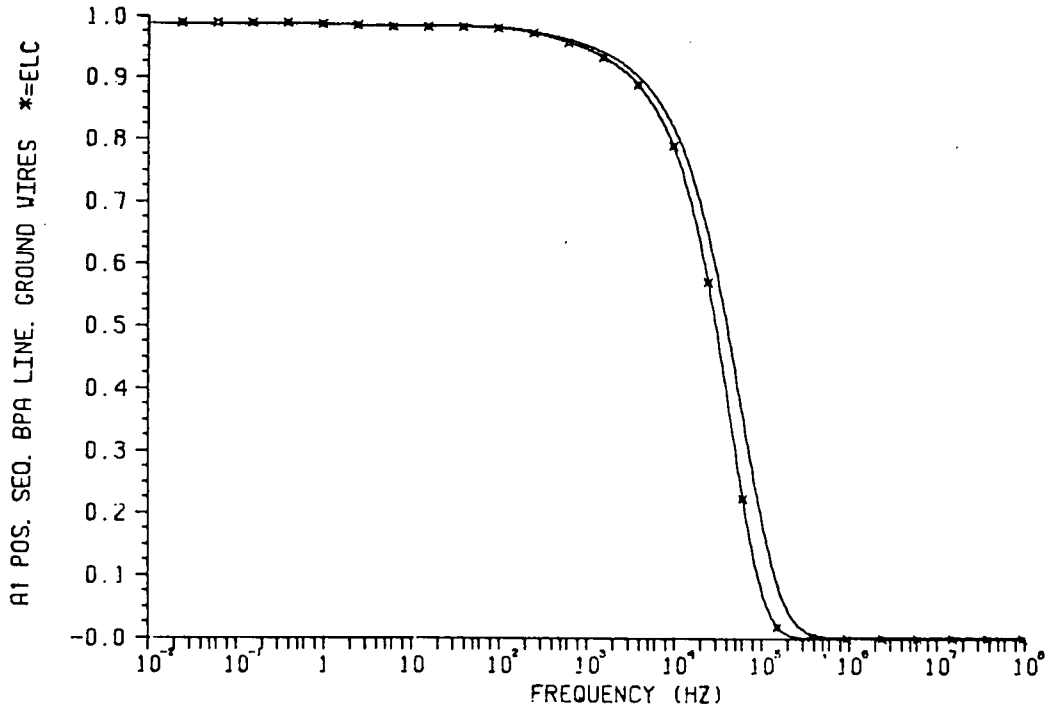

(a)

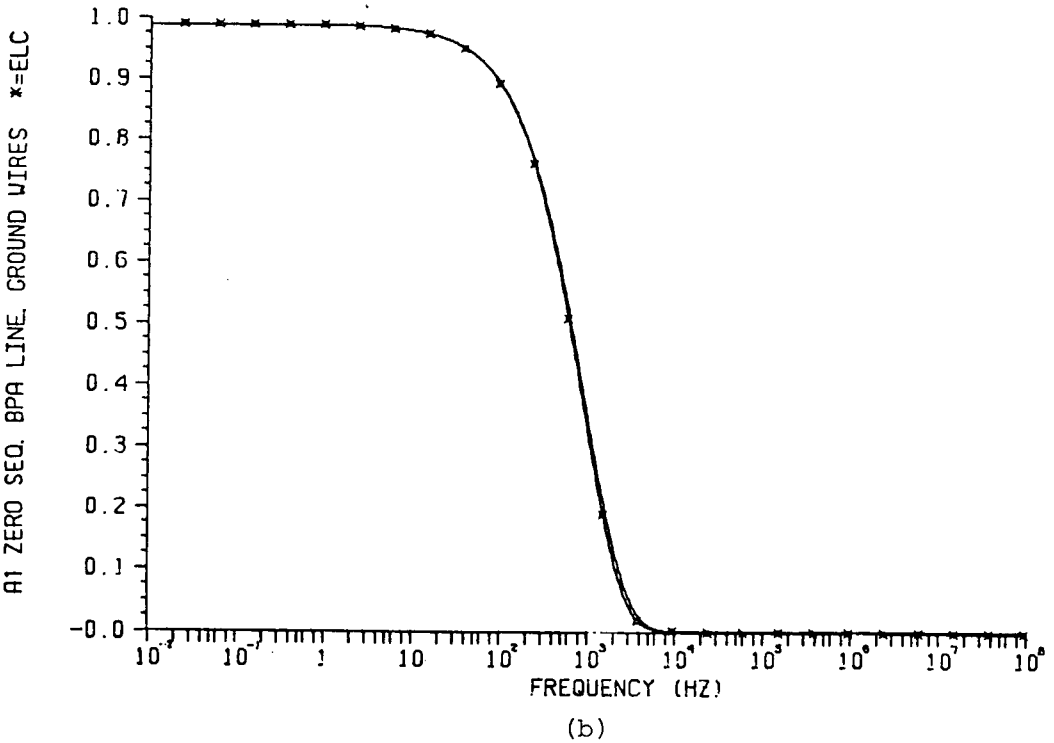

(b)

Graph II-C.1: A_1 magnitude function. Segmented ground wires, R_{dc} given. (a) Positive sequence (b) Zero sequence.

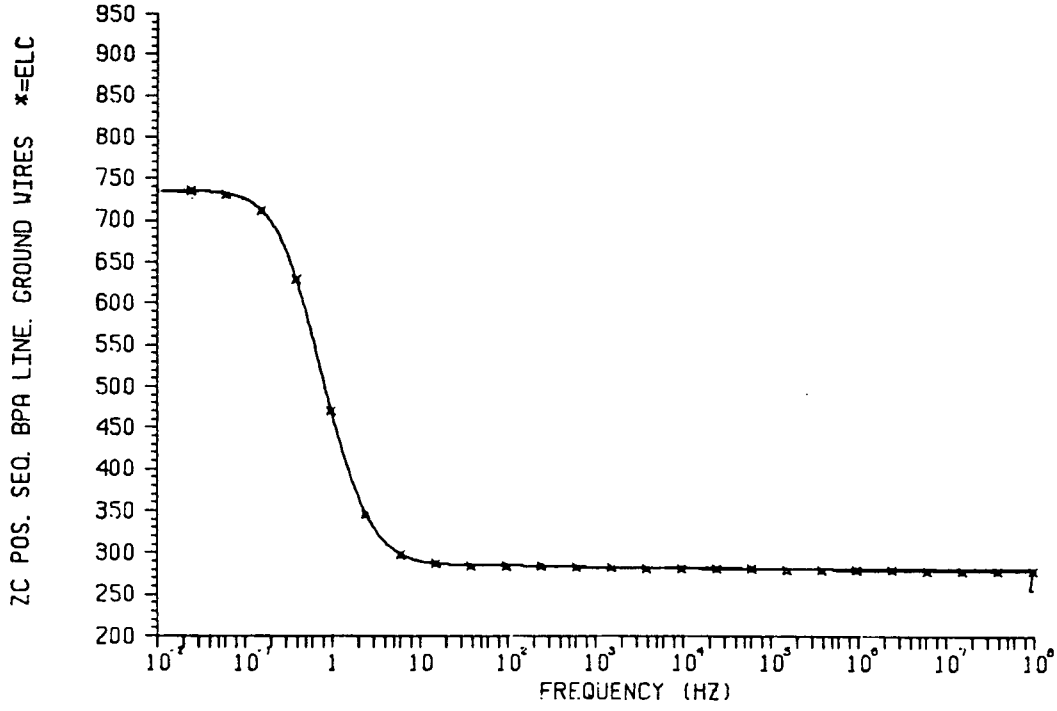

(a)

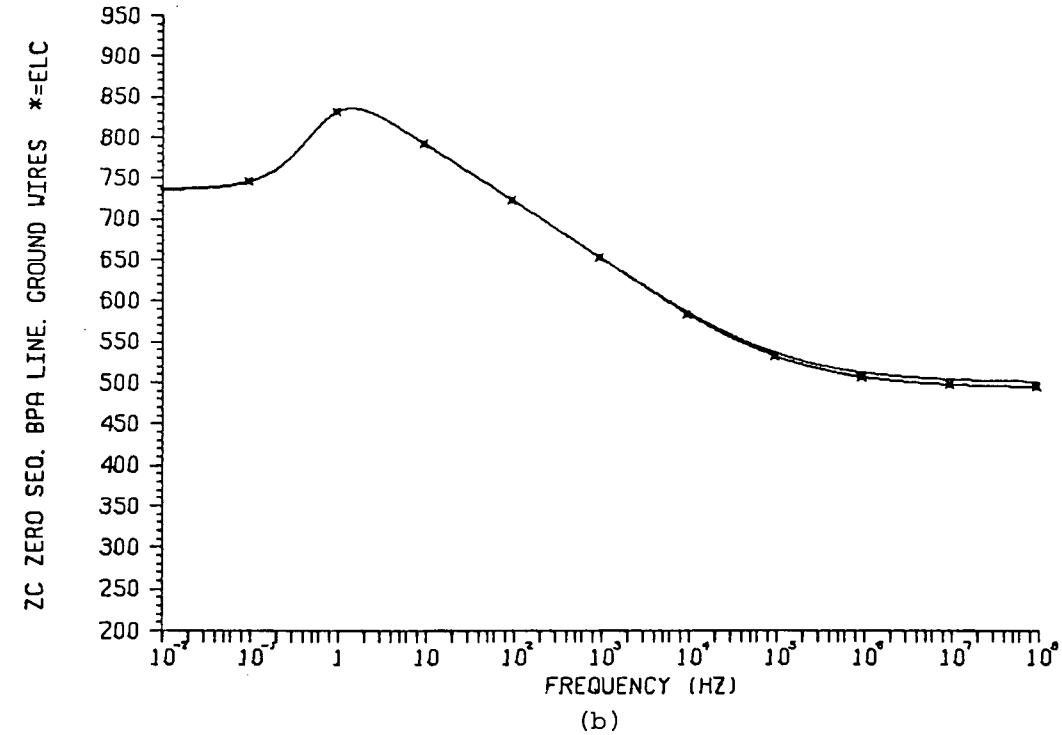

(b)

Graph II-C.2: Z_C magnitude function. Segmented ground wires, R_{dc} given. (a) Positive sequence (b) Zero sequence.

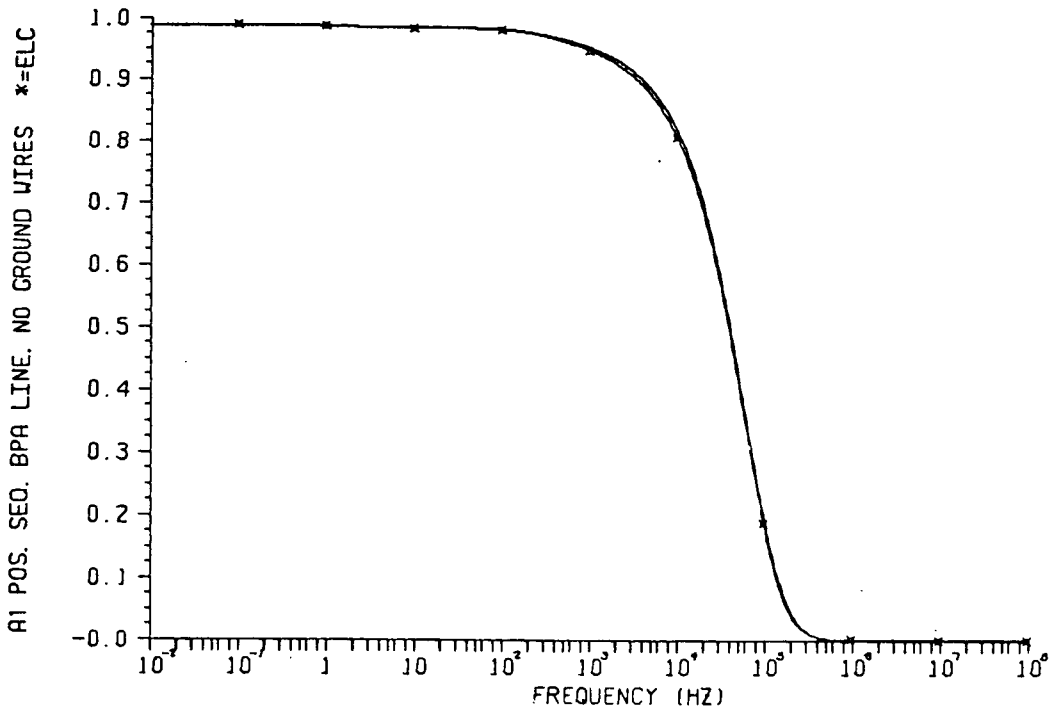

(a)

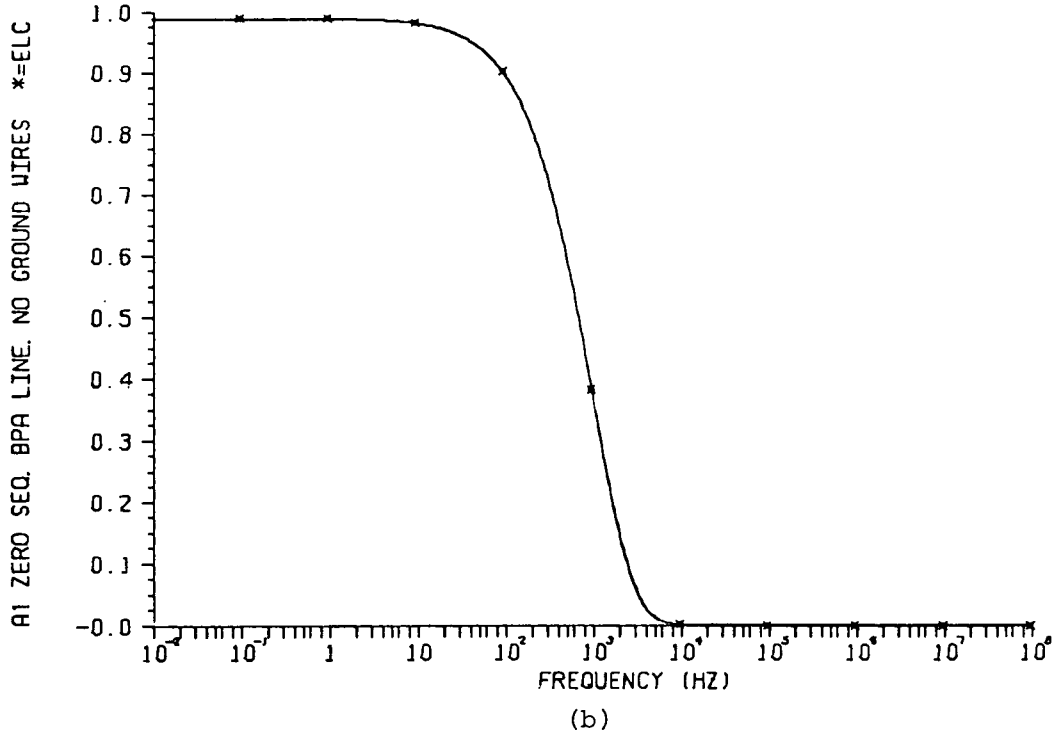

(b)

Graph II-C.3: A_1 magnitude function. No ground wires, R_{dc} given. (a) Positive sequence (b) Zero sequence.

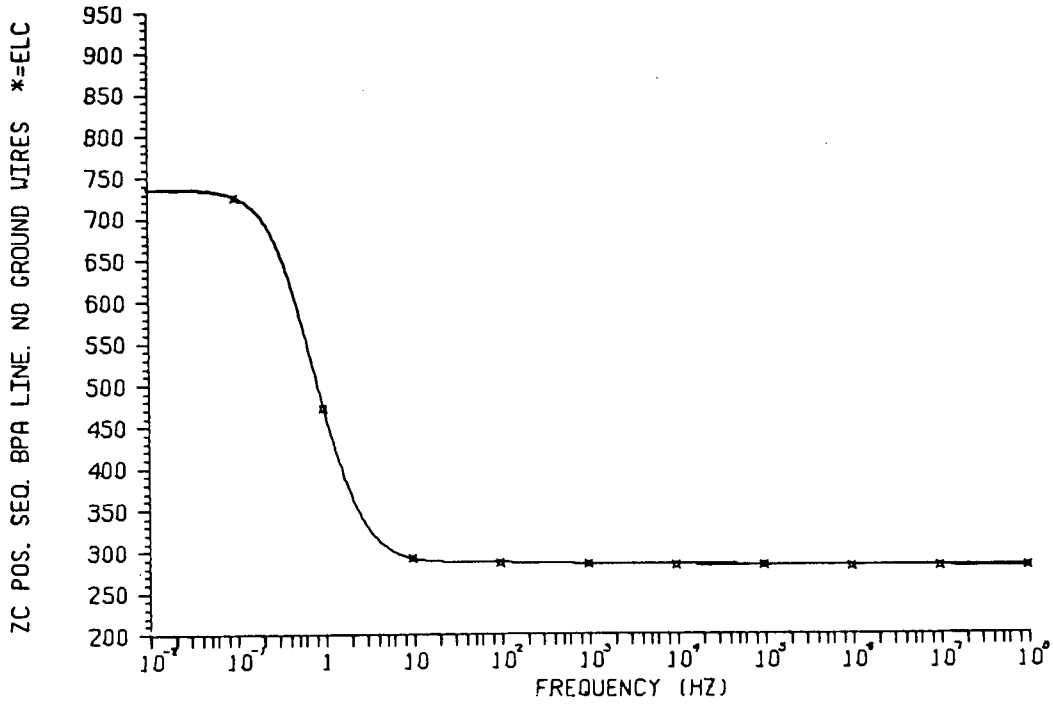

(a)

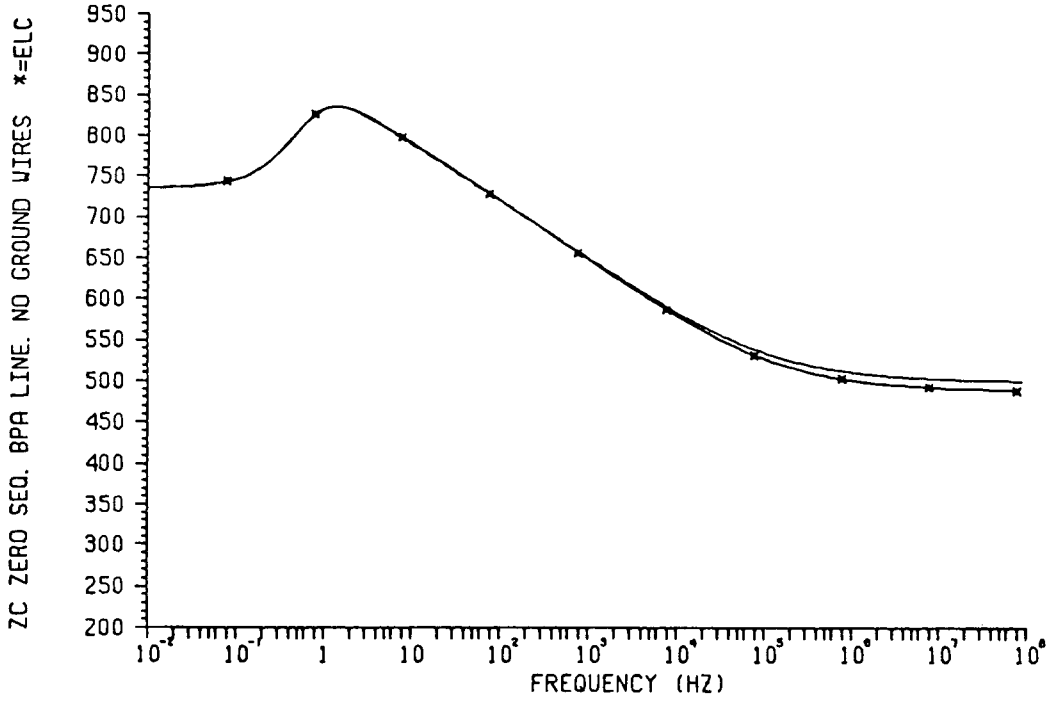

(b)

Graph II-C.4: Z_c magnitude function. No ground wires, R_{dc} given. (a) Positive sequence (b) Zero sequence.

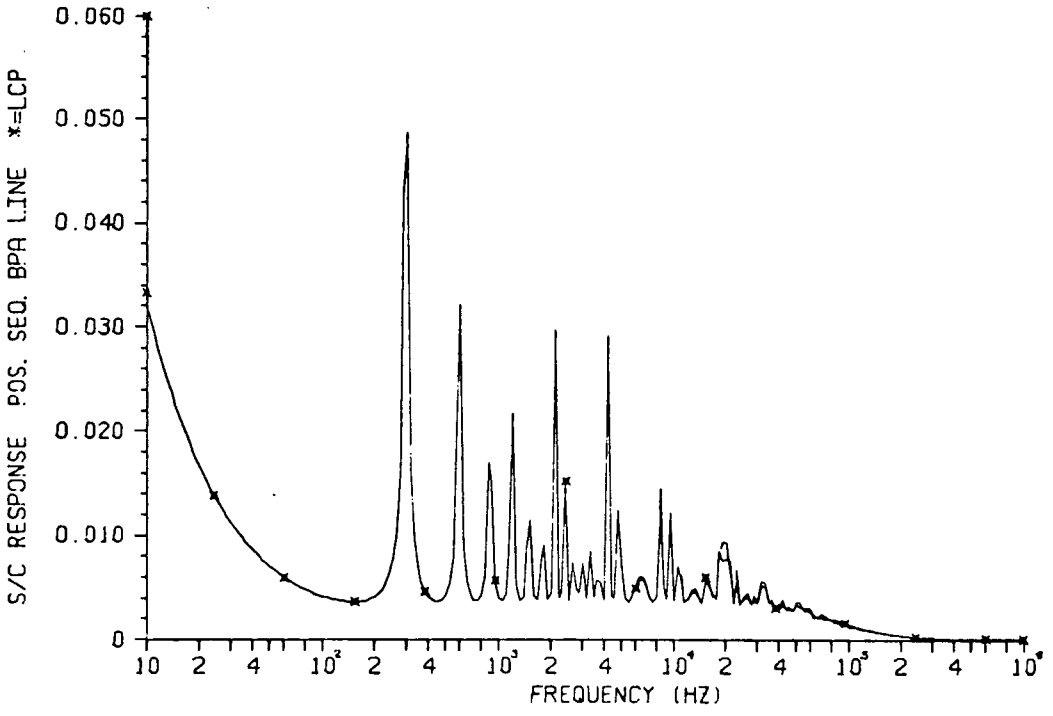

(a)

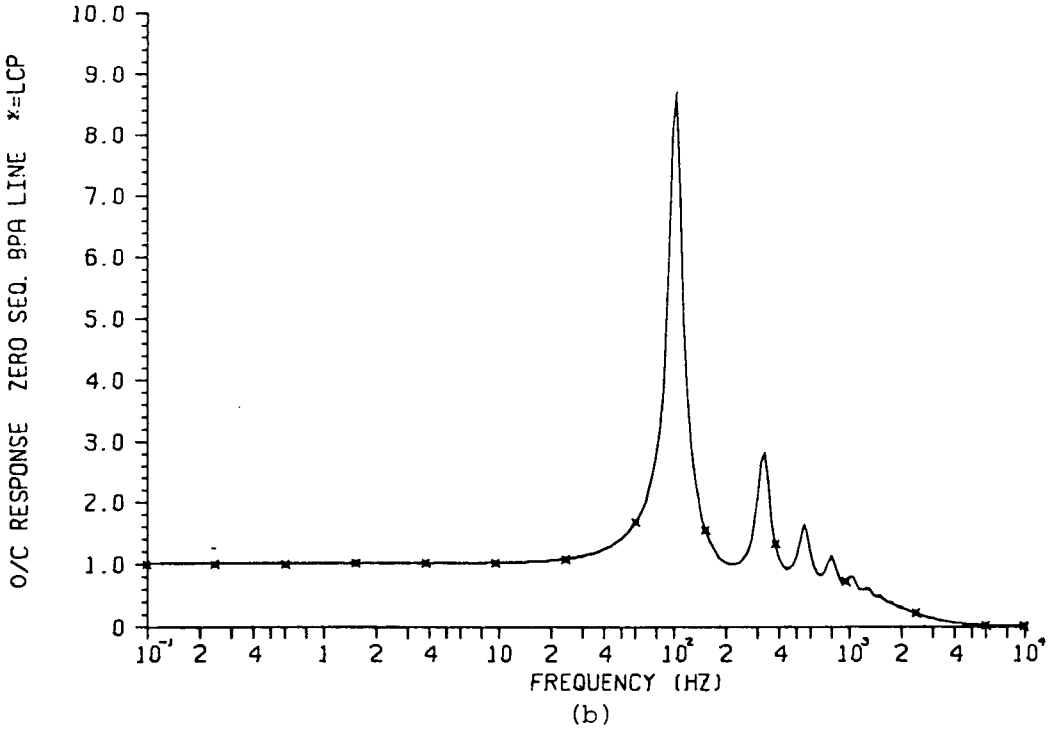

(b)

Graph II-C.5: O/C response. No ground wires, R_{dc} given.
(a) Positive sequence (b) Zero sequence.

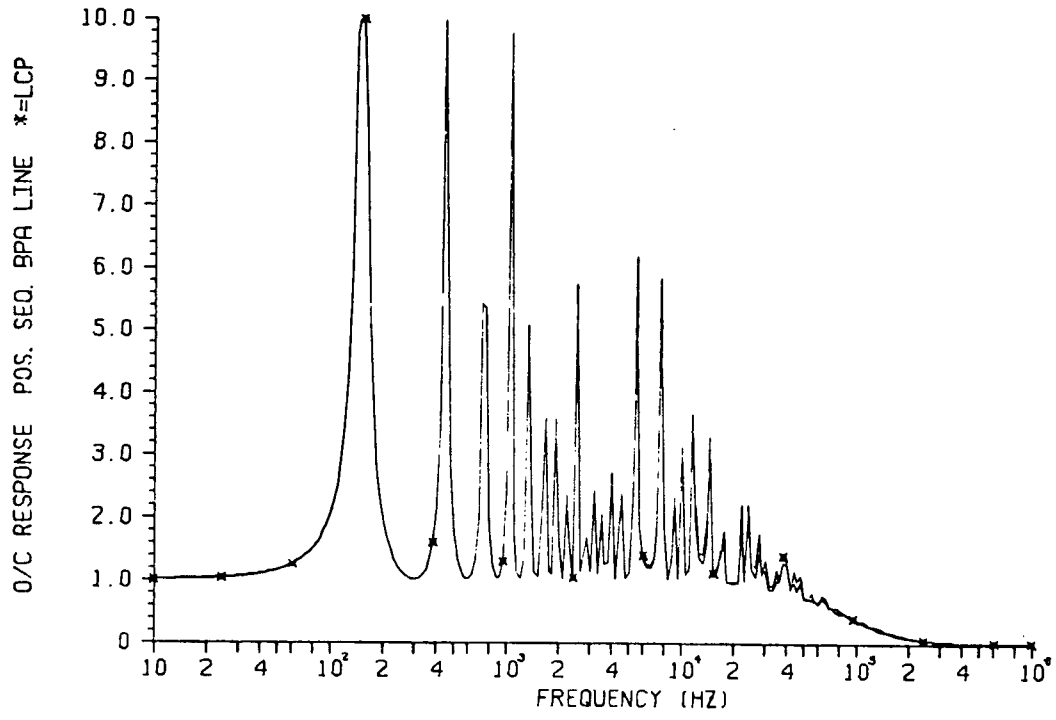

(a)

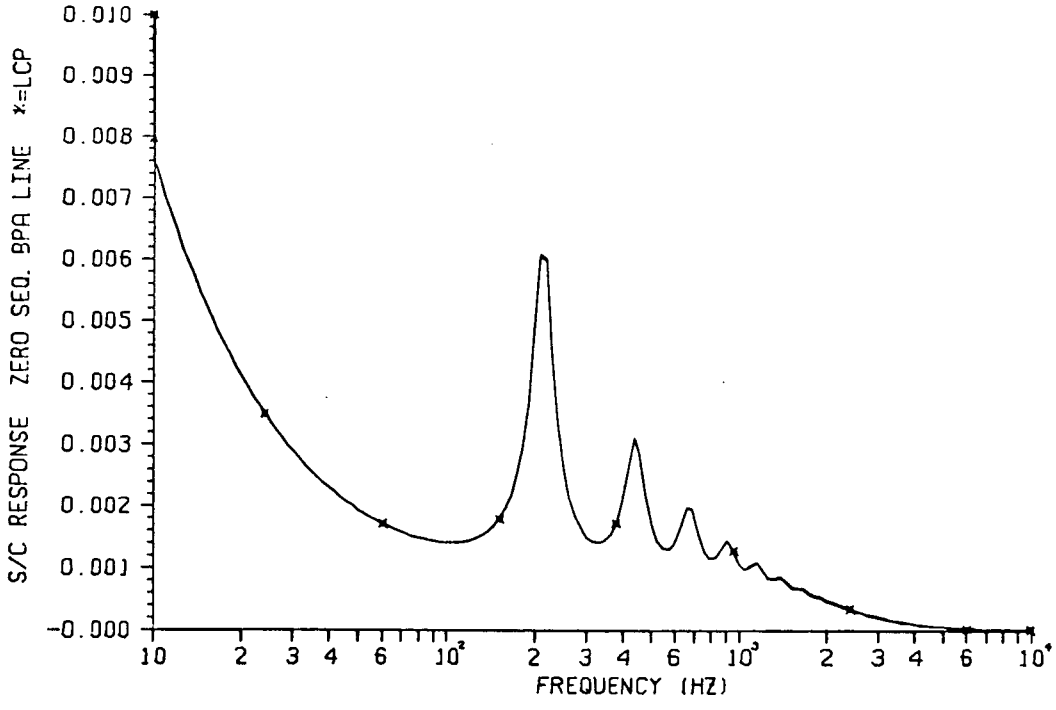

(b)

Graph II-C.6: S/C response. Mid to high frequencies.
No ground wires, R_{dc} given.
(a) Positive sequence (b) Zero sequence.

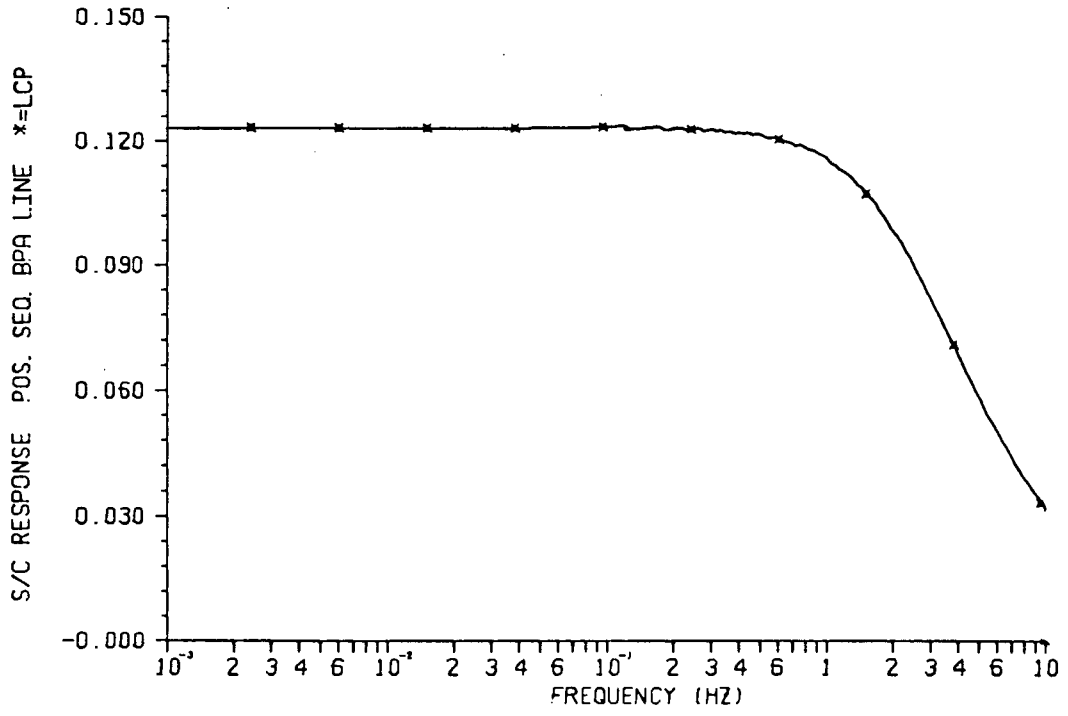

(a)

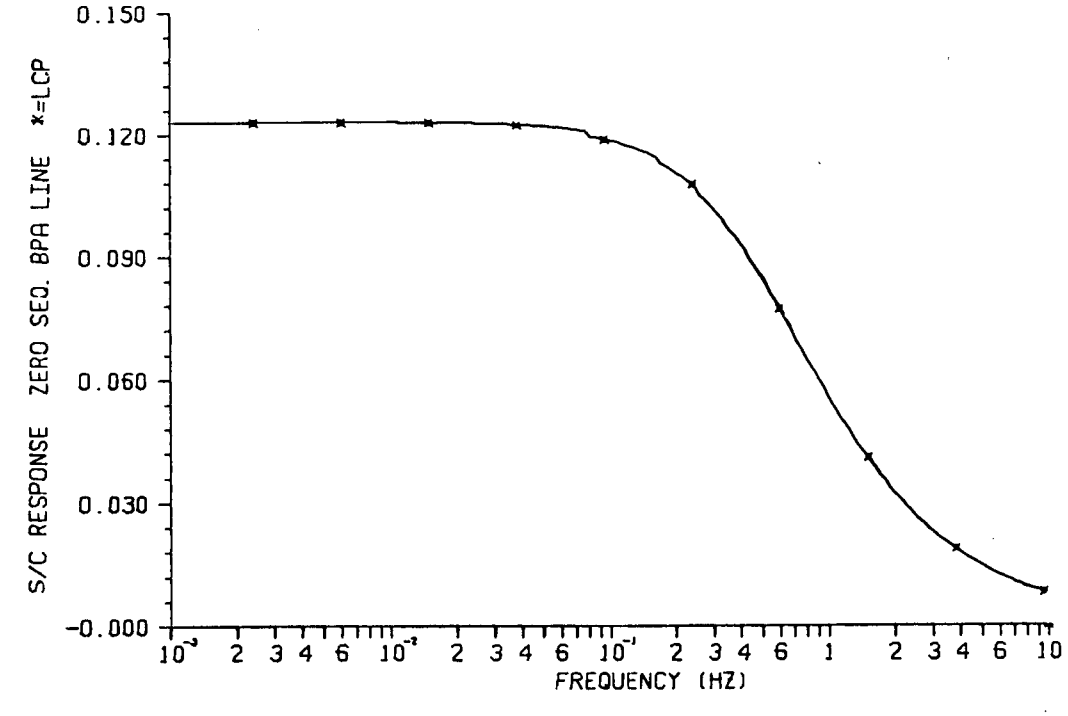

(b)

Graph II-C.7: S/C response. Low frequencies. No ground wires, R_{dc} given. (a) Positive sequence (b) Zero sequence.

APPENDIX II-D

USER'S GUIDE TO THE LOW-ORDER APPROXIMATION PROGRAM

The sequential file LO.O contains the object code of the low-order approximation routines. LO.O is available with READ ONLY status to UBC's MTS users.

A typical run command is shown below

```
$ RUN LUI: LO.O  5 = DA.LO  6 = -6  7 = -7  8 = -8  9 = -9  10 = -10
                            11 = -11  12 = -12
```

DA.LO contains the input data and the output control parameters. Logical units 6 through 12 contain output information. A typical data file is shown below (an example data file has been permitted on a READ ONLY basis. This file can be read under the name LUI: DA.LOT)

```
   1     3                                  NUMBER OF PHASES
   2     60.00                              FREQUENCY OF PARAMETERS
   3     500.0                              LINE LENGTH
   4     .00000003                          CONDUCTANCE
   5     100.0                              EARTH RESISTIVITY
   6     .88080000-03  3.330800D-03         L1(60HZ), LO(60HZ)
   7     .01330000000D-06   .008361000D-06  C1, CO
   8     .026190000 .02643000 .19740000     RDC,RF,RO
   9     .01                                FMIN
  10     10 10                              NO OF DEC, NO OF POINTS/DEC
  11     6 4                                NUMBER OF POLES IN ZCO AND ZC1
  12     5 4                                NUMBER OF POLES IN A10 AND A11
  13     0 5                                SHIFTING OF A10 AND A11 (0=NO)
  14     4 3                                SHIFTING OF ZCO AND ZC1 (0=NO)
  15     .5 .5                              ERROR (%) AT LINE FREQUENCY FOR ZC AND A1
  16     1                                  WRITE R(W), L(W)  (1=YES 0=NO)
  17     1                                  WRITE ZC(W), *ZC(W)* (1=YES 0=NO)
  18     1                                  WRITE A1, *A1*  (1=YES 0=NO)
End of File
```

Sample input parameters file.

The information from this file is read in free format, therefore a blank or a semi-colon can be used as delimitator between quantities.

Line 1 is the number of phases; the minimum is 2 and the maximum is 20. The violation of these limits is not detected internally by the program, but the system will discontinue execution due to array overflow.

Lines 2 through 8 are self-explanatory. Note that if the dc resistance is not known (line 8) and the 'RDC not given' option is required, a flag value of 0.0 must be introduced in the place of R_{dc}.

Line 9 contains the starting frequency at which the frequency-dependent response of the parameters is to be evaluated.

Line 10 contains the number of decades and points per decade of the desired frequency band.

Line 11 contains the number of poles required in the simulation of $Z_c(\omega)$ for zero and positive sequences. The maximum number permitted is 10 and the minimum is 1. No warning messages detect the violation of these limits, but an array overflow will result and the execution will stop.

Line 12 is the number of poles for the approximation of the propagation function $A_1(\omega)$; the maximum number is 10 and the minimum is 2. As in the case of $Z_c(\omega)$ no warning messages are provided, but if the limits are violated, execution will stop.

Line 13 controls the shifting option for the approximation of $A_1(\omega)$. Zero disables this option and matching at line frequency will be assumed. Values greater than zero specify the maximum number of shifting loops. If an improvement of more than 1% in the area between $|A_1(\omega)|$ and $|B(\omega)|$ is not obtained, or if the maximum number of loops is met, the shifting process stops and control is directed to the next part of the program.

Line 14 contains analogous information as line 13 for the approximation of $Z_c(\omega)$.

Line 15 is the error in (%) between the real (obtained from R,L and C given by the user) and approximated functions $Z_c(\omega)$ and $A_1(\omega)$ at the line frequency (line 2). Note that the same error level will be assumed for both zero and positive sequence.

If the shifting option is used, the matching procedure is disabled. If no shifting and no matching are desired, this error can be set to a large value (for example 50%). This will override the matching procedure.

Line 16 controls the information to be written in logical unit 7. An example is shown below.

1	FREQUENCY	R1 (OHMS)	L1 (MH)	RO (OHMS)	LO (MH)
2	0.1000000E-01	0.2619000E-01	0.8808493E+00	0.2621959E-01	0.5922672E+01
3	0.1258925E-01	0.2619000E-01	0.8808493E+00	0.2622725E-01	0.5853623E+01
4	0.1584893E-01	0.2619000E-01	0.8808493E+00	0.2623690E-01	0.5784579E+01
5	0.1995262E-01	0.2619000E-01	0.8808486E+00	0.2624904E-01	0.5715537E+01
6	0.2511886E-01	0.2619000E-01	0.8808486E+00	0.2626431E-01	0.5646500E+01
7	0.3162278E-01	0.2619000E-01	0.8808493E+00	0.2628355E-01	0.5577470E+01
8	0.3981072E-01	0.2619000E-01	0.8808493E+00	0.2630776E-01	0.5508444E+01
9	0.5011872E-01	0.2619000E-01	0.8808493E+00	0.2633823E-01	0.5439424E+01
10	0.6309573E-01	0.2619000E-01	0.8808486E+00	0.2637658E-01	0.5370411E+01

Sample output from logical unit 7.

Line 17 controls the output of the approximation process of $Z_C(\omega)$. Positive sequence is written in logical unit 9 and zero sequence in logical unit 8.

1	POSITIVE SEQUENCE SURGE IMPEDANCE			
2	FREQUENCY	ZC1	*ZC1*	ERROR (%)
3	0.1000000E-01	0.9341646E+03	0.9339930E+03	-0.1836608E-01
4	0.1258925E-01	0.9340593E+03	0.9338927E+03	-0.1783459E-01
5	0.1584893E-01	0.9338926E+03	0.9337339E+03	-0.1699431E-01
6	0.1995262E-01	0.9336287E+03	0.9334824E+03	-0.1566774E-01
7	0.2511886E-01	0.9332112E+03	0.9330845E+03	-0.1357827E-01
8	0.3162278E-01	0.9325514E+03	0.9324553E+03	-0.1029905E-01
9	0.3981072E-01	0.9315105E+03	0.9314622E+03	-0.5182284E-02
10	0.5011872E-01	0.9298727E+03	0.9298981E+03	0.2728810E-02

Sample output from logical unit 9.

1	ZERO SEQUENCE SURGE IMPEDANCE			
2	FREQUENCY	ZCO	*ZCO*	ERROR (%)
3	0.1000000E-01	0.9363715E+03	0.9363422E+03	-0.3129076E-02
4	0.1258925E-01	0.9363715E+03	0.9363251E+03	-0.4958766E-02
5	0.1584893E-01	0.9363715E+03	0.9362980E+03	-0.7857896E-02
6	0.1995262E-01	0.9363715E+03	0.9362550E+03	-0.1245087E-01
7	0.2511886E-01	0.9363715E+03	0.9361868E+03	-0.1972561E-01
8	0.3162278E-01	0.9363715E+03	0.9360790E+03	-0.3124371E-01
9	0.3981072E-01	0.9363715E+03	0.9359083E+03	-0.4946962E-01
10	0.5011872E-01	0.9363715E+03	0.9356385E+03	-0.7828299E-01

Sample output from logical unit 8.

In the output for $|Z_c(\omega)|$, zero sequence, ZCO is the magnitude of the characteristic impedance generated from the equivalent line configuration, *ZCO* is the rational-functions approximation of $|Z_c(\omega)|$ and ERROR (%) is the percentage error between them.

Line 18 controls the output of $|A_1(\omega)|$ in a similar way as in line 17. Units 10 and 11 contain the zero and positive magnitude functions, respectively.

```
1        ZERO SEQUENCE PROPAGATION FUNCTION
2          FREQUENCY          A10          *A10*          ERROR (%)
3       0.1000000E-01  0.9860748E+00  0.9860747E+00 -0.2222977E-05
4       0.1258925E-01  0.9860727E+00  0.9860747E+00  0.2027605E-03
5       0.1584893E-01  0.9860702E+00  0.9860747E+00  0.4610163E-03
6       0.1995262E-01  0.9860669E+00  0.9860747E+00  0.7865459E-03
7       0.2511886E-01  0.9860628E+00  0.9860746E+00  0.1197158E-02
8       0.3162278E-01  0.9860576E+00  0.9860745E+00  0.1715597E-02
9       0.3981072E-01  0.9860510E+00  0.9860744E+00  0.2371082E-02
10      0.5011872E-01  0.9860426E+00  0.9860742E+00  0.3201412E-02
```

Sample output from logical unit 10.

```
1      POSITIVE SEQUENCE PROPAGATION FUNCTION
2          FREQUENCY          A11          *A11*          ERROR (%)
3       0.1000000E-01  0.9860814E+00  0.9860810E+00 -0.4863591E-04
4       0.1258925E-01  0.9860808E+00  0.9860807E+00 -0.9226487E-05
5       0.1584893E-01  0.9860797E+00  0.9860802E+00  0.5319254E-04
6       0.1995262E-01  0.9860780E+00  0.9860795E+00  0.1520180E-03
7       0.2511886E-01  0.9860754E+00  0.9860784E+00  0.3083897E-03
8       0.3162278E-01  0.9860712E+00  0.9860766E+00  0.5555812E-03
9       0.3981072E-01  0.9860645E+00  0.9860738E+00  0.9457518E-03
10      0.5011872E-01  0.9860540E+00  0.9860694E+00  0.1560140E-02
```

Sample output from logical unit 11.

Logical unit 6 contains the record of the input parameters, equivalent line representation, and approximation process.

```
     RECORD OF INPUT PARAMETERS

     NUMBER OF PHASES=  3
     LINE LENGTH=     500.0000000
     LINE PARAMETERS PER UNIT LENGTH AT     60.000 HZ ARE:

     ZERO SEQUENCE
     RESISTANCE           0.1974000E+00 OHMS
     INDUCTANCE           0.3330800E-02 HENRYS
     CAPACITANCE          0.8361000E-08 FARADS
     EARTH RESISTIVITY    0.1000000E+03 OHMS


     POSITIVE SEQUENCE
     RESISTANCE           0.2643000E-01 OHMS
     INDUCTANCE           0.8808000E-03 HENRYS
     CAPACITANCE          0.1330000E-07 FARADS



     FROM THE GIVEN LINE PARAMETERS, THE ESTIMATED
     LINE CONFIGURATION IS:
     EQUIVALENT GEOMETRIC MEAN RADIUS       0.1844397E+00 METERS
     RADIUS OF EQUIVALENT BUNDLED
     CONDUCTOR                              0.1964899E+00 METERS
     AVERAGE DISTANCE BETWEEN CONDUCTORS    0.1508298E+02 METERS
     AVERAGE HEIGHT OF CONDUCTORS           0.1498967E+02 METERS
     AVERAGE DISTANCE BETWEEN CONDUCTORS
     AND THEIR IMAGES                       0.3400702E+02 METERS


     CORRECTION FACTOR FOR SKIN EFFECT
     S=(INTERNAL RADIUS)/(EXTERNAL RADIUS)=  0.8095438E+00
     DC RESISTANCE        0.2619000E-01 OHMS



     **** APROXIMATION PROCESS FOR ZCO ****
     NUMBER OF POLES=  6
     NUMBER OF ZEROS=  6
     SHIFTING OPTION SELECTED
     ERROR(%) AT        60.00000 HZ IS        -0.7488213379
     REACHED AFTER     4 SHIFTING LOOPS


     **** APROXIMATION PROCESS FOR A10 ****
     NUMBER OF POLES=  5
     NUMBER OF ZEROS=  4
     ERROR (%) AT        60.00000 HZ IS         0.2659203301
     REACHED AFTER     0 ITERATIONS


     **** APROXIMATION PROCESS FOR ZC1 ****
     NUMBER OF POLES=  4
     NUMBER OF ZEROS=  4
     SHIFTING OPTION SELECTED
     ERROR(%) AT        60.00000 HZ IS        -0.1188697158
     REACHED AFTER     3 SHIFTING LOOPS


     **** APROXIMATION PROCESS FOR A11 ****
     NUMBER OF POLES=  4
     NUMBER OF ZEROS=  3
     SHIFTING OPTION IS SELECTED
     ERROR AT 60.00 HZ IS  0.0160%
     REACHED AFTER   2 SHIFTING LOOPS


End of File
```

Sample output from logical unit 6.

Logical unit 12 contains the coefficients of the partial fractions expansion of the rational-functions approximation of the line. The output format is compatible with the frequency-dependence version of the EMTP, and it is the information to be introduced into logical unit 1.

It is important to take into account that the formatted writing of information is time consuming and computationally expensive. Therefore, for most applications it is recommended that the control parameters in lines 16 through 18 be set to zero.

BIBLIOGRAPHY

[1] H.W. Dommel, "Digital Computer Solution of Electromagnetic Transients in Single - and Multiphase Networks". IEEE Trans., PAS-88, pp. 388-399, April 1969.

[2] H.W. Dommel and W.S. Meyer, "Computation of Electromagnetic Transients". IEEE Proc., Vol. 62 (7), pp. 983-993, July 1974.

[3] J.R. Marti, "Accurate Modelling of Frequency-Dependent Transmission Lines in Electromagnetic Transients Simulations". IEEE Power Industry Computer Applications (PICA) Conference, Philadelphia, PA, 9 pages, May 1981.

[4] H.L. Leon, Profiles of Transient Voltages along Overhead Lines (M.A.Sc. thesis). Department of Electrical Engineering, University of Toronto, December, 1979.

[5] A. Semylen and A. Dabuleanu, "Fast and Accurate Switching Transient Calculations on Transmission Lines with Ground Return using Recursive Convolutions". IEEE Trans., PAS-94, pp. 561-571, March/ April 1975.

[6] Line Constants of Overhead Lines User's Manual. Methods Analysis Group, Branch of System Engineering, Bonneville Power Administration, Portland, Oregon, Appendix 2 by H.W. Dommel, August 1977.

[7] J.R. Marti, The Problem of Frequency Dependence in Transmission Line Modelling (PhD thesis). Department of Electrical Engineering, University of British Columbia, April 1981.

[8] Ibid., pp. 189-193.

[9] Ibid., p. 106

[10] D.E. Hedman, "Propagation on Overhead Transmission Lines: I. Theory of Modal Analysis; II. Earth Conduction Effects and Practical Results". IEEE Trans., PAS-84, pp. 200-211, March 1965.

[11] H.W. Dommel, Notes on Advanced Power Systems Analysis. University of British Columbia, 1975.

[12] UBC - Overhead Line Parameters Program. Originally written by H.W. Dommel at the Bonneville Power Administration, Portland, Oregon. Modified at the University of British Columbia (UBC), Canada, by I.I. Dommel, K.C. Lee, and T. Hung. User's Manual, UBC, August 1980.

BIBLIOGRAPHY

[13] UBC - Electromagnetic Transients Program (EMPT). Originally written by H.W. Dommel at the Bonneville Power Administration, Portland, Oregon. Modified at the University of British Columbia (UBC), Canada, by H.W. Dommel. Frequency-dependence version originally written by J.R. Marti at UBC. Modified by L. Marti. User's Manual, UBC, August 1978 (first published in 1976).

[14] J.P. Bickford, N. Mullineux, and J.R Reed, Computation of Power Systems Transients (book). Peregrinus (for the IEE), Herts (England), 1976.

[15] L.V. Bewley, Travelling Waves on Transmission Systems (book). Dover, New York, 1963 (first published in 1933).

[16] EHV Transmission Line Reference Book. Edison Electric Institute, New York, N.Y., 1968.